

Cyber Catalysis: N₂ Dissociation over Ruthenium Catalyst with Strong Metal-Support Interaction

Gerardo Valadez Huerta^{*,1}, Kaoru Hisama¹, Katsutoshi Sato², Katsutoshi Nagaoka², Michihisa Koyama^{*,1,3}

¹Research Initiative for Supra Materials, Shinshu University, Nagano 380-8553, Japan.

²Department of Chemical Systems Engineering, Nagoya University, Nagoya 464-8601, Japan.

³Open Innovation Institute, Kyoto University, Kyoto 606-8501, Japan

*Corresponding authors: valadez@shinshu-u.ac.jp, koyama_michihisa@shinshu-u.ac.jp

Abstract

Catalysis informatics is constantly developing, and significant advances in data mining, molecular simulation, and automation for computational design and high-throughput experimentation have been achieved. However, efforts to reveal the mechanisms of complex supported nanoparticle catalysts in cyberspace have proven to be unsuccessful thus far. This study fills this gap by exploring N₂ dissociation on a supported Ru nanoparticle as an example using a universal neural network potential. We calculated 200 catalyst configurations considering the reduction of the support and strong metal-support interaction (SMSI), eventually performing 15,600 calculations for various N₂ adsorption states. After successfully validating our results with experimental IR spectral data, we clarified key N₂ dissociation pathways behind the high activity of the SMSI surface and disclosed the maximum activity of catalysts reduced at 650 °C. Our method is well applicable to other complex systems, and we believe it represents a key first step toward the digital transformation of investigations on heterogeneous catalysis.

Catalysis informatics can be classified into three categories¹⁻³: i) data mining mainly based on machine learning^{2,4,5}; ii) first-principles calculations⁶, including the development of kinetic models⁷; iii) and computational automated design⁸. These approaches overlap within cyberspace^{4,9,10}. Recent developments in data-driven approaches have enabled the exploration of previously undiscovered catalysts without the need for numerous experiments and computations¹¹. Machine-learning approaches can guide high-throughput experiments as counterparts to traditional trial-and-error studies by narrowing the parameter space, resulting in an adaptive experimental design¹². Obtaining information on catalytic properties from supervised learning based on digital data is another data-driven approach in catalysis¹³. Rational catalyst design using first-principles calculations is ongoing^{14,15}, and the automated computational high-throughput design of catalysts is primarily practiced in organic chemistry⁸. However, despite the availability of countless catalysis studies and publicly available digital databases, such as Catalysis-Hub¹⁶, significant gaps inhibiting the full exploration of heterogeneous catalyst systems through catalysis informatics remain. This problem persists even in up-to-date discussions^{9,17,18} and was confirmed by a machine-generated summary of recent

publications for heterogeneous catalysis (see the Supplementary Data) created with the same tool¹⁹ used to obtain machine-generated books²⁰.

Supervised learning is a data-driven approach used to predict the catalytic properties of heterogeneous catalysts based on descriptors from first-principles data²¹. State-of-the-art first-principles calculations allow single calculations for isolated and supported nanoparticles^{22,23} containing up to 2,406 and 1,169 atoms, respectively²². This approach can also determine reaction paths for the dissociation of molecules on stepped surfaces²⁴ or supported clusters²⁵. Unfortunately, first-principles calculations, a critical tool for describing electronic and atomistic properties, are not yet widely applicable to the study of real heterogeneous catalysis systems requiring a simplified and ideal model³. A computationally inexpensive and widely applicable framework is necessary to examine heterogeneous systems with real solid catalysts, which may have local properties different from those of bulk phases owing to defects^{26,27}, surface site heterogeneity²⁸, or a strong metal-support interaction (SMSI)^{29–31}. Constant interfacial interactions between various phases may result in surface reconstruction processes³² influencing catalyst activity³³, which prevents the use of real system models in the first-principles method due to the computational cost³⁴. Higher-scaled computations can be performed with potentials such as the ReaxFF³⁵. However, the models obtained from such computations must be parameterised for each case, which limits their applicability and transferability^{36,37}. Moreover, ReaxFF parameterisation to achieve high accuracy is challenging³⁸. Neural network potentials have been used to reproduce first-principles results via machine learning. Calculations using such models are expected to have high computational performance^{39–41} and can break through the current theoretical barrier of high reductionist models⁴². Universal neural network potentials (UNNPs) have emerged as a result of the connatural evolution of catalysis informatics^{43–45}. The simultaneous calculation of different phases for multiple elements, including all interfacial interactions, is possible using these models. Chemical reactions and charge prediction can also be achieved^{43,45}. Thus, these models open the possibility of bringing automated computer design into the discipline of heterogeneous catalysis.

This study transcends the limits of DFT by exploiting the computational possibilities of a UNNP for exploring complex heterogeneous catalyst systems. From the countless material combinations that can be tackled with the UNNP, we chose, as a representative example, the dissociation of N₂ on a Ru nanoparticle on a La_{0.5}Ce_{0.5}O_{1.75-x} support for ammonia synthesis⁴⁶. Our modelling approach artificially reproduced the experimentally observed nanoparticle–cationic interfacial interaction resulting from the SMSI with 200 different catalyst configurations considering the reduction degree of the oxide support. We extensively observed N₂ adsorption on Ru on-top sites in all catalyst configurations. Calculations of the immense variety of adsorption configurations were unavoidable to obtain a wide-ranging perspective of the microscopic processes. We found catalyst configurations with N₂ wavenumbers similar to experimentally measured IR spectra⁴⁶. The activation energy of N₂ dissociation for select adsorption sites showed potential adsorption modes leading to the high activity observed in the literature⁴⁶.

Results

Strategy and Catalyst Model Preparation. Our approach for modelling and simulating N_2 dissociation on supported Ru nanoparticles is depicted in Fig. 1. First, we modelled the catalyst. We prepared $Ru/La_{0.5}Ce_{0.5}O_{1.75-x}$ models consisting of a Ru_{143} half-nanoparticle on a $4 \times 4 \times 3$ $La_{0.5}Ce_{0.5}O_{1.75-x}(111)$ slab with a fluorite structure (space group, $Fd\bar{3}m$) (Fig. 1a; Supplementary Fig. 1). We refer to the upper layer of the cationic slab as the cationic surface hereafter. We prepared Ce, La, superlattice (SL), and five solid solution (SS) cationic surfaces. The SL surface was prepared by intercalating the Ce and La cations and SS surfaces via random distribution. The remaining cationic bottom layers were modelled as an SS phase. After assembling the half-nanoparticle and support models, we reduced the slab by removing oxygen atoms from the cationic surface. The onset of an SMSI was observed experimentally for this particular catalyst⁴⁶, indicating an increase in nanoparticle–metal oxide interfacial area^{29,30}. To model the catalyst structure with an artificial SMSI, we randomly selected cations from the cationic surface and placed them on the lowest nanoparticle layer. The final catalyst configurations were obtained by optimising the models with different degrees of cationic surface reduction and artificial SMSI (Supplementary Fig. 2).

We observed different degrees of SMSI onset, depending on the extent of cationic surface reduction and artificial SMSI (Fig. 1b; Supplementary Note 1). For surfaces with full reduction, that is, all oxygen atoms in the surface layer were removed, surface reconstruction after optimisation resulted in only one or two cations moving toward the upper layers of the Ru nanoparticle without the artificial SMSI. When more cations are initially placed on the nanoparticle at this high reduction degree, they remain at this position or move toward upper layers. By contrast, the cations tend to descend to the support as the reduction degree decreases. We observed the nanoparticle beginning to convulse when the configuration with the highest SMSI and reduction degree simulated in this study was adopted (Supplementary Fig. 3). This type of system deterioration resulting from a high SMSI is a well-known experimentally observed process²⁹.

Next, we mapped the optimised catalyst configurations to obtain a complete picture of the configurational space. For this purpose, we need to find suitable descriptors. As widely discussed^{47,48}, the electronic metal-support interaction (EMSI) is more suitable for describing the catalyst support effect than the SMSI. The EMSI describes the charge transfer between a nanoparticle and its support. Therefore, it can be represented by the average charge of Ru. The charge distribution of Ru atoms and, thus, their average charge shift toward more negative values, depending on the degree of cationic surface reduction and SMSI (see blue atoms in Fig. 1c). Thus, we used the average charge $\bar{q}_{Ru,0}$ of the Ru atoms at the surface nanoparticle layer and the value of x in $La_{0.5}Ce_{0.5}O_{1.75-x}$ to spread the $Ru/La_{0.5}Ce_{0.5}O_{1.75-x}(111)$ optimised configurations. For simplicity, we only considered the composition of the whole $4 \times 4 \times 3$ slab, which does not correspond to the real system, owing to the size of the $La_{0.5}Ce_{0.5}O_{1.75-x}$ layer in our model. We refer to x as the reduction degree hereafter. The configuration map in Fig. 1d was constructed according to these descriptors. Using different upper cationic slab layer compositions and reduction degrees, as well as artificial modelling of the SMSI, we obtained 200 catalyst configurations.

Finally, we accounted for N₂ activation. For each of the 200 catalyst configurations, we placed a N₂ molecule with an end-on orientation on each available Ru on-top site by referring to previous experimental and theoretical observations of the adsorption structure^{46,49}. This step resulted in 15,600 optimisations. To work with this massive amount of data, we scanned, evaluated, and plotted the properties for each adsorption state using an automated screening approach (Fig. 1e). This step enabled us to automatically create spatial maps for each catalyst configuration by assigning, for example, specific N₂ wavenumber values to the Ru site position (compare Fig. 1e and Supplementary Fig. 4).

Exhaustive Calculation Results of N₂ Adsorption. Histograms showing the distribution of all calculated N₂ adsorption states over the N–N bond length are depicted in Fig. 2a. The coverage at 25 °C and 6 kPa is used as the weighting factor for the weighted histogram. Two dense regions with bond length peaks of approximately 1.14 and 1.17 Å were identified. Two adsorption peaks at approximately 2,150 and 1,850 cm⁻¹, corresponding to high and low wavenumbers, respectively, were also observed (see bottom diagram in Fig. 2a).

Spatial maps of the N₂ wavenumber are illustrated in Fig. 2c. Here, we used the top view of the nanoparticles and polar coordinate systems and kept the size of the markers proportional to the simulated N₂ coverage θ ($T = 25$ °C, $p = 6$ kPa) for better comparison. The adsorbed N₂ molecules had a high wavenumber ($>2,000$ cm⁻¹) when $x \approx \bar{q}_{Ru,0} \approx 0$. As the reduction degree x increased and the EMSI became stronger, a lower wavenumber ($<2,000$ cm⁻¹) was observed. Sites with a low wavenumber were located near Ce/La cations wrapped around the nanoparticle. Furthermore, adsorption sites became more active at higher reduction degrees and EMSI, as indicated by the size of the markers. To explain this effect, we constructed spatial maps of the N₂ adsorption energy, as shown in Fig. 2d. The adsorption on the edge and vertex sites is stronger than that on the (10 $\bar{1}$ 1) and (0001) surfaces for configurations with $x \approx \bar{q}_{Ru,0} \approx 0$. As the reduction degree and EMSI increased, the adsorption energy decreased at sites near Ce/La cations. Because of this effect, the coverage increased in these adsorption sites. When the non-weighted and weighted distributions of the histograms in Fig. 2a are compared, the activation of sites with a lower wavenumber become more evident. Moreover, as the number of cations wrapping the nanoparticle increased, the Ru sites became increasingly occupied, thereby preventing the adsorption of N₂ molecules (Fig. 2c, (10 $\bar{1}$ 1) surfaces for the catalyst configuration with $x = 0.27$ and $\bar{q}_{Ru,0} = -0.37$ e). Finally, the wavenumber and N₂ molecular charge showed a linear relationship with the N₂ bond length (see bottom diagram in Fig. 2a). The N–N bond became weaker owing to electron transfer to the N₂ antibonding π -orbital⁵⁰. While our calculations effectively reproduced this trend, we stress that this statement is simply an interpretation of the results because the UNNP model does not consider electron transfer explicitly.

After performing the exhaustive scan described above, we searched for representative adsorption states. A representative adsorption state should have high coverage and lie in the statistical bulk density within two defined regions. We depict, in Fig. 2b, examples of adsorption states following these criteria (A–I) (Supplementary Fig. 5). N₂ molecules adsorbed on the upper layers of the nanoparticle showed a high wavenumber. The wavenumber for adsorption state A, for example, is 2,161 cm⁻¹. We can identify two main mechanisms that determine by what extent the wavenumber may decrease. The first

effect is applicable to molecules near cations on the nanoparticle (e.g. states B, D, F, G, and H). When a large number of cations are present near the adsorption site, this effect is enriched. However, when these cations are (partially) oxidised, the effect is dampened (compare F and G). The second mechanism is applicable to molecules adsorbed at the interface between the nanoparticle and support, as depicted in adsorption states C and E; in this case, a lower wavenumber is observed even without cations near the adsorption site. However, this finding applies only to supports with a non-zero reduction degree or interfacial regions with oxygen vacancies when x is zero. When both mechanisms are combined, frequencies lower than $1,800\text{ cm}^{-1}$ can be observed, even when the cations attached to the nanoparticle are partially oxidised, as can be observed in adsorption state I.

Identification of a Real System Catalyst Configuration. We require validation to identify a catalyst configuration representing a real system. Thus, we calculated the spectrum of the wavenumber for each catalyst configuration by estimating weighted Gaussians for each adsorption state (middle diagram in Fig. 3a) and compared the results with experimental IR spectra. We considered the peak broadening of each vibrational state using the actual detector resolution, Doppler effect, and collisions. The collision contributions consider the gas atmosphere under experimental conditions, surrounding catalyst atoms, and neighbouring adsorbed N_2 molecules. The coverage at $25\text{ }^\circ\text{C}$ and 6 kPa was used as a weighting factor. The contribution of each effect is shown in the top diagram of Fig. 3a. The spectrum of the wavenumber of the catalyst configuration was obtained by summing the Gaussians of each adsorption configuration (Supplementary Note 2).

We identified regions with higher and lower wavenumbers using different distributions. In general, the shape of a distribution follows a single Gaussian. Lower coverage or higher broadening results in lower peaks; higher broadening also leads to a wider distribution. Because the simulated spectrum represents the sum of the Gaussians, the height of the spectrum increases with the number of N_2 molecules with wavenumbers close to a specific value. In our simulated spectra (see, for example, the bottom diagram in Fig. 3a), the broadening of the high wavenumber region can simply be represented by the collisions with the Ru site and adjacent N_2 molecules, as the Doppler and gas atmosphere effects are negligible. The asymmetry observed in this case is due to the wide distribution of adsorption states with wavenumbers between $2,000$ and $2,100\text{ cm}^{-1}$. The relatively low coverage within this wavenumber interval (see histograms in Fig. 2a) results in Gaussians with low peaks. The high number of neighbouring collisions in the low-frequency region causes a larger broadening of the calculated distribution compared with that observed in the high-frequency region. Moreover, the distribution curve around the high-frequency peak flattens as the distribution in the low-wavenumber region rises. This effect is consistent with the activation of adsorption sites within the low-frequency region discussed in the previous section.

The simulated spectra can be compared with the IR spectra of catalysts reduced at 500 and $650\text{ }^\circ\text{C}$ ⁴⁶. We can find 14 and 8 out of the 200 simulated spectra that are statistically similar to the experimental spectra measured at 500 and $650\text{ }^\circ\text{C}$, respectively (Supplementary Note 3). The average of these spectra, together with the experimental spectra, are provided in Fig. 3b. The average spectra (with $x = 0.095(21)$ and $\bar{q}_{\text{Ru},0} = -0.133(19)\text{ e}$ on average) corresponding to the catalyst reduced at $500\text{ }^\circ\text{C}$

showed a peak at a low wavenumber of $1,879\text{ cm}^{-1}$. The average spectra ($x = 0.175(72)$ and $\bar{q}_{\text{Ru},0} = -0.233(71)$ e on average) corresponding to the catalyst reduced at $650\text{ }^{\circ}\text{C}$ showed a peak at a low wavenumber of $1,852\text{ cm}^{-1}$. Thus, we can reproduce the measured values of $1,883$ and $1,844\text{ cm}^{-1}$, whereas all identified peaks correspond to frequencies with stretching vibrational modes. We further calculated the relative peak intensity by dividing the intensity of peaks at high wavenumbers by the intensity of peaks at low wavenumbers. The intensities were determined relative to the baselines of the spectra given by the thin solid lines in Fig. 3b. The simulated and experimental relative intensities were 7.4 and 6.8 , respectively, for a reduction temperature of $500\text{ }^{\circ}\text{C}$, and 5.9 and 4.1 , respectively, for a reduction temperature of $650\text{ }^{\circ}\text{C}$. While the simulated and experimental relative intensities show a discrepancy when the reduction temperature is $650\text{ }^{\circ}\text{C}$, the simulated and experimental values obtained for a reduction temperature of $500\text{ }^{\circ}\text{C}$ are in good agreement. Because the shape of the calculated spectra is similar to that observed in experimental observations, we can provide the experimental observations with a physical background. We note here that our simple bottom-up approach shows a certain discrepancy with the measured broadening, which may originate from the overestimation of the broadening mechanisms considered and other effects associated with the measurement proper that are not included in our calculations.

Analysis of Catalytic Activity. In experiments, $\text{Ru}/\text{La}_{0.5}\text{Ce}_{0.5}\text{O}_{1.75-x}$ catalysts show maximum activity when reduced at $650\text{ }^{\circ}\text{C}$ (Fig. 3c)⁴⁶. To elucidate the physical origin of this phenomenon, we calculated the dissociation paths (Fig. 3d) for the representative N_2 adsorption states A, C, F, G, H, and I (shown in Fig. 2b) at $350\text{ }^{\circ}\text{C}$. States A, F, G, and H show wavenumbers close to the experimental values. The activation Gibbs energy for the rate-determining step of dissociation on top of the nanoparticle (A) was 1.94 eV . This value is comparable with the reported energy barrier for N_2 dissociation on a Ru slab (Supplementary Table 1). The adsorption state at the interfacial layer on the $\text{Ru}(10\bar{1}1)$ surface (C) showed a lower activation Gibbs energy for dissociation of 0.90 eV , which could be expected from its lower wavenumber of $2,066\text{ cm}^{-1}$. The activation Gibbs energies for the rate-determining steps of adsorption states G and H were 1.09 and 0.98 eV , respectively. Lower values of 0.65 and 0.64 eV were observed for states F and I, respectively. Support reduction is fundamental to achieve a low dissociation barrier because the sites at the interface become active (Fig. 2c) and stabilise the onset of an SMSI. Moreover, wavenumbers lower than $2,000\text{ cm}^{-1}$ can be observed only when the onset of an SMSI occurs (Fig. 2c), resulting in sites corresponding to the states F, G, H, and I. Among these states, states G and H, with a relatively low wavenumber, show higher activation barriers than states F and I.

We further performed structural analysis to clearly differentiate these adsorption states. We counted the number of Ce/La/O atoms $N_{\text{Ce/La}}$ and N_{O} surrounding the N_2 molecule. A cut-off radius of 5 \AA was sufficiently large to consider different local structures. The cations surrounding the N_2 molecule for states F and I were partially oxidised ($N_{\text{Ce/La}} \geq N_{\text{O}}$ and $N_{\text{O}} > 0$), whereas the cations surrounding the N_2 molecule for states G and H were not ($N_{\text{Ce/La}} > 0$ and $N_{\text{O}} = 0$). Catalysts with a higher number of adsorption states F and I had higher catalytic activity. Finally, we sought to determine whether our hypothesis can explain the measured catalytic activity of the catalysts (Fig. 3c). We counted the emergences of states F and I for each configuration considering the N_2 coverage at $350\text{ }^{\circ}\text{C}$ and 1 MPa (Table 1). On average, we observed 20% more of these states in catalyst configurations corresponding to a reduction temperature of $650\text{ }^{\circ}\text{C}$

compared with those corresponding to a reduction temperature of 500 °C, thus supporting the higher activity of the catalyst system reduced at 650 °C.

Conclusions

This study shows the excellent validity of the proposed approach for investigating heterogeneous catalyst systems in cyberspace for catalysts based on supported nanoparticles showing the onset of an SMSI. In the proposed framework, the modelling approach for the catalyst is more compliant with an artificial mapping of configurations than a completely physics-based approach, that is, guided by the chemical potentials of the components and reducing atmosphere. This mapping was necessary to achieve the adequate and systematic preparation of catalyst models used to explore the adsorption and catalytic properties of molecules with which they interact. The exhaustive calculation of adsorbed molecules on the catalyst was unavoidable. The massive size of our models and extensive surface reconstruction necessary during the long optimisation of the supported nanoparticle systems prohibit the use of first-principles calculations. Even if optimising some adsorption sites via this technique is possible, the results obtained cannot be assumed to be meaningful for such a complex heterogeneous system, as discussed throughout the article. Moreover, we successfully validated the numerical results with experimental data and clarified specific experimental observations for these types of catalysts. Notably, we provided experimental observations for the IR spectra of N₂ molecules adsorbed on the studied catalyst with a robust physical background, which may be applicable to other similar catalysis systems.

Achieving the number of calculations required to obtain the dissociation reaction paths similar to that employed for the 15,600 calculated adsorption sites in our work will be challenging. However, we can produce an accurate state-of-the-art approximation of such properties for the heterogeneous catalyst system studied here. We believe that if the distribution of cations wrapped around a nanoparticle can be skilfully controlled by modifying the composition of the nanoparticle to avoid the deactivation of strategic adsorption sites, new catalysts with higher catalytic activity could be designed in cyberspace, synthesised, and characterised experimentally for use in real technical systems.

Our approach can be directly used to investigate other material combinations, including other supports and nanoparticles based on binary, ternary, and multinary alloys. Indiscriminate computationally guided high-throughput experimentation for material discovery may now be possible. Moreover, the many unresolved questions arising from the unique properties and behaviours of the innumerable synthesised complex supported nanoparticle catalysts developed thus far can now be solved using the proposed framework. Thus, we believe that this study is a key first step toward the true digital transformation of investigations on heterogeneous catalysis.

Methods

Model Preparation and Calculation. We configured the 4 × 4 × 3 La_{0.5}Ce_{0.5}O_{1.75} bulk models prior to optimisation using a well-known method for binary metal-oxides with vacancies⁵¹ by accounting for a Warren–Cowley⁵² parameter close to zero for the SS

cationic phase and a lattice parameter of 7.93 Å corresponding to the DFT value calculated from the Materials Project Database⁵³. Energy minimisation was applied to the cell size and atom positions. After optimisation, we added a 30 Å vacuum layer perpendicular to the (111) surface to create a slab and then optimised the atomic positions. We conducted a molecular dynamics (MD) simulation on the canonical ensemble to equilibrate the anions of the slab at 650 °C, corresponding to the reduction temperature reported in the literature⁴⁶ (Supplementary Fig. 9). The configuration of the slab trajectory obtained after equilibration was used for further calculations, and the upper cationic layer was reduced by different degrees by randomly removing oxygen anions.

We optimised a Ru₂₃₈ nanoparticle with an HCP structure and extracted a Ru₁₄₃ half-nanoparticle with a large (0001) facet downside. We tested different orientations of the nanoparticle on the slab and chose the most energetically favourable one (Supplementary Methods 1). Different supported nanoparticle configurations were created using this nanoparticle orientation. We then placed random cations from the cationic surface at the lower nanoparticle layer at various degrees and optimised the structure. Individual N₂ molecules were optimised and placed at all Ru on-top sites at a distance of 1.6 Å. The N atoms were oriented so that they pointed parallel to the direction from the Ru site to the middle of the nanoparticle (Supplementary Fig. 1). After optimisation, molecules that did not change the Ru site and with a distance to this site of less than 2.3 Å, bond length less than 2.5 Å, and wavenumber higher than 1,200 cm⁻¹ were used for further evaluation. These criteria ensured that the molecules to be analysed were end-on adsorbed on Ru on-top sites without repetition.

To approximate configurations for two different dissociated states per adsorption site, we placed N atoms at the neighbouring site of Ru in the \mathbb{R}^2 projection of the nanoparticle surface layer and optimised them. We calculated saddle-point configurations using two configurations estimated as the linear interpolation with a factor of 0.5 between the initial state and two approximated final states. Ten saddle points were calculated for each configuration. We minimised a second configuration downhill by extrapolating it 105% away from the initial state toward the saddle point and conducting a final optimisation to find the nearest local minima. We then calculated the minimum energy path and disregarded reaction paths that were repeated or inconsistent. We considered non-consistent paths as those with energies higher than the calculated transition state, energy barriers higher than 4 eV, a non-dissociated final state, or a poorly converged transition state showing more than one imaginary frequency.

Simulation Methods. All simulations were conducted using the commercial software UNNP Preferred Potential version 1.0.0 within the MatlantisTM distribution⁴⁵. Although MatlantisTM includes numerous features, we used the freely available ASE⁵⁴ tools for all calculations. All all-atom energy optimisations were performed using the FIRE algorithm⁵⁵ with a force threshold of 0.001 eV/Å unless otherwise stated. The MD simulation was performed with a timestep of 0.5 fs. The Nosé–Hoover⁵⁶ thermostat, as implemented in the FLARE library⁵⁷, was used with a damping factor Q corresponding to 100 timesteps⁵⁸. A simulation time of 100 ps was sufficient to achieve equilibration. The Dimer method⁵⁹ was used to search for saddle points. We performed downhill optimisation using the Broyden–Fletcher–Goldfarb–Shanno line search method⁵⁴. Only atoms within a cut-off radius of 3.0 Å relative to the N atoms were allowed to move. The

same was true for the NEB routine⁶⁰, which searched for the minimum energy path with a force threshold of 0.05 eV/Å. The NEB routine was performed by separately calculating segments of three images and adding in-between configurations along the path, resulting in nine images after two iterations, including the initial, transition, and final states. The NEB calculation was repeated for segments with a local maximum by climbing the images⁶¹ with a force threshold of 0.005 eV/Å. Configurations corresponding to the local minimum within the path were further all-atom optimised. A spring constant of 0.1 eV/Å was used for all NEB calculations. The UNNP is validated in Supplementary Methods 2.

Calculation of thermophysical properties. We calculated the coverage θ assuming Langmuir adsorption as $\theta = K_{ads} \cdot p / (1 + K_{ads} \cdot p)$ with the equilibrium constant K_{ads} calculated from $\ln(p^\ominus \cdot K_{ads}) = -\Delta G(T, p) / (k_B T)$. Here, p denotes the pressure, p^\ominus denotes the standard pressure, T refers to the temperature, and k_B is the Boltzmann constant. The adsorption Gibbs energy $\Delta G(T, p)$ for a single N₂ molecule was calculated by assuming the ideal gas limit, and the Gibbs energy for the adsorbed molecule was approximated using the Helmholtz energy from the harmonic limit; here, both models were used as implemented in ASE⁵⁴.

To calculate the wavenumber spectrum (Supplementary Fig. 10), we determined the Doppler broadening $\delta\tilde{\nu}_D$ as follows⁶²:

$$\delta\tilde{\nu}_D = \frac{2\nu}{c} \left(\frac{2 \cdot k_B T \ln(2)}{m_{N_2}} \right)^{\frac{1}{2}},$$

where ν denotes the wavenumber, c is the speed of light in vacuum, and m_{N_2} is the mass of the N₂ molecule. The broadening due to collisions was given by⁶²:

$$\delta\tilde{\nu}_{C,i} = \frac{\pi r^2}{2c} \left(\frac{8k_B T}{\pi \mu_{N_2-i}} \right)^{\frac{1}{2}} \cdot \rho_i,$$

where the reduced mass $\mu_{A-B} = m_A m_B / (m_A + m_B)$ and ρ_i is the number density of component i corresponding to the ideal gas density for collisions with the N₂ atmosphere or the number of atoms/molecules within the volume of the sphere with a radius equal to the collision cross-section $\pi r^2 = 3.4 \text{ nm}^2$ for N₂ molecules⁶². The density was weighted using the coverage θ by accounting for possible adjacent adsorbed N₂ molecules. Finally, we considered the detector resolution by applying the Sparrow rule⁶³ as follows:

$$\delta\tilde{\nu}_{Res} = \sqrt{2 \ln(2)} \cdot \text{FWHM},$$

where the full width at half maximum (FWHM) for each Gaussian is given by the experimental resolution⁴⁶ of 4 cm⁻¹.

Data availability

The data supporting the findings and statements presented in this study can be found in this article and Supplementary Information. Other data sources can be obtained from the authors upon reasonable request.

Figures

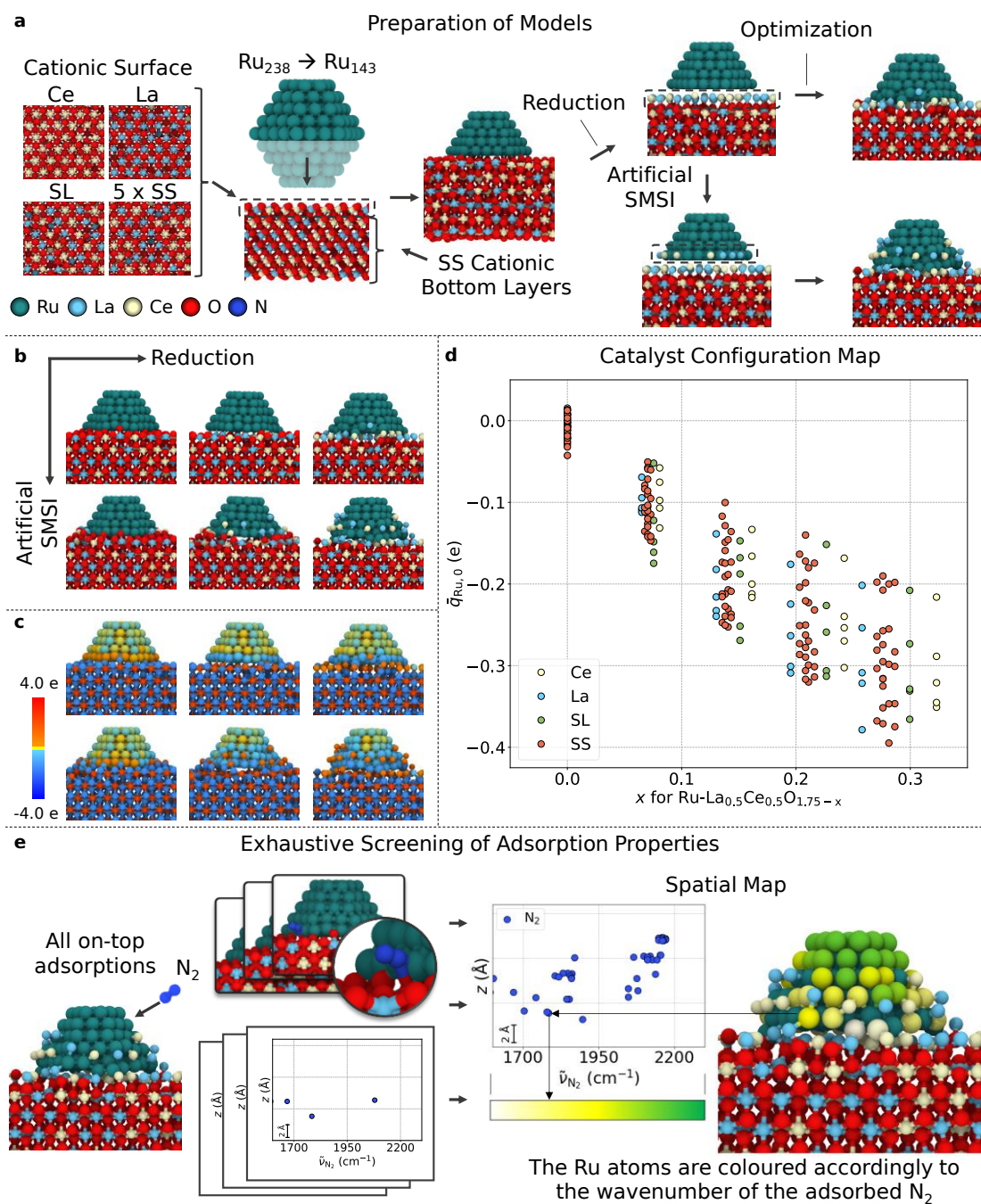


Fig. 1. Strategy for modelling and simulating N₂ dissociation on Ru/La_{0.5}Ce_{0.5}O_{1.75-x} catalysts. **a**, Automated preparation of the models. **b**, Optimised catalyst configurations for three reduction degrees of the cationic surface and two artificial SMSIs. **c**, Charge distribution for the configurations in **(b)**. **d**, Catalyst configuration map spread by the average charge $q_{\text{Ru},0}$ of Ru atoms on the nanoparticle surface layer and reduction degree x for all 200 catalyst configurations analysed in this study (x corresponds to the composition of the $4 \times 4 \times 3$ La_{0.5}Ce_{0.5}O_{1.75-x} slab). **e**, Screening method used to calculate

the N_2 properties and create the spatial maps. The N_2 wavenumber $\tilde{\nu}_{N_2}$ for each N_2 adsorption state was plotted over the position of the Ru site for each configuration. The Ru sites were then coloured according to the value of the wavenumber. The coordinate z is given arbitrarily for the Ru sites.

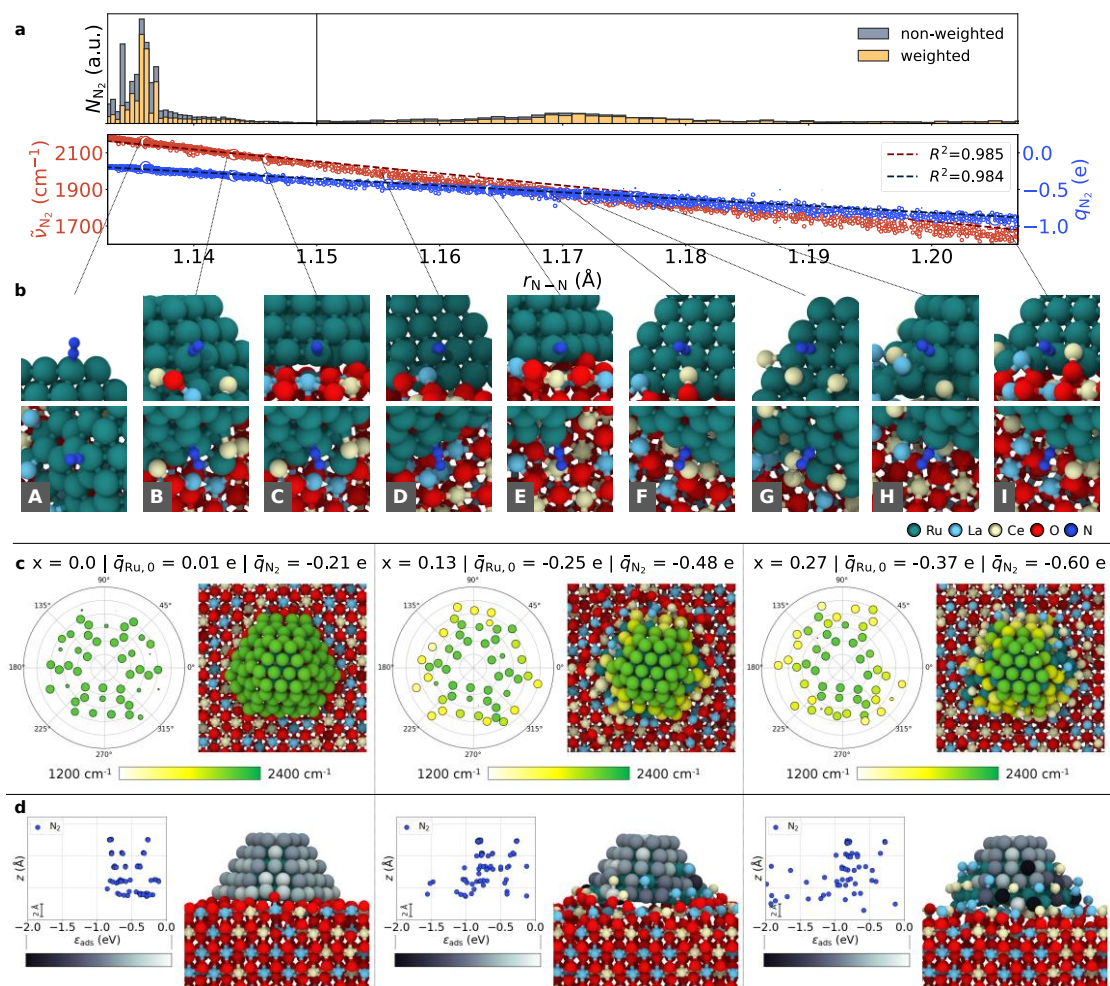


Fig. 2. Simulated N_2 adsorption on different $Ru/La_{0.5}Ce_{0.5}O_{1.75-x}$ catalyst configurations. a, Top: Weighted and non-weighted histograms of the N–N bond length r_{N-N} distribution. A total of 150 bins for $r_{N-N} > 1.15$ Å and 50 bins for $r_{N-N} < 1.15$ Å were arbitrarily chosen. The N_2 coverage θ at 25 °C and 6 kPa was used as the weighting factor. **Bottom:** Simulated wavenumbers $\tilde{\nu}_{N_2}$ and charges q_{N_2} of single adsorbed N_2 molecules for all adsorption sites within the depicted range. **b,** Representative adsorption sites. **c,** Calculated spatial maps of the N_2 wavenumber, which were built as described in Fig. 1e. Here, the top view and polar coordinates of the catalyst were used. The diameter of the markers is given according to the N_2 coverage θ at 25 °C and 6 kPa. **d,** Spatial maps of the N_2 adsorption energy ϵ_{ads} , which were built as described in Fig. 1e.

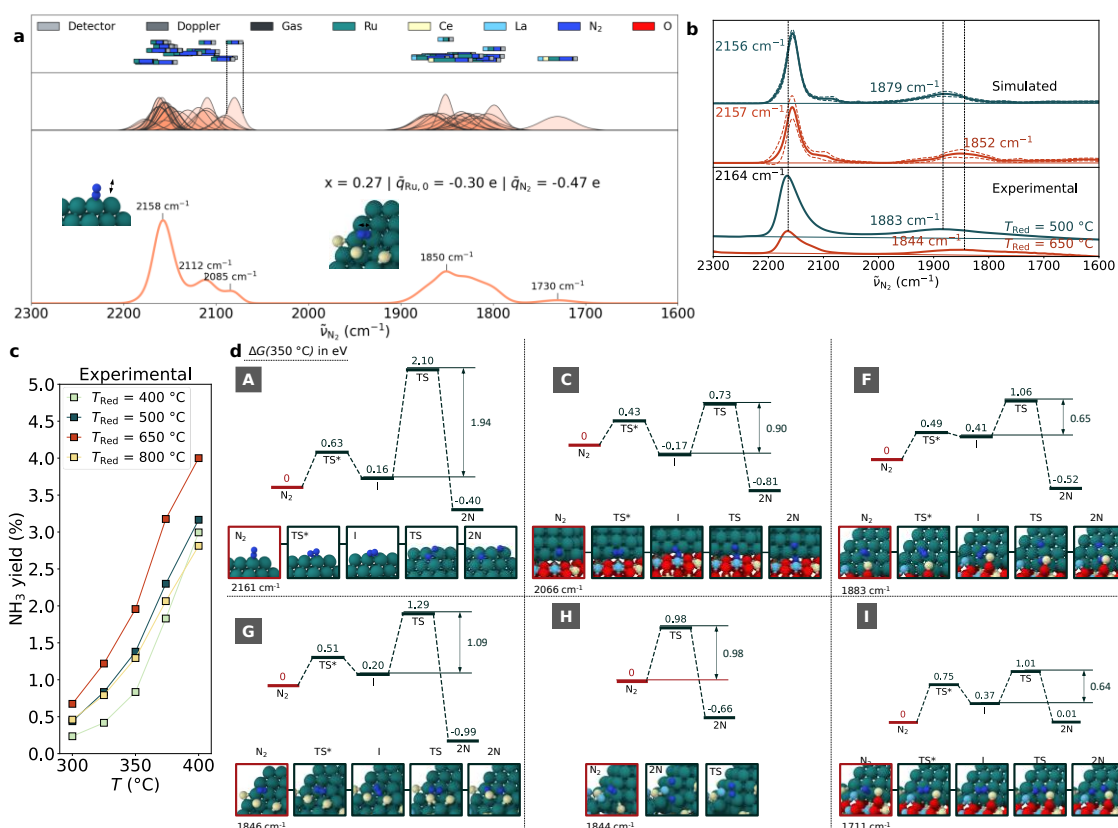


Fig. 3. Simulated catalytic properties for N₂ dissociation on different Ru/La_{0.5}Ce_{0.5}O_{1.75-x} catalyst configurations. **a**, Example of a simulated N₂ wavenumber distribution. **Top**: Calculated spectral line widths coloured according to the calculated contributions: broadening due to the detector resolution, Doppler effect, and collisions with the N₂ gas atmosphere and neighbouring Ru/Ce/La/O and adsorbed N₂. **Middle**: Weighted Gaussians (weighting factor: N₂ coverage θ). **Bottom**: Wavenumber distribution obtained from the sum of the Gaussians. The values were obtained at 25 °C and 6 kPa. **b**, Calculated average N₂ wavenumber distributions and measured IR spectra⁵⁹. Averaging was performed over the distributions that are statistically similar to the experimental IR spectra.⁵⁹ The dashed lines indicate the standard error of averaging with a 95% confidence interval. The thin solid lines are the baselines of the spectra. **c**, Measured NH₃ yield (in %) as a function of the reduction temperature of the catalysts⁴⁶. **d**, Calculated N₂ dissociation paths for the adsorption states A, C, F, G, H, and I shown in Fig. 2b. For each path, the label N₂ describes the initial state, TS* and TS indicate the transition states, I indicates the intermediate state, and 2N indicates the final dissociation state. The energy values indicated correspond to the Gibbs energy difference $\Delta G(350 \text{ }^\circ\text{C})$ relative to the initial state. The energies for the rate-determining step are also provided. All experimental data were taken from the literature⁴⁶.

Table

Table 1. Average number of adsorption states for the simulated configurations assigned to real catalysts.

States	A	C	G	H	F	I
$\Delta G(350\text{ }^\circ\text{C})$ (eV)	1.94	0.90	1.09	0.98	0.65	0.64
$\bar{N}_{N_2}(T_{\text{red}} = 500\text{ }^\circ\text{C})$	12.14	0.06	2.78		2.15	
$\bar{N}_{N_2}(T_{\text{red}} = 650\text{ }^\circ\text{C})$	12.26	0.50	1.69		2.56	

$\Delta G(350\text{ }^\circ\text{C})$ is the activation barrier at 350 °C. $\bar{N}_{N_2}(T_{\text{red}})$ is the average weighted number of adsorption states corresponding to the states A, C, G, H, F, and I (Fig. 1d) for the configurations assigned to the catalyst at a reduction temperature of T_{red} . The N_2 coverage $\theta(T = 350\text{ }^\circ\text{C}$ and 1 MPa) was used as the weighting factor.

References

1. Foscatto, M. & Jensen, V. R. Automated in silico design of homogeneous catalysts. *ACS Catal.* 10, 2354–2377 (2020). [10.1021/acscatal.9b04952](https://doi.org/10.1021/acscatal.9b04952).
2. Toyao, T., Maeno, Z., Takakusagi, S., Kamachi, T., Takigawa, I. & Shimizu, K. Machine learning for catalysis informatics: recent applications and prospects. *ACS Catal.* 10, 2260–2297 (2020). [10.1021/acscatal.9b04186](https://doi.org/10.1021/acscatal.9b04186).
3. Medford, A. J., Kunz, M. R., Ewing, S. M., Borders, T. & Fushimi, R. Extracting knowledge from data through catalysis informatics. *ACS Catal.* 8, 7403–7429 (2018). [10.1021/acscatal.8b01708](https://doi.org/10.1021/acscatal.8b01708).
4. Guan, Y., Chaffart, D., Liu, G., Tan, Z., Zhang, D., Wang, Y., Li, J. & Ricardez-Sandoval, L. Machine learning in solid heterogeneous catalysis: recent developments, challenges and perspectives. *Chem. Eng. Sci.* 248, 117224 (2022). [10.1016/j.ces.2021.117224](https://doi.org/10.1016/j.ces.2021.117224).
5. Esterhuizen, J. A., Goldsmith, B. R. & Linic, S. Interpretable machine learning for knowledge generation in heterogeneous catalysis. *Nat. Catal.* 5, 175–184 (2022). [10.1038/s41929-022-00744-z](https://doi.org/10.1038/s41929-022-00744-z).
6. Liao, X., Lu, R., Xia, L., Liu, Q., Wang, H., Zhao, K., Wang, Z. & Zhao, Y. Density functional theory for electrocatalysis. *Energy & Environ Materials* 5, 157–185 (2022). [10.1002/eem2.12204](https://doi.org/10.1002/eem2.12204).
7. Queiroz, V., de Almeida, D. S., de Oliveira Miglioranza, G. H., Steffani, E., Barbosa-Coutinho, E. & Schwaab, M. Analysis of commonly used batch adsorption kinetic models derived from mass transfer-based modelling. *Environ. Sci. Pollut. Res. Int.* 1, 1–15 (2022). [10.1007/s11356-021-18479-y](https://doi.org/10.1007/s11356-021-18479-y), Pubmed:[35015231](https://pubmed.ncbi.nlm.nih.gov/35015231/).
8. Burai Patrascu, M., Pottel, J., Pinus, S., Bezanson, M., Norrby, P. & Moitessier, N. From desktop to benchtop with automated computational workflows for computer-aided design in asymmetric catalysis. *Nat. Catal.* 3, 574–584 (2020). [10.1038/s41929-020-0468-3](https://doi.org/10.1038/s41929-020-0468-3).
9. Xu, J., Cao, X. M. & Hu, P. Perspective on computational reaction prediction using machine learning methods in heterogeneous catalysis. *Phys. Chem.*

- Chem. Phys.* 23, 11155–11179 (2021). [10.1039/d1cp01349a](https://doi.org/10.1039/d1cp01349a),
Pubmed:[33972971](https://pubmed.ncbi.nlm.nih.gov/33972971/).
10. Pracht, P., Bohle, F. & Grimme, S. Automated exploration of the low-energy chemical space with fast quantum chemical methods. *Phys. Chem. Chem. Phys.* 22, 7169–7192 (2020). [10.1039/c9cp06869d](https://doi.org/10.1039/c9cp06869d), Pubmed:[32073075](https://pubmed.ncbi.nlm.nih.gov/32073075/).
 11. Takahashi, K., Miyazato, I., Nishimura, S. & Ohyama, J. Unveiling hidden catalysts for the oxidative coupling of methane based on combining machine learning with literature data. *ChemCatChem* 10, 3223–3228 (2018). [10.1002/cctc.201800310](https://doi.org/10.1002/cctc.201800310).
 12. Liu, X., Liu, B., Ding, J., Deng, Y., Han, X., Zhong, C. & Hu, W. Building a library for catalysts research using high-throughput approaches. *Adv. Funct. Mater.* 32, 2107862 (2022). [10.1002/adfm.202107862](https://doi.org/10.1002/adfm.202107862).
 13. Wu, D., Kusada, K., Nanba, Y., Koyama, M., Yamamoto, T., Toriyama, T., Matsumura, S., Seo, O., Gueye, I., Kim, J., Rosantha Kumara, L. S., Sakata, O., Kawaguchi, S., Kubota, Y. & Kitagawa, H. Noble-metal high-entropy-alloy nanoparticles: atomic-level insight into the electronic structure. *J. Am. Chem. Soc.* 144, 3365–3369 (2022). [10.1021/jacs.1c13616](https://doi.org/10.1021/jacs.1c13616), Pubmed:[35166532](https://pubmed.ncbi.nlm.nih.gov/35166532/).
 14. Nørskov, J. K., Bligaard, T., Rossmeisl, J. & Christensen, C. H. Towards the computational design of solid catalysts. *Nat. Chem.* 1, 37–46 (2009). [10.1038/nchem.121](https://doi.org/10.1038/nchem.121), Pubmed:[21378799](https://pubmed.ncbi.nlm.nih.gov/21378799/).
 15. Dell'Angelo, D. Computational chemistry and the study and design of catalysts. in *Green Chemistry and Computational Chemistry* (ed. Mammino, L.) 299–332 (Elsevier, 2022).
 16. Winther, K. T., Hoffmann, M. J., Boes, J. R., Mamun, O., Bajdich, M. & Bligaard, T. Catalysis-Hub.org, an open electronic structure database for surface reactions. *Sci. Data* 6, 75 (2019). [10.1038/s41597-019-0081-y](https://doi.org/10.1038/s41597-019-0081-y), Pubmed:[31138816](https://pubmed.ncbi.nlm.nih.gov/31138816/).
 17. Studt, F. Grand challenges in computational catalysis. *Front. Catal.* 1, 658965 (2021). [10.3389/fctls.2021.658965](https://doi.org/10.3389/fctls.2021.658965).
 18. Morales-García, Á., Viñes, F., Gomes, J. R. B. & Illas, F. Concepts, models, and methods in computational heterogeneous catalysis illustrated through CO₂ conversion. *WIREs Comput. Mol. Sci.* 11, e1530 (2021). [10.1002/wcms.1530](https://doi.org/10.1002/wcms.1530).
 19. Hook, D. W., Porter, S. J. & Herzog, C. Dimensions: building context for search and evaluation. *Front. Res. Metr. Anal.* 3, 23 (2018). [10.3389/frma.2018.00023](https://doi.org/10.3389/frma.2018.00023).
 20. Writer, B. *Lithium-Ion Batteries* (Springer International Publishing, 2019).
 21. Yang, W., Fidelis, T. T. & Sun, W. H. Machine learning in catalysis, from proposal to practicing. *ACS Omega* 5, 83–88 (2020). [10.1021/acsomega.9b03673](https://doi.org/10.1021/acsomega.9b03673), Pubmed:[31956754](https://pubmed.ncbi.nlm.nih.gov/31956754/).
 22. Rivera Rocabado, D. S., Ishimoto, T. & Koyama, M. The effect of SnO₂(110) supports on the geometrical and electronic properties of platinum nanoparticles. *SN Appl. Sci.* 1, 1–15 (2019).
 23. Lykhach, Y., Kozlov, S. M., Skála, T., Tovt, A., Stetsovych, V., Tsud, N., Dvořák, F., Johánek, V., Neitzel, A., Mysliveček, J., Fabris, S., Matolín, V., Neyman, K.

- M. & Libuda, J. Counting electrons on supported nanoparticles. *Nat. Mater.* 15, 284–288 (2016). [10.1038/nmat4500](https://doi.org/10.1038/nmat4500), Pubmed:[26657332](https://pubmed.ncbi.nlm.nih.gov/26657332/).
24. Arevalo, R. L., Aspera, S. M., Escaño, M. C. S., Nakanishi, H. & Kasai, H. Tuning methane decomposition on stepped Ni surface: the role of subsurface atoms in catalyst design. *Sci. Rep.* 7, 1–8 (2017).
 25. Nguyen, T. Q., Escaño, M. C. S., Nakanishi, H., Kasai, H., Maekawa, H., Osumi, K. & Sato, K. DFT+U study on the oxygen adsorption and dissociation on CeO₂-supported platinum cluster. *Appl. Surf. Sci.* 288, 244–250 (2014). [10.1016/j.apsusc.2013.10.015](https://doi.org/10.1016/j.apsusc.2013.10.015).
 26. Xie, C., Yan, D., Li, H., Du, S., Chen, W., Wang, Y., Zou, Y., Chen, R. & Wang, S. Defect chemistry in heterogeneous catalysis: recognition, understanding, and utilization. *ACS Catal.* 10, 11082–11098 (2020). [10.1021/acscatal.0c03034](https://doi.org/10.1021/acscatal.0c03034).
 27. Chen, L. & Xu, Q. Fewer defects, better catalysis? *Science* 367, 737 (2020). [10.1126/science.aba6435](https://doi.org/10.1126/science.aba6435), Pubmed:[32054745](https://pubmed.ncbi.nlm.nih.gov/32054745/).
 28. Dean, J., Taylor, M. G. & Mpourmpakis, G. Unfolding adsorption on metal nanoparticles: connecting stability with catalysis. *Sci. Adv.* 5, eaax5101 (2019). [10.1126/sciadv.aax5101](https://doi.org/10.1126/sciadv.aax5101), Pubmed:[31548989](https://pubmed.ncbi.nlm.nih.gov/31548989/).
 29. Tauster, S. J. Strong metal-support interactions. *Acc. Chem. Res.* 20, 389–394 (1987). [10.1021/ar00143a001](https://doi.org/10.1021/ar00143a001).
 30. Zhang, Y., Yan, W., Qi, H., Su, X., Su, Y., Liu, X., Li, L., Yang, X., Huang, Y. & Zhang, T. Strong metal–support interaction of Ru on TiO₂ derived from the co-reduction mechanism of Ru_xTi_{1-x}O₂ interphase. *ACS Catal.* 12, 1697–1705 (2022). [10.1021/acscatal.1c04785](https://doi.org/10.1021/acscatal.1c04785).
 31. Wu, C., Cheng, D., Wang, M. & Ma, D. Understanding and application of strong metal–support interactions in conversion of CO₂ to methanol: a review. *Energy Fuels* 35, 19012–19023 (2021). [10.1021/acs.energyfuels.1c02440](https://doi.org/10.1021/acs.energyfuels.1c02440).
 32. Zhang, N., Zhang, X., Tao, L., Jiang, P., Ye, C., Lin, R., Huang, Z., Li, A., Pang, D., Yan, H., Wang, Y., Xu, P., An, S., Zhang, Q., Liu, L., Du, S., Han, X., Wang, D. & Li, Y. Silver single-atom catalyst for efficient electrochemical CO₂ reduction synthesized from thermal transformation and surface reconstruction. *Angew. Chem. Int Ed Engl* 60, 6170–6176 (2021). [10.1002/anie.202014718](https://doi.org/10.1002/anie.202014718), Pubmed:[33274797](https://pubmed.ncbi.nlm.nih.gov/33274797/).
 33. Trunschke, A., Bellini, G., Boniface, M., Carey, S. J., Dong, J., Erdem, E., Foppa, L., Frandsen, W., Geske, M., Ghiringhelli, L. M., Girgsdies, F., Hanna, R., Hashagen, M., Hävecker, M., Huff, G., Knop-Gericke, A., Koch, G., Kraus, P., Kröhnert, J., Kube, P., Lohr, S., Lunkenbein, T., Masliuk, L., Naumann d'Alnoncourt, R., Omojola, T., Pratsch, C., Richter, S., Rohner, C., Rosowski, F., Rüter, F., Scheffler, M., Schlögl, R., Tarasov, A., Teschner, D., Timpe, O., Trunschke, P., Wang, Y. & Wrabetz, S. Towards experimental handbooks in catalysis. *Top. Catal.* 63, 1683–1699 (2020). [10.1007/s11244-020-01380-2](https://doi.org/10.1007/s11244-020-01380-2).
 34. Zhao, Z. J., Li, Z., Cui, Y., Zhu, H., Schneider, W. F., Delgass, W. N., Ribeiro, F. & Greeley, J. Importance of metal-oxide interfaces in heterogeneous catalysis: A combined DFT, microkinetic, and experimental study of water-gas shift on Au/MgO. *J. Catal.* 345, 157–169 (2017). [10.1016/j.jcat.2016.11.008](https://doi.org/10.1016/j.jcat.2016.11.008).

35. Van Duin, A. C. T., Dasgupta, S., Lorant, F. & Goddard, W. A. ReaxFF: a reactive force field for hydrocarbons. *J. Phys. Chem. A* 105, 9396–9409 (2001). [10.1021/jp004368u](https://doi.org/10.1021/jp004368u).
36. Wang, Y., Shi, Y., Sun, Q., Lu, K., Kubo, M. & Xu, J. Development of a transferable ReaxFF parameter set for carbon- and silicon-based solid systems. *J. Phys. Chem. C* 124, 10007–10015 (2020). [10.1021/acs.jpcc.0c01645](https://doi.org/10.1021/acs.jpcc.0c01645).
37. Larentzos, J. P. & Rice, B. M. Transferable reactive force fields: extensions of ReaxFF-Ig to nitromethane. *J. Phys. Chem. A* 121, 2001–2013 (2017). [10.1021/acs.jpca.6b11761](https://doi.org/10.1021/acs.jpca.6b11761), Pubmed:[28177629](https://pubmed.ncbi.nlm.nih.gov/28177629/).
38. Liu, S. S., Saha, L.C., Iskandarov, A., Ishimoto, T., Yamamoto, T., Umeno, Y., Matsumura, S. & Koyama, M. Atomic structure observations and reaction dynamics simulations on triple phase boundaries in solid-oxide fuel cells. *Commun. Chem.* 2, 1–9 (2019).
39. Schmidt, J., Marques, M. R. G., Botti, S. & Marques, M. A. L. Recent advances and applications of machine learning in solid-state materials science. *npj Comput. Mater.* 5, 1–36 (2019).
40. Hodapp, M. & Shapeev, A. Machine-learning potentials enable predictive and tractable high-throughput screening of random alloys. *Phys. Rev. Mater.* 5, 113802 (2021). [10.1103/PhysRevMaterials.5.113802](https://doi.org/10.1103/PhysRevMaterials.5.113802).
41. Aghajamali, A. & Karton, A. Superior performance of the machine-learning GAP force field for fullerene structures. *Struct. Chem.* 33, 505–510 (2022). [10.1007/s11224-021-01864-1](https://doi.org/10.1007/s11224-021-01864-1).
42. Zubatyuk, R., Smith, J. S., Leszczynski, J. & Isayev, O. Accurate and transferable multitask prediction of chemical properties with an atoms-in-molecules neural network. *Sci. Adv.* 5, eaav6490 (2019). [10.1126/sciadv.aav6490](https://doi.org/10.1126/sciadv.aav6490), Pubmed:[31448325](https://pubmed.ncbi.nlm.nih.gov/31448325/).
43. Chanussot, L., Das, A., Goyal, S., Lavril, T., Shuaibi, M., Riviere, M., Tran, K., Heras-Domingo, J., Ho, C., Hu, W., Palizhati, A., Sriram, A., Wood, B., Yoon, J., Parikh, D., Zitnick, C. L. & Ulissi, Z. Open Catalyst 2020 (OC20) dataset and community challenges. *ACS Catal.* 11, 6059–6072 (2021). [10.1021/acscatal.0c04525](https://doi.org/10.1021/acscatal.0c04525).
44. Chen, C. & Ong, S. P. A universal graph deep learning interatomic potential for the periodic table. <https://arxiv.org/pdf/2202.02450>, (2022).
45. Takamoto, S., Shinagawa, C., Motoki, D., Nakago, K., Li, W., Kurata, I., Watanabe, T., Yayama, Y., Iriguchi, H., Asano, Y., Onodera, T., Ishii, T., Kudo, T., Ono, H., Sawada, R., Ishitani, R., Ong, M., Yamaguchi, T., Kataoka, T., Hayashi, A., Charoenphakdee, N. & Ibuka, T. Towards universal neural network potential for material discovery applicable to arbitrary combination of 45 elements. *Nat. Commun.* 13, 2991 (2022). [10.1038/s41467-022-30687-9](https://doi.org/10.1038/s41467-022-30687-9), Pubmed:[35637178](https://pubmed.ncbi.nlm.nih.gov/35637178/).
46. Ogura, Y., Sato, K., Miyahara, S. I., Kawano, Y., Toriyama, T., Yamamoto, T., Matsumura, S., Hosokawa, S. & Nagaoka, K. Efficient ammonia synthesis over a Ru/La_{0.5}Ce_{0.5}O_{1.75} catalyst pre-reduced at high temperature. *Chem. Sci.* 9, 2230–2237 (2018). [10.1039/c7sc05343f](https://doi.org/10.1039/c7sc05343f), Pubmed:[29719696](https://pubmed.ncbi.nlm.nih.gov/29719696/).

47. Campbell, C. T. Electronic perturbations. *Nat. Chem.* 4, 597–598 (2012). [10.1038/nchem.1412](https://doi.org/10.1038/nchem.1412), Pubmed:[22824888](https://pubmed.ncbi.nlm.nih.gov/22824888/).
48. Shi, Y., Ma, Z. R., Xiao, Y. Y., Yin, Y. C., Huang, W. M., Huang, Z. C., Zheng, Y. Z., Mu, F. Y., Huang, R., Shi, G. Y., Sun, Y. Y., Xia, X. H. & Chen, W. Electronic metal–support interaction modulates single-atom platinum catalysis for hydrogen evolution reaction. *Nat. Commun.* 12, 3021 (2021). [10.1038/s41467-021-23306-6](https://doi.org/10.1038/s41467-021-23306-6), Pubmed:[34021141](https://pubmed.ncbi.nlm.nih.gov/34021141/).
49. Rivera Rocabado, D. S., Noguchi, T. G., Hayashi, S., Maeda, N., Yamauchi, M. & Ishimoto, T. Adsorption states of N₂/H₂ activated on Ru nanoparticles uncovered by modulation-excitation infrared spectroscopy and density functional theory calculations. *ACS Nano* 15, 20079–20086 (2021). [10.1021/acsnano.1c07825](https://doi.org/10.1021/acsnano.1c07825), Pubmed:[34860010](https://pubmed.ncbi.nlm.nih.gov/34860010/).
50. Dooling, D. J. & Broadbelt, L. J. Investigation of the structure sensitivity of nitrogen adsorption on single crystal ruthenium clusters using density functional theory. *Stud. Surf. Sci. Catal.* 109, 251–259 (1997). [10.1016/S0167-2991\(97\)80412-0](https://doi.org/10.1016/S0167-2991(97)80412-0).
51. Schelling, P. K., Phillpot, S. R. & Wolf, D. Mechanism of the cubic-to-tetragonal phase transition in zirconia and yttria-stabilized zirconia by molecular-dynamics simulation. *J. Am. Ceram. Soc.* 84, 1609–1619 (2001). [10.1111/j.1151-2916.2001.tb00885.x](https://doi.org/10.1111/j.1151-2916.2001.tb00885.x).
52. Cowley, J. M. An approximate theory of order in alloys. *Phys. Rev.* 77, 669–675 (1950). [10.1103/PhysRev.77.669](https://doi.org/10.1103/PhysRev.77.669).
53. Jain, A., Ong, S. P., Hautier, G., Chen, W., Richards, W. D., Dacek, S., Cholia, S., Gunter, D., Skinner, D., Ceder, G. & Persson, K. A. Commentary: the Materials Project: a materials genome approach to accelerating materials innovation. *APL Mater.* 1, 011002 (2013). [10.1063/1.4812323](https://doi.org/10.1063/1.4812323).
54. Hjorth Larsen, A., Jørgen Mortensen, J., Blomqvist, J., Castelli, I. E., Christensen, R., Dułak, M., Friis, J., Groves, M. N., Hammer, B., Hargus, C., Hermes, E. D., Jennings, P. C., Bjerre Jensen, P., Kermode, J., Kitchin, J. R., Leonhard Kolsbjerg, E., Kubal, J., Kaasbjerg, K., Lysgaard, S., Bergmann Maronsson, J., Maxson, T., Olsen, T., Pastewka, L., Peterson, A., Rostgaard, C., Schiøtz, J., Schütt, O., Strange, M., Thygesen, K. S., Vegge, T., Vilhelmsen, L., Walter, M., Zeng, Z. & Jacobsen, K. W. The atomic simulation environment – A Python library for working with atoms. *J. Phys. Condens. Matter* 29, 273002 (2017). [10.1088/1361-648X/aa680e](https://doi.org/10.1088/1361-648X/aa680e), Pubmed:[28323250](https://pubmed.ncbi.nlm.nih.gov/28323250/).
55. Bitzek, E., Koskinen, P., Gähler, F., Moseler, M. & Gumbusch, P. Structural relaxation made simple. *Phys. Rev. Lett.* 97, 170201 (2006). [10.1103/PhysRevLett.97.170201](https://doi.org/10.1103/PhysRevLett.97.170201), Pubmed:[17155444](https://pubmed.ncbi.nlm.nih.gov/17155444/).
56. Nosé, S. A unified formulation of the constant temperature molecular dynamics methods. *J. Chem. Phys.* 81, 511–519 (1984). [10.1063/1.447334](https://doi.org/10.1063/1.447334).
57. Vandermause, J., Torrisi, S. B., Batzner, S., Xie, Y., Sun, L., Kolpak, A. M. & Kozinsky, B. On-the-fly active learning of interpretable bayesian force fields for atomistic rare events. *npj Comput. Mater.* 6, 1–11 (2020).
58. Moustafa, S. G., Schultz, A. J. & Kofke, D. A. Effects of thermostatting in molecular dynamics on anharmonic properties of crystals: application to fcc Al at

- high pressure and temperature. *J. Chem. Phys.* 149, 124109 (2018). [10.1063/1.5043614](https://doi.org/10.1063/1.5043614), Pubmed:[30278666](https://pubmed.ncbi.nlm.nih.gov/30278666/).
59. Henkelman, G. & Jónsson, H. A dimer method for finding saddle points on high dimensional potential surfaces using only first derivatives. *J. Chem. Phys.* 111, 7010–7022 (1999). [10.1063/1.480097](https://doi.org/10.1063/1.480097).
 60. Sheppard, D., Xiao, P., Chemelewski, W., Johnson, D. D. & Henkelman, G. A generalized solid-state nudged elastic band method. *J. Chem. Phys.* 136, 074103 (2012). [10.1063/1.3684549](https://doi.org/10.1063/1.3684549), Pubmed:[22360232](https://pubmed.ncbi.nlm.nih.gov/22360232/).
 61. Henkelman, G., Uberuaga, B. P. & Jónsson, H. A climbing image nudged elastic band method for finding saddle points and minimum energy paths. *J. Chem. Phys.* 113, 9901–9904 (2000). [10.1063/1.1329672](https://doi.org/10.1063/1.1329672).
 62. Atkins, P. W., de Paula, J. & Keeler, J. *Atkins' Physical Chemistry*. 11th ed (Oxford Univ., 2017).
 63. Lipson, A., Lipson, S. G. & Lipson, H. *Optical Physics* (Cambridge Univ., 2010).
 64. Stukowski, A. Visualization and analysis of atomistic simulation data with OVITO—the Open Visualization Tool. *Modell. Simul. Mater. Sci. Eng.* 18, 015012 (2010). [10.1088/0965-0393/18/1/015012](https://doi.org/10.1088/0965-0393/18/1/015012).

Acknowledgments

This work was supported by the Alexander von Humboldt Stiftung and by JSPS KAKENHI Grant Numbers JP21F30701 and JP20H05623. The authors are especially grateful to the participants of the Data-Driven AI Laboratory of the Research Initiative for Supra Materials at Shinshu University for their comments and suggestions during the whole project. All images of the atomic models within the article were rendered using OVITO.⁶⁴

Author contributions

M.K., K.N., and K.S. proposed and supervised the project. G.V.H. wrote the article, performed the modelling work, designed the numerical framework, and conducted the calculations and evaluation based on the universal neural network potential. K.H. contributed to the statistical evaluation of the data. All authors contributed to the discussion of the results and article preparation.

Competing interests

The authors declare no competing interests.

Supplementary Information

Cyber Catalysis: N₂ Dissociation over Ruthenium Catalyst with Strong Metal-Support Interaction

Gerardo Valadez Huerta^{*,1}, Kaoru Hisama¹, Katsutoshi Sato², Katsutoshi Nagaoka², Michihisa Koyama^{*,1,3}

¹Research Initiative for Supra Materials, Shinshu University, Nagano 380-8553, Japan. ²Department of Chemical Systems Engineering, Nagoya University, Nagoya 464-8601, Japan. ³Open Innovation Institute, Kyoto University, Kyoto 606-8501, Japan

*Correspondence to: valadez@shinshu-u.ac.jp, koyama_michihisa@shinshu-u.ac.jp

Table of Contents

Supplementary Notes	2
Supplementary Note 1. Catalyst Model Preparation.....	2
Supplementary Note 2. Simulated Spectra for Each Configuration.....	3
Supplementary Note 3. Similarity Analysis of the Simulated and Measured Spectra	3
Supplementary Note 4. Structural Analysis of Adsorption States	4
Supplementary Methods	5
1. Energetic Analysis of the Ru ₁₄₃ Half-Nanoparticle Orientation on the Support	5
2. Validation of the UNNP to Describe the Ru Nanoparticle, La _{0.5} Ce _{0.5} O _{1.75} Slab, and N ₂ Adsorption on Ru Slabs	5
Supplementary Figures	6
Supplementary Tables.....	10
Supplementary References	11

Supplementary Notes

Supplementary Note 1. Catalyst Model Preparation

Depictions of different views of all 25 initial configurations of the catalyst with a solid solution (SS) cationic surface, their optimised structures, and the resulting charge distribution can be found in the 'Supplementary Data' file (directory paths: Figures/Catalyst/Initial; Figures/Catalyst/Initial/Optimization). The depictions of other configurations may be obtained from the authors upon reasonable request. The optimised Ru₂₃₈ HCP nanoparticle structure and frames for the configuration labelled 165-La-1-1-xO25-1Cat75 are given in Supplementary Fig. 6. The directories containing the figures are labelled in the following manner. The number '165' refers to the rotational angle β of the nanoparticle relative to the optimised structure and is followed by the cationic surface composition of the support (here, 'La'). The first number in '1-1' refers to the configuration number, and the second refers to the number of reduced cationic layers. 'xO25' refers to the percentage of oxygen remaining in the layers after reduction (e.g. '25' corresponds to a 75% reduction in oxygen). The numbers '1' and '75' in '1Cat75' refer to the number of nanoparticle layers wrapped by cations and percentage of occupied Ru atoms at the lowest nanoparticle layer, respectively. All values are relative to the initial configuration.

Next, we provide an explanation of the catalyst configuration map in Fig. 1d in the article. A non-reduced surface results in a slab composition of La_{0.5}Ce_{0.5}O_{1.75} with Ce⁴⁺ and La³⁺ cations. Using our method, we can prepare slabs with a composition of La_{0.5}Ce_{0.5}O_{1.5} (or slightly lower oxygen concentrations) with Ce³⁺ and La³⁺ cations. Beyond these limits, further reduction of the cationic layers in the slab may not have any practical significance.

Supplementary Note 2. Simulated Spectra for Each Configuration

The dipole moment is not calculated by the UNNP version used in the article and, thus, it is not considered by the wavenumber calculation. We repeated the calculations for the wavenumber spectra by accounting for the ^{15}N isotope. Thus, we adjusted the N mass to 15 u and compared the results with the experimental data. The spectra depicted in Supplementary Fig. 7 correspond to that shown in Fig. 3a in the article. We can reproduce the red-shift of the peaks of ^{14}N relative to the peaks of ^{15}N by a factor of $(m(^{14}\text{N})/m(^{15}\text{N}))^{1/2}$ as physically expected and experimentally confirmed. All spectra are provided in the ‘Supplementary Data’ file (directory paths: ^{14}N : Figures/Catalytic/m14; ^{15}N : Figures/Catalytic/m15). The values of x , $\bar{q}_{\text{Ru},0}$, and \bar{q}_{N_2} are summarised in the ‘FreqHist_Legende_T25C-p6kPa.xlsx’ file within each directory.

Supplementary Note 3. Similarity Analysis of the Simulated and Measured Spectra

We first show that the simulated and measured curves are statistically comparable. We conducted a Kolmogorov–Smirnov (KS) test for the two-sided null hypothesis H_{01} : ρ_i is similar to ρ_{Exp} vs. H_{11} : ρ_i is not similar to ρ_{Exp} , where ρ_i and ρ_{Exp} are the calculated and measured vibrational frequency distributions, respectively (Fig. 3b in the article), at a significance level of $\alpha = 0.05$. We calculated the wavenumber distributions using the D value, which is given by:

$$D_i = \max |F_i(x) - F_{\text{Exp}}(x)|,$$

where $F(x)$ is the normalised cumulative distribution function. We calculated $F(x)$ by numerically integrating ρ_i and ρ_{Exp} using the trapezoidal method. The hypothesis cannot be rejected when the values are lower than the critical value

$$D_{\text{crit}} \approx \sqrt{\frac{-0.5 \cdot \ln\left(\frac{\alpha}{2}\right)}{n}} = 0.1537,$$

with $n = 78$ as the number of calculated adsorption states. We found 87 and 59 distributions that were comparable with the IR spectra obtained for a catalyst reduced at 500 and 650 °C, respectively, for which the hypothesis cannot be rejected.

After statistically confirming the similarity between the spectra, we searched for a suitable similarity factor. Recent literature¹ indicates that the Pearson correlation coefficient

$$S_{\text{PCC},i} = \frac{\sum_{j=1}^n (\rho(\tilde{\nu}_{\text{N}_2,j}) - \bar{\rho}_i) \cdot (\rho_{\text{Exp}}(x_j) - \bar{\rho}_{\text{Exp}})}{\sum_{j=1}^n (\rho(\tilde{\nu}_{\text{N}_2,j}) - \bar{\rho}_i)^2 \sum_{j=1}^n (\rho_{\text{Exp}}(x_j) - \bar{\rho}_{\text{Exp}})^2}$$

is the most suitable similarity factor for comparing the experimental and computed IR spectra. Scores of 0.684 or higher are considered to reflect high similarity. Note that a score of 1 is only given for an equal distribution. We first conducted a cross-check between the two experimental spectra depicted in Fig. 3b in the article and obtained a similarity factor of 0.98. Therefore, S_{PCC} is not a suitable similarity factor for comparing spectra in our study because this factor suggests that both experimental distributions are almost the same. Moreover, we did not observe any trend between the simulated distributions with high S_{PCC} factors and the experimental IR spectra, particularly in terms of wavenumber peaks. These observations agree with the literature¹, which states that established distance-based methods, such as the PCC, only weakly reflect any translation in the functions. Therefore, they may not be applicable for our case, where the distributions show a large broadening and relatively small differences between peaks. In addition, if we use a more traditional method of

comparing and matching peaks¹, the limited number of adsorption sites may result in a distribution with different peaks but similar intensities (see Supplementary Fig. 8a) owing to the size of the catalyst model. Thus, simply comparing and matching peaks is insufficient. To overcome this problem, we divided each of the experimental spectra (depicted in Fig. 3b in the article) into two distributions A, ranging from 1600 to 2000 cm⁻¹, and B, ranging from 2000 to 2400 cm⁻¹. Considering the baselines, we calculated the k -th percentiles $P(k_{\text{Exp}}^{\text{A,lo}}) = \tilde{\nu}_{\text{N}_2, \text{Exp}}^{\text{lo}}$ and $P(k_{\text{Exp}}^{\text{B,hi}}) = \tilde{\nu}_{\text{N}_2, \text{Exp}}^{\text{hi}}$ corresponding to the peaks (see Supplementary Table 2). Next, we calculated the percentiles $\tilde{\nu}_{\text{N}_2}(k_{\text{Exp}}^{\text{A,lo}})$ and $\tilde{\nu}_{\text{N}_2}(k_{\text{Exp}}^{\text{B,hi}})$ for the simulated distributions and performed the comparison. Finally, we calculated the root-mean-square deviation and combined this result with the D value obtained from the KS test to evaluate the similarity of the shapes of the distributions:

$$S = \left[\left(1 + \sqrt{\frac{|\tilde{\nu}_{\text{N}_2}(k_{\text{Exp}}^{\text{A,lo}}) - \tilde{\nu}_{\text{N}_2, \text{Exp}}^{\text{lo}}|^2 + |\tilde{\nu}_{\text{N}_2}(k_{\text{Exp}}^{\text{B,hi}}) - \tilde{\nu}_{\text{N}_2, \text{Exp}}^{\text{hi}}|^2}{2}} \right) \cdot D \right]^{-1}.$$

The higher the S , the higher the degree of similarity between the compared spectra. We cross-checked our results by comparing the experimental curves with each other and obtained a low S of 0.19. The calculated distributions considered similar in the article showed S values higher than 1.1, which means the so-defined similarity factor allows us to not only differentiate both experimental distributions but also find distributions with high similarity to each of the IR spectra considered. The wavenumber distribution with the highest similarity to the experimental IR spectrum of the catalyst reduced at 500 °C is depicted in Supplementary Fig. 8b. All results on the simulated distributions can be found in the 'FreqHist_T25C_p6kPa.xlsx' file within the 'Doc' directory of the 'Supplementary Data' file.

Supplementary Note 4. Structural Analysis of Adsorption States

To analyse the structures of the adsorption states (Fig. 3d in the article), we first searched for variables to determine the local structure of the adsorption state. We used the centre of mass of the N₂ molecule, defined a cut-off radius, and counted the number of cations $N_{\text{Ce/La}}$ and oxygen atoms N_{O} for the adsorption states given in Fig. 3d. The results for different cut-off radii are summarised in Supplementary Table 3.

Using a cut-off radius of 5 Å or higher, we found the following conditions to count the number of adsorption states in each configuration:

$$\begin{aligned} \text{A: } & \tilde{\nu}_{\text{N}_2} \geq 2100 \text{ cm}^{-1}, N_{\text{Ce/La}} = N_{\text{O}} = 0, \\ \text{C: } & 2100 \text{ cm}^{-1} \geq \tilde{\nu}_{\text{N}_2} \geq 2000 \text{ cm}^{-1}, N_{\text{Ce/La}} > 0, N_{\text{O}} > 0, \\ \text{G, H: } & \tilde{\nu}_{\text{N}_2} \leq 2000 \text{ cm}^{-1}, N_{\text{Ce/La}} > 0, N_{\text{O}} = 0, \\ \text{F, I: } & \tilde{\nu}_{\text{N}_2} \leq 2000 \text{ cm}^{-1}, N_{\text{Ce/La}} \geq N_{\text{O}}, N_{\text{O}} > 0. \end{aligned}$$

Supplementary Methods

1. Energetic Analysis of the Ru₁₄₃ Half-Nanoparticle Orientation on the Support

The nanoparticle is rotated by an angle of $\beta = 165^\circ$ for the 200 models used in the study. The calculated values of the interfacial energy $\varepsilon_{\text{inter}}$ between the nanoparticle and support for 20 catalyst models and 5 nanoparticle orientations are summarised in Supplementary Table 4. The chosen angle range was sufficiently wide to achieve accurate analysis owing to the symmetry of the support. The interfacial energy was calculated as follows:

$$\varepsilon_{\text{inter}} = \varepsilon_{\text{Ru}_{238}\text{-La}_{0.5}\text{Ce}_{0.5}\text{O}_{1.75}} - \frac{N_{\text{Ru}_{143}}}{N_{\text{Ru}_{238}}} \varepsilon_{\text{Ru}_{238}} - \varepsilon_{\text{La}_{0.5}\text{Ce}_{0.5}\text{O}_{1.75}},$$

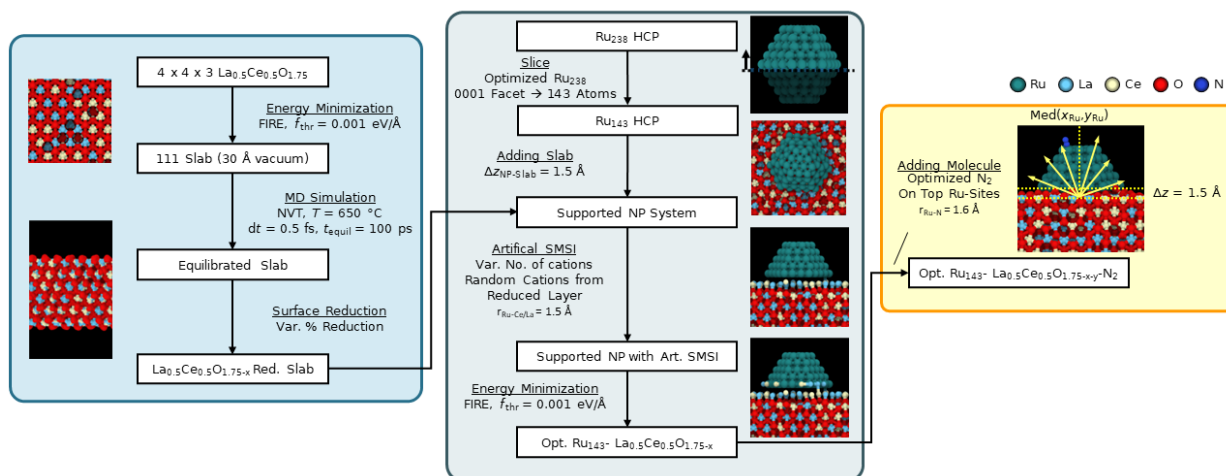
where $\varepsilon_{\text{Ru}_{238}\text{-La}_{0.5}\text{Ce}_{0.5}\text{O}_{1.75}}$ is the potential energy of the optimised catalyst structure with a non-reduced support, N is the number of atoms for the (half) Ru nanoparticle, and $\varepsilon_{\text{La}_{0.5}\text{Ce}_{0.5}\text{O}_{1.75}}$ is the potential energy of the non-reduced slab after the MD simulation. In general, the nanoparticle rotated by $\beta = 165^\circ$ is the most energetically favourable. The orientation for this particular case can be taken from the top view of Supplementary Fig. 6.

2. Validation of the UNNP to Describe the Ru Nanoparticle, La_{0.5}Ce_{0.5}O_{1.75} Slab, and N₂ Adsorption on Ru Slabs

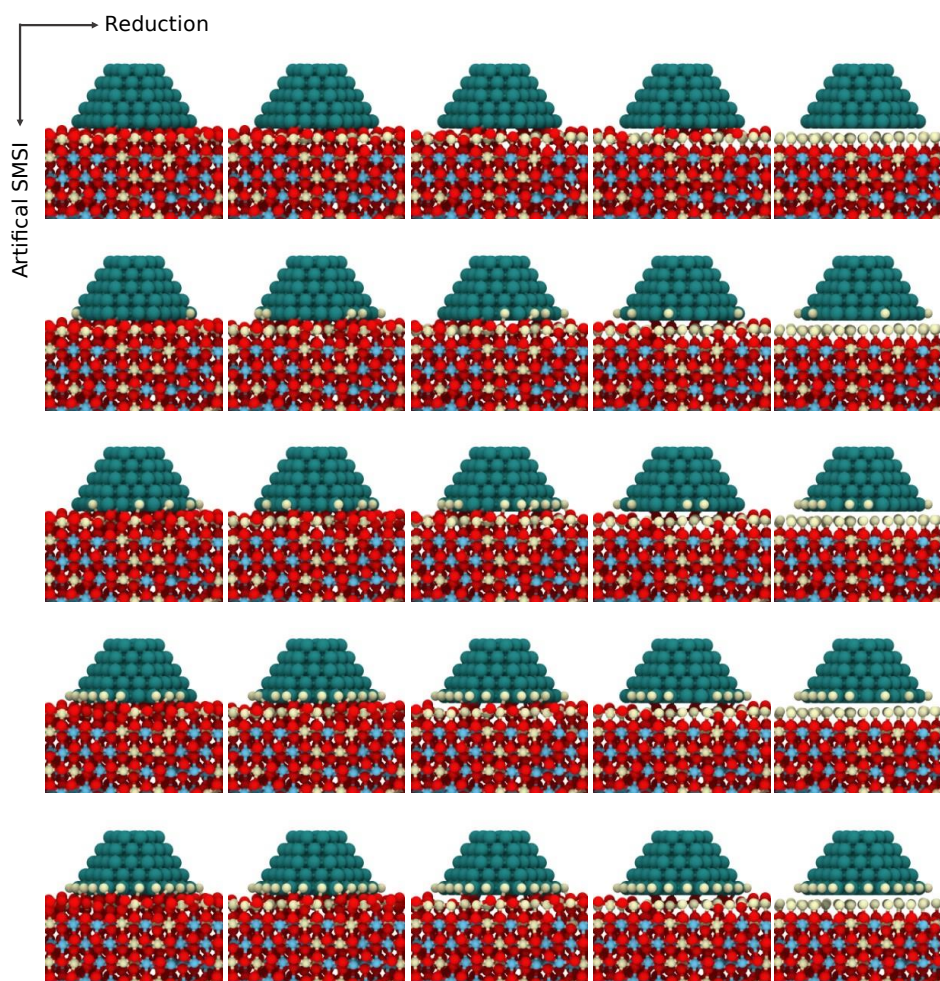
We validated the UNNP to describe Ru nanoparticles in previous work². Furthermore, we optimised the La_{0.5}Ce_{0.5}O_{1.75} configuration with the fluorite structure provided in the Materials Project Database³ using the UNNP. We calculated a lattice constant of 7.980 Å, which deviates from the DFT value of 7.939 Å by only 0.52%. The calculated bulk modulus (131 GPa) was also in good agreement with the value recorded in the Materials Project Database (130 GPa).

To validate the accuracy of the UNNP for calculating the adsorption of N₂ on Ru, we summarised all property values calculated using the UNNP, as well as DFT and experimental values obtained from previous studies, in Supplementary Table 5.

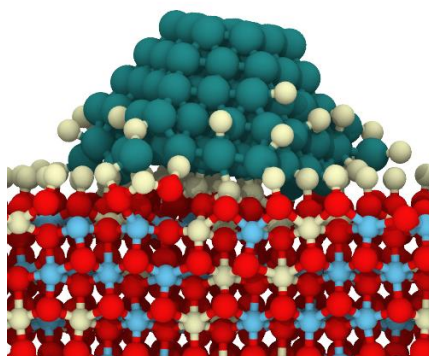
Supplementary Figures



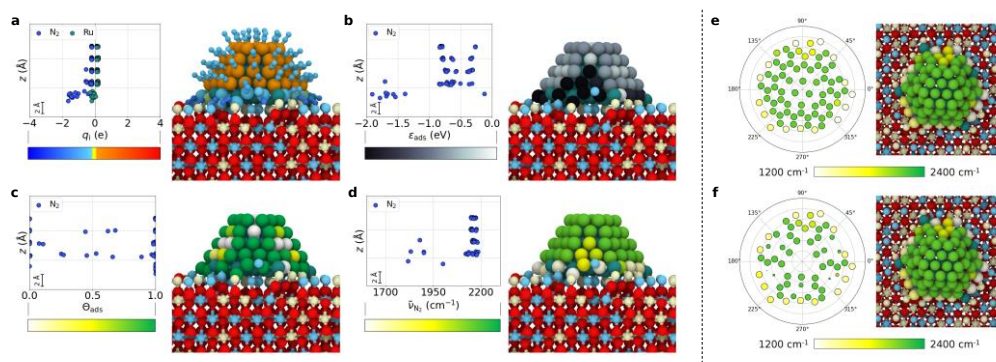
Supplementary Fig. 1 Methods applied to model the catalyst systems.



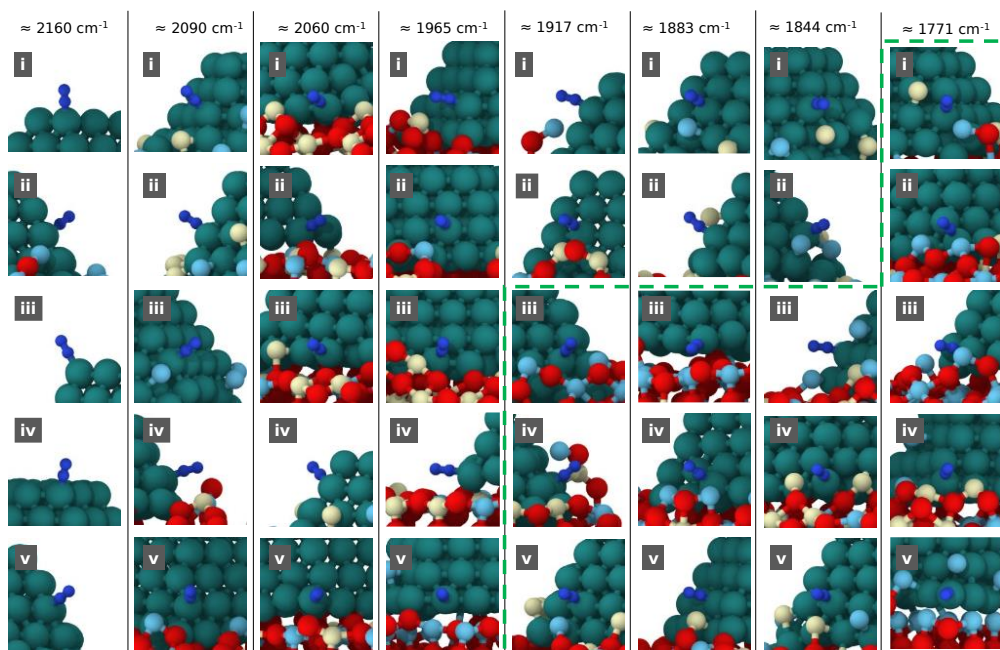
Supplementary Fig. 2. Example of 25 initial configurations obtained by varying the reduction of the Ce cationic surface and artificial SMSI. The cationic surface was reduced as follows from left to right: no removal of oxygen anions, removal of 1/4 of the oxygen anions, and so on, until the complete removal of oxygen anions on the cationic surface was achieved. The artificial SMSI follows a similar rule from top to bottom, and the number of cations attached to the lowest nanoparticle layer is varied.



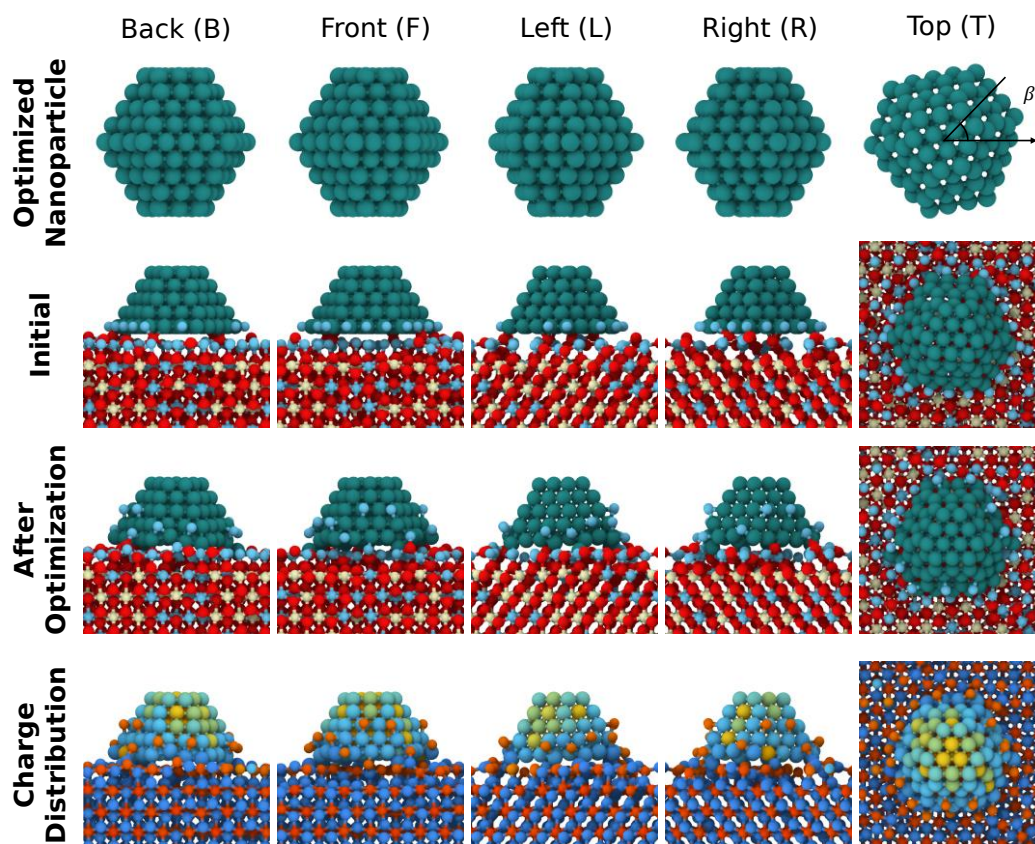
Supplementary Fig. 3. Optimised structure of the configuration with the highest SMSI and reduction degree.



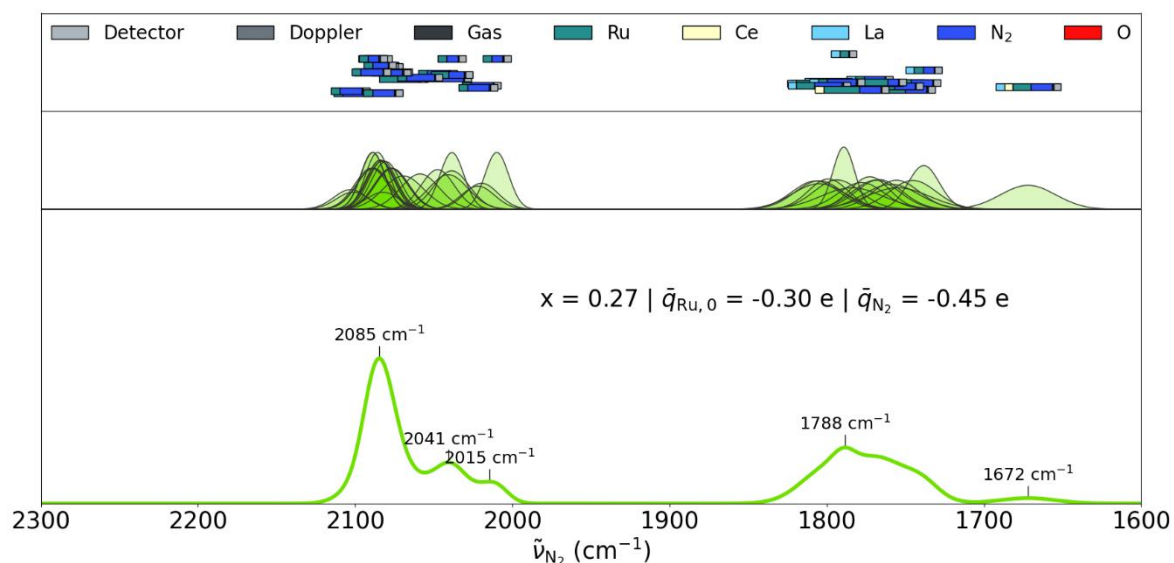
Supplementary Fig. 4. **a–d**, Spatial maps of the **(a)** charge q_i for individual adsorbed N_2 molecules and the Ru site, **(b)** adsorption energy ϵ_{ads} , **(c)** N_2 coverage θ ($T = 25^\circ\text{C}$, $p = 6\text{ kPa}$), and **(d)** wavenumber ν_{N_2} . **e, f**, **(e)** Weighted and **(f)** non-weighted spatial maps of the N_2 wavenumber in polar coordinates (weighting factor for the marker size: $\theta(T = 25^\circ\text{C}, p = 6\text{ kPa})$). The ‘Supplementary Data’ file (Directory: Figures/Adsorption) includes all figures for the 25 catalyst configurations with an SS cationic surface. Images for other configurations may be obtained from the authors upon reasonable request.



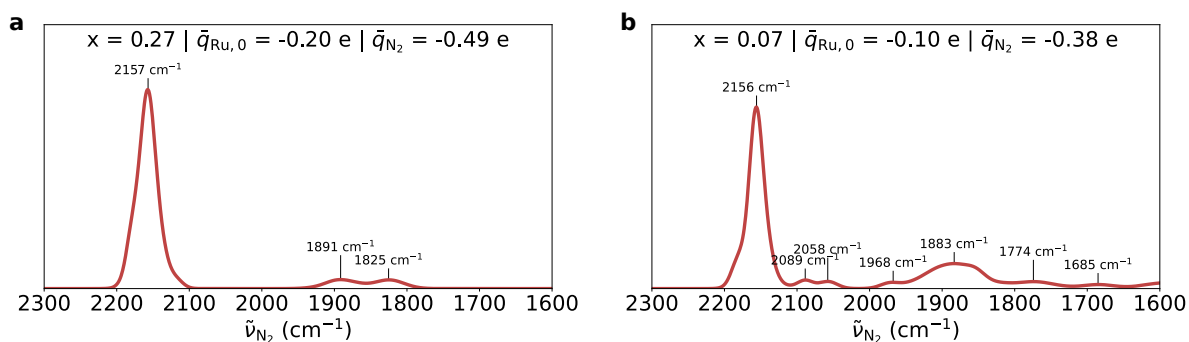
Supplementary Fig. 5. Additional adsorption states (compared with Fig. 2a in the article). Green regions mark adsorption states similar to F and I in Fig. 2 in the article that are expected to have a low activation barrier. All adsorption states have a high coverage of ≈ 1.0 at 25 °C and 6 kPa. The 'AdsorptionSites.xlsx' file in the 'Doc' directory of the 'Supplementary Data' file contains the properties of these and other adsorption states.



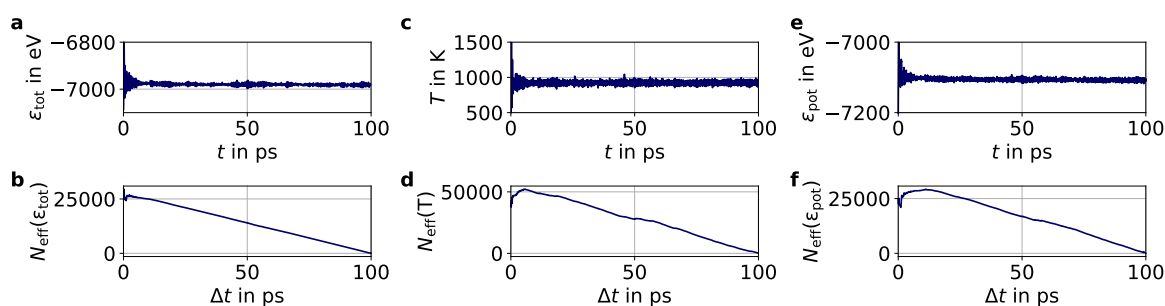
Supplementary Fig. 6 Optimised Ru_{238} HCP nanoparticle structure including the definition of the angle β and frames for the configuration labelled 165-La-1-1-xO25-1Cat75 (see Supplementary Note 1 for details).



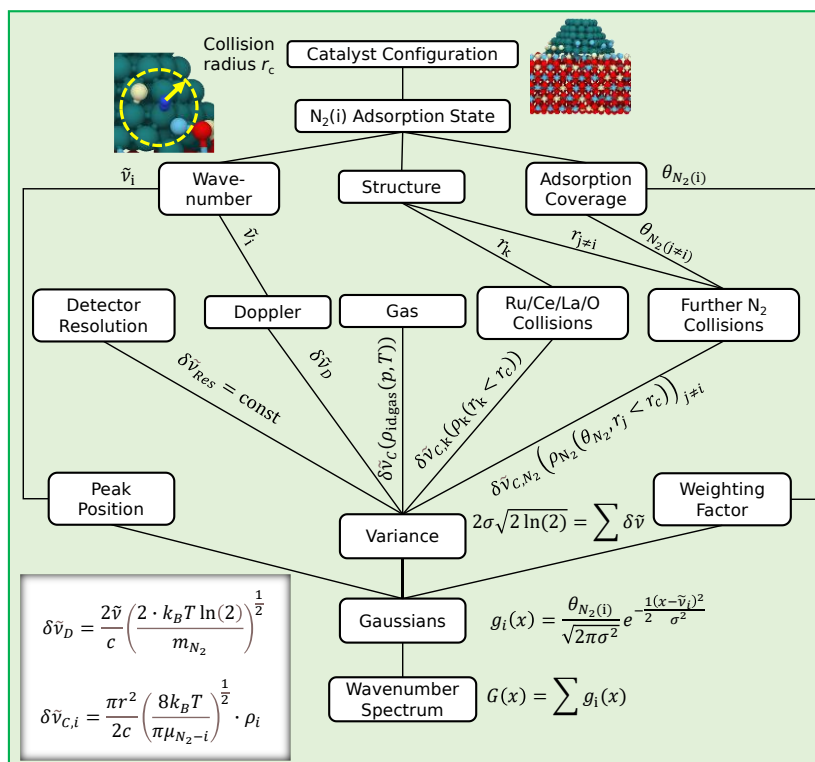
Supplementary Fig. 7 Wavenumber distribution corresponding to Fig. 3a in the article, but for a ^{15}N isotope.



Supplementary Fig. 8 a, Example wavenumber distribution for a configuration with a fully reduced SS surface and no artificial SMSI. **b**, Simulated wavenumber distribution with the highest similarity to the experimental IR spectrum of the catalyst reduced at 500 °C.



Supplementary Fig. 9 a, c, e, Changes in (a) total energy ϵ_{tot} , (c) temperature T , and (e) potential energy ϵ_{pot} over the simulation time t . **b, d, f**, Corresponding number of uncorrelated samples N_{eff} over the equilibration timespan Δt . All depictions are given as an example for a slab with a Ce surface and represent all other configurations. The system is considered to reach equilibrium over 100 ps because the number of uncorrelated samples is highest within this timespan and linearly approaches zero afterwards⁶.



Supplementary Fig. 10 Methods used to calculate the wavenumber distribution of adsorbed N₂ molecules on each catalyst configuration.

Supplementary Tables

Supplementary Table 1. Comparison of the calculated Gibbs energy barriers for the dissociation of a N₂ molecule on a Ru slab (on-top) toward two hollow sites (2N) using the UNNP and DFT values. The Gibbs energy is defined as $\Delta G = G(\text{TS}) - G(\text{N}_2)$, similar to the definition in Fig. 3d in the article. The DFT values correspond to $\Delta G = \Delta G^\ddagger + \Delta G_r$ because the values are given for $\Delta G^\ddagger = G(\text{TS}) - G(2\text{N})$ and $\Delta G_r = G(2\text{N}) - G(\text{N}_2)$ in the literature⁷. The UNNP calculations were performed for a $2 \times 2 \times 6$ Ru slab (HCP) with a 0001 surface by fixing the four lowest slab layers. The DFT calculations were performed for a $2 \times 2 \times 2$ Ru slab (HCP) by fixing the lowest layer⁷.

T in K	ΔG_{UNNP} (eV)	ΔG_{DFT} (eV)
100	1.56	1.66
300	1.60	1.70
700	1.73	1.80
1,000	1.83	1.88
1,400	1.97	1.99

Supplementary Table 2 Peaks at low and high wavenumbers in the experimental IR spectra depicted in Fig. 3b in the article and their corresponding location k . The IR spectra were divided into two distributions: A (range: 1600–2000 cm⁻¹) and B (range: 2000–2400 cm⁻¹).

T_{Red} in °C	$\tilde{\nu}_{\text{N}_2, \text{Exp}}^{\text{hi}}$ (cm ⁻¹)	$\tilde{\nu}_{\text{N}_2, \text{Exp}}^{\text{lo}}$ (cm ⁻¹)	$k_{\text{Exp}}^{\text{A, lo}}$	$k_{\text{Exp}}^{\text{B, hi}}$
500	2,164	1,883	60%	65%
650	2,164	1,846	60%	60%

Supplementary Table 3 Number of Ce/La/O ions considered in the local environment of the adsorbed nitrogen molecule depending on the chosen cut-off radius.

States	A	C	F	G	H	I
ν_{N_2} (cm ⁻¹)	2161	2066	1883	1846	1844	1711
$z-z_C$ (Å)	8.17	0.0	2.35	4.34	1.59	0.32
$r_{Cut} = 2 \text{ Å}: N_{Ce/La} N_O$	0 0	0 0	0 0	0 0	0 0	0 0
$r_{Cut} = 3 \text{ Å}: N_{Ce/La} N_O$	0 0	0 0	1 0	1 0	1 0	2 0
$r_{Cut} = 4 \text{ Å}: N_{Ce/La} N_O$	0 0	1 2	1 0	1 0	1 0	3 2
$r_{Cut} = 5 \text{ Å}: N_{Ce/La} N_O$	0 0	3 3	2 1	2 0	2 0	4 4
$r_{Cut} = 6 \text{ Å}: N_{Ce/La} N_O$	0 0	5 7	3 2	2 0	4 0	6 6

Supplementary Table 4 Angular variations of the Ru nanoparticle on the La_{0.5}Ce_{0.5}O_{1.75-x} slab (see Supplementary Fig. 6 for the definition of angle β) and corresponding interfacial energy ϵ_{inter} for different catalyst configurations.

β (°)	Ce-1	La-1	SL-1	SS-1
	ϵ_{inter} (eV)	ϵ_{inter} (eV)	ϵ_{inter} (eV)	ϵ_{inter} (eV)
75	-133.33	-132.33	-133.07	-126.42
105	-116.79	-135.11	-137.93	-131.94
135	-133.79	-129.65	-132.12	-127.40
165	-140.58	-137.59	-137.53	-132.51
195	-133.33	-132.33	-133.07	-126.42

Supplementary Table 5 Various properties of N₂ on-top adsorption on $\sqrt{3} \times \sqrt{3} \times 6$ and $2 \times 2 \times 6$ Ru slabs calculated using the UNNP, as well as DFT and experimental values obtained in previous studies. Properties: r_{i-j} = bond length between atoms i and j ; b = buckling; ϵ_{vib,N_2} = vibrational energy; ν_{N_2} = wavenumber; ϵ_{ads} = adsorption energy; $\Delta\epsilon_{act,top-b-top}$ = diffusion barrier for the on-top/bridge/on-top diffusion path; $\Delta\epsilon_{act,N_2 \rightarrow 2N}$ = activation barrier dissociation energy for N₂ (on-top site) to 2N (closest hollow sites); and ϵ_{def} = deformation energy of the slab.

$\sqrt{3} \times \sqrt{3} \times 6$ ($\theta = 1/3$)					
Property	DFT ⁴	DFT(PW91) ⁵	DFT(RPBE) ⁵	UNNP	Exp. ^{4,5}
r_{N-N} (Å)	1.11	-	-	1.13	1.10(4)
r_{Ru-N} (Å)	2.00	-	-	1.96	2.00(5)
b (Å)	0.15	-	-	0.00	0.00(5)
ϵ_{vib,N_2} (meV)	-	-	-	273	274
ν_{N_2} (cm ⁻¹)	2239	-	-	2202	2195
ϵ_{ads} (eV)	-0.61	-	-	-0.43	-0.44
$2 \times 2 \times 6$ ($\theta = 1/4$)					
Property	DFT ⁴	DFT(PW91) ⁵	DFT(RPBE) ⁵	UNNP	Exp. ^{4,5}
r_{N-N} (Å)		1.14		1.13	-
r_{Ru-N} (Å)		2.02		1.95	-
ν_{N_2} (cm ⁻¹)		2229		2202	-
ϵ_{ads} (eV)	-0.47	-0.74	-0.40	-0.44	-0.31
$\Delta\epsilon_{act,top-b-top}$ (eV)		0.45	0.51	0.56	-
$\Delta\epsilon_{act,N_2 \rightarrow 2N}$ (eV)	1.92	-	-	1.63	-
ϵ_{def} (eV)		0.08	0.07	0.07	-

Supplementary References

1. Esch, B. V., Peters, L. D. M., Sauerland, L. & Ochsenfeld, C. Quantitative comparison of experimental and computed IR-spectra extracted from ab initio molecular dynamics. *J. Chem. Theor. Comput.* 17, 985–995 (2021). [10.1021/acs.jctc.0c01279](https://doi.org/10.1021/acs.jctc.0c01279), Pubmed:[33512155](https://pubmed.ncbi.nlm.nih.gov/33512155/).
2. Huerta, G. V., Nanba, Y., Kurata, I., Nakago, K., Takamoto, S., Shinagawa, C. & Koyama, M.

Calculations of real-system nanoparticles using universal neural network potential PFP.
<https://arxiv.org/abs/2107.00963v1>, (2021).

3. Jain, A., Ong, S. P., Hautier, G., Chen, W., Richards, W. D., Dacek, S., Cholia, S., Gunter, D., Skinner, D., Ceder, G. & Persson, K. A. Commentary: the Materials Project: a materials genome approach to accelerating materials innovation. *APL Mater.* 1, 011002 (2013). [10.1063/1.4812323](https://doi.org/10.1063/1.4812323).
4. Mortensen, J. J., Morikawa, Y., Hammer, B. & Nørskov, J. K. Density functional calculations of N₂ adsorption and dissociation on a Ru(0001) surface. *J. Catal.* 169, 85–92 (1997). [10.1006/jcat.1997.1661](https://doi.org/10.1006/jcat.1997.1661).
5. Herron, J. A., Tonelli, S. & Mavrikakis, M. Atomic and molecular adsorption on Ru. *Surf. Sci.* 614 0001, 64–74 (2013).
6. Chodera, J. D. A simple method for automated equilibration detection in molecular simulations. *J. Chem. Theor. Comput.* 12, 1799–1805 (2016). [10.1021/acs.jctc.5b00784](https://doi.org/10.1021/acs.jctc.5b00784), Pubmed:[26771390](https://pubmed.ncbi.nlm.nih.gov/26771390/).
7. Lee, E. M. Y., Ludwig, T., Yu, B., Singh, A. R., Gygi, F., Nørskov, J. K. & de Pablo, J. J. Neural network sampling of the free energy landscape for nitrogen dissociation on ruthenium. *J. Phys. Chem. Lett.* 12, 2954–2962 (2021). [10.1021/acs.jpcllett.1c00195](https://doi.org/10.1021/acs.jpcllett.1c00195), Pubmed:[33729797](https://pubmed.ncbi.nlm.nih.gov/33729797/).

Auto-Summary for Heterogeneous Catalysis

Cyber Catalysis: N₂ Dissociation over Ruthenium Catalyst with Strong Metal-Support Interaction

Gerardo Valadez Huerta^{*,1}, Kaoru Hisama¹, Katsutoshi Sato², Katsutoshi Nagaoka², Michihisa Koyama^{*,1,3}

¹Research Initiative for Supra Materials, Shinshu University, Nagano 380-8553, Japan. ²Department of Chemical Systems Engineering, Nagoya University, Nagoya 464-8601, Japan. ³Open Innovation Institute, Kyoto University, Kyoto 606-8501, Japan

*Correspondence to: valadez@shinshu-u.ac.jp, koyama_michihisa@shinshu-u.ac.jp

Table of Contents

Introduction & Explanation Notes	1
Auto-Summary.....	2
1. Synthesis & Characterization.....	2
2. Towards Higher Catalytic Activity	15
3. Theoretical Studies	27
4. Recent Progress & Perspectives	43

Introduction & Explanation Notes

The following auto-summary was created using the Dimensions¹ Auto-Summarization 3.0 tool from Springer Nature. This tool is identical to that applied to create, e. g., the machine-generated review book 'Lithium-Ion Batteries'². The datasets for the first, second, and fourth chapters were prepared by searching for articles from 2016 up to the present using the keywords [heterogeneous AND (catalysis OR catalysis)] within the "SN Insights" database from Springer Nature. The database was divided into five clusters, from which only three were kept because we could not identify any content pattern within the other clusters. The cluster used to build the chapter 'Synthesis & Characterization' contained 120 samples, the cluster for 'Towards Higher Catalytic Activity' contained 336, and the cluster for 'Recent Progress & Perspectives' contained 337; these samples accounted for 1,026 of the most downloaded documents in the database. The final summary is given in the next section

and only considers the 30 samples with the highest metrics closest to the chapters' topic.

We applied the same methodology to create the cluster of the chapter 'Theoretical Studies'. Here, we use the keywords [heterogeneous AND (catalysis OR catalyst) and (DFT OR computational OR "machine learning" OR numerical OR simulation OR "neural network" OR ReaxFF OR "molecular dynamics" OR "monte carlo" OR "ab initio" OR "first principles" OR quantum OR "artificial intelligence" OR "neural network" OR descriptor OR "kinetic model" OR CFD OR "computational fluid dynamics")]. Finally, chapters 1–3 only include an (extended) abstract summary, whereas chapter 4 also includes a summary of the perspectives provided in the various summarised reviews. We thank Dr. Shin'ichi Koizumi from Springer for helping us prepare the datasets to be used with the auto-summarisation tool. After this section, the machine-generated section follows.

References

1. Hook, D. W., Porter, S. J. & Herzog, C. Dimensions:

building context for search and evaluation. *Front. Res. Metrics Anal.* **3**, 23 (2018).

2. Writer, B. *Lithium-Ion Batteries*. (Springer International Publishing, 2019).

Auto-Summary

1. Synthesis & Characterization

Immobilized N-Heterocyclic Carbene-Palladium(II) Complex on Graphene Oxide as Efficient and Recyclable Catalyst for Suzuki–Miyaura Cross-Coupling and Reduction of Nitroarenes

DOI: 10.1007/s10562-019-03083-0

Publication outline: Introduction | Experimental | Results and Discussion | Conclusions

Abstract-Summary

This new air- and moisture-stable NHC-Pd@GO heterogeneous catalytic system was found to be a highly active catalyst in the Suzuki–Miyaura cross-coupling between phenylboronic acid and various aryl halides (bromides/chlorides/iodides) and in the reduction of nitroarenes. NHC-Pd@GO heterogeneous catalyst could be recovered easily and reused at least eleven times in Suzuki–Miyaura cross-coupling and nine times in reduction of nitroarenes without any considerable loss of its catalytic activity. The stability and good selectivity of the NHC-Pd@GO heterogeneous catalyst in recycling experiments signify that it could be useful for practical application in various organic transformations.

Extended:

This new air- and moisture-stable heterogeneous catalyst was found to be highly active in Suzuki–Miyaura cross-coupling and reduction of nitroarenes reactions in an aqueous ethanol and aqueous methanol as green solvents using an extremely small amount of palladium under mild conditions (room temperature and short reaction time). NHC-Pd@GO heterogeneous catalyst could be easily recovered from the reaction media by simple filtration and reused at least 12 and ten cycles in the Suzuki–Miyaura cross-coupling and reduction of nitroarenes respectively without significant loss of its activity.

Pd Supported IRMOF-3: Heterogeneous, Efficient and Reusable Catalyst for Heck Reaction

DOI: 10.1007/s10562-019-02756-0

Publication outline: Introduction | Experimental | Results and Discussion | Conclusions

Abstract-Summary

The prepared porous catalyst was effectively used in the Heck coupling reaction in the presence of an organic base. The

reaction parameters such as the type of base, amounts of catalyst and solvents, temperature were optimized. The catalyst was then easily separated, washed, and reused 4 times without significant losses of catalytic activity.

Vanadium–Schiff base complex-functionalized SBA-15 as a heterogeneous catalyst: synthesis, characterization and application in pharmaceutical sulfoxidation of sulfids

DOI: 10.1007/s11164-016-2589-5

Publication outline: Introduction | Materials and methods | Results and discussion | Conclusion

Abstract-Summary

VO₂(picolinichydrazone) complex as a catalyst was stabilized on a SBA-15 mesoporous silica as a catalytic support by using (3-chloropropyl)triethoxysilane as a connector. The immobilization of a metal–Schiff base complex to the surface area of SBA-15 can improve its catalytic effects by increasing the catalytic surface area. A vanadium–Schiff base complex-functionalized SBA-15 was synthesized by covalency connected by a pre-synthesised VO₂(picolinichydrazone) complex to silanated SBA-15. The synthesized vanadium–Schiff base complex was characterized by proton nuclear magnetic resonance (¹H NMR) spectroscopy, carbon nuclear magnetic resonance (¹³C NMR) spectroscopy and Fourier transform infrared spectroscopy (FT-IR), and the final V/SBA-15 was characterized by FT-IR, ultraviolet–visible spectrophotometry and X-ray powder diffraction. The catalytic effect was examined by using V/SBA-15 as a heterogeneous catalyst in sulfoxidation reactions. Of modafinil and modafinic acid by pharmaceutical sulfoxidation of sulfides was carried out and the effects of different solvents, reaction times and also recoverability and reusability of the heterogeneous catalyst were investigated.

Extended:

Of mesoporous silicas was suggested for the first time in 1992 [9] and, since then, considerable progress has been made in the morphology and pore size regulation and application developments of various types of mesoporous silica [10–11].

Green Synthesis of Pd Nanoparticles Supported on Magnetic Graphene Oxide by *Origanum vulgare* Leaf Plant Extract: Catalytic Activity in the Reduction of Organic Dyes and Suzuki–Miyaura Cross-Coupling Reaction

DOI: 10.1007/s10562-017-2220-4

Publication outline: Introduction | Experimental | Result and Discussions | Conclusions

Abstract-Summary

The prepared magnetically nanocatalyst was characterized by transmission electron microscopy, scanning electron microscopy, X-ray diffraction, vibrating sample magnetometer (VSM) and Fourier transform infrared spectroscopy. The heterogeneous catalytic system was investigated for the reduction of 4-nitrophenol, methylene blue and methyl orange in

the presence of NaBH_4 as a reducing reagent and also for Suzuki–Miyaura cross-coupling reactions between phenylboronic acid and a range of aryl halides ($X = \text{I}, \text{Br}, \text{Cl}$).

A New Type of Magnetically-Recoverable Heteropolyacid Nanocatalyst Supported on Zirconia-Encapsulated Fe_3O_4 Nanoparticles as a Stable and Strong Solid Acid for Multicomponent Reactions

DOI: 10.1007/s10562-017-2015-7

Publication outline: Introduction | Result and Discussion | Conclusion

Abstract-Summary

The prepared HPW supported on nano- $\text{Fe}_3\text{O}_4@Zr\text{O}_2$ heterogeneous acid catalyst (or n- $\text{Fe}_3\text{O}_4@Zr\text{O}_2/\text{HPW}$) was fully characterized by several physicochemical techniques such as: Fourier transform infrared spectroscopy (FT-IR), field emission scanning electron microscopy, transmission electron microscopy, energy-dispersive X-ray spectroscopy, X-ray diffraction, vibrating sample magnetometry and thermogravimetric analysis. It was surprising that this very strong solid acid catalyst exhibited an excellent acid strength which was as a result of possessing a higher number of surface active sites compared to its homogeneous analogues. The catalytic activity of the as-prepared novel nano- $\text{Fe}_3\text{O}_4@Zr\text{O}_2/\text{HPW}$ was explored through the one-pot three-component synthesis of different 3,4-dihydropyrimidin-2(1H)-ones (i.e. Biginelli reaction) and 1,4-dihydropyridines (i.e. Hantzsh reaction) under solvent free condition. The sample of 40 wt% showed higher acidity and activity in the catalytic transformation. After the reaction, the catalyst/product isolation could be easily achieved with an external magnetic field and the catalyst could be easily recycled for at least five times without any decrease in its high catalytic activity.

Magnetic Nanoparticle-Supported N-Heterocyclic Carbene-Palladium(II): A Convenient, Efficient and Recyclable Catalyst for Suzuki–Miyaura Cross-Coupling Reactions

DOI: 10.1007/s10562-017-1987-7

Publication outline: Introduction | Experimental | Results and Discussion | Conclusion

Abstract-Summary

The nanomagnetic catalyst was used as convenient and efficient catalyst for the Suzuki–Miyaura cross-coupling reaction of various aryl bromides/chlorides/iodide with phenylboronic acid. The notable advantages of this heterogeneous nanomagnetic catalyst are excellent yields, mild reaction conditions, short reaction times and easy work-up. The new nanomagnetic catalyst could be easily recovered with an external magnet and could be reused at least five times without loss of its catalytic activity.

Extended:

The nanomagnetic catalyst is air- and water-stable, and can be synthesized in high yield with high purity from inexpensive commercially available starting materials.

Glycerol Cu(II) Complex Supported on Fe_3O_4 Magnetic Nanoparticles: A New and Highly Efficient Reusable Catalyst for the Formation of Aryl-Sulfur and Aryl-Oxygen Bonds

DOI: 10.1007/s10562-019-02973-7

Publication outline: Introduction | Experimental | Result and Discussion | Conclusion

Abstract-Summary

This magnetic nanocatalyst utilized as an effective catalyst for the C–S and C–O cross-coupling reactions of aryl halides with thiourea and phenol. A green and novel $\text{Fe}_3\text{O}_4@Si\text{O}_2$ -Glycerole-Cu(II) catalyst successfully was prepared and characterized. This catalyst can be used for the C– and C–O cross coupling reactions.

Extended:

The results show that the leaching of Cu into reaction media is negligible.

Magnetic cobalt ferrite composite as an efficient catalyst for photocatalytic oxidation of carbamazepine

DOI: 10.1007/s11356-016-7978-1

Publication outline: Introduction | Experimental | Results and discussion | Conclusions

Abstract-Summary

A magnetic spinel cobalt ferrite nanoparticle composite (CFO) was prepared via an ultrasonication-assisted co-precipitation method. The morphological structure and surface composition of CFO before and after reaction were investigated by using X-ray diffraction, scanning electron microscopy, transmission electron microscopy, energy dispersive X-ray, and Fourier transform infrared spectroscopy, indicating the consumption of iron oxide during photodegradation. The prepared CFO was then used for the photocatalytic degradation of carbamazepine (CBZ) as an example of pharmaceuticals and personal care products (PPCPs) from aqueous solution. The reactive species for CBZ degradation in the CFO/UV system was identified as hydroxyl radicals by the methanol scavenging method. Combined with the detection of leached iron ions during the process, the CBZ degradation mechanism can be presumed to be heterogeneous and homogeneous photocatalytic degradation in the CFO/UV system.

Design and development of a novel magnetic camphor nanospheres core/shell nanostructure

DOI: 10.1007/s40097-017-0224-7

Publication outline: Introduction | Experimental | Results and discussion | Conclusions

Abstract-Summary

The first synthesis, characterization and catalytic performance of Fe₃O₄/camphor core/shell nanospheres as a magnetic composite nanocatalyst were reported. Further advantages of this new protocol are short reaction times, high yields, easy workup procedure, inexpensive and eco-friendly protocol and magnetically recoverability and several times reusability of the nanocatalyst without significant decrease in catalytic activity.

Microspherical ReS₂ as a High-Performance Hydrodesulfurization Catalyst

DOI: 10.1007/s10562-017-2024-6

Publication outline: Introduction | Experimental | Results and Discussion | Conclusions

Abstract-Summary

An unsupported microspherical ReS₂ catalyst, consisting in self-assembled nano-layers, was evaluated in the hydrodesulfurization (HDS) of 3-methylthiophene showing an excellent catalytic activity. The presence of a defect-rich structure in the microspheres, with short and randomly-orientated ReS₂ slabs, results in the exposure of additional edge sites, which improve the catalytic performance of this material. This microspherical ReS₂ composite, with good HDS performance, is a promising catalyst for the desulfurization of fuel oils; the solvothermal reaction conditions are also useful to tune and create exotic morphologies for the design of new ReS₂ catalysts.

Synthesis and Characterization of Immobilized Lipase on Fe₃O₄ Nanoparticles as Nano biocatalyst for the Synthesis of Benzothiazepine and Spirobenzothiazine Chroman Derivatives

DOI: 10.1007/s10562-016-1797-3

Publication outline: Background | Experimental Section | Characterization | Results and Discussion | Conclusion

Abstract-Summary

A retrievable nanostructure heterogeneous catalyst, based on lipase (lipase from the fungus *Aspergillus niger*), namely Fe₃O₄-bonded lipase (Fe₃O₄ NPs@ lipase) was prepared in nano size and fully characterized by several techniques such as Fourier transform infrared spectroscopy, X-ray diffraction, Scanning electron microscopy, Transmission electron microscopy and Vibrating sample magnetometer.

Four-Component Synthesis of 2-Amino-3-Cyanopyridine Derivatives Catalyzed by Cu@imineZCMNPs as a Novel, Efficient and Simple Nanocatalyst Under Solvent-Free Conditions

DOI: 10.1007/s10562-018-2318-3

Publication outline: Introduction | Results and Discussion | Screening of Reaction Conditions | Conclusion | Experimental

Abstract-Summary

An efficient and convenient method was investigated for synthesis of 2-amino-3-cyanopyridine derivatives via a one-pot

four-component reaction of various types of aldehydes, acetophenone, malononitrile, and ammonium acetate in the presence of 10 mg Cu@imineZCMNPs catalyst. Due to the magnetic nature of the catalyst, it can be easily recovered by an external magnetic field and comfortably reused.

Synthesis and characterization of ceria-coated silica nanospheres: their application in heterogeneous catalysis of organic pollutants

DOI: 10.1007/s42452-019-1613-y

Publication outline: Introduction | Materials and methods | Results and discussion | Catalytic activity of ScP33%CeP and CeO₂ for 4NP reduction | Conclusions

Abstract-Summary

The present work investigates the parameters for the successful coating of silicon oxide nanoparticles surface with a homogeneous cerium oxide shell in an effort to develop core-shell nanostructures. Several processing conditions, such as the precipitation pH, the cerium precursor concentration and the treatment of silica cores (i.e., their use either as-received after their biomimetic formation, or after their calcination followed by surface modification), were examined and optimized. The analysis revealed the formation of spherical core-shell nanostructures bearing a uniform shell layer of crystalline cerium oxide around each silica core which after calcination at 600 °C was comprised of cubic CeO₂ nanocrystals with sizes ranging between 2 and 6 nm.

Magnetic nanoparticles tris(hydrogensulfato) boron as an efficient heterogeneous acid catalyst for the synthesis of α,α -benzylidene bis(4-hydroxycoumarin) derivatives under solvent-free condition

DOI: 10.1007/s11164-019-03881-6

Publication outline: Introduction | Experimental | Results and Discussion | Conclusions

Abstract-Summary

This effective and magnetically recoverable catalyst was employed for the synthesis of α,α -benzylidene bis(4-hydroxycoumarin) derivatives through the reaction of an aromatic aldehyde and 4-hydroxycoumarin under solvent-free conditions.

Gold nanoparticles immobilized on single-layer α -zirconium phosphate nanosheets as a highly effective heterogeneous catalyst

DOI: 10.1007/s42114-019-00091-x

Publication outline: Introduction | Experimental section | Results and discussion | Conclusions

Abstract-Summary

Gold nanoparticles (Au NPs) were immobilized on single-layered α -zirconium phosphate (ZrP) nanosheets as a highly efficient

heterogeneous catalyst. The characterizations showed that the Au NPs with a size distribution of 2.0 ± 1.0 nm were uniformly dispersed and immobilized on single-layer ZrP nanosheets.

Synthesis and Application of Hyperbranched Polyester-Grafted Polyethylene (HBPE-g-PE) Containing Palladium Nanoparticles as Efficient Nanocatalyst

DOI: 10.1007/s10562-016-1720-y

Publication outline: Introduction | Experimental | Results and Discussion | Conclusions

Abstract-Summary

In nowadays, palladium-catalyzed reactions are of utmost importance in synthetic organic chemistry. We report a facile approach to prepare hyperbranched polyester-grafted-polyethylene supported palladium nanoparticles as an efficient catalyst in Suzuki reaction and solvent-free aerobic oxidation of alcohols. Because of the amplification effect of hyperbranched polyester, high loading capacities (around $0.276 \text{ mmol g}^{-1}$ for Pd) was achieved. A hyperbranched polyester based on 2,2-bis(methylol) propionic acid (bis-MPA) was synthesized and grafted onto carboxylic acid functionalized polyethylene powder. The final nanocatalyst was prepared via solution loading of PdCl_2 and reduction to palladium nanoparticles on the HBPE-g-PE. The activity and stability of prepared polymer-supported heterogeneous catalyst was carefully examined for Suzuki reaction and solvent-free oxidation of alcohols.

Extended:

We chose a number of primary or secondary alcohols to perform oxidation reaction and prepare relevant aldehydes or ketones under solvent-free condition.

Five-membered N-Heterocycles Synthesis Catalyzed by Nano-silica Supported Copper(II)-2-imino-1,2-diphenylethan-1-ol Complex

DOI: 10.1007/s10562-017-2173-7

Publication outline: Introduction | Experimental Section | Results and Discussion | Conclusion

Abstract-Summary

A new amino functionalized nano silica was synthesized using 2-hydroxy-1,2-diphenylethan-1-one. The new 2-hydroxy-1,2-diphenylethan-1-one@amino functionalized nano-silica was used as a support material for copper(II) catalyst. The nano heterogeneous copper catalyst is recoverable up to 12 times without any significant leaching which indicated that the heterogeneous catalyst is stable and very active under the applied conditions.

In situ incorporation of well-dispersed Cu-Fe oxides in the mesochannels of AMS and their utilization as catalysts towards the Fenton-like degradation of methylene blue

DOI: 10.1007/s10853-016-0436-0

Publication outline: Introduction | Experimental section | Results and discussion | Conclusion

Abstract-Summary

Multi-components active metal oxide-supported catalysts are highly promising in heterogeneous catalysis due to some special promoting effects. The results revealed that bimetallic Cu-Fe oxides were directly formed and highly dispersed in the mesochannels during the calcinations and the introduction of Cu^{2+} and Fe^{2+} on the micelles has influence on the structure properties. As compared to the monometallic Fe-modified AMS, the presence of Cu promotes the effects between Fe species and silica wall, leading to the better dispersion of Fe in the mesochannels of AMS. A series of Cu-Fe-modified AMS were used as Fenton-like catalysts and exhibited good catalytic activity in the degradation of methylene blue (MB), which resulted from high dispersion of Fe species and synergetic effect between Cu and Fe active sites.

Synthesis of Polyhydroquinoline, 2,3-Dihydroquinazolin-4(1H)-one, Sulfide and Sulfoxide Derivatives Catalyzed by New Copper Complex Supported on MCM-41

DOI: 10.1007/s10562-018-2311-x

Publication outline: Introduction | Experimental | Result and Discussion | Conclusions

Abstract-Summary

A simple, efficient and less expensive protocol for the synthesis of Cu(II) immobilized on MCM-41@Serine has been reported. The obtained nanostructured compound were also employed as a green, efficient, heterogeneous and reusable catalytic system for the synthesis of polyhydroquinoline, 2,3-dihydroquinazolin-4(1H)-one, sulfide and sulfoxide derivatives. After characterization of this catalyst, the catalytic activity of this nanostructure compound has been investigated for the synthesis of polyhydroquinoline, 2,3-dihydroquinazolin-4(1H)-one, sulfide and sulfoxide derivatives.

Preparation, characterization and catalytic performance of polyoxometalate immobilized on the surface of halloysite

DOI: 10.1007/s10853-018-3142-2

Publication outline: Introduction | Experimental section | Results and discussion | Conclusions

Abstract-Summary

The catalytic performance of this catalyst was tested in green oxidation system of n-tetradecane using air as oxidant under the mild reaction condition with normal atmospheric pressure and low temperature and without adding any solvents and additives. In order to find the optimum catalytic reaction condition, we prepared five catalysts containing different amounts of SbWRu, 0.97%, 1.94%, 2.80%, 4.23% and 5.87%. The results of the controlled experiments confirmed that the catalyst containing SbWRu of 1.94% exhibited high activity with a conversion (53.30%) and turnover frequency (TOF: 52396 h^{-1}) at the

optimal reaction condition. The final conversion of n-tetradecane runs up to 87.97% after five consecutive cycles without the separation of the catalyst HNTs/Apts/SbWRu (1.94%).

Extended:

The catalytic performance of HNTs/Apts/SbWRu was evaluated in the oxidation reaction of n-tetradecane under environmentally friendly condition. This unique heterogeneous catalyst has bright potential application in the oxidation of n-alkanes in the future.

[P₄VPy–CuO nanoparticles as a novel and reusable catalyst: application at the protection of alcohols, phenols and amines](#)

DOI: 10.1007/s13738-016-0887-x

Publication outline: Introduction | Experiment | Results and discussion | Conclusions

Abstract-Summary

P₄VPy–CuO nanoparticles were synthesized using ultrasound irradiations. Relevant properties of the synthesized nanoparticles were investigated by X-ray diffraction, scanning electron microscopy, transmission electron microscopy and Fourier transform infrared spectroscopy.

Extended:

It bodes well for the future of P₄VPy reagents in which their properties can be fine-tuned in organic reactions [198].

[Supported Au/MIL-53\(Al\): a reusable green solid catalyst for the three-component coupling reaction of aldehyde, alkyne, and amine](#)

DOI: 10.1007/s11144-016-1034-5

Publication outline: Introduction | Experimental | Results and discussion | Conclusion

Abstract-Summary

A metal–organic-framework-supported Au-based heterogeneous catalyst (Au/MIL-53(Al)) was prepared using the impregnation method under mild conditions with HAuCl₄·4H₂O as the Au precursors. MIL-53(Al) indicates excellent chemical stability without structure degradation during the loading and catalysis process. The XPS spectra indicate that the catalyst Au/MIL-53(Al) contains coexisting Au⁰ and Au³⁺ ions. The results showed that the catalyst Au/MIL-53(Al) displayed high activity without any additives or an inert atmosphere (the yield reached 97.9% for 5 h at 120 °C). Au/MIL-53(Al) has proven to be applicable to a wide range of substrates. Various aromatic/aliphatic aldehydes, aromatic alkynes, and piperidine were able to undergo A³ coupling on the catalyst Au/MIL-53(Al).

Extended:

We believe that this methodology will find widespread use in organic synthesis for propargylamine preparation.

[Mixed cobalt/nickel metal–organic framework, an efficient catalyst for one-pot synthesis of substituted imidazoles](#)

DOI: 10.1007/s00706-016-1776-9

Publication outline: Introduction | Results and discussion | Conclusion | Experimental

Abstract-Summary

A three-dimensional bimetallic metal–organic framework, [CoNi(μ₃-tp)₂(μ₂-pyz)₂] (tp = terephthalic acid, pyz = pyrazine) was applied as a highly efficient and recoverable heterogeneous catalyst. The catalyzed reaction was the one-pot three-component condensation reaction between benzil or benzoin with various substituted aromatic aldehydes and ammonium acetate to synthesize the corresponding imidazoles in solvent-free conditions and high to quantitative yields. 2,4,5-trisubstituted 1H-imidazoles were not previously synthesized using MOFs as heterogeneous catalyst.

Extended:

There are a few reports on the application of bimetallic MOFs as a catalyst in MCRs.

[Magnetic Nanoparticle Decorated N-Heterocyclic Carbene–Nickel Complex with Pendant Ferrocenyl Group for C–H Arylation of Benzoxazole](#)

DOI: 10.1007/s10562-018-2514-1

Publication outline: Introduction | Experimental | Results and Discussion | Conclusion

Abstract-Summary

The complex proved to be an efficient heterogeneous catalyst for C–H arylation of benzoxazole with aryl boronic acids. The recycling studies revealed that complex could be reused for six times without significant decrease in catalytic activity.

[Facile synthesis of monodispersed Pd nanocatalysts decorated on graphene oxide for reduction of nitroaromatics in aqueous solution](#)

DOI: 10.1007/s11164-018-3621-8

Publication outline: Introduction | Experimental | Results and discussion | Conclusions

Abstract-Summary

We synthesized the reproducible heterogeneous catalyst of graphene oxide (GO)-supported palladium nanoparticles (NPs) via a simple and green process. The GO-supported Pd NPs (Pd/GO nanocatalyst) exhibited excellent catalytic activity for the reduction of nitroaromatics to aminoaromatics in aqueous sodium borohydride. These features ensured the high catalytic activity of the introduced graphene oxide supported Pd nanocatalysts.

[A facile green synthesis of silver nanoparticle-decorated hydroxyapatite for efficient catalytic activity towards 4-nitrophenol reduction](#)

DOI: 10.1007/s11164-017-3161-7

Publication outline: Introduction | Experimental | Characterization techniques | Results and discussion | Conclusion

Abstract-Summary

Silver nanoparticles (AgNPs) were gradually grown on a hydroxyapatite surface via a green self-reducing approach. Hydroxyapatite (HAP) was functionalized by dopamine and subsequently self-polymerized onto the HAP surface. Surface-adhered polydopamine acted as a self-reducing agent for the Ag⁺ ion; thus the process is considered to be green. The AgNP-decorated HAP was applied as a heterogeneous catalyst for the reduction of 4-nitrophenol (4-NP), which obeyed first-order reduction kinetics.

[Synthesis and characterization of oxo-vanadium complex anchored onto SBA-15 as a green, novel and reusable nanocatalyst for the oxidation of sulfides and oxidative coupling of thiols](#)

DOI: 10.1007/s11164-018-3367-3

Publication outline: Introduction | Experimental | Results and discussion | Conclusion

Abstract-Summary

The results of the developed procedure bring several benefits such as the use of commercially available, ecologically benign, operational simplicity, and cheap and chemically inert reagents. It shows good reaction times, practicability and high efficiency, and is easily recovered from the reaction mixture by simple filtration and reused for several consecutive cycles without noticeable change in its catalytic activity. High efficiency, simple and an inexpensive procedure, commercially available materials, easy separation, and an eco-friendly procedure are the several advantages of the currently employed heterogeneous catalytic system.

[Ru\(III\) complex anchored onto amino-functionalized MIL-101\(Cr\) framework via post-synthetic modification: an efficient heterogeneous catalyst for ring opening of epoxides](#)

DOI: 10.1007/s13738-017-1277-8

Publication outline: Introduction | Experimental | Results and discussion | Conclusion

Abstract-Summary

The metallo Schiff base-functionalized metal-organic framework was prepared by post-synthetic method and used as an electron-deficient catalyst for the alcoholysis of epoxides. This new catalyst, MIL-101-NH₂-PC-Ru, was characterized by Fourier transform infrared, UV-Vis spectroscopic techniques, X-ray

diffraction, BET, inductively coupled plasma atomic emission spectroscopy and field-emission scanning electron microscopy. In the presence of this heterogeneous catalyst, ring opening of epoxides was performed under mild condition to show the significant ability and successful applications of Lewis acid containing catalysts in corporation with metal-organic frameworks.

[A novel catalyst of MIL-101\(Fe\) doped with Co and Cu as persulfate activator: synthesis, characterization, and catalytic performance](#)

DOI: 10.1007/s11696-017-0276-7

Publication outline: Introduction | Experimental | Results and discussion | Conclusions

Abstract-Summary

Effective and novel heterogeneous catalysts of Metal-organic framework MIL-101(Fe) doped with cobalt (Co²⁺) or copper (Cu²⁺) have been synthesized by post-synthesis method, namely Co-MIL-101(Fe) and Cu-MIL-101(Fe). The initial and metal-doped samples were tested to activate persulfate (PS) for removal of Acid Orange 7 (AO7) in water. The addition of Cu²⁺ and Co²⁺ could alter structure characteristics of MIL-101(Fe) in crystal structure and morphology. The alteration was reflected in the catalytic capacity of PS activation. An interesting note was that, whether Co or Cu doping, metal-doped MIL-101(Fe) greatly improved the PS activation as compared to unmodified MIL-101(Fe). The removal rate of AO7 was about 66, 92, 98% in MIL-101(Fe)/PS, 6%wtCu-MIL-101(Fe)/PS and 6%wtCo-MIL-101(Fe)/PS system, respectively. Such an enhancement in activity may be attributed to the main reasons: the new active sites created by metal additives; an increase in number of active Fe sites produced by Co and Cu doping which results in alteration of morphology and structure of catalysts.

[Heterogeneous Ziegler-Natta catalysts with various sizes of MgCl₂ crystallites: synthesis and characterization](#)

DOI: 10.1007/s13726-016-0424-x

Publication outline: Introduction | Experimental | Results and discussion | Conclusion

Abstract-Summary

A MgCl₂-based Ziegler-Natta catalyst was characterized using X-ray diffraction (XRD) patterns, scanning electron microscopy (SEM) and transmission electron microscopy (TEM) and IR spectra. We focused on the XRD reflection at 2θ = 50° to determine the thickness of MgCl₂ crystals, and validated these results with TEM pictures. SEM pictures were taken in order to measure the size of the nanoparticles formed by the MgCl₂ crystals. The thickness of the catalyst crystals was calculated from the XRD reflection at 2θ = 50°. Changing the precipitation temperature within a range from 40 to 90 °C altered the thickness of the MgCl₂ crystal plates. We estimated that a typical catalyst particle with a diameter of 20 μm contained about one million nanoparticles, each of which consisted of about 25,000 MgCl₂ crystal units.

Extended:

We focused on the XRD at $50^\circ 2\theta$ to determine whether additional information can be gained from the crystallographic data. SEM pictures were used to find out whether a correlation exists between the size of the nanoparticles [267] in the produced material and the crystal thickness measured by X-ray at $50^\circ 2\theta$. The thickness of the $MgCl_2$ crystal was calculated from the reflection peak at $2\theta = 50^\circ$, on which our study concentrated. The thickness of the catalysts was measured by X-ray diffraction using the reflection at $2\theta = 50^\circ$. As part of future work, we will evaluate the effect of $MgCl_2$ crystal thickness on polymerization activity, molecular weight capability, width of molecular weight distribution, and amount of soluble polymer material in copolymers, especially when higher amounts of co-monomer are incorporated.

Bibliography

- [1] Vishal K, Fahlman BD, Sasidhar BS, Patil SA, Patil SA (2017) *Catal Lett* 147:900–918
- [2] Kandathil V, Fahlman BD, Sasidhar BS, Patil SA, Patil SA (2017) *New J Chem* 41:9531–9545
- [3] Manjunatha K, Koley TS, Kandathil V, Dateer RB, Balakrishna G, Sasidhar BS, Patil SA, Patil SA (2018) *Appl Organomet Chem* 32:e4266
- [4] Kandathil V, Koley TS, Manjunatha K, Dateer RB, Keri RS, Sasidhar BS, Patil SA, Patil SA (2018) *Inorg Chim Acta* 478:195–210
- [5] Kempasiddhaiah M, Kandathil V, Dateer RB, Sasidhar BS, Patil SA, Patil SA (2019) *Appl Organomet Chem* 33:e4846
- [6] Millward AR, Yaghi Millward OM (2005) Metal–organic frameworks with exceptionally high capacity for storage of carbon dioxide at room temperature. *J Am Chem Soc* 127:17998–17999
- [7] Yuanbiao H, Tao M, Ping H, Dongshuang W, Zujin L, Rong C (2013) Direct C-H bond arylation of indoles with aryl boronic acids catalyzed by palladium nanoparticles encapsulated in mesoporous metal-organic framework. *ChemCatChem* 5:1877–1883
- [8] Burés J (2016) A simple graphical method to determine the order in catalyst. *Angew Chem Int Ed Engl* 55:2028–2031
- [9] C.T. Kresge, M.E. Leonowicz, W.J. Roth, J.C. Vartuli, J.S. Beck, Ordered mesoporous molecular sieves synthesized by a liquid-crystal template mechanism. *Nature* 359, 710–712 (1992)
- [10] J.Y. Ying, C.P. Mehnert, M.S. Wong, Synthesis and applications of supramolecular templated mesoporous materials. *Angew. Chem. Int. Ed.* 38, 56–77 (1999)
- [11] Y. Wan, D.Y. Zhao, On the controllable soft-templating approach to mesoporous silicates. *Chem. Rev.* 107, 2821–2860 (2007)
- [12] A.P. Wight, M.E. Davis, Design and preparation of organic-inorganic hybrid catalysts. *Chem. Rev.* 102, 3589 (2002)
- [13] R. Breslow, Artificial enzymes. *Science* 218, 532 (1982)
- [14] S.L. Jain, B.S. Rana, B. Singh, A.K. Sinha, A. Bhaumik, M. Nandi, B. Sain, An improved high yielding immobilization of vanadium Schiff base complexes on mesoporous silica via azide–alkyne cycloaddition for the oxidation of sulfides. *Green Chem.* 12, 374–377 (2010)
- [15] M.R. Maurya, A.K. Chandrakar, S. Chand, Oxidation of phenol, styrene and methyl phenyl sulfide with H_2O_2 catalysed by dioxovanadium(V) and copper(II) complexes of 2-aminomethylbenzimidazole-based ligand encapsulated in zeolite-Y. *J. Mol. Catal. A: Chem.* 263, 227–237 (2007)
- [16] K. Srinivasan, P. Michaud, J.K. Kochi, Epoxidation of olefins with cationic (salen) manganese(III) complexes. The modulation of catalytic activity by substituents. *J. Am. Chem. Soc.* 108, 2309–2320 (1986)
- [17] D. Pérez-Quintanilla, A. Sánchez, I. del Hierro, M. Fajardo, I. Sierra, Preconcentration of Zn(II) in water samples using a new hybrid SBA-15-based material. *J. Hazard. Mater.* 166, 1449–1458 (2009)
- [18] Rumi L, Scheuermann GM, Mülhaupt R, Bannwarth W (2011) *Helv Chim Acta* 94:966–976
- [19] Siamaki A, Khder A, Abdelsayed V, et al. Microwave-assisted synthesis of palladium nanoparticles supported on graphene: a highly active and recyclable catalyst for carbon–carbon crosscoupling reactions. *J Catal*, 2011, 279: 1–11
- [20] Makharza S, Cirillo G, Bachmatiuk A, Ibrahim I, Ioannides N, Trzebicka B, Hampel S, Rummeli MH (2013) *J Nanopart Res* 15:2099
- [21] Scheuermann GM, Rumi L, Steurer P, Bannwarth W, Mülhaupt R (2009) *J Am Chem Soc* 131:8262–8270
- [22] Jia L, Zhang Q, Li Q, Song H (2009) *Nanotechnology* 20:385601
- [23] Jafar Hoseini S, Ghanavat Khozestan H, Hashemi Fath R (2015) *RSC Adv* 5:47701–47708
- [24] Karical RG, James KW, Fox M (2013) *Nano Lett* 3:1757–1760
- [25] Hosseini MM, Kolvari E, Koukabi N, Ziyaei M, Zolfigol MA (2016) *Catal Lett* 146:1040–1049
- [26] Koukabi N, Kolvari E, Zolfigol MA, Khazaei A, Shaghasemi BS, Fasahatib B (2012) *Adv Synth Catal* 354:2001–2008
- [27] Polshettiwar V, Varma RS (2010) *Green Chem* 12:743
- [28] Jin Z, Guo SX, Qiu LL, Wu GP, Fang JX (2011) *Appl Organomet Chem* 25:502
- [29] Ranganath KVS, Schäfer AH, Glorius F (2011) *Chem Cat Chem* 3:1889
- [30] Ke H, Chen X, Zou G (2014) *Appl Organometal Chem* 28:54
- [31] Serrano JL, Pérez J, García L, Sánchez G, García J, Lozano P, Zende V, Kapdi A (2015) *Organometallics* 34:522
- [32] Stevens PD, Li G, Fan J, Yen M, Gao Y (2005) *Chem Commun* 35:4435
- [33] Zheng Y, Stevens PD, Gao Y (2006) *J Org Chem* 71:537

- [34] Wang Z, YuY, Zhang YX, Li SZ, Qian H, Lin ZY (2015) Green Chem 17:413
- [35] Yang H, Wang Y, Qin Y, Chong Y, Yang Q, Li G, Zhang L, Li W 2011 Green Chem 13:1352
- [36] Liang D, Luo H, Liu YF et al (2013) Lysilactones A-C, three 6H-dibenzo[b, d]pyran-6-one glycosides from *Lysimachia clethroides*, total synthesis of Lysilactone A. *Tetrahedron* 69:2093–2097. <https://doi.org/10.1016/j.tet.2013.01.029>
- [37] Durmus Z, Sözeri H, Unal B et al (2011) Magnetic and dielectric characterization of alginate acid-Fe 3O4 nanocomposite. *Polyhedron* 30:322–328. <https://doi.org/10.1016/j.poly.2010.10.028>
- [38] Pirhayati M, Kakanejadifard A, Veisi H (2016) A new nano-Fe3O4-supported organocatalyst based on 3,4-dihydropyridine: an efficient heterogeneous nanocatalyst for one-pot synthesis of pyrazolo[3,4-b]pyridines and pyrano[2,3-d]pyrimidines. *Appl Organomet Chem* 30:1004–1008. <https://doi.org/10.1002/aoc.3534>
- [39] Heydari Z, Bahadorikhalili S, Ranjbar PR, Mahdavi M (2018) DABCO-modified super-paramagnetic nanoparticles as an efficient and water-compatible catalyst for the synthesis of pyrano[3,2-c:5,6-c']dichromene-6,8-dione derivatives under mild reaction conditions. *Appl Organomet Chem*. <https://doi.org/10.1002/aoc.4561>
- [40] Kabiri Esfahani F, Zareyee D, Shokuhi Rad A, Taher-Bahrami S (2017) Sulfonic acid supported on magnetic nanoparticle as an eco-friendly, durable and robust catalyst for the synthesis of β -amino carbonyl compounds through solvent free Mannich reaction. *Appl Organomet Chem*. <https://doi.org/10.1002/aoc.3865>
- [41] Yuan E, Wu C, Liu G et al (2018) Effects of SBA-15 physicochemical properties on performance of Pd/SBA-15 catalysts in 2-ethyl-anthraquinone hydrogenation. *J Ind Eng Chem* 66:158–167. <https://doi.org/10.1016/j.jiec.2018.05.025>
- [42] Vashurin A, Marfin Y, Tarasyuk I et al (2018) Sulfonated octa-substituted Co(II) phthalocyanines immobilized on silica matrix as catalyst for Thiuram E synthesis. *Appl Organomet Chem*. <https://doi.org/10.1002/aoc.4482>
- [43] Hassani H, Nasser MA, Zakerinasab B, Rafiee F (2016) Synthesis, characterization and application of sulfonic acid supported on ferrite-silica superparamagnetic nanoparticles. *Appl Organomet Chem* 30:408–413. <https://doi.org/10.1002/aoc.3447>
- [44] Saremi SG, Keypour H, Noroozi M, Veisi H (2018) Schiff base Mn(III) and Co(II) complexes coated on Co nanoparticles: an efficient and recyclable magnetic nanocatalyst for H2O2 oxidation of sulfides to sulfoxides. *RSC Adv* 8:3889–3898. <https://doi.org/10.1039/c7ra11225d>
- [45] Cui L, Pu T, Shen Z et al (2019) A facile strategy to synthesize Pd/TiO 2 nanotube arrays with high visible light photocatalytic performance. *Res Chem Intermed* 45:2167–2177
- [46] Keshavarz M, Vafaei-Nezhad M (2016) Design and Characterization of l-Proline-Amberlite as a Novel Heterogeneous Organocatalyst and Its Catalytic Application in the Synthesis of Pyrazol-Derivates. *Catal Letters* 146:353–363. <https://doi.org/10.1007/s10562-015-1668-3>
- [47] Karami B, Farahi M, Akrami S, Elhamifar D (2018) Tungstic acid-functionalized MCM-41 as a novel mesoporous solid acid catalyst for the one-pot synthesis of new pyrrolo[2,1- A] isoquinolines. *New J Chem* 42:12811–12816. <https://doi.org/10.1039/c8nj02699h>
- [48] Moosavi-Zare AR, Zolfigol MA, Zarei M et al (2013) Design, characterization and application of new ionic liquid 1-sulfonylpyridinium chloride as an efficient catalyst for tandem Knoevenagel-Michael reaction of 3-methyl-1-phenyl-1H-pyrazol-5(4H)-one with aldehydes. *Appl Catal A Gen* 467:61–68. <https://doi.org/10.1016/j.apcata.2013.07.004>
- [49] Jayaseeli AMI, Rajagopal S (2009) [Iron(III)-salen] ion catalyzed H2O2 oxidation of organic sulfides and sulfoxides. *J Mol Catal A: Chem* 309:103–110. <https://doi.org/10.1016/j.molcata.2009.05.004>
- [50] Feng YS, Li YY, Tang L et al (2010) Efficient ligand-free copper-catalyzed C–S cross-coupling of thiols with aryl iodides using KF/Al 2 O 3 as base. *Tetrahedron Lett* 51:2489–2492. <https://doi.org/10.1016/j.tetlet.2010.02.155>
- [51] Capozzi MAM, Fracchiolla G, Cardellicchio C (2013) The effect of nitrogen atoms in the enantioselective oxidation of aryl or heteroaryl benzyl sulfides. *J Sulfur Chem* 34:646–650. <https://doi.org/10.1080/17415993.2013.779697>
- [52] Yavari I, Nematpour M, Damghani T (2014) Copper-catalyzed S-arylation of tetramethylguanidine-heterocumulene adducts. *Tetrahedron Lett* 55:1323–1325. <https://doi.org/10.1016/j.tetlet.2014.01.006>
- [53] Liu X, Zhu H, Zhang SB et al (2018) Facile synthesis of S-arylisothioureas via the S-arylation of arylthioureas with aryl iodides in water. *Tetrahedron Lett* 59:3165–3170. <https://doi.org/10.1016/j.tetlet.2018.07.012>
- [54] Rout L, Saha P, Jammi S, Punniyamurthy T (2008) Efficient copper(I)-catalyzed C–S cross coupling of thiols with aryl halides in water. *European J Org Chem* 2008:640–643. <https://doi.org/10.1002/ejoc.200700978>
- [55] Kang HY, Wang HP (2013) Preparation of magnetic recoverable nanosize Cu-Fe2O3/Fe photocatalysts. *Environ Sci Technol* 47:7380–7387
- [56] Li XY, Hou Y, Zhao QD, Teng W, Hu XJ, Chen GH (2011a) Capability of novel ZnFe2O4 nanotube arrays for visible-light induced degradation of 4-chlorophenol. *Chemosphere* 82:581–586
- [57] Li XY, Hou Y, Zhao QD, Wang LZ (2011b) A general, one-step and template-free synthesis of sphere-like zinc ferrite nanostructures with enhanced photocatalytic activity for dye degradation. *J Colloid Interf Sci* 358:102–108
- [58] Liu SQ et al (2013) Graphene oxide enhances the Fenton-like photocatalytic activity of nickel ferrite for degradation of dyes under visible light irradiation. *Carbon* 64:197–206
- [59] Senapati KK, Borgohain C, Phukan P (2012) CoFe2O4-ZnS nanocomposite: a magnetically recyclable photocatalyst. *Catal Sci Technol* 2:2361–2366

- [60] Singh C, Goyal A, Singhal S (2014) Nickel-doped cobalt ferrite nanoparticles: efficient catalysts for the reduction of nitroaromatic compounds and photo-oxidative degradation of toxic dyes. *Nanoscale* 6:7959–7970
- [61] Guan YH, Ma J, Ren YM, Liu YL, Xiao JY, Lin LQ, Zhang C (2013) Efficient degradation of atrazine by magnetic porous copper ferrite catalyzed peroxydisulfate oxidation via the formation of hydroxyl and sulfate radicals. *Water Res* 47:5431–5438
- [62] Zhang T, Li WW, Croue JP (2012) A non-acid-assisted and non-hydroxyl-radical-related catalytic ozonation with ceria supported copper oxide in efficient oxalate degradation in water. *Appl Catal B-Environ* 121:88–94
- [63] Andreozzi R, Marotta R (2004) Removal of benzoic acid in aqueous solution by Fe(III) homogeneous photocatalysis. *Water Res* 38:1225–1236
- [64] Zeynizadeh, B., Karimkoshteh, M.: Magnetic Fe₃O₄ nanoparticles as recovery catalyst for preparation of oximes under solvent-free condition. *J. Nanostruct. Chem.* 3, 57–63 (2013)
- [65] Polshettiwar, V., Luque, R., Fihri, A., Zhu, H., Bouhrara, M., Basset, J.M.: Magnetically recoverable nanocatalysts. *Chem. Rev.* 111, 3036–3075 (2011)
- [66] Maleki, A., Kamalzare, M., Aghaei, M.: Efficient one-pot four-component synthesis of 1,4-dihydropyridines promoted by magnetite/chitosan as a magnetically recyclable heterogeneous nanocatalyst. *J. Nanostruct. Chem.* 5, 95–105 (2015)
- [67] Wang L, Sofer Z, Luxa J, Sedmidubský D, Ambrosi A, Pumera M (2016) *Electrochem Commun* 63:39
- [68] Chianelli R (1984) *Cat Rev Sci Eng* 26:361
- [69] Wildervanck JC, Jellineck F (1971) *J Less Common Met* 24:73
- [70] Hafeez M, Gan L, Li H, Ma Y, Zhai T (2016) *Adv Funct Mater* 26:4551
- [71] Yella A, Therese HA, Zink N, Panthöfer M, Tremel W (2008) *ChemMater* 20:3587
- [72] Tu W, Denizot B (2007) *J Colloid Interface Sci* 310:167
- [73] Tang N, Tu W (2009) *J MagnMagn Mater* 321:3311
- [74] Brorson M, Hansen TW, Jacobsen CJ (2002) *J Am Chem Soc* 124: 11582
- [75] Aliaga JA, Araya JF, Lozano H, Benavente E, Alonso-Nuñez G, González G (2015) *Mater Chem Phys* 151:372
- [76] Qi F, Cheng Y, Zheng B, He J, Li Q, Wang X, Yu B, Lin J, Zhang J, Li P, Zhang W (2017) *J Mater Sci* 52:3622
- [77] Itoh T, Kuroda K, Tomosada M, Takagi Y (1991) Design of a-alkyl @-hydroxy esters suitable for providing optical resolution by lipase hydrolysis. *J Org Chem* 56:797–804
- [78] Huang H, Liao MH, Chen DH (2003) Direct binding and characterization of lipase onto magnetic nanoparticles. *Biotechnol Prog* 19:1095–1100
- [79] Kim M, Ham HO, Oh SD, Park HG, Chang HN, Choi SH (2006) Immobilization of *Mucor javanicus* lipase on effectively functionalized silica nanoparticles. *J Mol Catal B* 39:62–68
- [80] Liu X, Ma Z, Xing J, Liu H, Magn J (2004) Preparation and characterization of amino-silane modified superparamagnetic silica nanospheres. *J Magn Magn Mater* 270:1–6
- [81] Shaw SY, Chen YJ, Ou JJ, Ho L (2006) Preparation and characterization of *Pseudomonas putida* esterase immobilized on magnetic nanoparticles. *Enzyme Microb Technol* 39:1089–1095
- [82] Girgis AS, Kalmouch A, Hosni HM (2004) *Amino Acids* 26:139
- [83] Kambe S, Saito K (1980) *Synthesis* 1980:366
- [84] Shi F, Tu S, Fang F, Li T (2005) *Arkivoc* I:137
- [85] Tu SJ, Jiang H, Zhuang QY, Miao CB, Shi DQ, Wang XS, Gao YC (2003) *Chin J Org Chem* 23:488
- [86] Zhou WJ, Ji SJ, Shen ZL (2006) *J Organomet Chem* 691:1356
- [87] Safari J, Zarnegar Z, Heydarian M (2012) *Bull Chem Soc Jpn* 85:1332
- [88] Bala H, Zhang Y, Ynag H, Wang C, Li M, Lv X, Wang Z (2007) Preparation and characteristics of calcium carbonate/silica nanoparticles with core-shell structure. *Colloids Surf A: Physicochem Eng Asp* 294:8–13
- [89] Hwang HS, Bae JH, Kim HG, Lim KT (2010) Synthesis of silica-polystyrene core-shell nanoparticles via surface thiol-lactam initiated radical polymerization. *Eur Polym J* 46:1654–1659
- [90] Srdić VV, Mojić B, Nikolić M, Ognjanović S (2013) Recent progress on synthesis of ceramics core/shell nanostructures. *Process Appl Ceram* 7:45–62
- [91] He B, Zhao Q, Zeng Z, Wang X, Han S (2015) Effect of hydrothermal reaction time and calcination temperature on properties of Au@CeO₂ core-shell catalyst for CO oxidation at low temperature. *J Mater Sci* 50:6339–6348
- [92] Lin K-F, Cheng H-M, Hsu H-C, Lin L-J, Hsieh W-F (2005) Band gap variation of size-controlled ZnO quantum dots synthesized by sol-gel method. *Chem Phys Lett* 409:208–211
- [93] Ullah S et al (2015) Enhanced photocatalytic properties of core@shell SiO₂@TiO₂ nanoparticles. *Appl Catal B* 179:333–343
- [94] A. Khalafi-Nezhad, H. Foroughi, M.M. Doroodmand, F. Panahi, *J. Mater. Chem.* 21, 12842 (2011)
- [95] M. Farahi, B. Karami, R. Keshavarz, F. Khosravian, *RSC Adv.* 7, 46644 (2017)
- [96] M. Kidwai, V. Bansal, P. Mothsra, S. Saxena, R.K. Somvanshi, S. Dey, T.P. Singh, *J. Mol. Catal. A: Chem.* 268, 76 (2007)
- [97] J.M. Khurana, S. Kumar, *Monatsh. Chem.* 141, 561 (2010)
- [98] J.M. Khurana, S. Kumar, *Tetrahedron Lett.* 50, 4125 (2009)
- [99] H. Mehrabi, H. Abusaidi, *J. Iran. Chem. Soc.* 7, 890 (2010)

- [100] B. Karmakar, A. Nayak, J. Banerji, *Tetrahedron Lett.* 53, 4343 (2012)
- [101] W. Li, Y. Wang, Z. Wang, L. Dai, Y. Wang, *Catal. Lett.* 141, 1651 (2011)
- [102] K. Parvanak Boroujeni, P. Ghasemi, Z. Rafienia, *Monatsh Chem.* 145, 1651 (2014)
- [103] M.M. Heravi, F. Nahavandi, S. Sadjadi, H.A. Oskooie, F.F. Bamoharram, *Synth. Commun.* 145, 498 (2010)
- [104] K. Parvanak Boroujeni, S. Hadizadeh, S. Hasani, A. Fadavi, M. Shahrokh, *Acta Chim. Slov.* 64, 692 (2017)
- [105] J. Albadi, A. Mansournezhad, S. Salehnasab, *Res. Chem. Intermed.* 41, 5713 (2015)
- [106] S. Rahmani, B. Zeynizadeh, *Res. Chem. Intermed.* 45, 1227 (2019)
- [107] Z. Karimi-Jaberi, M.R. Nazarifar, B. Pooladian, *Chin. Chem. Lett.* 23, 781 (2012)
- [108] R. Rezaei, F. Moezzi, M.M. Doroodmand, *Chin. Chem. Lett.* 25, 183 (2014)
- [109] R. Rezaei, M.R. Sheikhi, *Res. Chem. Intermed.* 41, 1283 (2015)
- [110] Overbury SH, Schwartz V, Mullim DR, Yan WF, Dai S (2006) Evaluation of the Au size effect: CO oxidation catalyzed by Au/TiO₂. *J Catal* 241(1):56–65. <https://doi.org/10.1016/j.jcat.2006.04.018>
- [111] Xie MR, Ding L, You ZW, Gao DY, Yang GD, Han HJ (2012) Robust hybrid nanostructures comprising gold and thiol-functionalized polymer nanoparticles: facile preparation, diverse morphologies and unique properties. *J Mater Chem* 22(28):14108–14118. <https://doi.org/10.1039/c2jm31228j>
- [112] Praharaj S, Nath S, Ghosh SK, Kundu S, Pal T (2004) Immobilization and recovery of Au nanoparticles from anion exchange resin: resin-bound nanoparticle matrix as a catalyst for the reduction of 4-nitrophenol. *Langmuir* 20(23):9889–9892. <https://doi.org/10.1021/la0486281>
- [113] Ferrara MC, Mirengi L, Mevoli A, Tapfer L (2008) Synthesis and characterization of sol-gel silica films doped with size-selected gold nanoparticles. *Nanotechnology* 19(36):9. <https://doi.org/10.1088/0957-4484/19/36/365706>
- [114] Zhu KK, Hu JC, Richards R (2005) Aerobic oxidation of cyclohexane by gold nanoparticles immobilized upon mesoporous silica. *Catal Lett* 100(3–4):195–199. <https://doi.org/10.1007/s10562-004-3454-5>
- [115] Li J, Liu CY, Liu Y (2012) Au/graphene hydrogel: synthesis, characterization and its use for catalytic reduction of 4-nitrophenol. *J Mater Chem* 22(17):8426–8430. <https://doi.org/10.1039/c2jm16386a>
- [116] Porta F, Prati L (2004) Selective oxidation of glycerol to sodium glycerate with gold-on-carbon catalyst: an insight into reaction selectivity. *J Catal* 224(2):397–403. <https://doi.org/10.1016/j.jcat.2004.03.009>
- [117] Xiong ZG, Zhang LL, Ma JZ, Zhao XS (2010) Photocatalytic degradation of dyes over graphene-gold nanocomposites under visible light irradiation. *Chem Commun* 46(33):6099–6101. <https://doi.org/10.1039/c0cc01259a>
- [118] Haruta M (2002) *CATTECH* 6(3):102–115
- [119] Ousmane M, Liotta LF, Pantaleo G, Venezia AM, Di Carlo G, Aouine M, Retailleau L, Giroir-Fendler A (2011) Supported Au catalysts for propene total oxidation: study of support morphology and gold particle size effects. *Catal Today* 176(1):7–13. <https://doi.org/10.1016/j.cattod.2011.07.009>
- [120] Schubert MM, Hackenberg S, Van Veen AC, Muhler M, Plzak V, Behm RJ (2001) CO oxidation over supported gold catalysts—“inert” and “active” support materials and their role for the oxygen supply during reaction. *J Catal* 197(1):113–122. <https://doi.org/10.1006/jcat.2000.3069>
- [121] Liotta LF, Di Carlo G, Pantaleo G, Venezia AM (2010) Supported gold catalysts for CO oxidation and preferential oxidation of CO in H₂ stream: support effect. *Catal Today* 158(1–2):56–62. <https://doi.org/10.1016/j.cattod.2010.04.049>
- [122] Miyamura H, Matsubara R, Miyazaki Y, Kobayashi S (2007) Aerobic oxidation of alcohols at room temperature and atmospheric conditions catalyzed by reusable gold nanoclusters stabilized by the benzene rings of polystyrene derivatives. *Angew Chem Int Edit* 46(22):4151–4154. <https://doi.org/10.1002/anie.200700080>
- [123] Sun L, Boo WJ, Sue H-J, Clearfield A (2007) Preparation of α -zirconium phosphate nanoplatelets with wide variations in aspect ratios. *New J Chem* 31(1):39–43. <https://doi.org/10.1039/b604054c>
- [124] Sun LY, Boo WJ, Clearfield A, Sue HJ, Pham HQ (2008) Barrier properties of model epoxy nanocomposites. *J Membr Sci* 318(1–2):129–136. <https://doi.org/10.1016/j.memsci.2008.02.041>
- [125] Alonso F, Beletskaya IP, Yus M (2008) Non-conventional methodologies for transition-metal catalysed carbon-carbon coupling: A critical overview. Part 2: the Suzuki reaction. *Tetrahedron* 64(14):3047–3101
- [126] Yin L, Liebscher J. Carbon-carbon coupling reactions catalyzed by heterogeneous palladium catalysts. *Chem Rev*, 2007, 107: 133–173
- [127] Li H, Wang L, Yang M, Qi Y (2012) Palladium supported on amine-functionalized mesoporous silica: Highly efficient phosphine-free catalyst for alkyne-alkyne cross-coupling reaction. *Catal Commun* 17:179–183
- [128] Zhu J, Zhou J, Zhao T, Zhou X, Chen D, Yuan W (2009) Carbon nanofiber-supported palladium nanoparticles as potential recyclable catalysts for the Heck reaction. *Appl Catal A* 352(1):243–250
- [129] Datta K, Eswaramoorthy M, Rao C (2007) Water-solubilized aminoclay-metal nanoparticle composites and their novel properties. *J Mater Chem* 17(7):613–615
- [130] Su FZ, Liu YM, Wang LC, Cao Y, He HY, Fan KN (2008) Ga-Al mixed-oxide-supported gold nanoparticles with enhanced

- activity for aerobic alcohol oxidation. *Angew Chem* 120(2):340–343
- [131] Moussa S, Siamaki A, Gupton B, et al. Pd-partially reduced graphene oxide catalysts (Pd/PRGO): laser synthesis of Pd nanoparticles supported on PRGO nanosheets for carbon-carbon cross coupling reactions. *ACS Catal*, 2012, 2: 145–154
- [132] Veerakumar P, Balakumar S, Velayudham M, Lu K-L, Rajagopal S (2012) Ru/Al₂O₃ catalyzed N-oxidation of tertiary amines by using H₂O₂. *Catal Sci Technol* 2(6):1140–1145
- [133] Veerakumar P, Velayudham M, Lu K-L, Rajagopal S (2013) Silica-supported PEI capped nanopalladium as potential catalyst in Suzuki, Heck and Sonogashira coupling reactions. *Appl Catal A* 455:247–260
- [134] Bertolini G, Casagrande C, Santangelo F (1992) 1,2,3-triazole compounds active as inhibitors of the enzyme hmg-coa reductase and pharmaceutical compositions containing them. US Patent 5,081,136, 14 Jan
- [135] Lattmann R, Acklin P (2003) Substituted 3,5-diphenyl-1,2,4-triazoles and their use as pharmaceutical metal chelators. US Patent 6,596,750, 22 Jul
- [136] Aher NG, Pore VS, Mishra NN, Kumar A, Shukla PK, Sharma A, Bhat MK (2009) *Bioorg Med Chem Lett* 19:759
- [137] Wang XL, Wan K, Zhou CH (2010) *Eur J Med Chem* 45:4631
- [138] Agalave SG, Maujan SR, Pore VS (2011) *Chem Asian J* 6:2696
- [139] Nagarajan S, Shanmugavelan P, Sathishkumar M, Selvi R, Ponnuswamy A, Harikrishnan H, Shanmugaiah V (2014) *Chin Chem Lett* 25:419
- [140] Whiting M, Muldoon J, Lin YC, Silverman SM, Lindstrom W, Olson AJ, Kolb HC, Finn MG, Sharpless KB, Elder JH, Fokin VV (2006) *Angew Chem Int Ed* 45:1435
- [141] da Silva FC, de Souza MCBV, Frugulhetti IIP, Castro HC, Souza SLdO, de Souza TML, Rodrigues DQ, Souza AMT, Abreu PA, Passamani F, Rodrigues CR, Ferreira VF (2009) *Eur J Med Chem* 44:373
- [142] Singh P, Raj R, Kumar V, Mahajan MP, Bedi PMS, Kaur T, Saxena AK (2012) *Eur J Med Chem* 47:594
- [143] Kumar A, Ahmad I, Chhikara BS, Tiwari R, Mandal D, Parang K (2011) *Bioorg Med Chem Lett* 21:1342
- [144] Bratsos I, Urankar D, Zangrando E, Genova-Kalou P, Kosmrlj J, Alessio E, Turel I (2011) *Dalton Trans* 40:5188
- [145] Kamal A, Prabhakar S, Ramaiah MJ, Reddy PV, Reddy CR, Mallareddy A, Shankaraiah N, Reddy TLN, Pushpavalli SNCVL, Pal-Bhadra M (2011) *Eur J Med Chem* 46:3820
- [146] Shafi S, Mahboob Alam M, Mulakayala N, Mulakayala C, Vanaja G, Kalle AM, Pallu R, Alam MS (2012) *Eur J Med Chem* 49:324
- [147] Rao PS, Kurumurthy C, Veeraswamy B, Santhosh Kumar GS, Poornachandra Y, Ganesh Kumar CG, Vasamsetti SB, Kotamraju S, Narsaiah B (2014) *Eur J Med Chem* 80:184
- [148] Shanmugavelan P, Nagarajan S, Sathishkumar M, Ponnuswamy A, Yogeewari P, Sriram D (2011) *Bioorg Med Chem Lett* 21:7273
- [149] Jordão AK, Sathler PC, Ferreira VF, Campos VR, de Souza MCBV, Castro HC, Lannes A, Lourenco A, Rodrigues CR, Bello ML, Lourenco MCS, Carvalho GSL, Almeida MCB, Cunha AC (2011) *Bioorg Med Chem* 19:5605
- [150] Ruijter E, Scheffelaar R, Orru RVA (2011) *Angew Chem Int Ed* 50:6234
- [151] Candeias NR, Montalbano F, Cal PMSD, Gois PMP (2010) *Chem Rev* 110:6169
- [152] Li M, Zuo Z, Wen L, Wang S (2008) *J Comb Chem* 10:436
- [153] Guchhait SK, Chandgude AL, Priyadarshani G (2012) *J Org Chem* 77:4438
- [154] Liéby-Muller F, Constantieux T, Rodriguez J (2005) *J Am Chem Soc* 127:17176
- [155] Sharghi H, Shiri P, Aberi M (2014) *Mol Divers* 18:559
- [156] Sharghi H, Aberi M (2014) *Synlett* 25:1111
- [157] Sharghi H, Beyzavi MH, Doroodmand MM (2008) *Eur J Org Chem* 2008:4126
- [158] Amantini D, Beleggia R, Fringuelli F, Pizzo F, Vaccaro L (2004) *J Org Chem* 69:2896
- [159] Sharghi H, Aberi M, Doroodmand MM (2008) *Adv Synth Catal* 350:2380
- [160] Sharghi H, Beyzavi MH, Safavi A, Doroodmand MM, Khalifeh R (2009) *Adv Synth Catal* 351:2391
- [161] Sharghi H, Ebrahimpourmoghaddam S, Doroodmand MM, Purkhosrow A (2012) *Asian J Org Chem* 1:377
- [162] Sharghi H, Shiri P, Aberi M (2014) *Synthesis* 46:2489
- [163] Sharghi H, Hosseini-Sarvari M, Moeini F, Khalifeh R, Beni AS (2010) *Helv Chim Acta* 93:435
- [164] Balamurugan V, Shankar S, Chandramohan S (2014) *J Biol Chem* 8:85
- [165] Yang F, Gao S, Xiong CR, Long SF, Li XM, Xi T, Kong Y (2015) Direct templating assembly route for the preparation of highly-dispersed vanadia species encapsulated in mesoporous MCM-41 channel. *RSC Adv* 5:72099–72106
- [166] Aguila G, Gracia F, Araya P (2008) CuO and CeO₂ catalysts supported on Al₂O₃, ZrO₂, and SiO₂ in the oxidation of CO at low temperature. *Appl Catal A* 343:16–24
- [167] Kuniarska-Biernacka I, Raposo MMM, Batista R, Parpot P, Biernacki K, Magalhaes AL, Fonseca AM (2016) Highly efficient heterogeneous catalysts for phenol oxidation: binuclear pyrrolyl-azine metal complexes encapsulated in NaY zeolite. *Microporous Mesoporous Mater* 227:272–280

- [168] Wu N, Li B, Liu J, Zuo S, Zhao Y (2016) Preparation and catalytic performance of a novel highly dispersed bifunctional catalyst Pt@Fe-MCM-41. *Rsc Adv* 6:13461–13468
- [169] Yu X, Chen J, Ren T (2014) Promotional effect of Fe on performance of Ni/SiO₂ for deoxygenation of methyl laurate as a model compound to hydrocarbons. *Rsc Adv* 4:46427–46436
- [170] Lu R, Mao D, Yu J, Guo Q (2015) Enhanced activity of Cu-Fe/SiO₂ catalyst for CO hydrogenation to higher alcohols by pretreating the support with ammonia. *J Ind Eng Chem* 25:338–343
- [171] Braganca LFFPG, Avillez RR, Moreira CR, Pais da Silva MI (2013) Synthesis and characterization of Co-Fe nanoparticles supported on mesoporous silicas. *Mater Chem Phys* 138:17–28
- [172] Tsoncheva T, Genova I, Stoyanova M (2014) Effect of mesoporous silica topology on the formation of active sites in copper supported catalysts for methanol decomposition. *Appl Catal B* 147:684–697
- [173] Yamashita T, Hayes P (2008) Analysis of XPS spectra of Fe²⁺ and Fe³⁺ ions in oxide materials. *Appl Surf Sci* 254:2441–2449
- [174] Gao J, Lu L, Zhou W, Gao G, He M (2008) *J Porous Mater* 15:127
- [175] Fernandez I, Khiar N (2003) *Chem Rev* 103:3651
- [176] Darabi M, Tamoradi T, Ghadermazi M, Ghorbani-Choghamarani A (2017) *Transit Met Chem* 42:703
- [177] Rezaeifard A, Jafarpour M, Raissi H, Ghiamati E, Tootoonchi A (2011) *Polyhedron* 30:592
- [178] Kazemi M, Shiri L (2015) *J Sulfur Chem* 36:613
- [179] Jeon HB, Kim KT, Kim SH (2014) *Tetrahedron Lett* 55:3905
- [180] Khanmoradi M, Nikoorazm M, Ghorbani-Choghamarani A (2017) *Appl Organomet Chem*. <https://doi.org/10.1002/aoc.3693>
- [181] Shiri L, Ghorbani-Choghamarani A, Kazemi M (2017) *Res Chem Intermed* 43:2707
- [182] Behroozi SJ, Kim W, Gates KS (1995) *J Org Chem* 60:3964
- [183] Ghorbani-Choghamarani A, Zamani P (2011) *J Iran Chem Soc* 8:142
- [184] Davarpanah J, Kiasat AR (2014) *Catal Commun* 46:75
- [185] Weissbach H, Etienne F, Hoshi T, Heinemann SH, Lowther WT, Matthews B, Johne GS, Nathane C, Brote N (2002) *Arch Biochem Biophys* 397:172
- [186] Noori N, Nikoorazm M, Ghorbani-Choghamarani A (2017) *Catal Lett* 147:204
- [187] Nikoorazm M, Ghorbani-Choghamarani A, Noori N (2015) *J Porous Mater* 22:877
- [188] Kiasat AR, Davarpanah J (2015) *Catal Commun* 69:179
- [189] Hajipour AR, Mostafavi M, Ruoho AE (2009) *Sulfur Silicon Relat Elem* 184:1920
- [190] Tamoradi T, Ghadermazi M, Ghorbani-Choghamarani A (2018) *Appl Organomet Chem*. <https://doi.org/10.1002/aoc.3974>
- [191] Zheng DM, Wang RQ, Du Y, Hou GF, Wu LX, Bi LH (2016) A new organo-ruthenium substituted tungstotellurate: synthesis, structural characterization and catalytic properties. *New J Chem* 40:8829–8836
- [192] Wang RQ, Suo L, Zheng DM, Du Y, Wu LX, Bi LH (2016) A heterogeneous catalyst containing tetra-ruthenium (IV)-substituted silicotungstate: preparation, characterization and catalytic performance toward oxidation of n-tetradecane with air. *Inorg Chim Acta* 443:218–223
- [193] Zhou Y, Chen G, Long Z, Wang J (2014) Recent advances in polyoxometalate-based heterogeneous catalytic materials for liquid-phase organic transformations. *RSC Adv* 4:42092–42113
- [194] Xing W, Ni L, Huo P, Lu Z, Liu X, Luo Y, Yan Y (2012) Preparation high photocatalytic activity of CdS/halloysite nanotubes (HNTs) nanocomposites with hydrothermal method. *Appl Surf Sci* 259:698–704
- [195] Moslehyani A, Ismail AF, Othman MHD, Matsuura T (2015) Hydrocarbon degradation and separation of bilge water via a novel TiO₂-HNTs/PVDF-based photocatalytic membrane reactor (PMR). *RSC Adv* 5:14147–14155
- [196] Das S, Jana S (2015) A facile approach to fabricate halloysite/metal nanocomposites with preformed and in situ synthesized metal nanoparticles: a comparative study of their enhanced catalytic activity. *Dalton Trans* 44:8906–8916
- [197] Kalinina IV, Izarova NV, Kortz U (2012) Bis[tetra-ruthenium(IV)]-containing polyoxometalates: [Ru^{IV}O₆(H₂O)₉]₂Sb₂W₂O₆₈(OH)₂]⁴⁻ and [Ru^{IV}O₆(H₂O)₉]₂[Fe(H₂O)₂]₂[β-TeW₉O₃₃]₂H]⁻. *Inorg Chem* 51:7442–7444
- [198] J. Albadi, N. Iravani, M. Khoshakhlagh, Iran. *J. Catal.* 2, 85 (2012)
- [199] K. Tanaka, F. Toda, *Chem. Rev.* 100, 1025 (2000)
- [200] D. Zareyee, B. Karimi, *Tetrahedron Lett.* 48, 1277 (2007)
- [201] N.A. Ibrahim, M. Shahmiri, K. Shameli, N. Zainuddin, H. Jahangirian, *Adv. Sci. Eng. Med.* 5, 193 (2013)
- [202] Liu LL, Zhang X, Gao JS, Xu CM (2012) *Green Chem* 14:1710–1720
- [203] Zhang X, Corma A (2008) *Angew Chem Int Ed* 47:4358–4361
- [204] Nasrollahzadeh M, Sajadi SM (2015) *RSC Adv* 5(57):46240–46246
- [205] Villaverde G, Corma A, Iglesias M, Sánchez F (2012) *ACS Catal* 2(3):399–406
- [206] Lo VKY, Liu Y, Wong MK, Che CM (2006) *Org Lett* 8:1529–1532
- [207] Wei C, Li Z, Li CJ (2003) *Org Lett* 5:4473–4475
- [208] Palchak ZL, Lussier DJ, Pierce CJ, Larsen CH (2015) *Green Chem* 17(3):1802–1810

- [209] Hua P, Lei W (2005) *Chin J Chem* 23(8):1076–1080
- [210] Li CJ, Wei C (2002) *Chem Commun* 3:268–269
- [211] Yoon M, Srirambalaji R, Kim K (2011) *Chem Rev* 112:1196
- [212] Horike SM, Dincă K, Tamaki K, Long GR (2008) *J Am Chem Soc* 130:5854–5855
- [213] Chughtai A, Ahmad N, Younus H, Laypkov A, Verpoort F (2015) Metal–organic frameworks: versatile heterogeneous catalysts for efficient catalytic organic transformations. *Chem Soc Rev* 44:6804–6849
- [214] Song F, Wang C, Falkowski JM, Ma L, Lin W (2010) *J Am Chem Soc* 132:15390
- [215] Jiang H-L, Makal TA, Zhou H-C (2013) *Coord Chem Rev* 257:2232
- [216] Keller TC, Isabettini S, Verboekend D, Rodrigues EG, Pérez-Ramírez J (2014) *Chem Sci* 5:677
- [217] Ibanez S, Poyatos M, Dawe LN, Gusev D, Peris E (2016) *Organometallics* 35:2747
- [218] Loxq P, Debono N, Gulcernal S, Daran JC, Manoury E, Poli R, Cetinkaya B, Labande A (2014) *New J Chem* 38:338
- [219] Liu C-X, Liu Q, Guo C-C (2010) *Catal Lett* 138:96
- [220] Nasir Baig RB, Varma RS (2013) *Chem Commun* 49:752
- [221] Rossi LM, Vono LLR, Silva FP, Kiyohara PK, Duarte EL, Matos JR (2007) *Appl Catal A* 330:139
- [222] Hajipour AR, Tadayoni NS, Khorsandi Z (2016) *Appl Organomet Chem* 30:590
- [223] Gawande MB, Luque R, Zboril R (2014) *ChemCatChem* 6:3312
- [224] de Resende Filho JBM, Pires GP, de Oliveira Ferreira JMG, Teotonio EES, Vale JA (2017) *Catal Lett* 147:167
- [225] Gawande MB, Branco PS, Varma RS (2013) *Chem Soc Rev* 42:3371–3393
- [226] Karimi B, Mansouri F, Mirzaei HM (2015) *ChemCatChem* 7:1736
- [227] Kurane R, Jadhav J, Khanpure S, Salunkhe R, Rashinkar G (2013) *Green Chem* 15:1849
- [228] A.M. Tafesh, J. Weiguny, *Chem. Rev.* 96, 2035 (1996)
- [229] W. Wang, Y. Xi, S. Zhang, X. Liu, M. Haruta, J. Huang, *Catalysts* 8, 60 (2018)
- [230] E. Menumerov, R.A. Hughes, S. Neretina, *Nano Lett.* 16, 7791 (2016)
- [231] Z. Wu, X. Yuan, H. Zhong, H. Wang, G. Zeng, X. Chen, H. Wang, L. Zhang, J. Shao, *Sci. Rep.* 6, 25638 (2016)
- [232] M. Shokouhimehr, M.S. Asl, B. Mazinani, *Res. Chem. Intermed.* 44, 1617 (2018)
- [233] A. Haghightzadeh, B. Mazinani, M. Shokouhimehr, L. Samiee, *Desalin. Water Treat.* 92, 145 (2018)
- [234] Y. Lee, T.G. Park, *Langmuir* 27, 2971 (2011)
- [235] M. Scampicchio, J. Wang, A.J. Blasco, A. Sanchez Arribas, S. Mannino, A. Escarpa, *Anal. Chem.* 78, 2063 (2006)
- [236] H. Lee, S.M. Dellatore, W.M. Miller, P.B. Messersmith, *Science* 318, 430 (2007)
- [237] K.C. Black, Z. Liu, P.B. Messersmith, *Chem. Mater.* 23, 1135 (2011)
- [238] X.Q. Wu, D.D. Huang, Z.H. Zhou, W.W. Dong, Y.P. Wu, J. Zhao, D.S. Li, Q. Zhang, X. Bu, *Dalton Trans.* 46, 2438 (2017)
- [239] A. Masahiko, Z. Fengyu, *Catalyst* 5, 868 (2015)
- [240] D. Zhao, J. Feng, Q. Huo, N. Melosh, G.H. Fredrickson, B.F. Chmelka, G.D. Stucky, Triblock copolymer syntheses of mesoporous silica with periodic 50–300 Angstrom pores. *Science* 279, 548–552 (1998)
- [241] X.B. Li, Z.J. Li, Y.J. Gao, Q.Y. Meng, S. Yu, R.G. Weiss, G.H. Tung, L.Z. Wu, *Angew. Chem. Int. Ed.* 53, 2085 (2014)
- [242] E. Rattanangkool, W. Krailat, T. Vilaivan, P. Phuwapraisirisan, M. Sukwattanasinitt, S. Wacharasindhu, *Eur. J. Org. Chem.* 22, 4795 (2014)
- [243] M. Hajjami, F. Ghorbani, Z. Yousofvand, *Appl. Organometal. Chem.* 2017
- [244] J.G. Smith, *Synthesis* 629, 629–656 (1984)
- [245] H. Firouzabadi, N. Iranpoor, A.A. Jafari, S. Makarem, *J. Mol. Catal. A: Chem.* 250, 237 (2006)
- [246] V. Mirkani, S. Tangestaninejad, B. Yadollahi, L. Alipanah, *Tetrahedron* 59, 8213 (2003)
- [247] K. Fagnou, M. Lautens, *Org. Lett.* 2, 2319 (2000)
- [248] S. Tangestaninejad, M. Moghadam, V. Mirkhani, B. Yadollahi, S.M.R. Mirmohammadi, *Monat. fur Chem.* 137, 235 (2006)
- [249] N. Iranpoor, H. Adibi, *Bull. Chem. Soc. J* 73, 675 (2000)
- [250] S. Mohammadpoor-Baltork, H. Tangestaninejad, V. Aliyan, Mirkhani. *Synth. Commun.* 30, 2365 (2000)
- [251] C. Grundwald, O. Gevert, J. Wolf, P. Gonzales-Herrero, H. Werner, *Organometallics* 15, 1960 (1996)
- [252] S.T. Nguyen, L.K. Johnson, R.H. Grubbs, J.W. Ziller, *J. Am. Chem. Soc.* 114, 3974 (1992)
- [253] B.M. Novak, R.H. Grubbs, *J. Am. Chem. Soc.* 110, 7542 (1988)
- [254] A.J. Ancieux, A.J. Hubert, A.F. Noels, N. Petiniot, P. Teyssie, *J. Org. Chem.* 45, 695 (1980)
- [255] E.A. Demonceau, C.A. Diaz, A.V. Lemoine, C. Stumpf, J. Petraszuk, B. Gulinski, Marcinec. *Tetrahedron Lett.* 36, 3519 (1995)
- [256] K.Q. Tfouni, F.G. Ferreira, R.S. Doro, Z.N. DaSilva, DaRocha. *Coord. Chem. Rev.* 249, 405 (2005)
- [257] M. Zaja, S.J. Connon, A.M. Dunne, M. Rivard, N. Buschmann, J. Jiricek, S. Blechert, *Tetrahedron* 59, 6545 (2003)

- [258] I.J. Munslow, K.M. Gillespie, R.J. Deeth, P. Scott, Chem. Commun. 1638, (2001)
- [259] R. Kardanpour, S. Tangestaninejad, V. Mirkhani, M. Moghadam, I. Mohammadpoor-Baltork, F. Zadehahmadi, J. Solid State Chem. 226, 262 (2015)
- [260] C.J. Doonan, W. Morris, H. Furukawa, O.M. Yaghi, J. Am. Chem. Soc. 131, 9492 (2009)
- [261] R. Kitaura, G. Onoyama, H. Sakamoto, S. Matsuda, R. Noro, S. Kitagawa, Angew. Chem. Int. Ed. 43, 2684 (2004)
- [262] M. Shultz, A.A. Sarjeant, O.K. Farha, J.T. Hupp, S.T. Nguyen, J. Am. Chem. Soc. 133, 13252 (2011)
- [263] P.W. Roesky, A. Bhunia, Y. Lan, A.K. Powell, S. Kureti, Chem. Commun. 47, 2035 (2011)
- [264] Zhou HC, Long JR, Yaghi OM (2012) Introduction to metal-organic frameworks. Chem Rev 112:673–674. doi: 10.1021/cr300014x
- [265] Alaerts L, Seguin E, Poelman H, Thibault-Starzyk H, Jacobs PA, De Vos DE (2006) Chem Eur J 12:7353
- [266] Wu F, Qiu LG, Ke F, Jiang X (2013) Copper nanoparticles embedded in metal-organic framework MIL-101(Cr) as a high performance catalyst for reduction of aromatic nitro compounds. Inorg Chem Commun 32:5–8. doi: 10.1016/j.inoche.2013.03.003
- [267] Dwivedi S, Taniike T, Terano M (2014) Understanding the chemical and physical transformations of a Ziegler-Natta catalyst at the initial stage of polymerization kinetics: the key role of alkylaluminum in the catalyst activation process. Macromol Chem Phys 215:1698–1706
- [268] Cipullo R, Mellino S, Busico V (2014) Identification and count of the active sites in olefin polymerization catalysis by oxygen quench. Macromol Chem Phys 215:1728–1734
- [269] Chien JCW, Wu JC, Kuo CI (1982) Magnesium chloride supported high-mileage catalysts for olefin polymerization. I. Chemical composition and oxidation states of titanium. J Polym Sci Polym Chem Ed 20:2019–2032
- [270] Chien JCW, Wu JC, Kuo CI (1983) Magnesium chloride supported high-mileage catalysts for olefin polymerization. IV. FTIR and quantitative analysis of modifiers in the catalysts. J Polym Sci Polym Chem Ed 21:725–736

2. Towards Higher Catalytic Activity

Highly Efficient and Convenient Supported Ionic Liquid $\text{TiCl}_5\text{-DMIL@SiO}_2\text{@Fe}_3\text{O}_4\text{-Catalyzed Cycloaddition of CO}_2\text{ and Epoxides to Cyclic Carbonates}$

DOI: 10.1007/s10562-017-2051-3

Publication outline: Introduction | Experimental | Results and Discussion | Conclusion

Abstract-Summary

A series of silica coated magnetic nanoparticles supported ILS were prepared, characterized and their catalytic performances

in cycloaddition of CO_2 to epoxides were investigated. Research shows that $\text{TiCl}_5\text{-DMIL@SiO}_2\text{@Fe}_3\text{O}_4$ could be used as the highest efficient catalyst in cycloaddition of CO_2 and epoxides to gives the corresponding cyclic carbonates. The heterogeneous supported catalyst is easily recoverable by filtration, and could be used for five consecutive runs without significant loss in catalytic activity.

Extended:

Research shows that $\text{TiCl}_5\text{-DMIL@SiO}_2\text{@Fe}_3\text{O}_4$ is the most effective catalyst in the titled reaction.

Eco-friendly highly efficient solvent free synthesis of benzimidazole derivatives over sulfonic acid functionalized graphene oxide in ambient condition

DOI: 10.1007/s11164-016-2745-y

Publication outline: Introduction | Experimental | Results and discussion | Conclusions

Abstract-Summary

Using prepared heterogeneous catalyst GO-HSO_3 , benzimidazole synthesis was carried out by means of reacting diamine and aldehyde at room temperature in solvent free condition. The catalyst GO-HSO_3 showed tremendous catalytic activity in selective synthesis of benzimidazole, as a result 100 % conversion of reactants and up to 89.0 % yield of respective benzimidazole was achieved using 0.1 mg of catalyst in very short reaction duration. The present method is found eco-friendly, highly efficient, solvent free, high yielding, and clean method for the synthesis benzimidazole derivatives at room temperature.

Extended:

These results indicate that, the present methodology is highly eco-friendly and green approach for the preparation of benzimidazole derivatives.

Ruthenium Nanoparticles Immobilized on Nano-silica Functionalized with Thiol-Based Dendrimer: A Nanocomposite Material for Oxidation of Alcohols and Epoxidation of Alkenes

DOI: 10.1007/s10562-018-2313-8

Publication outline: Introduction | Experimental Section | Results and Discussion | Conclusion

Abstract-Summary

Ruthenium nanoparticles were immobilized on thiol-based dendrimer functionalized nano-silica and its catalytic activity was investigated in the oxidation reactions. The catalytic activity of this nanocomposite material as a heterogeneous catalyst was studied in the epoxidation of alkenes and oxidation of alcohols with tert-butyl hydroperoxide (tert-BuOOH) and the corresponding products were obtained in good to excellent yields. $\text{Ru}_{\text{np-nSTDP}}$ provided a highly stable, active, reusable, and solid-phase catalyst for preparation of a series of epoxides and aldehydes.

Extended:

The average core diameter (D) is about 2 nm.

[Suzuki–Miyaura Cross-Coupling in Aqueous Medium Using Recyclable Palladium/Amide-Silica Catalyst](#)

DOI: 10.1007/s10562-016-1796-4

Publication outline: Introduction | Results and Discussion | Conclusions | Experimental Sections | Preparation of Catalyst

Abstract-Summary

The complex exhibits excellent catalytic activity and stability for Suzuki–Miyaura cross-coupling reaction under mild aqueous reaction condition. Various aryl bromides were coupled with arylboronic acids in *i*-PrOH/H₂O, under open air at room temperature, in the presence of 0.22 mol% of the catalyst to afford corresponding cross-coupled products in high yields.

[Highly Active and Recyclable Mesoporous Molecular Sieves CaO\(SrO,BaO\)/SBA-15 with Base Sites as Heterogeneous Catalysts for Methanolysis of Polycarbonate](#)

DOI: 10.1007/s10562-017-2193-3

Publication outline: Introduction | Experimental | Results and Discussion | Conclusion

Abstract-Summary

Mesoporous molecular sieves CaO(BaO, SrO)/SBA-15, which can produce basic sites, were synthesized by impregnation of a certain amount of CaO(BaO, SrO) on the synthesis of SBA-15 support, and used as heterogeneous catalysts for the methanolysis of polycarbonate (PC). The results showed that CaO/SBA-15 exhibited better catalytic activity than BaO/SBA-15 and SrO/SBA-15, and its catalytic activity was related to the loading amount of CaO. Moreover, the obtained product from the methanolysis of PC was mainly bisphenol A (BPA) with high purity. The influences on reaction conditions of PC methanolysis catalyzed by 10%CaO/SBA-15 were also investigated. The stability of catalyst showed that 10%CaO/SBA-15 catalysts could be recycled and reused with negligible loss in activity over five cycles.

[Highly active recyclable SBA-15-EDTA-Pd catalyst for Mizoroki-Heck, Stille and Kumada C–C coupling reactions](#)

DOI: 10.1007/s10934-016-0323-8

Publication outline: Introduction | Experimental | Results and discussion | Catalytic activity | Conclusions

Abstract-Summary

SBA-15-EDTA-Pd(II) catalyst was found to exhibit excellent catalytic activity in appreciable yield for Heck, Stille and Kumada cross-coupling reactions. Covalently anchored heterogeneous SBA-15-EDTA-Pd(II) catalyst can be recycled for more than five times without noticeable loss in activity and selectivity.

[Sustainable Oxidative Cleavage of Vegetable Oils into Diacids by Organo-Modified Molybdenum Oxide Heterogeneous Catalysts](#)

DOI: 10.1007/s11746-017-3047-2

Publication outline: Introduction | Experimental | Results and Discussion | Catalytic Test Results | Conclusions

Abstract-Summary

A novel catalytic system based on organo-modified molybdenum trioxide was synthesized by a green hydrothermal method in one simple step, using Mo powder as precursor, hydrogen peroxide, and amphiphilic surfactants cetyltrimethylammonium bromide (CTAB) and tetramethylammonium bromide (TMAB) as capping agents. The synthesized catalysts were employed in oxidative cleavage of oleic acid, the most abundant unsaturated fatty acid, to produce azelaic and pelargonic acids with a benign oxidant, H₂O₂.

Excellent catalytic activities resulting in full conversion of initial oleic acid were obtained, particularly for CTAB-capped molybdenum oxide (CTAB/Mo molar ratio of 1:3) that gave 83 and 68% yields of production of azelaic and pelargonic acids, respectively. The CTAB-capped catalyst could be conveniently separated from the reaction mixture by simple centrifugation and reused without significant loss of activity up to at least four cycles.

Extended:

We have tried to push the proved potential of molybdenum oxide as an oxidizing solid catalyst [46, 47–48] to oxidative cleavage reaction of unsaturated fatty acids.

[Functionalized Polystyrene Supported Copper\(I\) Complex as an Effective and Reusable Catalyst for Propargylamines Synthesis in Aqueous Medium](#)

DOI: 10.1007/s10562-016-1728-3

Publication outline: Introduction | Experimental | Results and Discussion | Test for Heterogeneity | Recycling of Catalyst | Comparative Study | Conclusions

Abstract-Summary

An efficient procedure for the one-pot synthesis of propargylamines is A³ coupling in which an alkyne, an aldehyde, and an amine are coupled together. We report that polystyrene supported Cu(I) catalyst is excellent for A³ coupling in water without using any additives or hazardous organic solvents. The polystyrene supported Cu(I) catalyst was synthesized and its catalytic activity was also evaluated in the synthesis of propargylamines in oxidative A³-coupling reaction with benzyl alcohols instead of their aldehydes in water. Polymer supported copper catalyst, Cu-PS-ala, acts as a heterogeneous catalyst for the one pot synthesis of propargylamines via A³ coupling reaction in water using aldehydes or alcohols, amines and alkynes.

Extended:

The simple protocol, broad scope of the substrates and recycling of the catalyst permitted us to look forward to a good future of this process in academic as well as in industry.

Modified Montmorillonite Clay Stabilized Silver Nanoparticles: An Active Heterogeneous Catalytic System for the Synthesis of Propargylamines

DOI: 10.1007/s10562-015-1679-0

Publication outline: Introduction | Experimental | Results and Discussion | Conclusion

Abstract-Summary

We have synthesized size selective silver nanoparticles (Ag-NPs) in the nanopores of modified montmorillonite clay by an "in situ" approach. The modification of montmorillonite K-10 was carried out with HCl under controlled condition for generating a high surface area and porous matrix which acted as hosts for the "in situ" generation of silver nanoparticles. The Ag-NPs stabilized on modified montmorillonite serves as an efficient green heterogeneous catalyst for the three component one-pot synthesis of propargylamines with 83–95 % yield and 100 % selectivity under mild reaction condition. Ag-NPs@mmt is found to be an efficient and robust heterogeneous catalyst for the synthesis of propargylamines under mild reaction condition.

Synthesis of Dowex functionalised half-sandwich Ru (II) (η^6 -p-cymene) complex as effective and selective hydrogenation of furfural to levulinic acid

DOI: 10.1007/s10965-021-02454-9

Publication outline: Introduction | Experimental section | Results and discussion | Conclusions

Abstract-Summary

The ruthenium(II) complex $[(\eta^6\text{-p-cymene})\text{Ru}(\text{Cl})(8\text{-amino quinoline})]$ and $[(\eta^6\text{-p-cymene})\text{Ru}(\text{OH}_2)(8\text{-amino quinoline})]$ were synthesised, characterised, and used to prepare novel ruthenium(II) based Dowex resin polymer $[(\eta^6\text{-p-cymene})\text{Ru}(\text{Cl} / \text{or } \text{OH}_2)(8\text{-amino quinoline})]@\text{Dowex}$. The ruthenium(II) complex based Dowex catalyst is synthesised by treatment of $[(\eta^6\text{-p-cymene})\text{Ru}(\text{Cl})(8\text{-amino quinoline})]$ or $[(\eta^6\text{-p-cymene})\text{Ru}(\text{OH}_2)(8\text{-amino quinoline})]$ with Dowex@Na via ion exchange synthesis, in the presence of DCM as a solvent forming $[(\eta^6\text{-p-cymene})\text{Ru}(\text{Cl} / \text{OH}_2)(8\text{-amino quinoline})]@\text{Dowex}$, respectively. The catalytic transfer hydrogenation of furfural over both Ru(II) complex based Dowex catalyst were investigated with formic acid as the hydrogen donor and water as the solvent at 80 °C after 19 h. The $[(\eta^6\text{-p-cymene})\text{RuCl} (8\text{-amino quinoline})]@\text{Dowex}$ and $[(\eta^6\text{-p-cymene})\text{RuOH}_2(8\text{-amino quinoline})]@\text{Dowex}$ catalysts were shown to exhibit high activity in the transfer hydrogenation of furfural to form a sole levulinic acid (Lv) giving good conversion and excellent selectivity under mild reaction conditions. Recyclability and leaching tests confirmed $[(\eta^6\text{-p-cymene})\text{Ru}(\text{OH}_2)(8\text{-amino quinoline})]$ complex to function as a heterogeneous catalyst which could be reused for at least four consecutive reaction runs without significant loss of catalytic activity.

Synthesis of a Cellulosic Pd(salen)-Type Catalytic Complex as a Green and Recyclable Catalyst for Cross-Coupling Reactions

DOI: 10.1007/s10562-020-03172-5

Publication outline: Introduction | Materials and Methods | Results and Discussion | Conclusion

Abstract-Summary

A green recyclable cellulose-supported Pd(salen)-type catalyst was synthesized through sequential three steps: chlorination with thionyl chloride, modification by ethylenediamine, and the formation of Schiff base with salicylaldehyde to immobilize palladium chloride through multiple binding sites. This novel heterogeneous cellulosic Pd(salen)-type catalytic complex was fully characterized by FT-IR, SEM, TEM, XPS, ICP-AES and TG. Studies have shown that the synthesized catalyst shows high activity and efficiency for all types of transformations, providing the corresponding carbon-carbon or carbon-heteroatom coupling products in a general and mild manner.

Heteropolyacid supported on amine-functionalized halloysite nano clay as an efficient catalyst for the synthesis of pyrazolopyranopyrimidines via four-component domino reaction

DOI: 10.1007/s11164-016-2756-8

Publication outline: Introduction | Experimental | Results and discussion | Conclusion

Abstract-Summary

An efficient heterogeneous hybrid catalyst was developed by functionalization of halloysite clay nanotubes by γ -aminopropyltriethoxysilane and then immobilization of a Keggin type heteropolyacid, phosphotungstic acid. This hybrid catalyst was characterized by SEM/EDX, FTIR and XRD and its catalytic activity for the synthesis of pyrazolopyranopyrimidine derivatives via four-component domino reaction of barbituric acid, hydrazine hydrate, ethyl acetoacetate and benzaldehyde was investigated. The results indicated that the hybrid system can promote the reaction to afford the desired products in high yields and short reaction times. It was re-used at least three times with negligible loss of activity.

Extended:

The results indicated the formation of the desired product in negligible yield after 1 h; this also can prove the slight leaching of HPA. The results indicated that microwave irradiation promoted the reaction in very short reaction time, 5 min.

Synthesis, characterization and catalytic activity of melamine immobilized MCM-41 for condensation reactions

DOI: 10.1007/s10934-017-0481-3

Publication outline: Introduction | Experimental | Results and discussion | Conclusions

Abstract-Summary

Melamine immobilized MCM-41 is synthesized by grafting on modified MCM-41. The surface area, pore size and pore volume of MCM-41-Mela were found to be decreased after immobilization of melamine. FTIR and Raman spectroscopy results revealed the successful grafting of melamine on the surface of MCM-41. The catalytic activity of MCM-41-Mela was then successfully carried out for Knoevenagel condensation with different substrates, giving excellent yields of the corresponding products. Simple preparation methods, high efficiency and reusability of the heterogeneous MCM-41-Mela catalyst demonstrate a great potential for future catalysis application.

Extended:

Melamine immobilized MCM-41 catalyst is successfully synthesized by feasible low cost route and utilised in condensation of furfural and acetylacetone under solvent-free reaction conditions.

[Citric acid stabilized on the surface of magnetic nanoparticles as an efficient and recyclable catalyst for transamidation of carboxamides, phthalimide, urea and thiourea with amines under neat conditions](#)

DOI: 10.1007/s13738-018-1523-8

Publication outline: Introduction | Results and discussion | Experimental procedures | Conclusion

Abstract-Summary

This magnetic nanocatalyst was employed as an efficient, recyclable, and environmentally benign heterogeneous catalyst for the transamidation of carboxamides, phthalimide, urea and thiourea with amines. The catalyst could be easily separated from the reaction mixture using an external magnet and can be reused six times without any significant loss in its catalytic activity.

[Cu\(OAc\)₂ entrapped on ethylene glycol-modified melamine–formaldehyde polymer as an efficient heterogeneous catalyst for Suzuki–Miyaura coupling reactions](#)

DOI: 10.1007/s11164-019-03984-0

Publication outline: Introduction | Result and discussion | Conclusions | Experimental section

Abstract-Summary

Morphological, physicochemical characteristics and catalytic activity of the heterogeneous catalyst (Cu@MCOP) were analyzed by various instrumental methods including powder X-ray diffraction, FT-IR, UV-DRS, X-ray photoelectron spectroscopy, SEM and elemental mapping which have been used to authenticate the polymeric materials Cu@MCOP. The catalytic performance of Cu@MCOP as solid heterogeneous catalyst was evaluated in synthesis of various biphenyl derivatives through Suzuki–Miyaura cross-coupling reactions of various aryl halides with substituted organoboranes under normal reaction conditions.

[Ru–PPh₃@porous organic polymer: efficient and stable catalyst for the trickle bed regioselective hydrogenation of cinnamaldehyde](#)

DOI: 10.1007/s11144-016-1130-6

Publication outline: Introduction | Experimental | Results and discussion | Conclusions

Abstract-Summary

Ru supported on the porous vinyl-functional triphenylphosphine organic polymer (Ru–PPh₃@POP) as a heterogeneous catalyst for the selective hydrogenation of cinnamaldehyde (CAL) was synthesized. This catalyst, which combines the advantages of heterogeneous and homogeneous catalyst, showed much higher catalytic activity of continuous trickle bed hydrogenation of CAL than traditional inorganic material supported heterogeneous catalysts. The high efficiency of the Ru–PPh₃@POP catalyst was attributed to the formation of the strong coordination bonds between the Ru species and the exposure phosphorus atoms on the surface of PPh₃@POP support according to the results of EDS-mapping, ³¹P NMR, XPS analysis and HRTEM. Ru species maintained their nanoparticles without further aggregation during the long-term reaction, and thus the catalyst exhibited a high conversion of CAL of 55% and selectivity towards cinnamyl alcohol (COL) of 63% even over 312 h of time on stream of hydrogenation of CAL.

[Pd Nanoparticles Immobilized on Supported Magnetic GO@PAMPS as an Auspicious Catalyst for Suzuki–Miyaura Coupling Reaction](#)

DOI: 10.1007/s10562-017-2089-2

Publication outline: Introduction | Experimental | Results and Discussion | Conclusion

Abstract-Summary

A novel catalytic system based on palladium nanoparticles (Pd-NPs) immobilized onto the surface of graphene oxide (GO) modified by poly 2-acrylamido-2-methyl-1-propanesulfonic acid decorated with magnetic Fe₃O₄ was designed, prepared and fully characterized. The results showed excellent catalytic activity for the cross coupling of aryl bromides, alkyl iodides as well as aryl chlorides as the challenging substrates. It was easily separated by an external magnet and reused without any pre-activation at least in seven consecutive runs without any loss in its catalytic activity as well as any detectable Pd leaching.

[Characterization and catalytic performance evaluation of a novel heterogeneous mesoporous catalyst for methanol–acetic acid esterification](#)

DOI: 10.1007/s10934-019-00764-4

Publication outline: Introduction | Experimental | Results and discussion | Conclusions

Abstract-Summary

A novel heterogeneous catalyst based on silicotungstic acid (STA) has been synthesised using hydrothermal and wet-impregnation methods for methanol–acetic acid esterification. Characterizations of MCM-48 and STA/MCM-48 catalysts were performed using BET, XRD, FT-IR, DRIFT, TGA/DTA, SEM, and EDX mapping analysis. The catalytic activity was also investigated in methyl acetate esterification reaction and it was shown that temperature, reaction time and the molar ratio of the reactants had significant effect on conversion rate. The highest catalytic activity was obtained as 84% with 20% catalyst at feed ratio of 1:3 (methanol:acetic acid, 353 K, 27 h).

Extended:

A novel heterogeneous mesoporous catalyst for MeOH–AA ER was prepared using silicotungstic acid (STA, surface area < 1 m²/g) as an active agent and MCM-48 as a mesoporous support material. Characterization and catalytic performance of a novel heterogeneous catalyst, STA/MCM-48, has been reported for MeOH–AA ER. The highest catalytic activity was obtained as 84% with 20% STA loadings at the feed ratio of 1:3 (MeOH:AA) and 353 K at 27 h. However, the reaction did not yet reach its equilibrium which suggests further optimizations needed for reactant molar ratios and experiment duration.

Immobilization of new macrocyclic Schiff base copper complex on graphene oxide nanosheets and its catalytic activity for olefins epoxidation

DOI: 10.1007/s10853-018-3035-4

Publication outline: Introduction | Experimental procedures | Results and Discussion | Conclusion

Abstract-Summary

A new heterogeneous copper–salophen catalyst was fabricated through the nucleophilic attack and esterification reaction of salophen Schiff base with graphene oxide (GO). The Schiff base was covalently grafted to the activated carboxyl group on GO through esterification reaction and also through the nucleophilic attack to epoxy groups. The prepared heterogeneous catalyst was used in the oxidation of olefins with H₂O₂/NaHCO₃ under mild condition. The influence of various parameters such as catalyst dosage, reaction time as well as reaction temperature on the epoxidation of norbornene was evaluated. The catalyst exhibits high activity and selectivity to target product; cyclohexene showed 100% conversion, without any by-product, and norbornene gave 100% conversion and 93% selectivity. The catalyst reused up to four more consecutive times without significant sacrificing activity. The high activity of catalyst can be ascribed to strong π–π stacking interaction between GO sheet and aromatic rings of salophen complex.

Extended:

The influence of various parameters such as reaction time, the dose of catalyst, as well as the reaction temperature on the epoxidation of norbornene was investigated, and the reaction was followed by GC. The high activity and high selectivity of GO–Cu–L as a heterogeneous catalyst can be attributed to the active sites of the Schiff base complex as a privileged ligand and the

synergistic catalytic interaction between the copper complex and GO as support [127, 128].

Palladium Nanoparticles Anchored on Thiol Functionalized Xylose Hydrochar Microspheres: An Efficient Heterogeneous Catalyst for Suzuki Cross-Coupling Reactions

DOI: 10.1007/s10562-019-02984-4

Publication outline: Introduction | Experimental Section | Results and Discussions | Conclusions

Abstract-Summary

Novel thiol functionalized xylose hydrochar microspheres supported palladium nanoparticles (C–SH–Pd) were synthesized by gentle heating of palladium (II) acetate and thiol functionalized xylose hydrochar (C–SH) in ethanol. The as-prepared C–SH–Pd exhibited high catalytic activity towards Suzuki reactions with a yield of high up to 100%. Due to the superior catalytic performance and stability of the C–SH–Pd catalyst, it can be exploited in other cross coupling reactions in the long run.

First Report About the Use of Micellar Keggin Heteropolyacids as Catalysts in the Green Multicomponent Synthesis of Nifedipine Derivatives

DOI: 10.1007/s10562-016-1784-8

Publication outline: Introduction | Experimental | Results and Discussion | Conclusion

Abstract-Summary

Micellar Keggin heteropolyacid catalysts were prepared using hexadecyltrimethylammonium bromide (cetyltrimethylammonium bromide—CTAB), 1-hexadecylpyridinium chloride, and Keggin heteropolyacids H₃PMo₁₂O₄₀ and H₄PMo₁₁VO₄₀ as precursors. This methodology requires a reaction time of 8 h, and a temperature of 78 °C to obtain good to excellent yields of 1,4-dihydropyridine derivatives. The micellar Keggin catalysts are insoluble in polar media, which allows easy removal of the reaction products without affecting their catalytic activity. The leaching test showed that they have an excellent stability and can be used five times as heterogeneous catalysts without appreciable loss of the catalytic activity.

Nitrogen-doped reduced graphene oxide-supported Mn₃O₄: An efficient heterogeneous catalyst for the oxidation of vanillyl alcohol to vanillin

DOI: 10.1007/s10853-016-0318-5

Publication outline: Introduction | Experimental section | Results and discussion | Conclusion

Abstract-Summary

The as-made N-RGO/Mn₃O₄ catalyst was used for the oxidation of vanillyl alcohol to vanillin. N,N-Dimethylformamide was found to be the best solvent, affording both high conversion and

vanillin selectivity. 92.5 % conversion of vanillyl alcohol and 91.4 % selectivity of vanillin were achieved after 12 h at 120 °C under oxygen balloon by the use of 40 mg of the N-GO/Mn₃O₄ catalyst. Kinetic studies revealed that the active energy for the oxidation of vanillyl alcohol to vanillin over N-GO/Mn₃O₄ catalyst was 39.67 kJ.mol⁻¹.

Harnessing CO₂ into Carbonates Using Heterogeneous Waste Derivative Cellulose-Based Poly(ionic liquids) as Catalysts

DOI: 10.1007/s10562-018-2637-4

Publication outline: Introduction | Experimental | Results and Discussion | Conclusion

Abstract-Summary

CPILs were used as heterogeneous catalysts for CO₂ chemical transformation into cyclic carbonates by cycloaddition of CO₂ with epoxides [propylene (PO) and styrene oxides (SO)]. The effect of the cation present in CPILs in catalytic performance, use of ZnBr₂ as a co-catalyst and catalytic reaction parameters (temperature, pressure and time) were investigated just as well. Results demonstrate that CPILs cation variation influence their catalytic activity. A higher CO₂ yield and selectivity of 81.9%/95.3% for propylene carbonate (PC) and 78.7%/100% for styrene carbonate (SC) was obtained by CPIL-TBP/ZnBr₂ at conditions of 40 bar, 110 °C and 6 h, being easily separated and recycled without significant loss of catalytic activity until the fourth cycle.

Preparation of metallic Pd nanoparticles using supercritical CO₂ deposition: An efficient catalyst for Suzuki cross-coupling reaction

DOI: 10.1007/s11051-018-4252-0

Publication outline: Introduction | Experimental | Results and discussion | Conclusions

Abstract-Summary

Ligand-free palladium nanoparticles supported on multi-walled carbon nanotubes (Pd/MWCNT) were prepared by the supercritical carbon dioxide (scCO₂) deposition method using a novel scCO₂-soluble Pd organometallic complex as a precursor. Pd/MWCNT was utilized as a heterogeneous catalyst in Suzuki cross-coupling reaction. The nanocatalyst was found very effective in Suzuki reaction and it could also be recovered easily from the reaction media and reused over several cycles without significant loss of catalytic activity under mild conditions.

Copper(II)-Substituted Polyoxotungstates Immobilized on Amine-Functionalized SBA-15: Efficient Heterogeneous Catalysts for Liquid Phase Oxidative Reaction

DOI: 10.1007/s10562-016-1874-7

Publication outline: Introduction | Experimental | Results and Discussion | Conclusions

Abstract-Summary

Results demonstrated that the heteropolyanions are highly dispersed on mesoporous materials. The resulting catalysts exhibited highly efficient catalytic activity for both the selective oxidation of benzyl alcohol to the benzaldehyde and the oxidation of thiophene with 30 % hydrogen peroxide as oxidant.

Carbon Quantum Dots-TiO₂ Nanocomposites with Enhanced Catalytic Activities for Selective Liquid Phase Oxidation of Alcohols

DOI: 10.1007/s10562-017-2065-x

Publication outline: Introduction | Experimental | Results and Discussion | Conclusions

Abstract-Summary

The obtained catalyst showed enhanced catalytic activities compared to the pure CQDs catalyst. The enhanced catalytic activities were mainly attributed to the highly dispersive CQDs with more active centers which caused by the TiO₂ support. The CQDs-TiO₂ catalyst can also be reused without any significant loss in their catalytic activities after five times.

A Novel Magnetic Immobilized Para-Aminobenzoic Acid-Cu(II) Complex: A Green, Efficient and Reusable Catalyst for Aldol Condensation Reactions in Green Media

DOI: 10.1007/s10562-020-03216-w

Publication outline: Introduction | Experimental | Results and Discussion | Conclusion

Abstract-Summary

The structure of the newly synthesized heterogeneous magnetic nanocatalyst with enhanced and improved catalytic efficiency were determined by various instrumental techniques, including SEM, VSM, TGA, XRD, UV-VIS FT-IR and EDXA. The catalytic activity and efficient performance of Fe₃O₄@PABA-Cu(II) MNPs were analyzed toward the synthesis of novel 5-arylidenthiazolidine-2,4-diones and 5-arylidene-2-imidazolidine-2,4-dione derivatives via aldol condensation reactions between a variety of (hetero) aromatic aldehydes and hydantoin or thiazolidine-2,4-dione multifunctional privileged scaffolds under reflux condensations in ethanol as a benign solvent. It is the first report of aldol synthesis of new 5-arylidenthiazolidine-2,4-dione, and 5-arylidene-imidazolidine-2,4-dione derivatives using a reusable copper-PABA complex supported on Fe₃O₄ MNPs (Fe₃O₄@PABA-Cu(II)) catalyst in Green media.

Extended:

These results show that Fe₃O₄@PABA-Cu(II) as an efficient catalyst increase the reaction yields and rate with easy conditions, simple workup and reduced unwanted side product.

Direct oxidative esterification of alcohols catalyzed by a nitrogen-doped carbon black-supported PdBi bimetallic catalyst under ambient conditions

DOI: 10.1007/s10853-020-05726-9

Publication outline: Introduction | Experimental section | Characterization | Results and discussion | Conclusions

Abstract-Summary

The optimal PdBi/NCB shows outstanding catalytic performance with broad substrate scope, good functional group tolerance towards direct oxidative esterification of alcohols under mild conditions in a heterogeneous catalytic system with air as the sole oxidant. Superior catalytic activity is mainly attributable to the unique structure of the catalyst, including synergetic electronic effect between Pd and Bi, as well as modulated surface character by acidification and N doping for better active components' anchoring and dispersion, as well as reactants' adsorption. This study provides a facile, practical, eco-friendly and efficient catalytic system for oxidative esterification of alcohols and shows promising prospect in industrial production.

Novel and Efficient Heterogeneous 4-Methylbenzenesulfonic Acid-Based Ionic Liquid Supported on Silica Gel for Greener Fischer Indole Synthesis

DOI: 10.1007/s10562-016-1721-x

Publication outline: Introduction | Experimental | Results and Discussion | Conclusion

Abstract-Summary

IL-SO₃H-SiO₂ was utilized as an efficient and heterogeneous catalyst for the synthesis of indoles via the one-pot Fischer reaction of phenyl hydrazines with ketones or aldehydes at room temperature.

The Efficient Oxidation of Biomass-Derived 5-Hydroxymethyl Furfural to Produce 2,5-Diformylfuran Over Supported Cobalt Catalysts

DOI: 10.1007/s12649-016-9724-9

Publication outline: Introduction | Experimental Section | Result and Discussions | Conclusions

Abstract-Summary

We report a novel cobalt-based catalyst (Co_xO_y-N@TiO₂) for the oxidation of HMF to DFF with 30 % aqueous tert-butyl hydroperoxide as the oxidant. Of catalytic test, it is found that a 91 % conversion of HMF and 40 % selectivity of DFF was obtained with the Co_xO_y-N@TiO₂ catalyst at 80 °C within 5 h. In addition, the Co_xO_y-N@TiO₂ can be recycled up to five times without significant loss of activity. The efficient oxidation of 5-hydroxymethyl furfural, a biomass-derived platform compound, to produce 2,5-diformylfuran is achieved using Co_xO_y-N@TiO₂ catalyst under mild conditions.

Bibliography

- [1] Cui G, Wang J, Zhang S (2016) Chem Soc Rev 45:4307
- [2] Amarasekara AS (2016) Chem Rev 116:6133
- [3] Pohako-Esko K, Bahlmann M, Schulz PS, Wasserscheid P (2016) Ind Eng Chem Res 55:7052
- [4] Rostamizadeh S, Nojavan M, Aryan R, Azad M (2014) Catal Lett 144:1772
- [5] Xin B, Hao J (2014) Chem Soc Rev 43:7171
- [6] Bagheri M, Masteri-Farahani M, Ghorbani M (2013) J Magn Magn Mater 327:58
- [7] B. Sadeghi, M.G. Nejad, J. Chem. 2013 (2013) (Article ID: 581465)
- [8] C. Mukhopadhyay, P.K. Tapaswi, Tetrahedron Lett. 49, 6237 (2008)
- [9] Sheldon RM, van Bekkum H (2001) Eds., Fine chemicals through heterogeneous catalysis. Wiley-VCH, Weinheim
- [10] Z. Dong, X. Le, X. Li, W. Zhang, C. Dong, J. Ma, Appl. Catal. B-Environ. 158, 129 (2014)
- [11] Le X, Dong Z, Li X et al (2015) Fibrous nano-silica supported palladium nanoparticles: An efficient catalyst for the reduction of 4-nitrophenol and hydrodechlorination of 4-chlorophenol under mild conditions. Catal Commun 59:21–25
- [12] Dhiman M, Chalke B, Polshettiwar V (2015) Efficient synthesis of monodisperse metal (Rh, Ru, Pd) nanoparticles supported on fibrous nanosilica (KCC-1) for catalysis. ACS Sustain Chem Eng 3:3224–3230
- [13] Das SK, Khan Md MR, Guha AK et al (2013) Bio-inspired fabrication of silver nanoparticles on nanostructured silica: characterization and application as a highly efficient hydrogenation catalyst. Green Chem 15:2548–2557
- [14] Tojo G, Fernandez M (2006) Oxidation of alcohols to aldehydes and ketones. Springer New York
- [15] Shinde VM, Skupien E, Makkee M (2015) Synthesis of highly dispersed Pd nanoparticles supported on multi-walled carbon nanotubes for their excellent catalytic performance for oxidation of benzyl alcohol. Catal Sci Technol 5:4144–4153
- [16] Ventura-Espinosa D, Vicent C, Bayac M et al (2016) Ruthenium molecular complexes immobilized on graphene as active catalysts for the synthesis of carboxylic acids from alcohol dehydrogenation. Catal Sci Technol 6:8024–8035
- [17] Bianchini C, Shen PK (2009) Palladium-based electrocatalysts for alcohol oxidation in half cells and in direct alcohol fuel cells. Chem Rev 109:4183–4206
- [18] Sheldon RA, Arends IWCE., Dijkstra A (2000) New developments in catalytic alcohol oxidations for fine chemicals synthesis. Catal Today 57:157–166

- [19] Allen SE, Walvoord RR, Padilla-Salinas R et al (2013) Aerobic copper-catalyzed organic reactions. *Chem Rev* 113:6234–6458
- [20] Daneshvar A, Moghadam M, Tangestaninejad S et al (2016) Ruthenium hydride complex supported on gold nanoparticle cored triazine dendrimers for C–C coupling reactions. *Organometallics* 35:1747–1755
- [21] Asadi B, Mohammadpoor-Baltork I, Tangestaninejad S et al (2016) Synthesis and characterization of Bi(III) immobilized on triazine dendrimer-stabilized magnetic nanoparticles: A reusable catalyst for synthesis of aminonaphthoquinones and bisaminonaphthoquinones. *New J Chem* 40:6171–6184
- [22] Landarani Isfahani A, Mohammadpoor-Baltork I, Mirkhani V et al (2014) Pd nanoparticles immobilized on nanosilica triazine dendritic polymer: a reusable catalyst for the synthesis of mono-, di-, and trialkynylaromatics by Sonogashira cross-coupling in water. *Eur J Org Chem* 2014: 5603–5609
- [23] Landarani Isfahani A, Mohammadpoor-Baltork I, Mirkhani V et al (2014) Palladium nanoparticles immobilized on nanosilica triazine dendritic polymer (P_{dn}p-nSTDP) as catalyst in the synthesis of mono-, di-, and trisulfides through C–S cross-coupling reactions. *Synlett* 25:645–652
- [24] Mohammadpoor-Baltork I, Moghadam M, Nasr-Esfahani M et al (2014) Copper immobilized on nano-silica triazine dendrimer (Cu(II)-TD@nSiO₂) catalyzed synthesis of symmetrical and unsymmetrical 1,3-diynes under aerobic conditions at ambient temperature. *RSC Adv* 4:14291–14296
- [25] Nasr-Esfahani M, Mohammadpoor-Baltork I, Khosropour AR et al (2014) Copper immobilized on nanosilica triazine dendrimer (Cu(II)-TD@nSiO₂) catalyzed regioselective synthesis of 1,4-disubstituted 1,2,3-triazoles and bis- and tris-triazoles via a one-pot multicomponent click reaction. *J Org Chem* 79:1437–1443
- [26] Landarani Isfahani A, Mohammadpoor-Baltork I, Mirkhani V et al (2013) Palladium nanoparticles immobilized on nano-silica triazine dendritic polymer (P_{dn}p-nSTDP): an efficient and reusable catalyst for Suzuki–Miyaura cross-coupling and heck reactions. *Adv Synth Catal* 355:957–972
- [27] Zakeri M, Moghadam M, Mirkhani V et al (2016) Synthesis and characterization of a host (a new thiol based dendritic polymer)-guest (Pd nanoparticles) nanocomposite material: an efficient and reusable catalyst for C–C coupling reactions. *RSC Adv* 6:104608–104619
- [28] Miyaura N, Suzuki A (1995) *Chem Rev* 95:2457
- [29] Das P, Linert W (2016) *Coord Chem Rev* 311:1
- [30] Veerakumar P, Velayudham M, Lu K-L, Rajagopal S (2013) Silica-supported PEI capped nanopalladium as potential catalyst in Suzuki, Heck and Sonogashira coupling reactions. *Appl Catal A* 455:247–260
- [31] Polshettiwar V, Len C, Fihri A (2009) *Coord Chem Rev* 253:2599
- [32] Xie W, Yang X, Fan M (2015) *Renew Energy* 80:230–237
- [33] Liu X, Sun L, Liu X, Li A, Lu F, Liu X (2013) *ACS Appl Mater Interfaces* 5:9823 – 9829
- [34] Thitsartarn W, Maneerung T, Kawi S (2015) *Energy* 89:946–956
- [35] Albuquerque MCG, Jimenez-Urbistondo I, Santamaria-Gonzalez J, Mérida-Robles JM, Moreno-Tost R, Rodríguez-Castellón E, Jiménez-López A, Azevedo DCS, Jr Cavalcante CL, Maireles-Torres P (2008) *Appl Catal A* 334:35–43
- [36] Kim D, Kim BK, Cho Y, Han M, Kim BS (2009) *Ind Eng Chem Res* 48:6591–6599
- [37] I.P. Beletskaya, A.V. Cheprakov, *Chem. Rev.* 100, 3009–3066 (2000)
- [38] S.P. Stanforth, *Tetrahedron* 54, 263–303 (1998)
- [39] A. Dahan, M. Portnoy, *Org. Lett.* 5, 1197–1200 (2003)
- [40] A. Dandapat, D. Jana, G. De, *Appl. Catal. A Gen.* 396, 34–39 (2011)
- [41] J.Y. Ying, C.P. Mehnert, M.S. Wong, Synthesis and applications of supramolecular templated mesoporous materials. *Angew. Chem. Int. Ed.* 38, 56–77 (1999)
- [42] R.I. Kureshy, I. Ahmad, N.-U.H. Khan, S.H.R. Abdi, K. Pathak, R.V. Jasra, *Tetrahedron Asymm.* 16, 3562–3569 (2005)
- [43] P. Sharma, A.P. Singh, *Catal. Sci. Technol.* 4, 2978–2989 (2014)
- [44] J. Huang, F. Zhang, *Appl. Organomet. Chem.* 24, 767–773 (2010)
- [45] X.J. Feng, M. Yan, X. Zhang, M. Bao, *Chin. Chem. Lett.* 22, 643–646 (2011)
- [46] Chandra P, Doke DS, Umbarkar SB, Biradar AV (2014) One-pot synthesis of ultrasmall MoO₃ nanoparticles supported on SiO₂, TiO₂, and ZrO₂ nanospheres: an efficient epoxidation catalyst. *J Mater Chem A* 2(44):19060–19066. doi: 10.1039/C4TA03754E
- [47] Li Z, Li Y, Zhan E, Ta N, Shen W (2013) Morphology-controlled synthesis of [small alpha]-MoO₃ nanomaterials for ethanol oxidation. *J Mater Chem A* 1(48):15370–15376. doi: 10.1039/C3TA13402D
- [48] Ma Z, Wu Y, He Y, Wu T (2013) A novel protocol for the oxidative degradation of chitosan with hydrogen peroxide catalyzed by peroxomolybdate in aqueous solution. *RSC Adv* 3(30):12049–12051. doi: 10.1039/C3RA40424B
- [49] Enferadi Kerenkan A, Beland F, Do T-O (2016) Chemically catalyzed oxidative cleavage of unsaturated fatty acids and their derivatives into valuable products for industrial applications: a review and perspective. *Catal Sci Technol* 6(4):971–987. doi: 10.1039/C5CY01118C

- [50] Turnwald SE, Lorier MA, Wright LJ, Mucalo MR (1998) Oleic acid oxidation using hydrogen peroxide in conjunction with transition metal catalysis. *J Mater Sci Lett* 17(15):1305–1307. doi: 10.1023/a:1006532314593
- [51] Metcalfe LD, Schmitz AA (1961) The rapid preparation of fatty acid esters for gas chromatographic analysis. *Anal Chem* 33(3):363–364. doi: 10.1021/ac60171a016
- [52] Metcalfe LD, Schmitz AA, Pelka JR (1966) Rapid preparation of fatty acid esters from lipids for gas chromatographic analysis. *Anal Chem* 38(3):514–515. doi: 10.1021/ac60235a044
- [53] Mao Y, Li W, Sun X, Ma Y, Xia J, Zhao Y, Lu X, Gan J, Liu Z, Chen J, Liu P, Tong Y (2012) Room-temperature ferromagnetism in hierarchically branched MoO₃ nanostructures. *CrystEngComm* 14(4):1419–1424. doi: 10.1039/C1CE05700F
- [54] Boulton AA, Davis BA, Durden DA, Dyck LE, Juorio AV, Li X-M, Paterson IA, Yu PH (1997) *Drug Dev Res* 42:150–156
- [55] Zani L, Bolm C (2006) *Chem Commun* 4263–4275
- [56] Frechet JM, Schuerch C (1971) *J Am Chem Soc* 93:492–496
- [57] Albaladejo MJ, Alonso F, Moglie Y, Yus M (2012) *Eur J Org Chem* 16:3093–3104
- [58] Borah BJ, Borah SJ, Saikia L, Dutta DK (2014) *Catal Sci Technol* 4:1047–1054
- [59] Kidwai M, Bansal V, Kumar A, Mozumdar S (2007) *Green Chem* 9:742–745
- [60] Kidwai M, Bansal V, Mishra NK, Kumar A, Mozumdar S (2007) *Synlett* 1581
- [61] Zhou X, Lu Y, Zhai LL, Zhao Y, Liu Q, Sun WY (2013) *RSC Adv* 3:1732
- [62] Layek K, Chakravarti R, LakshmiKantam M, Maheswaran H, Viru A (2011) *Green Chem* 13:2878
- [63] Borah BJ, Borah SJ, Saikia K, Dutta DK (2014) *Catal Sci Technol* 4(11):4001–4009
- [64] Yin D, Ren H, Li C, Liu J, Liang C (2018) *Chin J Catal* 39:319–326
- [65] Gupta K, Tyagi D, Dwivedi AD, Mobin SM, Singh SK (2015) *Green Chem* 17:4618–4627
- [66] Kobayashi H, Komanoya T, Guha SK, Hara K, Fukuoka A (2011) *Appl Catal A* 409:13–20
- [67] Fukuoka A, Dhepe PL (2009) *Chem Rec* 9:224–235
- [68] Reddy KR, Kumar NS, Reddy PS, Sreedhar B, Kantam ML (2006) *J Mol Catal A* 252:12–16
- [69] Mirosanloo A, Zareyee D, Khalilzadeh MA (2018) *Appl Organomet Chem* 32:e4546
- [70] Du QW, Li YQ (2012) *Res Chem Intermediat* 38:1807–1817
- [71] Y. Zhang, J. Ouyang, H. Yang, *Appl. Clay Sci.* 95, 252 (2014)
- [72] X.T. Cao, A.M. Showkat, D.W. Kim, Y.T. Jeong, J.S. Kim, K.T. Lim, *J. Nanosci. Nanotechnol.* 15, 8617 (2015)
- [73] Y. Ren, B. Liu, Z. Zhang, J. Lin, *J. Ind. Eng. Chem.* 21, 1127 (2015)
- [74] B. Yang, J.J. Pignatello, D. Qu, B. Xing, *J. Phys. Chem. A* 119, 1055 (2015)
- [75] S. Sadjadi, M.M. Heravi, *Curr. Org. Chem.* 20, 1404 (2016)
- [76] J. Xiong, W. Zhu, W. Ding, L. Yang, Y. Chao, H. Li, F. Zhu, H. Li, *Ind. Eng. Chem. Res.* 53, 19895 (2014)
- [77] E. Rafiee, F. Mirnezami, *J. Mol. Liq.* 199, 156 (2014)
- [78] M.M. Heravi, S. Sadjadi, H.A. Oskooie, R.H. Shoar, F.F. Bamoharram, *Tetrahedron Lett.* 50, 662 (2009)
- [79] M.M. Heravi, S. Sadjadi, N.M. Haj, H.A. Skooief, F. Bamoharram, *Catal. Commun.* 10, 1643 (2009)
- [80] M.M. Heravi, M. Saeedi, Y.S. Beheshtiha, H.A. Oskooie, *Mol. Divers.* 15, 239 (2011)
- [81] A. Ying, L. Wang, F. Qiu, H. Hu, J. Yang, *Comptes Rendus Chimie* 18 223–232 (2015)
- [82] M. Hajjami, F. Ghorbani, S. Rahimipannah, S. Roshani, *Chin. J. Catal.* 36, 1852–1860 (2015)
- [83] L. Martins, W. Hölderich, P. Hammer, D. Cardoso, *J. Catal.* 271, 220–227 (2010)
- [84] H. Zhao, N. Yu, Y. Ding, R. Tan, C. Liu, D. Yin, H. Qiu, D. Yin, *Microporous Mesoporous Mater.* 136, 10–17 (2010)
- [85] K.M. Parida, D. Rath, *J. Mol. Catal. A* 310, 93–100 (2009)
- [86] L. Martins, T.J. Bonagamba, E.R. de Azevedo, P. Bargiela, D. Cardoso, *Appl. Catal. A* 312, 77–85 (2006)
- [87] X. Chen, M. Arruebo, K.L. Yeung, *Catal. Today* 204, 140–147 (2013)
- [88] W.L. Craig, *Molecule of the Month. Curr. Top. Med. Chem.* 8, 434–434 (2008)
- [89] M.A. Ali, S.H. Siddiki, K. Kon, K.-i. Shimizu, Fe³⁺-exchanged clay catalyzed transamidation of amides with amines under solvent-free condition. *Tetrahedron Lett.* 55, 1316–1319 (2014)
- [90] S.C. Ghosh, C.C. Li, H.C. Zeng, J.S. Ngiam, A.M. Seayad, A. Chen, Mesoporous niobium oxide spheres as an effective catalyst for the transamidation of primary amides with amines. *Adv. Synth. Catal.* 356, 475–484 (2014)
- [91] M. Tamura, T. Tonomura, K. Shimizu, A. Satsuma, Transamidation of amides with amines under solvent-free

- conditions using a CeO₂ catalyst. *Green Chem.* 14, 717–724 (2012)
- [92] S.P. Pathare, A.K.H. Jain, K.G. Akamanchi, Sulfated tungstate: a highly efficient catalyst for transamidation of carboxamides with amines. *RSC Adv.* 3, 7697–7703 (2013)
- [93] B.Y. No, M.G. Kim, *J. Appl. Polym. Sci.* 93, 2559 (2004)
- [94] Y.S. He, X. Liu, Y.Z. Chen, L.M. Qu, *Appl. Mater. Inter.* 42, 1482 (2013)
- [95] A. Baliani, V. Peal, L. Gros, R. Brun, M. Kaiser, M.P. Barrett, I.H. Gilbert, *Org. Biomol. Chem.* 7, 1154 (2009)
- [96] V. Sadhasivam, R. Balasaravanan, A. Siva, *Appl. Organomet. Chem.* 33, e4994 (2019).
- [97] V. Sadhasivam, M. Mariyappan, A. Siva, *Chem. Sel.* 3, 13442 (2018)
- [98] S. Zhang, W. Ji, Y. Han, X. Gu, H. Li, J. Sun, *J. Appl. Polym. Sci.* 135, 1 (2018)
- [99] J.A. Faniran, K.S.J. Patel, *J. Inorg. Nucl. Chem.* 36, 2261 (1974)
- [100] S. Barua, G. Das, L. Aidew, A.K. Buragohainc, N. Karak, *RSC Adv.* 3, 14997 (2013)
- [101] Y. Han, M. Zhang, Y.Q. Zhang, Z.H. Zhang, *Green Chem.* 20, 4891 (2018)
- [102] P. Puthiaraj, K. Pitchumani, *Chem. Eur. J.* 20, 8761 (2014)
- [103] Dongil AB, Bachiller-Baeza B, Guerrero-Ruiz A, Rodríguez-Ramos I (2011) *J Catal* 282(2):299–309
- [104] Bhanage B (1999) *Chem Commun* 14(14):1277–1278
- [105] Fujita S, Akihara S, Zhao FY, Liu RX, Hasegawa M, Arai M (2005) *J Catal* 236(1):101–111
- [106] Cole-Hamilton DJ (2003) *Science* 299(5613):1702–1706
- [107] Sun Q, Jiang M, Shen Z, Jin Y, Pan S, Wang L, Meng X, Chen W, Ding Y, Li J, Xiao F-S (2014) *Chem Commun* 50(80):11844–11847
- [108] Hajek J, Kumar N, Maki-Arvela P, Salmi T, Murzin DY (2004) *J Mol Catal A Chem* 217(1–2):145–154
- [109] Mahmoud S, Hammoudeh A, Gharaibeh S, Melshemer J (2002) *J Mol Catal A Chem* 178:161–167
- [110] Miyaura N, Yamada K, Suzuki A (1979) *Tetrahedron Lett* 20:3437–3440
- [111] Heravi MM, Hashemi E (2012) *Tetrahedron* 68:9145–9178
- [112] Heravi MM, Hashemi E (2012) *Monatshefte für Chemie* 143:861–880
- [113] Suzuki A (2011) *Angew Chem Int Ed* 50:6722
- [114] Heravi MM, Kivanloo A, Rahimzadeh M, Bakavoli M, Ghassemzadeh M, Neumüller B (2005) *Tetrahedron Lett* 46:1607–1610
- [115] Oskooie H, Heravi MM, Behbahani F (2007) *Molecules* 12:1438
- [116] Heravi MM, Keivanloo A, Rahimizadeh M, Bakavoli M, Ghassemzadeh M (2004) *Tetrahedron Lett* 45:5747–5749
- [117] Sakai T, Matsunaga T, Yamamoto Y, Ito C, Yoshida R, Suzuki S, Sasaki N, Shibayama M, Chung U-i (2008) *Macromolecules* 41:5379–5384
- [118] Lee Y, Hong MC, Ahn H, Yu J, Rhee H (2014) *J Organomet Chem* 769:80–93
- [119] Sivudu KS, Reddy NM, Prasad MN, Raju KM, Mohan YM, Yadav J, Sabitha G, Shailaja D (2008) *J Mol Catal A* 295:10–17
- [120] Song H-q, Zhu Q, Zheng X-j, Chen X-g (2015) *J Mater Chem A* 3:10368–10377
- [121] Sheldon RA, Wallau M, Arends IW, Schuchardt U (1998) *Acc Chem Res* 31:485–493
- [122] Y. Liu, E. Lotero, J.G. Goodwin Jr., A comparison of the esterification of acetic acid with methanol using heterogeneous versus homogeneous acid catalysis. *J. Catal.* 242(2), 278–286 (2006)
- [123] S. Veli, A. Pinar, Characterization and catalytic performance of modified sba-16 in liquid phase reaction. *Int. J. Chem. Reactor Eng.* (2018). <https://doi.org/10.1515/ijcre-2017-0246>
- [124] R. Koster, B. van der Linden, E. Poels, A. Blik, The mechanism of the gas-phase esterification of acetic acid and ethanol over MCM-41. *J. Catal.* 204(2), 333–338 (2001)
- [125] M.A. Hanif, S. Nisar, U. Rashid, Supported solid and heteropoly acid catalysts for production of biodiesel. *Catal. Rev.* 59(2), 165–188 (2017)
- [126] K. Schumacher, P.I. Ravikovitch, A. Du Chesne, A.V. Neimark, K.K. Unger, Characterization of MCM-48 materials. *Langmuir* 16(10), 4648–4654 (2000)
- [127] Li Z, Wu S, Ding H, Zheng D, Hu J, Wang X, Huo Q, Guan J, Kan Q (2013) Immobilized Cu(II) and Co(II) salen complexes on graphene oxide and their catalytic activity for aerobic epoxidation of styrene. *New J Chem* 37:1561–1568
- [128] González-Arellano C, Corma A, Iglesias M, Sánchez F (2004) Heterogenised Rh (I), Ir(I) metal complexes with chiral triaza donor ligands: a cooperative effect between support and complex. *Inorg Chim Acta* 357:3071–3078
- [129] Irie R, Noda K, Ito Y, Matsumoto N, Katsuki T (1990) Catalytic asymmetric epoxidation of unfunctionalized olefins. *Tetrahedron Lett* 31:7345–7348

- [130] Jacobsen EN, Zhang W, Muci AR, Ecker JR, Deng L (1991) Highly enantioselective epoxidation catalysts derived from 1,2-diaminocyclohexane. *J Am Chem Soc* 113:7063–7064
- [131] Holbach M, Weck M (2006) Modular approach for the development of supported, monofunctionalized, salen catalysts. *J Org Chem* 71:1825–1836
- [132] Keilitz J, Haag R (2009) Intramolecular acceleration of asymmetric epoxide ring-opening by dendritic polyglycerol salen–Cr(III) complexes. *Eur J Org Chem* 2009:3272–3278
- [133] Yang Q, Pan X, Clarke K, Li K (2011) Covalent functionalization of graphene with polysaccharides. *Ind Eng Chem Res* 51:310–317
- [134] Collman JP, Lee VJ, Kellen-Yuen CJ, Zhang X, Ibers JA, Brauman JI (1995) Threitol-strapped manganese porphyrins as enantioselective epoxidation catalysts of unfunctionalized olefins. *J Am Chem Soc* 117:692–703
- [135] Balkus KJ Jr, Khanmamedova AK, Dixon KM, Bedioui F (1996) Oxidations catalyzed by zeolite ship-in-a-bottle complexes. *Appl Catal A* 143:159–173
- [136] Tan R, Yin D, Yu N, Jin Y, Zhao H, Yin D (2008) Ionic liquid-functionalized salen Mn(III) complexes as tunable separation catalysts for enantioselective epoxidation of styrene. *J Catal* 255:287–295
- [137] Huang Q, Zhou L, Jiang X, Zhou Y, Fan H, Lang W (2014) Synthesis of copper graphene materials functionalized by amino acids and their catalytic applications. *ACS Appl Mater Interfaces* 6:13502–13509
- [138] Zhang H, Xiang S, Li C (2005) Enantioselective epoxidation of unfunctionalised olefins catalyzed by Mn (salen) complexes immobilized in porous materials via phenyl sulfonic group. *Chem Commun* 39:1209–1211
- [139] Khatri PK, Choudhary S, Singh R, Jain SL, Khatri OP (2014) Grafting of a rhenium–oxo complex on Schiff base functionalized graphene oxide: an efficient catalyst for the oxidation of amines. *Dalton Trans* 43:8054–8061
- [140] Mungse HP, Verma S, Kumar N, Sain B, Khatri OP (2012) Grafting of oxo–vanadium Schiff base on graphene nanosheets and its catalytic activity for the oxidation of alcohols. *J Mater Chem* 22:5427–5433
- [141] Su H, Li Z, Huo Q, Guan J, Kan Q (2014) Immobilization of transition metal (Fe²⁺, Co²⁺, V²⁺ or Cu²⁺) Schiff base complexes onto graphene oxide as efficient and recyclable catalysts for epoxidation of styrene. *RSC Adv* 4:9990–9996
- [142] Połtowicz J, Pamin K, Tabor E, Haber J, Adamski A, Sojka Z (2006) Metallosalen complexes immobilized in zeolite NaX as catalysts of aerobic oxidation of cyclooctane. *Appl Catal A* 299:235–242
- [143] Dong WH, Zhang L, Wang CH, Feng C, Shang NZ, Gao ST, Wang C (2016) *RSC Adv* 6:37118–37123
- [144] Gholinejad M, Zareh F, Nájera C (2018) *Appl Organomet Chem* 32:e3984
- [145] Huo JJ, Johnson RL, Duan P, Pham HN, Mendivelso-Perez D, Smith EA, Datye AK, Schmidt-Rohr K, Shanks BH (2018) *Catal Sci Technol* 8:1151–1160
- [146] Diyarbakir S, Can H, Metin O (2015) *ACS Appl Mater Interfaces* 7:3199–3206
- [147] Elazab HA, Siamaki AR, Moussa S, Gupton BF, El-Shall MS (2015) *Appl Catal A* 491:58–69
- [148] Jadhav S, Kumbhar A, Salunkhe R (2015) *Appl Organomet Chem* 29:339–345
- [149] Mori K, Masuda S, Tanaka H, Yoshizawa K, Che M, Yamashita H (2017) *Chem Commun* 53:4677–4680
- [150] Ayodele OB, Farouk HU, Mohammed J, Uemura Y, Daud WMAW (2015) *J Mol Catal A* 400:179–186
- [151] Fu WQ, Zhang L, Tang TD, Ke QP, Wang S, Hu JB, Fang GY, Li JX, Xiao FS (2011) *J Am Chem Soc* 133:15346–15349
- [152] Baran T, Menteş A (2016) *J Mol Struct* 1122:111–116
- [153] Sharma YC, Singh B (2011) *Biofuels Bioprod Bioref* 5:69–92
- [154] Clark J (2002) *Acc Chem Res* 35:791–797
- [155] Cheng M, Shi T, Guan H, Wang S, Wang X, Jiang Z (2011) *Appl Catal B* 107:104–109
- [156] Hu J, Hu Y, Mao J, Yao J, Chena Z, Li H (2012) A cobalt schiff base with ionic substituents on the ligand as an efficient catalyst for the oxidation of 4-methyl guaiacol to vanillin. *Green Chem* 14:2894–2898
- [157] Zhang Y, Li X, Cao X, Zhao J (2014) Liquid-phase oxidation of 2-methoxy-p-cresol to vanillin with oxygen catalyzed by a combination of CoCl₂ and N-hydroxyphthalimide. *Res Chem Intermed* 40:1303–1311
- [158] Pérez-Mayoral E, Calvino-Casilda V, Soriano E. Metal-supported carbon-based materials: opportunities and challenges in the synthesis of valuable products. *Catal Sci Technol*, 2016, 6: 1265–1291
- [159] Zhou M, Wang HL, Guo SJ (2016) Towards high-efficiency nanoelectrocatalysts for oxygen reduction through engineering advanced carbon nanomaterials. *Chem Soc Rev* 45:1273–1307
- [160] Saptal VB, Bhanage BM (2017) Current advances in heterogeneous catalysts for the synthesis of cyclic carbonates from carbon dioxide. *Curr Opin Green Sustain Chem* 3:1–10. <https://doi.org/10.1016/j.cogsc.2016.10.006>
- [161] Xiao L, Lv D, Wu W (2011) Brønsted acidic ionic liquids mediated metallic salts catalytic system for the chemical fixation of carbon dioxide to form cyclic carbonates. *Catal Lett* 141:1838–1844. <https://doi.org/10.1007/s10562-011-0682-3>

- [162] Aquino AS, Bernard FL, Vieira MO et al (2014) A new approach to CO₂ capture and conversion using imidazolium based-ionic liquids as sorbent and catalyst. *J Braz Chem Soc* 25:2251–2257. <https://doi.org/10.5935/0103-5053.20140176>
- [163] He Q, O'Brien JW, Kitselman KA et al (2014) Synthesis of cyclic carbonates from CO₂ and epoxides using ionic liquids and related catalysts including choline chloride–metal halide mixtures. *Catal Sci Technol* 4:1513–1528. <https://doi.org/10.1039/C3CY00998J>
- [164] Kawanami H, Sasaki A, Matsui K, Ikushima Y (2003) A rapid and effective synthesis of propylene carbonate using a supercritical CO₂–ionic liquid system. *Chem Commun*. <https://doi.org/10.1039/b212823c>
- [165] Xu B-H, Wang J-Q, Sun J et al (2015) Fixation of CO₂ into cyclic carbonates catalyzed by ionic liquids: a multi-scale approach. *Green Chem* 17:108–122. <https://doi.org/10.1039/C4GC01754D>
- [166] Bobbink FD, Dyson PJ (2016) *J Catal* 343:52
- [167] Neto D, Brenno A, Spencer J (2012) The impressive chemistry, applications and features of ionic liquids: properties, catalysis & catalysts and trends. *J Braz Chem Soc* 23:987–1007. <https://doi.org/10.1590/S0103-50532012000600002>
- [168] Xiong Y, Bai F, Cui Z et al (2013) Cycloaddition reaction of carbon dioxide to epoxides catalyzed by polymer-supported quaternary phosphonium salts. *J Chem* 2013:1–9. <https://doi.org/10.1155/2013/261378>
- [169] Meng X-L, Nie Y, Sun J et al (2014) Functionalized dicyandiamide–formaldehyde polymers as efficient heterogeneous catalysts for conversion of CO₂ into organic carbonates. *Green Chem* 16:2771–2778. <https://doi.org/10.1039/C3GC42331J>
- [170] Xie Y, Zhang Z, Jiang T et al (2007) CO₂ cycloaddition reactions catalyzed by an ionic liquid grafted onto a highly cross-linked polymer matrix. *Angew Chem Int Ed* 46:7255–7258. <https://doi.org/10.1002/anie.200701467>
- [171] Wang J-Q, Sun J, Cheng W-G et al (2012) Experimental and theoretical studies on hydrogen bond-promoted fixation of carbon dioxide and epoxides in cyclic carbonates. *Phys Chem Chem Phys* 14:11021. <https://doi.org/10.1039/c2cp41698k>
- [172] Rojas MF, Bernard FL, Aquino A et al (2014) Poly(ionic liquid)s as efficient catalyst in transformation of CO₂ to cyclic carbonate. *J Mol Catal A* 392:83–88. <https://doi.org/10.1016/j.molcata.2014.05.007>
- [173] Shim JJ, Kim D, Choon SR (2006) Carboxylation of styrene oxide catalyzed by quaternary onium salts under solvent-free conditions. *Bull Korean Chem Soc* 27:744–746. <https://doi.org/10.5012/bkcs.2006.27.5.744>
- [174] Wang JQ, Dong K, Cheng WG et al (2012) Insights into quaternary ammonium salts-catalyzed fixation carbon dioxide with epoxides. *Catal Sci Technol* 2:1480–1484. <https://doi.org/10.1039/c2cy20103h>
- [175] Chen Q, Peng C, Xie H et al (2015) Cellulosic poly(ionic liquid)s: synthesis, characterization and application in the cycloaddition of CO₂ to epoxides. *RSC Adv* 5:44598–44603. <https://doi.org/10.1039/C5RA05667E>
- [176] Erkey C (2009) Preparation of metallic supported nanoparticles and films using supercritical fluid deposition. *J Supercrit Fluids* 47:517–522
- [177] Škerget M, Knez Ž, Knez-Hrnčič MŠ (2011) Solubility of solids in sub- and supercritical fluids: a review. *J Chem Eng Data* 56:694–719
- [178] Ulusal F, Darendeli B, Erünal E, Egitmen A, Guzel B (2017) Supercritical carbondioxide deposition of γ -alumina supported Pd nanocatalysts with new precursors and using on Suzuki-Miyaura coupling reactions. *J Supercrit Fluids* 127:111–120
- [179] Collins G, Schmidt M, O'Dwyer C, Holmes JD, McGlacken GP (2014) The origin of shape sensitivity in palladium-catalyzed Suzuki-Miyaura cross coupling reactions. *Angew Chem Int Ed Engl* 53:4142–4145
- [180] Ulusal F, Güzel B (2018) Deposition of palladium by the hydrogen assisted on SBA-15 with a new precursor using supercritical carbon dioxide. *J Supercrit Fluids* 133:233–238
- [181] Pan H-B, Yen CH, Yoon B, Sato M, Wai CM (2006) Recyclable and ligandless Suzuki coupling catalyzed by carbon nanotube-supported palladium nanoparticles synthesized in supercritical fluid. *Synth Commun* 36:3473–3478
- [182] Li X-H, Baar M, Blechert S, Antonietti M (2013) Facilitating room-temperature Suzuki coupling reaction with light: Mott-Schottky photocatalyst for C-C-coupling. *Sci Rep* 3:1743
- [183] Molnar A (2011) Efficient, selective, and recyclable palladium catalysts in carbon-carbon coupling reactions. *Chem Rev* 111:2251–2320
- [184] Dumbre D, Choudhary VR, Selvakannan PR (2016) Cu–Fe layered double hydroxide derived mixed metal oxide: environmentally benign catalyst for Ullmann coupling of aryl halides. *Polyhedron* 120:180–184
- [185] Chen L, Zhu K, Bi L, Suchopar A, Reicke M, Mathys G, Jaensch H, Kortz U, Richards RM (2007) *Inorg Chem* 46:8457–8459
- [186] Song X, Zhu W, Li K, Wang J, Niu H, Gao H, Gao W, Zhang W, Yu J (2015) *Catal Today* 259:59–65
- [187] Hu J, Li K, Li W, Ma F, Guo Y (2009) *Appl Catal A Gen* 364:211–220
- [188] Zhang X, Fu XB, Zhang YM, Zhu Y, Yang J (2016) Transition metal-free carbon quantum dots for selective liquid phase oxidation of alcohols using water as an only solvent. *Catal Lett* 146:945–950

- [189] Zhang LW, Fu HB, Zhu YF (2008) Efficient TiO₂ photocatalysts from surface hybridization of TiO₂ particles with graphite-like carbon. *Adv Funct Mater* 18:2180–2189
- [190] Zhang H, Lv XJ, Li YM, Wang Y, Li JH (2010) P25-graphene composite as a high performance photocatalyst. *ACS Nano* 4:380–386
- [191] Ji HB, Shi DP, Shao M, Li Z, Wang LF (2005) Transition metal-free and substrate-selective oxidation of alcohols using water as an only solvent in the presence of beta-cyclodextrin. *Tetrahedron Lett* 46:2517–2520
- [192] Khajeh-Amiri A, Foroughifar N, Hassannejad F et al (2019) Microwave assisted highly efficient synthesis of rhodanine and -2, 4-thiazolidinedione derivatives under solvent free conditions. *Curr Microw Chem* 06:215–224. <https://doi.org/10.2174/2213335606666190118163108>
- [193] Jawale DV, Pratap UR, Lingampalle DL, Mane RA (2011) Dicationic ionic liquid mediated synthesis of 5-arylidine-2,4-thiazolidinediones. *Chin J Chem* 29:942–946. <https://doi.org/10.1002/cjoc.201190192>
- [194] Kumar KK, Sharma RSK, Babu PC et al (2017) Synthesis, characterization and pharmacological evaluation of novel spiro heterocyclic compounds as anti diabetic agents. *Asian J Res Chem* 10:393. <https://doi.org/10.5958/0974-4150.2017.00067.0>
- [195] Nikalje A, Nikalje G, Deshpande D, Une H (2012) Facile synthesis and in vivo hypoglycemic activity of novel 2,4-thiazolidinedione derivatives. *Eur J Exp Biol* 2:343–353
- [196] Ceylan-Ünlüsoy M, Verspohl EJ, Ertan R (2010) Synthesis and antidiabetic activity of some new chromonyl-2,4-thiazolidinediones. *J Enzyme Inhib Med Chem* 25:784–789. <https://doi.org/10.3109/14756360903357544>
- [197] Ashraf MA, Liu Z, Peng W-X, Gao C (2020) New copper complex on Fe₃O₄ nanoparticles as a highly efficient reusable nanocatalyst for synthesis of polyhydroquinolines in water. *Catal Lett* 150:683–701. <https://doi.org/10.1007/s10562-019-02986-2>
- [198] Hu Y, Chen L, Li B (2016) NHPI/ tert -butyl nitrite: a highly efficient metal-free catalytic system for aerobic oxidation of alcohols to carbonyl compounds using molecular oxygen as the terminal oxidant. *Catal Commun* 83:82–87. <https://doi.org/10.1016/j.catcom.2016.05.017>
- [199] Hu Y, Chen L, Li B (2018) Fe(NO₃)₃ / 2,3-dichloro-5,6-dicyano-1,4-benzo quinone (DDQ): an efficient catalyst system for selective oxidation of alcohols under aerobic conditions. *Catal Commun* 103:42–46. <https://doi.org/10.1016/j.catcom.2017.09.019>
- [200] Ryland BL, Stahl SS (2014) Practical aerobic oxidations of alcohols and amines with homogeneous copper/TEMPO and related catalyst systems. *Angew Chem Int Ed Engl* 53:8824–8838
- [201] Xia J, Zhang L, Fu Y, He G, Sun X, Wang X (2017) Nitrogen-doped carbon black supported NiCo₂S₄ catalyst for hydrogenation of nitrophenols under mild conditions. *J Mater Sci* 53(6):4467–4481. <https://doi.org/10.1007/s10853-017-1852-5>
- [202] Candu N, Rizescu C, Podolean I, Tudorache M, Parvulescu VI, Coman SM (2015) *Catal Sci Technol* 5:729
- [203] Amarasekara, A.S., Green, D., McMillan, E.: Efficient oxidation of 5-hydroxymethylfurfural to 2,5-diformylfuran using Mn(III)-salen catalysts. *Catal. Commun.* 9, 286–288 (2008)
- [204] Tong, X., Sun, Y., Bai, X., Li, Y.: Highly efficient aerobic oxidation of biomass derived 5-hydroxymethyl furfural to produce 2,5-diformylfuran in the presence of copper salts. *RSC Adv.* 4, 44307–44311 (2014)
- [205] Sádaba, I., Gorbanev, Y.Y., Riisager, A., Putluru, S.S.R., Berg, R.W., Riisager, A.: Catalytic performance of zeolite-supported vanadia in the aerobic oxidation of 5-hydroxymethylfurfural to 2,5-diformylfuran. *ChemCatChem* 5, 284–293 (2013)

3. Theoretical Studies

Carbon Permeation: The Prerequisite Elementary Step in Iron-Catalyzed Fischer–Tropsch Synthesis

DOI: 10.1007/s10562-018-02651-0

Publication outline: Introduction | Molecular Dynamic (MD) Simulation Methods | DFT Methods | Energy and Rate Constants | Model Surfaces | Carbon Permeation from MD Simulations | Dicarboxyl | Permeation Will Vary Substantially with Surface | Permeation vs Surface Migration | Rate Constant Estimates for Permeation | Conclusions

Abstract-Summary

The interaction of C atoms with five model surfaces (Fe (100), (110), (111), (211), (310)) was studied in six distinct ways. In the first, the random deposition of C atoms on the Fe surfaces was simulated by molecular dynamics, with C atoms released gradually. It shows that the early stages of carburization is a C permeation process, without much disturbance to the Fe surfaces. C atoms were approached to the surfaces sequentially. They bind readily (by 7–9 eV per C) to the surfaces, but to a different extent—strongest on Fe (100), and weakest on Fe (111). At a certain coverage, different on each surface, C atoms prefer in calculation to go subsurface. In a third approach, detailed transition paths of C permeation subsurface were calculated, with associated barriers in the order Fe (100) > (111) > (310) > (211) > (110). Comparing C permeation with surface migration on clean surfaces, the barrier of the former is smaller than that of the latter for most of the surfaces, except Fe (111). At intermediate C coverage, the (100) surface also prefers migration to permeation. In a fifth approach, the position in energy of the d-band centers of the Fe surfaces upon C permeation was studied. For all the surfaces, the d-band

centers move away from the Fermi level with increasing C coverage, and start to resemble those of the bulk carbide phases at high C coverage. A general picture emerges of C permeation on Fe surfaces as a stepwise process with opposite thermodynamic and kinetic preferences.

Extended:

For all the surfaces studied, C permeation moves the d-band centers of the surfaces further away from the Fermi level.

[First-principles-based multiscale modelling of heterogeneous catalysis](#)

DOI: 10.1038/s41929-019-0298-3

Publication outline: Main | A generic multiscale modelling framework | Mechanistic complexity | Structural complexity | Environmental complexity | Conclusion and perspective

Abstract-Summary

They provide invaluable mechanistic insight and allow screening of vast materials spaces for promising new catalysts — in silico and at predictive quality. We briefly review methodological cornerstones of existing approaches and highlight successes and ongoing developments. On the road towards a higher structural, mechanistic and environmental complexity, it is, in particular, the fusion with machine learning methodology that promises rapid advances in the years to come.

[Achievements and Expectations in the Field of Computational Heterogeneous Catalysis in an Innovation Context](#)

DOI: 10.1007/s11244-021-01489-y

Publication outline: Introduction | Understanding the Nature of the Surface Active Sites | Quantification of Reaction Profiles | Prediction of the Reaction Rates and of Catalytic Performance | Prediction of New Active Phases | Current Challenges: Towards More Relevance, Accuracy, Efficiency

Abstract-Summary

The present short review discusses and illustrates these various stages of the catalyst understanding and performance prediction where computational catalysis has a crucial role to play. Selected achievements in the field are reviewed, with a focus on the simulation of complex metallic and zeolite catalysts of industrial relevance. Future directions are suggested, on the basis of the need for ever more exhaustive and accurate models of catalytic sites and catalytic reactions representative of industrial systems, and for speed up in catalyst understanding and discovery.

[The Role of Zeolite Framework in Zeolite Stability and Catalysis from Recent Atomic Simulation](#)

DOI: 10.1007/s11244-021-01473-6

Publication outline: Introduction | Theoretical Advances in Understanding Zeolite Stability | Atomic Simulations on the Zeolite–Molecule Interaction | Perspective

Abstract-Summary

Theoretical simulations, particularly those based on first principles calculations, have advanced significantly the understandings on zeolite, from structure to adsorption kinetics and to catalytic reactivity. This short review overviews the theoretical insights into the role of zeolite framework in zeolite stability and catalysis revealed from atomic simulation in recent years. We will mainly focus on two key aspects: (i) the theory on zeolite stability, including the templating effect of structure directing agents and the zeolite bonding pattern analysis; (ii) the confinement effect of zeolite pores that affects the catalytic conversion of molecules in zeolite.

[Catalysis at Metal/Oxide Interfaces: Density Functional Theory and Microkinetic Modeling of Water Gas Shift at Pt/MgO Boundaries](#)

DOI: 10.1007/s11244-020-01257-4

Publication outline: Introduction | Methods | Results and Discussion | Conclusions

Abstract-Summary

The impact of metal/oxide interfaces on the catalytic properties of oxide-supported metal nanoparticles is a topic of longstanding interest in the field of heterogeneous catalysis. Using a combination of periodic Density Functional Theory calculations and microkinetic modeling, we present a comprehensive analysis of the WGS mechanism at the interface between a quasi-one dimensional platinum nanowire and an irreducible MgO support. The nanowire is lattice matched to the MgO support to remove spurious strain at the metal/oxide interface, and reactions both on the nanowire and at the three-phase boundary itself are considered in the mechanistic analysis. These results are combined with detailed calculations of adsorbate entropies and dual-site microkinetic modeling to determine the kinetically significant features of the WGS reaction network which are subsequently, validated through experimental measurements of apparent reaction orders and activation barrier. The analysis demonstrates the important role that the metal/oxide interface plays in the reaction, with the water dissociation step being facile at the interface compared to the pure metal or oxide surfaces. Further, explicit consideration of CO interactions with other adsorbates at the metal/oxide interface is found to be central to correctly determining reaction mechanisms, rate determining steps, reaction orders, and effective activation barriers.

Extended:

The nanowire is lattice matched to the MgO surface to remove spurious strain effects that sometimes arise in models of metal/oxide interfaces, and the irreducibility of the MgO, in turn, leads to simplification of the space of possible reaction mechanisms, since lattice oxygen does not directly affect the WGS chemistry.

[DFT calculations on subnanometric metal catalysts: a short review on new supported materials](#)

DOI: 10.1007/s00214-018-2236-x

Publication outline: Introduction | Computational details | Discussion | Conclusions

Abstract-Summary

Metal clusters have been used in catalysis for a long time, even in industrial production protocols, and a large number of theoretical and experimental studies aimed at characterizing their structure and reactivity, either when supported or not, are already present in the literature. In the last years the advances made in the control of the synthesis and stabilization of subnanometric clusters promoted a renewed interest in the field. If supported, subnanometric clusters could be highly influenced by the interactions with the support that could affect geometric and electronic properties of the catalyst. The outstanding position of this corner of science will be highlighted through a selected number of examples present in the literature, concerning the growth and reactivity of subnanometric supported metal catalysts.

Theory-guided design of catalytic materials using scaling relationships and reactivity descriptors

DOI: 10.1038/s41578-019-0152-x

Publication outline: Introduction | [Section 2] | Descriptors on metal surfaces | Descriptors on metal-oxide surfaces | Universal and other descriptors | How to break scaling relationships | Outlook

Abstract-Summary

A physical or chemical property of the reaction system, termed as a reactivity descriptor, scales with another property often in a linear manner, which can describe and/or predict the catalytic performance. In this Review, we describe scaling relationships and reactivity descriptors for heterogeneous catalysis, including electronic descriptors represented by d-band theory, structural descriptors, which can be directly applied to catalyst design, and, ultimately, universal descriptors. The prediction of trends in catalytic performance using reactivity descriptors can enable the rational design of catalysts and the efficient screening of high-throughput catalysts.

Extended:

In this Review, we discuss reactivity descriptors in different catalytic systems, taking into consideration the limitations of scaling relationships and strategies to break these established scaling relationships. We aim to lay foundations for the future computational design of catalysts.

Modelling heterogeneous interfaces for solar water splitting

DOI: 10.1038/nmat4803

Publication outline: Main | Computational methods | Photoelectrode/water interfaces | Photoelectrode/catalyst/water interfaces | Outlook and conclusions

Abstract-Summary

The key of a successful solar-to-fuel technology is the design of efficient, long-lasting and low-cost photoelectrochemical cells, which are responsible for absorbing sunlight and driving water splitting reactions. We review recent progress and open challenges in predicting physicochemical properties of heterogeneous interfaces for solar water splitting applications using first-principles-based approaches, and highlights the key role of these calculations in interpreting increasingly complex experiments.

Computational optimization of electric fields for better catalysis design

DOI: 10.1038/s41929-018-0109-2

Publication outline: Main | Natural and synthetic biocatalysis | Porous supermolecular capsules and zeolite catalysts | Electric fields for heterogeneous and homogeneous catalysis | Summary and future directions

Abstract-Summary

We illustrate how electric fields have been used to computationally optimize biocatalytic performance of a synthetic enzyme, and how they could be used as a unifying descriptor for catalytic design across a range of homogeneous and heterogeneous catalysts.

Extended:

The data that supports the findings of this study are available from the corresponding author upon request.

Properties of Isolated and TiO₂(110) Supported Pt₁₃ Clusters: A Theoretical Study

DOI: 10.1007/s11244-019-01182-1

Publication outline: Introduction | Computational Details and Cluster Models | Results and Discussion | Conclusions

Abstract-Summary

We determine their equilibrium geometries, cohesive energies, magnetic moments, electronic and vibrational density of states. The analysis of the vibrational modes reveal that the Oh and Ih structures are dynamically unstable unlike the layered structures that have lower energies. We then examine the Pt₁₃-titania system to characterize the cluster/substrate interaction for both the stoichiometric and reduced surfaces. We characterize different aspects of the metal-oxide interaction by determining their equilibrium geometries, adsorption energies, charge transfer effects and electronic density of states. We find that the Pt₁₃ cluster suffers a strong restructuring when adsorbed on the surface, it deforms towards increasing the interaction of the platinum atoms with the surface, leading to a high value of the adsorption energy and getting oxidized. The calculated surface oxygen vacancy formation energy is preferred by the cluster deposition as a fact that favours the use of this system in the CO oxidation reactions from a surface oxygen, an important step in the water gas shift reaction.

Extended:

The analysis of the vibrational modes reveal that the Oh and Ih structures are dynamically unstable, while the layered configurations, named DT-1 and DT-2, are dynamically stable. We find that the Pt₁₃ cluster suffers a restructuring when adsorbed on the surface.

[Evaluating differences in the active-site electronics of supported Au nanoparticle catalysts using Hammett and DFT studies](#)

DOI: 10.1038/nchem.2911

Publication outline: Main | Results | Additional information

Abstract-Summary

Supported metal catalysts, which are composed of metal nanoparticles dispersed on metal oxides or other high-surface-area materials, are ubiquitous in industrially catalysed reactions. Metal-support interactions have an enormous impact on the chemistry of the catalytic active site and can determine the optimum support for a reaction; however, few direct probes of these interactions are available. We show how benzyl alcohol oxidation Hammett studies can be used to characterize differences in the catalytic activity of Au nanoparticles hosted on various metal-oxide supports.

[Optimum Performance of Vanadyl Pyrophosphate Catalysts](#)

DOI: 10.1007/s11244-016-0673-0

Publication outline: Introduction | Experimental | Results and Discussion | Summary

Abstract-Summary

A scheme is proposed for the dynamic, catalytically active vanadium-phosphorus-mixed oxide surface of industrially used catalysts for the selective oxidation of n-butane to maleic anhydride. This scheme is used as basis for a two-dimensional, heterogeneous reactor model describing the observed performance changes as function of the underlying phosphorus surface dynamics. The dynamic model comprises two reversible reactions: slow phosphorus adsorption, and water adsorption reaching its equilibrium faster. The kinetic model distinguishes explicitly between the intrinsic kinetics and phosphorus/water induced activity dynamics. In the presented study all phosphorus and water related processes appeared to be completely reversible, and the developed reactor model fully describes dynamic performance changes up to 400 h on stream.

[Oxygen evolution reaction over catalytic single-site Co in a well-defined brookite TiO₂ nanorod surface](#)

DOI: 10.1038/s41929-020-00550-5

Publication outline: Main | Results | Conclusions | Methods

Abstract-Summary

The structural complexity of heterogeneous electrocatalysts makes it a great challenge to elucidate the surface catalytic sites

and OER mechanisms. We report that catalytic single-site Co in a well-defined brookite TiO₂ nanorod (210) surface (Co-TiO₂) presents turnover frequencies that are among the highest for Co-based heterogeneous catalysts reported to date, reaching 6.6 ± 1.2 and 181.4 ± 28 s⁻¹ at 300 and 400 mV overpotentials, respectively. Based on grand canonical quantum mechanics calculations and the single-site Co atomic structure validated by in situ and ex situ spectroscopic probes, we have established a full description of the catalytic reaction kinetics for Co-TiO₂ as a function of applied potential, revealing an adsorbate evolution mechanism for the OER.

[Dependency of solvation effects on metal identity in surface reactions](#)

DOI: 10.1038/s42004-020-00428-4

Publication outline: Introduction | Results | Discussion | Methods

Abstract-Summary

Solvent interactions with adsorbed moieties involved in surface reactions are often believed to be similar for different metal surfaces. To reveal the importance of metal identity on aqueous solvent effects in heterogeneous catalysis, we studied solvent effects on the activation free energies of the O-H and C-H bond cleavages of ethylene glycol over the (111) facet of six transition metals (Ni, Pd, Pt, Cu, Ag, Au) using an explicit solvation approach based on a hybrid quantum mechanical/molecular mechanical (QM/MM) description of the potential energy surface. The main reason for this dependence could be traced back to a different amount of charge-transfer between the adsorbed moieties and metals in the reactant and transition states for the different metal surfaces.

[Using statistical learning to predict interactions between single metal atoms and modified MgO\(100\) supports](#)

DOI: 10.1038/s41524-020-00371-x

Publication outline: Introduction | Results | Discussion | Methods

Abstract-Summary

We use density functional theory (DFT) and statistical learning (SL) to derive models for predicting how the adsorption strength of metal atoms on MgO(100) surfaces can be enhanced by modifications of the support. We use SL methods (i.e., LASSO, Horseshoe prior, and Dirichlet-Laplace prior) that are trained against DFT data to identify physical descriptors for predicting how the adsorption energy of metal atoms will change in response to support modification. These SL-derived feature selection tools are used to screen through more than one million candidate descriptors that are generated from simple chemical properties of the adsorbed metals, MgO, dopants, and adsorbates. Among the tested SL tools, we demonstrate that Dirichlet-Laplace prior predicts metal adsorption energies on MgO most accurately, while also identifying descriptors that are most transferable to chemically similar oxides, such as CaO, BaO, and ZnO.

Extended:

We will explore the performance of both LASSO-based FS methods and state-of-the-art Bayesian FS methods [164, 165] for finding descriptors that can predict changes in metal binding energy caused by MgO surface modification.

[Integration of theory and experiment in the modelling of heterogeneous electrocatalysis](#)

DOI: 10.1038/s41560-021-00827-4

Publication outline: Main | Critical elements to model heterogeneous systems | Modelling reactions at metal electrodes | Modelling reactions at oxides | Outlook

Abstract-Summary

Theoretical and computational approaches are essential to interpret experimental data and provide the mechanistic understanding necessary to design more effective catalysts. Automated general procedures to build predictive theoretical and computational frameworks are not readily available; specific choices must be made in terms of the atomistic structural model and the level of theory, as well as the experimental data used to inform and validate these choices. The level of theory should be chosen for the specific system and properties of interest, and experimental validation is essential from the beginning to the end of the study.

[CO Oxidation Promoted by a Pt₄/TiO₂ Catalyst: Role of Lattice Oxygen at the Metal/Oxide Interface](#)

DOI: 10.1007/s10562-018-2610-2

Publication outline: Introduction | Computational Details | Results and Discussion | Conclusions

Abstract-Summary

CO oxidation promoted by a subnano Pt₄ cluster deposited on the anatase a-TiO₂(101) surface has been investigated by means of DFT + U calculations. The focus of the study is on the role of supported Pt₄ in favoring the formation of an oxygen vacancy at interface sites between Pt₄ and the TiO₂ surface, a key step in CO oxidation reactions according to a Mars-van Krevelen mechanism. The motivation is to compare this reaction mechanism with other processes described in the literature for Pt clusters on anatase TiO₂ where the reaction involves O₂ dissociation at the surface of the metal particle or its activation at the metal/oxide interface. The processes is slightly endothermic, and occurs with barriers comparable, or even lower, than found for the case of Au nanoparticles supported on the same a-TiO₂ (101) surface.

Extended:

The motivation is to compare, using the same approach, the behavior of the Pt/TiO₂ catalyst with that of Au/TiO₂ [188], or Au/ZrO₂ [189] systems, where a MvK mechanism has been established [188] or suggested [189].

[Structural diversity of metallacycle intermediates for ethylene dimerization on heterogeneous NiMCM-41 catalyst: a quantum chemical perspective](#)

DOI: 10.1007/s11224-018-1184-3

Publication outline: Introduction | Computational | Results and discussion | Conclusion

Abstract-Summary

Nanocluster models were investigated to explore the diversity of metallacycle intermediates for ethylene dimerization over NiMCM-41 at B3LYP/6-311+G* and M06/Def2-TZVP. The thermodynamic favorability of the formation of metallacycle with respect to the ring size of silica varied in the sequence of 6T < 3T < 2T < 5T < 4T in terms of Gibbs free energy (ranging from -10.01 to 16.66 kcal/mol at B3LYP/6-311+G*). The formation of the intermediate and π complexation of 1-butene led to positive total charges on the hydrocarbon segment of the complex, being maximized on four-membered sites and minimized on two-membered ones.

Extended:

The formation of the catalytically active species from such pre-catalysts is an interesting less-addressed topic for which molecular simulation can be extremely useful. The formation of both types of clusters were found to be exothermic on all of the active sites at both levels of theory with the A4T and A5T complexes to be the most exothermic intermediates (with the enthalpies of -43.03 and -40.66 kcal/mol at L2, respectively).

[A review on the computational studies of the reaction mechanisms of CO₂ conversion on pure and bimetals of late 3d metals](#)

DOI: 10.1007/s00894-021-04811-3

Publication outline: Introduction | CO₂ conversion studies on single metal crystals | Scope of review | Reaction mechanisms | Conclusions

Abstract-Summary

Despite series of experimental studies that reveal unique activities of late 3d transition metals and their role in microorganisms known for CO₂ conversion, these surfaces are not industrially viable yet. This review covers both experimental and theoretical studies into the mechanisms of CO₂ reduction into CO and methane, on single metals and bimetals of late 3d transition metals, i.e. Fe, Co, Ni, Cu and Zn. These mechanistic studies reveal CO₂ activation and reduction mechanisms are specific to both composition and surface facet. Surfaces with least CO₂ binding potential are seen to favour CO and O binding and provide higher barriers to dissociation. Hydrogen-assisted dissociation is seen to be generally favoured kinetically on Cu and Ni surfaces over direct dissociation except on the Ni (211) surface. Methane production on Cu and Ni surfaces is seen to occur via the non-formate pathway. Hydrogenation reactions have focused on Cu and Ni, and more needs to be done on other surfaces, i.e. Co, Fe and Zn.

First principles investigation on the applicability of ruthenium as a potential ORR catalyst

DOI: 10.1007/s12039-019-1691-9

Publication outline: Introduction | Models and computational details | Results and Discussion | Conclusions

Abstract-Summary

Realizing the wide acceptance of ruthenium as a promising catalyst for various catalytic reactions, we have investigated the plausibility of Ru to perform in the bulk as well as nanoparticle forms as an efficient oxygen reduction reaction catalyst. We report here that Ru cannot be an alternative to the Pt-based catalysts owing to a high overpotential. The catalytic activity of ruthenium catalysts for ORR was investigated with reference to the recent advancements in the development of ruthenium catalysts for various electrochemical reactions. The results reveal that both the surface as well as nanocluster based ruthenium systems do not outperform the Pt(111) catalyst.

Ability of density functional theory methods to accurately model the reaction energy pathways of the oxidation of CO on gold cluster: A benchmark study

DOI: 10.1007/s00214-016-1852-6

Publication outline: Introduction | Methods | Results and discussion | Summary

Abstract-Summary

Density functional theory (DFT) is the method of choice for the investigation of energy pathways of reactions assisted by metal nanoparticles due to their computational efficiency. The reliability of such theoretical studies depends to a large extent on the choice of the DFT functional used. The adsorption energies, barrier heights and reaction energies calculated using the DFT methods lie in a wide range with some methods showing high deviations from the CCSD(T) results. The percentage of Hartree-Fock exchange included in the DFT functional also plays a crucial role in predicting the correct pathway. Extensive benchmark study, it is suggested that the computationally less expensive hybrid density functionals, PBE0, B3PW91 and B3P86, are better suited for accurate modeling of this class of reactions.

Effects of correlated parameters and uncertainty in electronic-structure-based kinetic modelling

DOI: 10.1038/nchem.2454

Publication outline: Main | Results | Discussion | Conclusions | Methods

Abstract-Summary

Kinetic models based on first principles are becoming common place in heterogeneous catalysis because of their ability to interpret experimental data, identify the rate-controlling step, guide experiments and predict novel materials. To overcome the tremendous computational cost of estimating parameters of

complex networks on metal catalysts, approximate quantum mechanical calculations are employed that render models potentially inaccurate. We rationalize why models often underpredict reaction rates and show that, despite the uncertainty being large, the method can, in conjunction with experimental data, identify influential missing reaction pathways and provide insights into the catalyst active site and the kinetic reliability of a model.

Stability of heterogeneous single-atom catalysts: a scaling law mapping thermodynamics to kinetics

DOI: 10.1038/s41524-020-00411-6

Publication outline: Introduction | Results | Discussion | Methods

Abstract-Summary

We extend the current thermodynamic view of SAC stability in terms of the binding energy (E_{bind}) of single-metal atoms on a support to a kinetic (transport) one by considering the activation barrier for metal atom diffusion. A rapid computational screening approach allows predicting diffusion barriers for metal-support pairs based on E_{bind} of a metal atom to the support and the cohesive energy of the bulk metal (E_c). This diffusion scaling-law provides a simple model for screening thermodynamics to kinetics of metal adatom on a support.

Bulk and surface theoretical investigation of Nb-doped δ -FeOOH as a promising bifunctional catalyst

DOI: 10.1007/s00894-021-04864-4

Publication outline: Introduction | Theoretical methods | Results and discussion | Final remarks

Abstract-Summary

Iron oxyhydroxides have been identified as low-cost bifunctional catalysts. This work consists in the study, through DFT calculations, of the properties of the bulk and the surface of feroxyhyte (δ -FeOOH) doped with niobium, as a potential bifunctional catalyst. We identified the formation of stronger van der Waals interactions among the doped δ -FeOOH layers, which can increase the thermal stability of the catalyst. Evidence has been found that the insertion of Nb increases Brønsted acidity and gives rise to new Lewis acid sites on the catalyst surface.

Methanol Oxidation on Pt(111) from First-Principles in Heterogeneous and Electrocatalysis

DOI: 10.1007/s12678-017-0370-1

Publication outline: Introduction | Computational Details | Chemical and Electrochemical Environments | Energetics of Reaction Intermediates | Hydrogen-Covered Pt(111) Electrode | Conclusion

Abstract-Summary

We find characteristic differences between the methanol oxidation paths in heterogeneous and electro-catalysis. The

presence of the aqueous electrolyte stabilizes reaction intermediates containing hydrophilic groups thus also influencing the selectivity in the methanol oxidation. Adsorbed hydrogen on Pt(111) is shown to render the electro-oxidation of methanol less efficient.

Extended:

The presence of the aqueous electrolyte leads to the stabilization of reaction intermediates that contain hydrophilic groups such as hydroxyl when isomers are compared. The presence of adsorbed hydrogen atoms on Pt(111) is shown to be detrimental for methanol oxidation.

[Graph theory approach to determine configurations of multidentate and high coverage adsorbates for heterogeneous catalysis](#)

DOI: [10.1038/s41524-020-0345-2](https://doi.org/10.1038/s41524-020-0345-2)

Publication outline: [Introduction](#) | [Results and discussion](#) | [Methods](#)

Abstract-Summary

Growing computational power has permitted the extension of such studies to complex reaction networks involving either high adsorbate coverages or multidentate adsorbates, which bind to the surface through multiple atoms. Describing all possible adsorbate configurations for such systems, however, is often not possible based on chemical intuition alone. To systematically treat such complexities, we present a generalized Python-based graph theory approach to convert atomic scale models into undirected graph representations. These representations, when combined with workflows such as evolutionary algorithms, can systematically generate high coverage adsorbate models and classify unique minimum energy multidentate adsorbate configurations for surfaces of low symmetry, including multi-elemental alloy surfaces, steps, and kinks. Two case studies are presented which demonstrate these capabilities; first, an analysis of a coverage-dependent phase diagram of adsorbate NO on the Pt₃Sn(111) terrace surface, and second, an investigation of adsorption energies, together with identifying unique minimum energy configurations, for the reaction intermediate propyne (CHCCH₃^{*}) adsorbed on a PdIn(021) step surface.

[A Bayesian framework for adsorption energy prediction on bimetallic alloy catalysts](#)

DOI: [10.1038/s41524-020-00447-8](https://doi.org/10.1038/s41524-020-00447-8)

Publication outline: [Introduction](#) | [Results and discussion](#) | [Methods](#)

Abstract-Summary

We extend the single descriptor linear scaling relation to a multi-descriptor linear regression models to leverage the correlation between adsorption energy of any two pair of adsorbates. With a large dataset, we use Bayesian Information Criteria (BIC) as the model evidence to select the best linear regression model.

Gaussian Process Regression (GPR) based on the meaningful convolution of physical properties of the metal-adsorbate complex can be used to predict the baseline residual of the selected model. This integrated Bayesian model selection and Gaussian process regression, dubbed as residual learning, can achieve performance comparable to standard DFT error (0.1 eV) for most adsorbate system. For sparse and small datasets, we propose an ad hoc Bayesian Model Averaging (BMA) approach to make a robust prediction.

Extended:

We demonstrate a Bayesian framework for the model selection and model averaging for efficient and robust prediction of chemisorption energies of a few important multi-atom monodentate adsorbates on a bimetallic alloy dataset with the goal of novel catalytic materials discovery for hydrocarbon or nitrogen containing chemical reaction processes, such as, methanation, Fischer–Tropsch synthesis, and ammonia synthesis.

[The Effect of Hartree-Fock Exchange on Scaling Relations and Reaction Energetics for C–H Activation Catalysts](#)

DOI: [10.1007/s11244-021-01482-5](https://doi.org/10.1007/s11244-021-01482-5)

Publication outline: [Introduction](#) | [Reaction Mechanism](#) | [Computational Details](#) | [Results and Discussion](#) | [Conclusions](#)

Abstract-Summary

In open shell transition metal complexes (TMCs) that are promising for challenging reactions (e.g., C–H activation), the predictive power of DFT has been challenged, and properties are known to be strongly dependent on the admixture of Hartree-Fock (HF) exchange. We carry out a large-scale study of the effect of HF exchange on the predicted catalytic properties of over 1200 mid-row (i.e., Cr, Mn, Fe, Co) 3d TMCs for direct methane-to-methanol conversion. Narrower metal/oxidation/spin-state specific LFERs perform better and are less sensitive to HF exchange than absolute reaction energetics, except in the case of some intermediate/high-spin states. The interplay between spin-state dependent reaction energetics and exchange effects on spin-state ordering means that the choice of DFT functional strongly influences whether the minimum energy pathway is spin-conserved. Despite these caveats, LFERs involving catalysts that can be expected to have closed shell intermediates and low-spin ground states retain significant predictive power.

[Microscopic understanding of electrocatalytic reduction of CO₂ on Pd-polyaniline composite: an ab initio study](#)

DOI: [10.1007/s00894-018-3762-0](https://doi.org/10.1007/s00894-018-3762-0)

Publication outline: [Introduction](#) | [Methods](#) | [Results and discussion](#) | [Conclusions](#)

Abstract-Summary

It is found that both PANI and Pd/PANI show high selectivity for the formation of formic acid (HCOOH) over the methanol (CH₃OH) production. The electroreduction of CO₂ towards formic acid (HCOOH) follows two different pathways, depending

on the catalyst: on PANI the formation of HCOOH occurs through the *COOH intermediate, whereas for the case of Pd/PANI, the same reaction proceeds through the formation of formate (*OCHO). While the formation of CH₃OH from CO₂ on PANI is not feasible, electroreduction of CO₂ towards CH₃OH on Pd/PANI occurs through the formation of CO.

Extended:

It is also observed that the smaller-sized nanoparticles are more efficient for this reduction reaction [257]. It is found that the formation of *OCHO is 0.34 eV more favorable than that of *COOH.

Molecular Insights on the Role of (CTA⁺)(SiO⁻) Ion Pair into the Catalytic Activity of [CTA⁺]-Si-MCM-41

DOI: 10.1007/s11244-019-01181-2

Publication outline: Introduction | Method and Calculation Details | Results and Discussion | Conclusions

Abstract-Summary

A theoretical study in conjunction with a spectroscopic analysis by FTIR were carried out in order to obtain molecular insights on the role of (CTA⁺)(≡SiO⁻) ion pair into the catalytic activity of [CTA⁺]-Si-MCM-41, the non-calcined form of Si-MCM-41. The reaction of transesterification of ethyl acetate with methanol was used as a model of transesterification of vegetal oils using the mesoporous heterogeneous catalyst. It is found that the most favorable reaction mechanism is the dual site mechanism and that the presence of the (CTA⁺)(≡SiO⁻) ionic pair is fundamental for the catalytic activity.

Extended:

The reaction of transesterification of ethyl acetate (which is the simplest known ester) with methanol was used as a model of transesterification of vegetal oils. Further studies on the nature of interactions on these systems are under investigation in our laboratory, and results will be published in the near future.

Bibliography

[1] Huo CF, Wu BS, Gao P, Yang Y, Li YW, Jiao H (2011) *Angew Chem Int Ed* 50:7403

[2] Wang T, Wang S, Luo Q, Li Y-W, Wang J, Beller M, Jiao H (2014) *J Phys Chem C* 118:4181

[3] Blöchl PE (1994) *Phys Rev B* 50:17953

[4] Kresse G, Joubert D (1999) *Phys Rev B* 59:1758

[5] Methfessel M, Paxton AT (1989) *Phys Rev B* 40:3616

[6] Jónsson H, Mills G, Jacobsen KW (1998) *Classical and quantum dynamics in condensed phase simulations*. World Scientific, Singapore

[7] de Smit E, Cinquini F, Beale AM, Safonova OV, van Beek W, Sautet P, Weckhuysen BM (2010) *J Am Chem Soc* 132:14928

[8] Le Caer G, Dubois JM, Pijolat M, Perrichon V, Bussiere P (1982) *J Phys Chem* 86:4799

[9] Govender NS, de Croon MHJM, Schouten JC (2010) *Appl Catal A* 373:81

[10] Sutton, J. E. & Vlachos, D. G. Building large microkinetic models with first-principles' accuracy at reduced computational cost. *Chem. Eng. Sci.* 121, 190–199 (2015).

[11] Reuter, K. Ab initio thermodynamics and first-principles microkinetics for surface catalysis. *Catal. Lett.* 146, 541–563 (2016).

[12] Nørskov, J. K., Studt, F., Abild-Pedersen, F. & Bligaard, T. *Fundamental Concepts in Heterogeneous Catalysis* (Wiley, 2014).

[13] Andersen, M., Panosetti, C. & Reuter, K. A practical guide to surface kinetic monte carlo simulations. *Front. Chem.* 7, 202 (2019).

[14] Reuter, K., Frenkel, D. & Scheffler, M. The steady state of heterogeneous catalysis, studied by first-principles statistical mechanics. *Phys. Rev. Lett.* 93, 116105 (2004). One of the first couplings of first-principles calculations with kinetic Monte Carlo models that explored the steady state of CO oxidation on RuO₂ (110) and provided valuable mechanistic insight.

[15] Gokhale, A. A., Dumesic, J. A. & Mavrikakis, M. On the mechanism of low-temperature water gas shift reaction on copper. *J. Am. Chem. Soc.* 130, 1402–1414 (2008).

[16] Honkala, K. et al. Ammonia synthesis from first-principles calculations. *Science* 307, 555–558 (2005).

[17] Inderwildi, O. R., Jenkins, S. J. & King, D. A. An unexpected pathway for the catalytic oxidation of methylidyne on Rh(111) as a route to syngas. *J. Am. Chem. Soc.* 129, 1751–1759 (2007).

[18] Saeys, M., Reyniers, M. F., Neurock, M. & Marin, G. B. Ab initio reaction path analysis of benzene hydrogenation to cyclohexane on Pt(111). *J. Phys. Chem. B* 109, 2064–2073 (2005).

[19] Pilot, I. A. W., Van Santen, R. A. & Hensen, E. J. M. The optimally performing Fischer–Tropsch catalyst. *Angew. Chem. Int. Ed.* 53, 12746–12750 (2014).

[20] Greeley, J. Theoretical heterogeneous catalysis: scaling relationships and computational catalyst design. *Annu. Rev. Chem. Biomol. Eng.* 7, 605–635 (2016).

[21] Vlachos, D. G. Multiscale integration hybrid algorithms for homogeneous–heterogeneous reactors. *AIChE J.* 43, 3031–3041 (1997).

[22] Deutschmann, O. (ed.) *Modeling and Simulation of Heterogeneous Catalytic Reactions* (Wiley, 2012).

[23] Maestri, M. & Cuoci, A. Coupling CFD with detailed microkinetic modeling in heterogeneous catalysis. *Chem. Eng. Sci.* 96, 106–117 (2013).

- [24] Matera, S. & Reuter, K. First-principles approach to heat and mass transfer effects in model catalyst studies. *Catal. Lett.* 133, 156–159 (2009).
- [25] Matera, S. & Reuter, K. Transport limitations and bistability for in situ CO oxidation at RuO₂(110): First-principles based multiscale modeling. *Phys. Rev. B Condens. Matter Mater. Phys.* 82, 085446 (2010).
- [26] Matera, S., Maestri, M., Cuoci, A. & Reuter, K. Predictive-quality surface reaction chemistry in real reactor models: Integrating first-principles kinetic Monte Carlo simulations into computational fluid dynamics. *ACS Catal.* 4, 4081–4092 (2014).
- [27] Sabbe, M. K., Reyniers, M.-F. & Reuter, K. First-principles kinetic modeling in heterogeneous catalysis: an industrial perspective on best-practice, gaps and needs. *Catal. Sci. Technol.* 2, 2010–2024 (2012).
- [28] Jørgensen, M. & Grönbeck, H. The site-assembly determines catalytic activity of nanoparticles. *Angew. Chem. Int. Ed.* 57, 5086–5089 (2018). Constructing kinetic Monte Carlo models on metal nanoparticles allowed addressing structural complexity of metal catalysts and revealed synergistic effects between assemblies of active sites.
- [29] Jørgensen, M. & Grönbeck, H. Scaling relations and kinetic Monte Carlo simulations to bridge the materials gap in heterogeneous catalysis. *ACS Catal.* 7, 5054–5061 (2017).
- [30] Calle-Vallejo, F., Loffreda, D., Koper, M. T. M. & Sautet, P. Introducing structural sensitivity into adsorption–energy scaling relations by means of coordination numbers. *Nat. Chem.* 7, 403–410 (2015).
- [31] Keil, F. J. Molecular modelling for reactor design. *Annu. Rev. Chem. Biomol. Eng.* 9, 201–227 (2018).
- [32] Hohenberg P, Kohn W (1964) *Phys Rev* 136:B864–B871
- [33] Kohn W, Sham LJ (1965) *Phys Rev* 140:A1133–A1138
- [34] Hu CH, Chizallet C, Mager-Maury C, Corral Valero M, Sautet P, Toulhoat H, Raybaud P (2010) *J Catal* 274:99–110
- [35] Briquet LGV, Catlow CRA, French SA (2009) *J Phys Chem C* 113:16747–16756
- [36] Corral Valero M, Raybaud P, Sautet P (2007) *Phys Rev B* 75(045427):045421
- [37] Iachella M, Wilson A, Naitabdi A, Bernard R, Prévot G, Loffreda D (2016) *Nanoscale* 8:16475–16485
- [38] Van Speybroeck V, De Wispelaere K, Van der Mynsbrugge J, Vandichel M, Hemelsoet K, Waroquier M (2014) *Chem Soc Rev* 43:7326–7357
- [39] Rey J, Bignaud C, Raybaud P, Bucko T, Chizallet C (2020) *Angew Chem Int Ed* 59:18938–18942
- [40] Rey J, Gomez A, Raybaud P, Chizallet C, Bučko T (2019) *J Catal* 373:361–373
- [41] Bučko T, Hafner J (2015) *J Catal* 329:32–48
- [42] Cnudde P, De Wispelaere K, Vanduyfhuys L, Demuynck R, Van der Mynsbrugge J, Waroquier M, Van Speybroeck V (2018) *ACS Catal* 8:9579–9595
- [43] Cnudde P, De Wispelaere K, Van der Mynsbrugge J, Waroquier M, Van Speybroeck V (2017) *J Catal* 345:53–69
- [44] Laloué N, Laroche C, Jobic H, Méthivier A (2009) *Oil & Gas Science and Technology - Revue de l'IFP* 64:773–793
- [45] Laloué N, Laroche C, Jobic H, Méthivier A (2007) *Adsorption* 13:491–500
- [46] Huang WL, Li J, Liu Z, Zhou J, Ma C, Wen L-X (2019) *Chem Eng Sci* 198:253–259
- [47] Krishna R, van Baten JM, Dubbeldam D (2004) *J Phys Chem B* 108:14820–14822
- [48] Krishna R, van Baten JM (2019) *ACS Omega* 4:10761–10766
- [49] Teixeira AR, Qi X, Conner WC, Mountziaris TJ, Fan W, Dauenhauer PJ (2015) *Chem Mater* 27:4650–4660
- [50] Calle-Vallejo F, Loffreda D, Koper MTM, Sautet P (2015) *Nat Chem* 7:403–410
- [51] Calle-Vallejo F, Martinez JI, Garcia-Lastra JM, Sautet P, Loffreda D (2014) *Angew Chem Int Ed* 53:8316–8319
- [52] Calle-Vallejo F, Tymoczko J, Colic V, Vu QH, Pohl MD, Morgenstern K, Loffreda D, Sautet P, Schuhmann W, Bandarenko AS (2015) *Science* 350:185–189
- [53] Shakouri K, Behler J, Meyer J, Kroes GJ (2017) *J Phys Chem Lett* 8:2131–2136
- [54] Jinnouchi R, Lahnsteiner J, Karsai F, Kresse G, Bokdam M (2019) *Phys Rev Lett* 122:225701
- [55] Zhang L, Lin DY, Wang H, Car R (2019) *Phys Rev Mater* 3:0804
- [56] Artrith N, Kolpak AM (2014) *Nano Lett* 14:2670–2676
- [57] Burkett SL, Davis ME (1995) *Chem Mater* 7:920–928
- [58] Li J, Corma A, Yu J (2015) *Chem Soc Rev* 44:7112–7127
- [59] Dusselier M, Davis ME (2018) *Chem Rev* 118:5265–5329
- [60] Gallego EM, Portilla MT, Paris C, León-Escamilla A, Boronat M, Moliner M, Corma A (2017) *Science* 355:1051–1054
- [61] Van Speybroeck V, Hemelsoet K, Joos L, Waroquier M, Bell RG, Catlow CRA (2015) *Chem Soc Rev* 44:7044–7111
- [62] Gounder R, Iglesia E (2012) *Acc Chem Res* 45:229–238

- [63] Van der Mynsbrugge J, De Ridder J, Hemelsoet K, Waroquier M, Van Speybroeck V (2013) *Chem Eur J* 19:11568–11576
- [64] Chen YY, Zhao XH, Qin ZF, Wang S, Wei ZH, Li JF, Dong M, Wang JG, Fan WB (2020) *J Phys Chem C* 124:13789–13798
- [65] Sabnis KD et al (2015) Water-gas shift catalysis over transition metals supported on molybdenum carbide. *J Catal* 331:162–171
- [66] Pazmiño JH et al (2012) Metallic Pt as active sites for the water-gas shift reaction on alkali-promoted supported catalysts. *J Catal* 286:279–286
- [67] Williams WD et al (2010) Metallic corner atoms in gold clusters supported on rutile are the dominant active site during water-gas shift catalysis. *J Am Chem Soc* 132(40):14018–14020
- [68] Choksi T, Majumdar P, Greeley JP (2018) Electrostatic origins of linear scaling relationships at bifunctional metal/oxide interfaces: a case study of Au nanoparticles on doped MgO Substrates. *Angew Chemie* 130(47):15636–15640
- [69] Mehta P, Greeley J, Delgass WN, Schneider WF (2017) Adsorption energy correlations at the metal-support boundary. *ACS Catal* 7(7):4707–4715
- [70] Aranifard S, Ammal SC, Heyden A (2014) On the importance of metal-oxide interface sites for the water-gas shift reaction over Pt/CeO₂ catalysts. *J Catal* 309:314–324
- [71] Song W, Hensen EJM (2014) Mechanistic aspects of the water-gas shift reaction on isolated and clustered Au atoms on CeO₂ (110): a density functional theory study. *ACS Catal* 4(6):1885–1892
- [72] Kauppinen MM, Melander MM, Bazhenov AS, Honkala K (2018) Unraveling the role of the RhZrO₂ interface in the water-gas shift reaction via a first-principles microkinetic study. *ACS Catal* 8(12):11633–11647
- [73] Flaherty DW, Yu WY, Pozun ZD, Henkelman G, Mullins CB (2011) Mechanism for the water-gas shift reaction on monofunctional platinum and cause of catalyst deactivation. *J Catal* 282(2):278–288
- [74] Hammer, B. & Nørskov, J. K. Why gold is the noblest of all the metals. *Nature* 376, 238–240 (1995).
- [75] Nørskov, J. K. Electronic structure factors in catalysis. *Prog. Surf. Sci.* 38, 103–144 (1991).
- [76] Nilsson, A. et al. The electronic structure effect in heterogeneous catalysis. *Catal. Lett.* 100, 111–114 (2005).
- [77] Hammer, B. & Nørskov, J. K. Theoretical surface science and catalysis—calculations and concepts. *Adv. Catal.* 45, 71–129 (2000).
- [78] Kitchin, J. R., Nørskov, J. K., Barteau, M. A. & Chen, J. G. Modification of the surface electronic and chemical properties of Pt(111) by subsurface 3d transition metals. *J. Chem. Phys.* 120, 10240–10246 (2004).
- [79] Logadottir, A. et al. The Brønsted–Evans–Polanyi relation and the volcano plot for ammonia synthesis over transition metal catalysts. *J. Catal.* 197, 229–231 (2001).
- [80] Wang, S. et al. Universal Brønsted–Evans–Polanyi relations for C–C, C–O, C–N, N–O, N–N, and O–O dissociation reactions. *Catal. Lett.* 141, 370–373 (2010).
- [81] Nørskov, J. K. et al. The nature of the active site in heterogeneous metal catalysis. *Chem. Soc. Rev.* 37, 2163–2171 (2008).
- [82] Michaelides, A. et al. Identification of general linear relationships between activation energies and enthalpy changes for dissociation reactions at surfaces. *J. Am. Chem. Soc.* 125, 3704–3705 (2003).
- [83] Bligaard, T. et al. The Brønsted–Evans–Polanyi relation and the volcano curve in heterogeneous catalysis. *J. Catal.* 224, 206–217 (2004).
- [84] Loffreda, D., Delbecq, F., Vigne, F. & Sautet, P. Fast prediction of selectivity in heterogeneous catalysis from extended Brønsted–Evans–Polanyi relations: a theoretical insight. *Angew. Chem. Int. Ed.* 48, 8978–8980 (2009).
- [85] Vojvodic, A. et al. On the behavior of Brønsted–Evans–Polanyi relations for transition metal oxides. *J. Chem. Phys.* 134, 244509 (2011).
- [86] Wang, S. et al. Universal transition state scaling relations for (de)hydrogenation over transition metals. *Phys. Chem. Chem. Phys.* 13, 20760–20765 (2011).
- [87] Viñes, F., Vojvodic, A., Abild-Pedersen, F. & Illas, F. Brønsted–Evans–Polanyi relationship for transition metal carbide and transition metal oxide surfaces. *J. Phys. Chem. C* 117, 4168–4171 (2013).
- [88] Yang, B., Burch, R., Hardacre, C., Headdock, G. & Hu, P. Understanding the optimal adsorption energies for catalyst screening in heterogeneous catalysis. *ACS Catal.* 4, 182–186 (2013).
- [89] Fajín, J. L. C., Cordeiro, M. N. D. S., Illas, F. & Gomes, J. R. B. Generalized Brønsted–Evans–Polanyi relationships and descriptors for O–H bond cleavage of organic molecules on transition metal surfaces. *J. Catal.* 313, 24–33 (2014).
- [90] Greeley, J., Jaramillo, T. F., Bonde, J., Chorkendorff, I. & Nørskov, J. K. Computational high-throughput screening of electrocatalytic materials for hydrogen evolution. *Nat. Mater.* 5, 909–913 (2006).
- [91] Zhang, Y.-J., Sethuraman, V., Michalsky, R. & Peterson, A. A. Competition between CO₂ reduction and H₂ evolution on transition-metal electrocatalysts. *ACS Catal.* 4, 3742–3748 (2014).

- [92] Cave, E. R. et al. Trends in the catalytic activity of hydrogen evolution during CO₂ electroreduction on transition metals. *ACS Catal.* 8, 3035–3040 (2018).
- [93] Greeley, J., Nørskov, J. K., Kibler, L. A., El-Aziz, A. M. & Kolb, D. M. Hydrogen evolution over bimetallic systems: understanding the trends. *ChemPhysChem* 7, 1032–1035 (2006).
- [94] Calle-Vallejo, F., Loffreda, D., Koper, M. T. & Sautet, P. Introducing structural sensitivity into adsorption–energy scaling relations by means of coordination numbers. *Nat. Chem.* 7, 403–410 (2015).
- [95] Hong, W. T. et al. Toward the rational design of non-precious transition metal oxides for oxygen electrocatalysis. *Energy Environ. Sci.* 8, 1404–1427 (2015).
- [96] Tsai, C., Chan, K., Nørskov, J. K. & Abild-Pedersen, F. Understanding the reactivity of layered transition-metal sulfides: a single electronic descriptor for structure and adsorption. *J. Phys. Chem. Lett.* 5, 3884–3889 (2014).
- [97] Xu, H., Cheng, D., Cao, D. & Zeng, X. C. A universal principle for a rational design of single-atom electrocatalysts. *Nat. Catal.* 1, 339–348 (2018).
- [98] Wang, A., Li, J. & Zhang, T. Heterogeneous single-atom catalysis. *Nat. Rev. Chem.* 2, 65–81 (2018).
- [99] Marcinkowski, M. D. et al. Pt/Cu single-atom alloys as coke-resistant catalysts for efficient C–H activation. *Nat. Chem.* 10, 325–332 (2018).
- [100] Zhang, Z. et al. Thermally stable single atom Pt/m-Al₂O₃ for selective hydrogenation and CO oxidation. *Nat. Commun.* 8, 16100 (2017).
- [101] Mehta, P. et al. Overcoming ammonia synthesis scaling relations with plasma-enabled catalysis. *Nat. Catal.* 1, 269–275 (2018).
- [102] Sun, G. et al. Breaking the scaling relationship via thermally stable Pt/Cu single atom alloys for catalytic dehydrogenation. *Nat. Commun.* 9, 4454 (2018).
- [103] Nie, L. et al. Activation of surface lattice oxygen in single-atom Pt/CeO₂ for low-temperature CO oxidation. *Science* 358, 1419–1423 (2017).
- [104] Liu, J. et al. Tackling CO poisoning with single-atom alloy catalysts. *J. Am. Chem. Soc.* 138, 6396–6399 (2016).
- [105] Lucci, F. R. et al. Selective hydrogenation of 1,3-butadiene on platinum–copper alloys at the single-atom limit. *Nat. Commun.* 6, 8550 (2015).
- [106] Qiao, B. et al. Single-atom catalysis of CO oxidation using Pt₁/FeO_x. *Nat. Chem.* 3, 634–641 (2011).
- [107] Bruix, A. et al. Maximum noble-metal efficiency in catalytic materials: atomically dispersed surface platinum. *Angew. Chem. Int. Ed.* 53, 10525–10530 (2014).
- [108] Wei, H. et al. FeO_x-supported platinum single-atom and pseudo-single-atom catalysts for chemoselective hydrogenation of functionalized nitroarenes. *Nat. Commun.* 5, 5634 (2014).
- [109] Zhang, S. et al. Catalysis on singly dispersed bimetallic sites. *Nat. Commun.* 6, 7938 (2015).
- [110] Cheng, M.-J., Clark, E. L., Pham, H. H., Bell, A. T. & Head-Gordon, M. Quantum mechanical screening of single-atom bimetallic alloys for the selective reduction of CO₂ to C₁ hydrocarbons. *ACS Catal.* 6, 7769–7777 (2016).
- [111] Lin, L. et al. A highly CO-tolerant atomically dispersed Pt catalyst for chemoselective hydrogenation. *Nat. Nanotechnol.* 14, 354–361 (2019).
- [112] Liu, D. et al. Atomically dispersed platinum supported on curved carbon supports for efficient electrocatalytic hydrogen evolution. *Nat. Energy* 4, 512–518 (2019).
- [113] Darby, M. T., Stamatakis, M., Michaelides, A. & Sykes, E. C. H. Lonely atoms with special gifts: breaking linear scaling relationships in heterogeneous catalysis with single-atom alloys. *J. Phys. Chem. Lett.* 9, 5636–5646 (2018).
- [114] Liao, P. & Carter, E. A. New concepts and modeling strategies to design and evaluate photo-electro-catalysts based on transition metal oxides. *Chem. Soc. Rev.* 42, 2401–2422 (2013).
- [115] Bhatt, M. D. & Lee, J. S. Recent theoretical progress in the development of photoanode materials for solar water splitting photoelectrochemical cells. *J. Mater. Chem. A* 3, 10632–10659 (2015).
- [116] Skone, J. H., Govoni, M. & Galli, G. Self-consistent hybrid functional for condensed systems. *Phys. Rev. B* 89, 195112 (2014).
- [117] Wood, B. C., Schwegler, E., Choi, W. I. & Ogitsu, T. Hydrogen-bond dynamics of water at the interface with InP/GaP (001) and the implications for photoelectrochemistry. *J. Am. Chem. Soc.* 135, 15774–15783 (2013).
- [118] Wood, B. C., Schwegler, E., Choi, W. I. & Ogitsu, T. Surface chemistry of GaP (001) and InP (001) in contact with water. *J. Phys. Chem. C* 118, 1062–1070 (2014).
- [119] Shen, X. et al. Photocatalytic water oxidation at the GaN (101E0)- water interface. *J. Phys. Chem. C* 114, 13695–13704 (2010).
- [120] Wang, J., Pedroza, L. S., Poissier, A. & Fernández-Serra, M. Water dissociation at the GaN (10 0) surface: structure, dynamics and surface acidity. *J. Phys. Chem. C* 116, 14382–14389 (2012).
- [121] Kharche, N., Muckerman, J. T. & Hybertsen, M. S. First-principles approach to calculating energy level alignment at aqueous semiconductor interfaces. *Phys. Rev. Lett.* 113, 176802 (2014).

- [122] Ping, Y., Sundararaman, R. & Goddard, W. A. III Solvation effects on the band edge positions of photocatalysts from first principles. *Phys. Chem. Chem. Phys.* 17, 30499–30509 (2015).
- [123] Ping, Y., Goddard, W. A. III & Galli, G. A. Energetics and solvation effects at the photoanode/catalyst interface: ohmic contact versus Schottky barrier. *J. Am. Chem. Soc.* 137, 5264–5267 (2015).
- [124] Kim, T. W. & Choi, K.-S. Nanoporous BiVO₄ photoanodes with dual-layer oxygen evolution catalysts for solar water splitting. *Science* 343, 990–994 (2014).
- [125] Kim, T. W., Ping, Y., Galli, G. A. & Choi, K.-S. Simultaneous enhancements in photon absorption and charge transport of bismuth vanadate photoanodes for solar water splitting. *Nat. Commun.* 6, 8769 (2015).
- [126] Cheng, H. & Selloni, A. Hydroxide ions at the water/anatase TiO₂ (101) interface: structure and electronic states from first principles molecular dynamics. *Langmuir* 26, 11518–11525 (2010).
- [127] Cheng, J. & Sprik, M. The electric double layer at a rutile TiO₂ water interface modelled using density functional theory based molecular dynamics simulation. *J. Phys. Condens. Matter* 26, 244108 (2014).
- [128] Warshel, A. Energetics of enzyme catalysis. *Proc. Natl Acad. Sci. USA* 75, 5250–5254 (1978).
- [129] Bhowmick, A., Sharma, S. C. & Head-Gordon, T. The importance of the scaffold for de novo enzymes: a case study with kemp eliminase. *J. Am. Chem. Soc.* 139, 5793–5800 (2017).
- [130] Liu, C. T. et al. Probing the electrostatics of active site microenvironments along the catalytic cycle for Escherichia coli dihydrofolate reductase. *J. Am. Chem. Soc.* 136, 10349–10360 (2014).
- [131] Mansoor, E., Mynsbrugge, J. Vd, Head-Gordon, M. & Bell, A. T. Impact of long-range electrostatic and dispersive interactions on theoretical predictions of adsorption and catalysis in zeolites. *Catal. Today* 312, 51–65 (2018).
- [132] Deshlahra, P. & Iglesia, E. Toward more complete descriptors of reactivity in catalysis by solid acids. *ACS Catal* 6, 5386–5392 (2016).
- [133] Gorin, C. F., Beh, E. S. & Kanan, M. W. An electric field-induced change in the selectivity of a metal oxide-catalyzed epoxide rearrangement. *J. Am. Chem. Soc.* 134, 186–189 (2012).
- [134] Levin, M. D. et al. Scope and mechanism of cooperativity at the intersection of organometallic and supramolecular catalysis. *J. Am. Chem. Soc.* 138, 9682–9693 (2016).
- [135] Aragonés, A. C. et al. Electrostatic catalysis of a Diels–Alder reaction. *Nature* 531, 88–91 (2016).
- [136] Akamatsu, M., Sakai, N. & Matile, S. Electric-field-assisted anion- π catalysis. *J. Am. Chem. Soc.* 139, 6558–6561 (2017).
- [137] Dinpajoo, M. & Matyushov, D. V. Dielectric constant of water in the interface. *J. Chem. Phys.* 145, 014504 (2016).
- [138] Zhang, C., Gygi, F. & Galli, G. Strongly anisotropic dielectric relaxation of water at the nanoscale. *J. Phys. Chem. Lett.* 4, 2477–2481 (2013).
- [139] Sundararaman, R. & Schwarz, K. Evaluating continuum solvation models for the electrode–electrolyte interface: challenges and strategies for improvement. *J. Chem. Phys.* 146, 084111 (2017).
- [140] Hansen, H. A., Viswanathan, V. & Nørskov, J. K. Unifying kinetic and thermodynamic analysis of 2e⁻ and 4e⁻ reduction of oxygen on metal surfaces. *J. Phys. Chem. C* 118, 6706–6718 (2014).
- [141] Ghosh, S., Castillo-Lora, J., Soudackov, A. V., Mayer, J. M. & Hammes-Schiffer, S. Theoretical insights into proton-coupled electron transfer from a photoreduced ZnO nanocrystal to an organic radical. *Nano Lett.* 17, 5762–5767 (2017).
- [142] Wang, L., Fried, S. D. & Markland, T. E. Proton network flexibility enables robustness and large electric fields in the ketosteroid isomerase active site. *J. Phys. Chem. B* 121, 9807–9815 (2017).
- [143] Xiao L, Wang L (2004) Structures of platinum clusters: planar or spherical? *J Phys Chem A* 108:8605–8614
- [144] Wang L, Johnson DD (2007) Density functional study of structural trends for late-transition-metal 13-atom clusters. *Phys Rev B* 75:235405–235410
- [145] Bhattacharyya K, Majumder Ch (2007) Growth pattern and bonding trends in Ptn (n = 2–13) clusters: theoretical investigation based on first principle calculations. *Chem Phys Lett* 446:374–379
- [146] Perdew JP, Chevary JA, Vosko SH, Jackson KA, Pederson MR, Singh DJ, Fiolhais C (1992) Atoms, molecules, solids, and surfaces: applications of the generalized gradient approximation for exchange and correlation. *Phys Rev B* 46:6671–6687
- [147] Perdew JP, Chevary JA, Vosko SH, Jackson KA, Pederson MR, Singh DJ, Fiolhais C (1993) Erratum: donor transition energy in GaAs superlattices in a magnetic field along the growth axis. *Phys Rev B* 48:4978
- [148] Hammett, L. P. The effect of structure upon the reactions of organic compounds. Benzene derivatives. *J. Am. Chem. Soc.* 59, 96–103 (1937).
- [149] Centi G, Trifirò F, Ebner JR, Franchetti VM (1988) *Chem Rev* 88:55–80
- [150] Centi G, Fornaseri G, Trifiro F (1985) n-butane oxidation to maleic anhydride on vanadium-phosphorus oxides: kinetic analysis with a tubular flow stacked-pellet reactor. *Ind Eng Chem Prod Res Dev* 24:32–37

- [151] Gascón J, Valenciano R, Téllez C, Herguido J, Menéndez M (2006) A generalized kinetic model for the partial oxidation of n-butane to maleic anhydride under aerobic and anaerobic conditions. *Chem Eng Sci* 61:6385–6394
- [152] Huang XF, Li CY, Chen BH, Silveston PL (2002) Transient kinetics of n-Butane oxidation to maleic anhydride over a VPO catalyst. *Am Inst Chem Eng J* 48:846–855
- [153] Lesser D, Mestl G, Turek T (2016) Transient behavior of vanadyl pyrophosphate catalysts during the partial oxidation of n-butane in industrial-sized, fixed bed reactors. *Appl Catal A Gen* 510:1–10
- [154] Lesser D, Mestl G, Turek T (2016) *Chem Eng Sci* (to be published)
- [155] Ping, Y., Nielsen, R. J. & Goddard, W. A. The reaction mechanism with free energy barriers at constant potentials for the oxygen evolution reaction at the IrO₂ (110) surface. *J. Am. Chem. Soc.* 139, 149–155 (2017).
- [156] Xiao, H., Shin, H. & Goddard, W. A. Synergy between Fe and Ni in the optimal performance of (Ni,Fe)OOH catalysts for the oxygen evolution reaction. *Proc. Natl Acad. Sci. USA* 115, 5872–5877 (2018).
- [157] Li, X., Rong, H., Zhang, J., Wang, D. & Li, Y. Modulating the local coordination environment of single-atom catalysts for enhanced catalytic performance. *Nano Res.* 13, 1842–1855 (2020).
- [158] Mathew, K., Sundararaman, R., Letchworth-Weaver, K., Arias, T. A. & Hennig, R. G. Implicit solvation model for density-functional study of nanocrystal surfaces and reaction pathways. *J. Chem. Phys.* 140, 084106 (2014).
- [159] Huang, Y., Nielsen, R. J. & Goddard, W. A. Reaction mechanism for the hydrogen evolution reaction on the basal plane sulfur vacancy site of MoS₂ using grand canonical potential kinetics. *J. Am. Chem. Soc.* 140, 16773–16782 (2018).
- [160] Deshpande, S. & Greeley, J. First-Principles Analysis of Coverage, Ensemble, and Solvation Effects on Selectivity Trends in NO Electroreduction on Pt₃Sn Alloys. *ACS Catal.* 10, 9320–9327 (2020).
- [161] Clayborne, A., Chun, H.-J., Rankin, R. B. & Greeley, J. Elucidation of Pathways for NO Electroreduction on Pt(111) from First Principles. *Angew. Chem. Int. Ed.* 54, 8255–8258 (2015).
- [162] Faheem, M. & Heyden, A. Hybrid Quantum Mechanics/Molecular Mechanics Solvation Scheme for Computing Free Energies of Reactions at Metal-Water Interfaces. *J. Chem. Theory Comput.* 10, 3354–3368 (2014).
- [163] Ryde, U. How Many Conformations Need To Be Sampled To Obtain Converged QM/MM Energies? The Curse of Exponential Averaging. *J. Chem. Theory Comput.* 13, 5745–5752 (2017).
- [164] Bhattacharya, A., Pati, D., Pillai, N. S. & Dunson, D. B. Dirichlet–Laplace priors for optimal shrinkage. *J. Am. Stat. Assoc.* 110, 1479–1490 (2015).
- [165] Carvalho, C. M., Polson, N. G. & Scott, J. G. The horseshoe estimator for sparse signals. *Biometrika* 97, 465–480 (2010).
- [166] Stavale, F. et al. Donor characteristics of transition-metal-doped oxides: Cr-doped MgO versus Mo-doped CaO. *J. Am. Chem. Soc.* 134, 11380–11383 (2012).
- [167] Rumble, J. R. *CRC Handbook of Chemistry and Physics*, 99th (Internet Version 2018) (CRC Press/Taylor & Francis, Boca Raton, FL).
- [168] Greeley, J. Theoretical heterogeneous catalysis: scaling relationships and computational catalyst design. *Annu. Rev. Chem. Biomol.* 7, 605–635 (2016).
- [169] Bruix, A., Margraf, J. T., Andersen, M. & Reuter, K. First-principles-based multiscale modelling of heterogeneous catalysis. *Nat. Catal.* 2, 659–670 (2019).
- [170] Quesne, M. G., Silveri, F., de Leeuw, N. H. & Catlow, C. R. A. Advances in sustainable catalysis: a computational perspective. *Front. Chem.* 7, 182 (2019).
- [171] Schlexer Lamoureux, P. et al. Machine learning for computational heterogeneous catalysis. *ChemCatChem* 11, 3581–3601 (2019).
- [172] Cheng, J. & Sprik, M. Alignment of electronic energy levels at electrochemical interfaces. *Phys. Chem. Chem. Phys.* 14, 11245–11267 (2012).
- [173] Pham, T. A., Ping, Y. & Galli, G. Modelling heterogeneous interfaces for solar water splitting. *Nat. Mater.* 16, 401–408 (2017).
- [174] Rousseau, R., Glezakou, V.-A. & Selloni, A. Theoretical insights into the surface physics and chemistry of redox-active oxides. *Nat. Rev. Mater.* 5, 460–475 (2020).
- [175] Venkataraman, C., Soudackov, A. V. & Hammes-Schiffer, S. Theoretical formulation of nonadiabatic electrochemical proton-coupled electron transfer at metal–solution interfaces. *J. Phys. Chem. C* 112, 12386–12397 (2008).
- [176] Goldsmith, Z. K., Lam, Y. C., Soudackov, A. V. & Hammes-Schiffer, S. Proton discharge on a gold electrode from triethylammonium in acetonitrile: theoretical modeling of potential-dependent kinetic isotope effects. *J. Am. Chem. Soc.* 141, 1084–1090 (2019).
- [177] Jackson, M. N. & Surendranath, Y. Donor-dependent kinetics of interfacial proton-coupled electron transfer. *J. Am. Chem. Soc.* 138, 3228–3234 (2016).
- [178] Lam, Y.-C., Soudackov, A. V. & Hammes-Schiffer, S. Theory of electrochemical proton-coupled electron transfer in diabatic vibronic representation: application to proton discharge on metal electrodes in alkaline solution. *J. Phys. Chem. C* 124, 27309–27322 (2020).

- [179] Sakaushi, K. Quantum proton tunneling in multi-electron/-proton transfer electrode processes. *Faraday Discuss.* 221, 428–448 (2020).
- [180] Schkolnik, G. et al. Vibrational Stark effect of the electric-field reporter 4-mercaptobenzonitrile as a tool for investigating electrostatics at electrode/SAM/solution interfaces. *Int. J. Mol. Sci.* 13, 7466–7482 (2012).
- [181] Patrow, J. G., Sorenson, S. A. & Dawlaty, J. M. Direct spectroscopic measurement of interfacial electric fields near an electrode under polarizing or current-carrying conditions. *J. Phys. Chem. C* 121, 11585–11592 (2017).
- [182] Sorenson, S. A., Patrow, J. G. & Dawlaty, J. M. Solvation reaction field at the interface measured by vibrational sum frequency generation spectroscopy. *J. Am. Chem. Soc.* 139, 2369–2378 (2017).
- [183] Gerosa, M., Gygi, F., Govoni, M. & Galli, G. The role of defects and excess surface charges at finite temperature for optimizing oxide photoabsorbers. *Nat. Mater.* 17, 1122–1127 (2018).
- [184] Hoster, H. E., Alves, O. B. & Koper, M. T. M. Tuning adsorption via strain and vertical ligand effects. *ChemPhysChem* 11, 1518–1524 (2010).
- [185] van der Niet, M. J. T. C., Garcia-Araez, N., Hernández, J., Feliu, J. M. & Koper, M. T. M. Water dissociation on well-defined platinum surfaces: the electrochemical perspective. *Catal. Today* 202, 105–113 (2013).
- [186] Rossmesl, J. et al. Realistic cyclic voltammograms from ab initio simulations in alkaline and acidic electrolytes. *J. Phys. Chem. C* 124, 20055–20065 (2020).
- [187] Tiwari, A. et al. Fingerprint voltammograms of copper single crystals under alkaline conditions: a fundamental mechanistic analysis. *J. Phys. Chem. Lett.* 11, 1450–1455 (2020).
- [188] Schlexer P, Widmann D, Behm RJ, Pacchioni G (2018) CO oxidation on a Au/TiO₂ nanoparticle catalyst via the Au-Assisted Mars–van Krevelen mechanism. *ACS Catal* 8:6513–6525
- [189] Puigdollers AR, Pacchioni G (2017) CO oxidation on Au nanoparticles supported on ZrO₂: role of metal/oxide interface and oxide reducibility. *ChemCatChem* 9:1119–1127
- [190] Zhou H, Chen X, Wang J (2016) CO oxidation over supported Pt clusters at different CO coverage. *Int J Quantum Chem* 116:939–944
- [191] Dudarev S, Botton G, Savrasov S, Humphreys C, Sutton A (1998) Electron-energy-loss spectra and the structural stability of nickel oxide: an LSDA + U study. *Phys Rev B* 57:1505–1509
- [192] Chen HYT, Tosoni S, Pacchioni G (2015) Adsorption of ruthenium atoms and clusters on anatase TiO₂ and tetragonal ZrO₂ surfaces: a comparative DFT study. *J Phys Chem C* 119:10856–10868
- [193] Jia C, Zhong W, Deng M, Jiang J (2018) CO oxidation on Ru-Pt bimetallic nanoclusters supported on TiO₂(101): the effect of charge polarization. *J Chem Phys* 148:124701
- [194] Martínez A, Arribas MA, Concepción P, Moussa S (2013) New bifunctional Ni–H-Beta catalysts for the heterogeneous oligomerization of ethylene. *Appl Catal A Gen* 467:509–518. <https://doi.org/10.1016/j.apcata.2013.08.021>
- [195] Ghashghaee M, Farzaneh V (2018) Nanostructured hydrotalcite-supported RuBaK catalyst for direct conversion of ethylene to propylene. *Russ J Appl Chem* 91(6):970–974. <https://doi.org/10.1134/S1070427218060149>
- [196] Finiels A, Fajula F, Hulea V (2014) Nickel-based solid catalysts for ethylene oligomerization - a review. *Catal Sci Technol* 4(8):2412–2426. <https://doi.org/10.1039/c4cy00305e>
- [197] Hulea V, Fajula F (2004) Ni-exchanged AlMCM-41—an efficient bifunctional catalyst for ethylene oligomerization. *J Catal* 225(1):213–222. <https://doi.org/10.1016/j.jcat.2004.04.018>
- [198] Andrei RD, Popa MI, Fajula F, Hulea V (2015) Heterogeneous oligomerization of ethylene over highly active and stable Ni-ALSBA-15 mesoporous catalysts. *J Catal* 323:76–84. <https://doi.org/10.1016/j.jcat.2014.12.027>
- [199] Andrei RD, Popa MI, Fajula F, Cammarano C, Khudhair AA, Bouchemella K, Mutin PH, Hulea V (2015) Ethylene to propylene by one-pot catalytic cascade reactions. *ACS Catal* 5(5):2774–2777. <https://doi.org/10.1021/acscatal.5b00383>
- [200] Cai FX, Lepetit C, Kermarec M, Olivier D (1987) Dimerization of ethylene into 1-butene over supported tailor-made nickel catalysts. *J Mol Catal* 43(1):93–116. [https://doi.org/10.1016/0304-5102\(87\)87024-4](https://doi.org/10.1016/0304-5102(87)87024-4)
- [201] Bonneviot L, Olivier D, Che M (1983) Dimerization of olefins with nickel-surface complexes in X-type zeolite or on silica. *J Mol Catal* 21(1):415–430. [https://doi.org/10.1016/0304-5102\(93\)80138-K](https://doi.org/10.1016/0304-5102(93)80138-K)
- [202] Brogaard RY, Olsbye U (2016) Ethene oligomerization in Ni-containing zeolites: theoretical discrimination of reaction mechanisms. *ACS Catal* 6(2):1205–1214. <https://doi.org/10.1021/acscatal.5b01957>
- [203] Balar M, Azizi Z, Ghashghaee M (2016) Theoretical identification of structural heterogeneities of divalent nickel active sites in NiMCM-41 nanoporous catalysts. *J Nanostruct Chem* 6(4):365–372. <https://doi.org/10.1007/s40097-016-0208-z>
- [204] Kendall RA, Dunning TH, Harrison RJ (1992) Electron affinities of the first-row atoms revisited. Systematic basis sets and wave functions. *J Chem Phys* 96(9):6796–6806. <https://doi.org/10.1063/1.462569>
- [205] EUROPEAN UNION (2017) EUROPEAN COMMISSION Directorate-General for Internal Market, Industry, Entrepreneurship and SMEs Directorate I — Space Policy, Copernicus and Defence Unit I.2 — Copernicus

- [206] Jiang Z, Xiao T, Kuznetsov VL, Edwards PP (2010) Turning carbon dioxide into fuel. *Philos Trans A Math Phys Eng Sci* 368:3343–3364. <https://doi.org/10.1098/rsta.2010.0119>
- [207] Wächtershäuser G (1992) Groundworks for an evolutionary biochemistry: the iron-sulphur world. *Prog Biophys Mol Biol* 58:85–201. [https://doi.org/10.1016/0079-6107\(92\)90022-X](https://doi.org/10.1016/0079-6107(92)90022-X)
- [208] Saito M a, Sigman DM, Morel FM. (2003) The bioinorganic chemistry of the ancient ocean: the co-evolution of cyanobacterial metal requirements and biogeochemical cycles at the Archean–Proterozoic boundary? *Inorg Chim Acta* 356:308–318. [https://doi.org/10.1016/S0020-1693\(03\)00442-0](https://doi.org/10.1016/S0020-1693(03)00442-0)
- [209] Liu C, Cundari T, Wilson A (2012) CO₂ reduction on transition metal (Fe, Co, Ni, and Cu) surfaces: in comparison with homogeneous catalysis. *J Phys Chem* 116(9):5681–5688
- [210] Ye R, Liu Y, Peng Z, Wang T, Jalilov A S, Yakobson B I, Wei S-H and Tour J M 2017 High performance electrocatalytic reaction of hydrogen and oxygen on ruthenium nanoclusters *ACS Appl. Mater. Interfaces* 9 3785
- [211] Demir E, Akbayrak S, Önal A M and Özkar S 2017 Nanoceria-supported Ruthenium(0) nanoparticles: highly active and stable catalysts for hydrogen evolution from water *ACS Appl. Mater. Interfaces* 10 6299
- [212] Wang Y-J, Long W, Wang L, Yuan R, Ignaszak A, Fang B and Wilkinson D P 2018 Unlocking the door to highly active ORR catalysts for PEMFC applications: polyhedron-engineered Pt-based nanocrystals *Energy Environ. Sci.* 11 258
- [213] Miyazaki K and Mori H 2017 Origin of high oxygen reduction reaction activity of Pt₁₂ and strategy to obtain better catalyst using sub-nanosized Pt-alloy clusters *Sci. Rep.* 7 45381
- [214] Stolobov S 2012 Nature of the selenium submonolayer effect on the oxygen electroreduction reaction activity of Ru(0001) *J. Phys. Chem. C* 116 7173
- [215] Zuluaga S and Stolobov S 2012 First principles studies of the size and shape effects on reactivity of the Se modified Ru nanoparticles *J. Phys.: Condens. Matter.* 24 345303
- [216] Zhao Y, Truhlar DG (2005) *Phys Chem Chem Phys* 7:2701–2705
- [217] Ricca A, Bauschlicher CW Jr (1995) *Theor Chem Acc* 92:123–131
- [218] Cramer CJ, Truhlar DG (2009) *Phys Chem Chem Phys* 11:10757–10816
- [219] Stegelmann, C., Andreasen, A. & Campbell, C. T. Degree of rate control: how much the energies of intermediates and transition states control rates. *J. Am. Chem. Soc.* 131, 8077–8082 (2009).
- [220] Kucherenko, S., Rodriguez-Fernandez, M., Pantelides, C. & Shah, N. Monte Carlo evaluation of derivative-based global sensitivity measures. *Reliab. Eng. Syst. Safety* 94, 1135–1148 (2009).
- [221] Chen, Z. et al. Single-atom heterogeneous catalysts based on distinct carbon nitride scaffolds. *National Sci. Rev.* 5, 642–652 (2018).
- [222] Wang, A., Li, J. & Zhang, T. Heterogeneous single-atom catalysis. *Nat. Rev. Chem.* 2, 65–81 (2018).
- [223] Qiao, B. et al. Single-atom catalysis of CO oxidation using Pt₁/FeO_x. *Nat. Chem.* 3, 634–641 (2011).
- [224] Chen, Z. et al. A heterogeneous single-atom palladium catalyst surpassing homogeneous systems for Suzuki coupling. *Nat. Nanotechnol.* 13, 702–707 (2018).
- [225] Wang, H. et al. Quasi Pd₁Ni single-atom surface alloy catalyst enables hydrogenation of nitriles to secondary amines. *Nat. Comm.* 10, 1–9 (2019).
- [226] Albani, D. et al. Selective ensembles in supported palladium sulfide nanoparticles for alkyne semi-hydrogenation. *Nat. Comm.* 9, 1–11 (2018).
- [227] O'Connor, N. J., Jonayat, A., Janik, M. J. & Senftle, T. P. Interaction trends between single metal atoms and oxide supports identified with density functional theory and statistical learning. *Nat. Catal.* 1, 531–539 (2018).
- [228] Figueroba, A., Kovács, G., Bruix, A. & Neyman, K. M. Towards stable single-atom catalysts: strong binding of atomically dispersed transition metals on the surface of nanostructured ceria. *Catal. Sci. Technol.* 6, 6806–6813 (2016).
- [229] Fiedorow, R. M., Chahar, B. & Wanke, S. E. The sintering of supported metal catalysts: II. Comparison of sintering rates of supported Pt, Ir, and Rh catalysts in hydrogen and oxygen. *J. Catal.* 51, 193–202 (1978).
- [230] Chen, Z. et al. Stabilization of single metal atoms on graphitic carbon nitride. *Adv. Funct. Mater.* 27, 1605785 (2017).
- [231] Daelman, N., Capdevila-Cortada, M. & López, N. Dynamic charge and oxidation state of Pt/CeO₂ single-atom catalysts. *Nat. Mater.* 18, 1215–1221 (2019).
- [232] Wang JJ et al (2020) Earth-abundant transition-metal-based bifunctional catalysts for overall electrochemical water splitting: a review. *J Alloy Compd* 819:153346. <https://doi.org/10.1016/j.jallcom.2019.153346>
- [233] Tavares TS (2020) Delta-FeOOH as support for immobilization peroxidase: optimization via a chemometric approach. *Molecules* 25:259. <https://doi.org/10.3390/molecules25020259>
- [234] Pereira AF (2019) Development of technologies applied to the biodegradation of warfare nerve agents: theoretical evidence for asymmetric homogeneous catalysis. *Chem Biol Interact* 308:323–331. <https://doi.org/10.1016/j.cbi.2019.06.007>

- [235] Oliveira LCA et al (2009) Nb-doped hematites for decomposition of isopropanol: evidence of surface reactivity by in situ CO adsorption. *Applied Catalysis a-General* 368:17–21. <https://doi.org/10.1016/j.apcata.2009.08.001>
- [236] C. Shi, H.A. Hansen, A.C. Lausche, J.K. Norskov, Trends in electrochemical CO₂ reduction activity for open and close-packed metal surfaces. *Phys. Chem. Chem. Phys.* 16, 4720 (2014). doi: 10.1039/C3CP54822H
- [237] Norskov, J. K., Abild-Pedersen, F., Studt, F. & Bligaard, T. Density functional theory in surface chemistry and catalysis. *Proc. Natl Acad. Sci. USA* 108, 937–943 (2011).
- [238] S. Sakong, A. Groß, The importance of the electrochemical environment in the electro-oxidation of methanol on Pt(111). *ACS Catal.* 6, 5575 (2016). doi: 10.1021/acscatal.6b00931
- [239] Gunceler, D., Letchworth-Weaver, K., Sundararaman, R., Schwarz, K. A. & Arias, T. The importance of nonlinear fluid response in joint density-functional theory studies of battery systems. *Model. Simul. Mater. Sci.* 21, 074005 (2013).
- [240] S.A. Petrosyan, J.F. Briere, D. Roundy, T.A. Arias, Joint density-functional theory for electronic structure of solvated systems. *Phys. Rev. B.* 75, 205105 (2007). doi: 10.1103/PhysRevB.75.205105
- [241] K. Tonigold, A. Groß, Dispersive interactions in water bilayers at metallic surfaces: A comparison of the pbe and rpbe functional including semiempirical dispersion corrections. *J. Comput. Chem.* 33(6), 695 (2012). doi: 10.1002/jcc.22900
- [242] G. Mercurio, E.R. McNellis, I. Martin, S. Hagen, F. Leyssner, S. Soubatch, J. Meyer, M. Wolf, P. Tegeder, F.S. Tautz, K. Reuter, Structure and energetics of azobenzene on ag(111): Benchmarking semiempirical dispersion correction approaches. *Phys. Rev. Lett.* 104, 036102 (2010). doi: 10.1103/PhysRevLett.104.036102
- [243] M. Fishman, H.L. Zhuang, K. Mathew, W. Dirschka, R.G. Hennig, Accuracy of exchange-correlation functionals and effect of solvation on the surface energy of copper. *Phys. Rev. B.* 87, 245402 (2013). doi: 10.1103/PhysRevB.87.245402
- [244] Andreussi, O., Dabo, I. & Marzari, N. Revised self-consistent continuum solvation in electronic-structure calculations. *J. Chem. Phys.* 136, 064102 (2012).
- [245] O. Andreussi, N. Marzari, Electrostatics of solvated systems in periodic boundary conditions. *Phys. Rev. B.* 90, 245101 (2014). doi: 10.1103/PhysRevB.90.245101
- [246] F. Gossenberger, T. Roman, A. Groß, Hydrogen and halide co-adsorption on Pt(111) in an electrochemical environment: A computational perspective. *Electrochim. Acta.* 216, 152 (2016). doi: 10.1016/j.electacta.2016.08.117
- [247] X. Lin, F. Gossenberger, A. Groß, Ionic adsorbate structures on metal electrodes calculated from first-principles. *Ind. Eng. Chem. Res.* 55(42), 11107 (2016). doi: 10.1021/acs.iecr.6b03087
- [248] Greeley, J. et al. Alloys of platinum and early transition metals as oxygen reduction electrocatalysts. *Nat. Chem.* 1, 552–556 (2009).
- [249] Winther, K. T. et al. Catalysis-Hub.org, an open electronic structure database for surface reactions. *Sci. Data* 6, 75 (2019).
- [250] Mamun, O., Winther, K. T., Boes, J. R. & Bligaard, T. High-throughput calculations of catalytic properties of bimetallic alloy surfaces. *Sci. Data* 6, 76 (2019).
- [251] Gaggioli CA, Stoneburner SJ, Cramer CJ, Gagliardi L (2019) Beyond density functional theory: the multiconfigurational approach to model heterogeneous catalysis. *ACS Catal* 9(9):8481–8502
- [252] Kulik HJ (2015) Perspective: treating electron over-delocalization with the DFT plus U method. *J Chem Phys* 142(24):240901
- [253] Yu HS, Li SL, Truhlar DG (2016) Perspective: Kohn-Sham density functional theory descending a staircase. *J Chem Phys* 145(13):130901
- [254] Nandy A, Kulik HJ (2020) Why conventional design rules for C–H activation fail for open-shell transition-metal catalysts. *ACS Catal* 10(24):15033–15047. <https://doi.org/10.1021/acscatal.0c04300>
- [255] Nandy A, Zhu J, Janet JP, Duan C, Getman RB, Kulik HJ (2019) Machine learning accelerates the discovery of design rules and exceptions in stable metal-oxo intermediate formation. *ACS Catal* 9:8243–8255
- [256] Gani TZH, Kulik HJ (2017) Unifying exchange sensitivity in transition metal spin-state ordering and catalysis through bond valence metrics. *J Chem Theory Comput* 13:5443–5457
- [257] Weiran Z, Wing MH, Lin Y, Edman TSC (2017) Electroreduction of carbon dioxide to formic acid and methanol over a palladium/polyaniline catalyst in acidic solution: A study of the palladium size effect. *Energ Technol* 5(6):937. <https://doi.org/10.1002/ente.201600659>. <https://onlinelibrary.wiley.com/doi/abs/10.1002/ente.201600659>
- [258] Azuma M, Hashimoto K, Hiramoto M, Watanabe M, Sakata T (1990) Electrochemical reduction of carbon dioxide on various metal electrodes in low-temperature aqueous KHCO₃ media. *J Electrochem Soc* 137(6):1772. <https://doi.org/10.1149/1.2086796>. <http://jes.ecsdl.org/content/137/6/1772.abstract>
- [259] Kuhl KP, Hatsukade T, Cave ER, Abram DN, Kibsgaard J, Jaramillo TF (2014) Electrocatalytic conversion of carbon dioxide to methane and methanol on transition metal surfaces. *J Am Chem Soc* 136(40):14107. <https://doi.org/10.1021/ja505791r>
- [260] Lee S, Ju H, Machunda R, Uhm S, Lee JK, Lee HJ, Lee J (2015) Sustainable production of formic acid by electrolytic reduction of gaseous carbon dioxide. *J Mater Chem A* 3(6):3029. <https://doi.org/10.1039/C4TA03893B>

<http://pubs.rsc.org/en/content/articlelanding/2015/ta/c4ta03893b>

[261] Chaplin R, Wragg A (2003) Effects of process conditions and electrode material on reaction pathways for carbon dioxide electroreduction with particular reference to formate formation. *J Appl Electrochem* 33(12):1107. <https://doi.org/10.1023/B:JACH.0000004018.57792.b8>

[262] Kas R, RKortlever R, Ylmaz H, Koper MTM, Mul G (2015) Manipulating the hydrocarbon selectivity of copper nanoparticles in CO₂ electroreduction by process conditions. *ChemElectroChem* 2(3):354. <https://doi.org/10.1002/celec.201402373>. <https://onlinelibrary.wiley.com/doi/abs/10.1002/celec.201402373>

[263] Zheng W, Nayak S, Yuan W, Zeng Z, Hong X, Vincent KA, Edman Tsang SC (2016) A tunable metal–polyaniline interface for efficient carbon dioxide electro-reduction to formic acid and methanol in aqueous solution. *Chem Comm* 52(96):13901. <https://doi.org/10.1039/C6CC07212G>. <http://pubs.rsc.org/en/Content/ArticleLanding/2016/CC/C6C07212G>

[264] Shanmugam R, Thamarachelvan A, Kuppusamy Ganesan T, Viswanathan B (2016) Carbon dioxide activation and transformation to HCOOH on metal clusters (M = Ni, Pd, Pt, Cu, Ag & Au) anchored on a polyaniline conducting polymer surface—an evaluation study by hybrid density functional theory. *RSC Adv* 6(103):100829. <https://doi.org/10.1039/C6RA20715D>. <http://pubs.rsc.org/en/Content/ArticleLanding/2016/RA/C6RA20715D>

[265] Zhao C, Yin Z, Wang J (2015) Efficient electrochemical conversion of CO₂ to HCOOH using pd-polyaniline/CNT nanohybrids prepared in situ. *ChemElectroChem* 2(12):1974. <https://doi.org/10.1002/celec.201500328>. <https://onlinelibrary.wiley.com/doi/abs/10.1002/celec.201500328>

[266] Peterson A, Abild-Pedersen F, Studt F et al (2010) How copper catalyzes the electroreduction of carbon dioxide into hydrocarbon fuels. *Energy Environ Sci* 3:1311. <https://doi.org/10.1039/c0ee00071j>

[267] J.K. Nørskov, J. Rossmeisl, A. Logadottir, L. Lindqvist, J.R. Kitchin, T. Bligaard, H. Jónsson, Origin of the overpotential for oxygen reduction at a fuel-cell cathode. *J. Phys. Chem. B.* 108(46), 17886 (2004). doi: 10.1021/jp047349j

[268] Millikan RC, Pitzer KS (1957) Infrared spectra and vibrational assignment of monomeric formic acid. *J Chem Phys* 27(6):1305. <https://doi.org/10.1063/1.1743996>

[269] Graciani J, Mudiyansele K, Xu F, Baber AE, Evans J, Senanayake SD, Stacchiola DJ, Liu P, Hrbek J, Sanz JF, Rodriguez JA (2014) Highly active copper–ceria and copper–ceria–titania catalysts for methanol synthesis from CO₂. *Science* 345(6196):546. <http://science.sciencemag.org/content/345/6196/546>

[270] Philipp K, RajabhauBajirao U, Christoph K, Andreas J (2013) Production of liquid hydrocarbons with CO₂ as carbon source based on reverse water–gas shift and Fischer–Tropsch synthesis. *Chemie Ingenieur Technik* 85 (4):489. <https://doi.org/10.1002/cite.201200179>. <https://onlinelibrary.wiley.com/doi/abs/10.1002/cite.201200179>

[271] Daza YA, Kuhn JN (2016) CO₂ conversion by reverse water gas shift catalysis: comparison of catalysts, mechanisms and their consequences for CO₂ conversion to liquid fuels. *RSC Adv* 6:49675–49691. <https://doi.org/10.1039/C6RA05414E>

[272] Uzunova EL, Seriani N, Mikosch H (2015) CO₂ conversion to methanol on Cu(i) oxide nanolayers and clusters: an electronic structure insight into the reaction mechanism. *Phys Chem Chem Phys* 17(16):11088. <https://doi.org/10.1039/C5CP01267H>

[273] Ranucci CR, Colpini LMS, Monteiro MR, Kothe V, Gasparrini LJ, Alves HJ (2015) Preparation, characterization and stability of KF/Si-MCM-41 basic catalysts for application in soybean oil transesterification with methanol. *J Environ Chem Eng* 3(2):703–707. <https://doi.org/10.1016/j.jece.2015.02.023>

[274] Kothe V, Alves HJ, Silveira MHL, Pereira L (2016) Synthesis, characterization and application of [CTA+]-MCM-41 in the catalytic conversion of soybean oil to fatty acid methyl esters. *J Adv Chem* 12(6):4117–4126. <https://doi.org/10.24297/jac.v12i6.4348>

[275] Ugliengo P, Sodupe M, Musso F, Bush IJ, Orlando R, Dovesi R (2008) Realistic models of hydroxylated amorphous silica surfaces and MCM-41 mesoporous material simulated by large-scale periodic B3LYP calculations. *Adv Mater* 20(23):4579–4583. <https://doi.org/10.1002/adma.200801489>

[276] Gao Y, Chen H, Tay-Agbozo S, Kispert LD (2017) Photo-induced electron transfer of carotenoids in mesoporous sieves (MCM-41) and surface modified MCM-41: the role of hydrogen bonds on the electron transfer. *J Photochem Photobiol A* 341:1–11. <https://doi.org/10.1016/j.jphotochem.2017.03.013>

[277] Grün M, Unger KK, Matsumoto A, Tsutsumi K (1999) Novel pathways for the preparation of mesoporous MCM-41 materials: control of porosity and morphology. *Microporous Mesoporous Mater* 27(2):207–216. [https://doi.org/10.1016/S1387-1811\(98\)00255-8](https://doi.org/10.1016/S1387-1811(98)00255-8)

4. Recent Progress & Perspectives

Non-Colloidal Nanocatalysts Fabricated Using Arc Plasma Deposition and Their Application in Heterogeneous Catalysis and Photocatalysis

DOI: 10.1007/s11244-017-0746-8

Abstract-Summary

To understand technologically complex catalytic systems and to tailor both activity and selectivity in heterogeneous catalysis and photocatalysis, there is the challenge of bridging the materials

gap that exists between two- and three-dimensional model catalytic systems and real catalysts, which are comprised of highly dispersed, oxide-supported metal nanoparticles. Coaxial vacuum arc plasma deposition (APD) is a method to fabricate non-colloidal nanocatalysts that has the potential for large-scale synthesis of nanocatalysts and, at the same time, allows for systematic investigation of intrinsic factors that affect catalytic activity. Direct vaporization of metallic materials to deposit active materials on two-dimensional or three-dimensional oxide supports has drawn considerable interest due to its simplicity, high reproducibility, and the possibility for large-scale production. In the case of photocatalysis, APD was used to fabricate metal nanoparticles on a hierarchically porous oxide; enhanced hydrogen evolution by doping and porosity was also demonstrated. The materials gap in catalysis can be bridged by the potential for large-scale synthesis of a variety of catalysts using APD.

Extended:

In the case of powder-type substrates, the powder is constantly stirred for effective dispersion of the deposited nanoparticles on the powder.

Conclusion

We have discussed the most recent advances in the preparation of catalyst nanoparticles on catalyst supports fabricated using APD. With the advent of pulsed APD, new applications for preparing metallic nanoparticles in a direct and dry process are emerging. It is also easy to control the size of the generated nanoparticles at nanometer scale by controlling the APD parameters, e.g. the number of arc plasma pulse shots, the arc discharge voltage, and the arc discharge condenser capacitance. As for the substrates for deposition, the APD method provides a simple and easy method for direct and dry deposition of metallic nanoparticles on a variety of substrates, e.g. 2-dimensional thin films and 3-dimensional powders.

Graphitized nanocarbon-supported metal catalysts: synthesis, properties, and applications in heterogeneous catalysis

DOI: 10.1007/s40843-017-9160-7

Abstract-Summary

Graphitized nanocarbon materials can be an ideal catalyst support for heterogeneous catalytic systems. This review summarizes recent relevant applications in supported catalysts that use graphitized nanocarbon as supports for catalytic oxidation, hydrogenation, dehydrogenation, and C–C coupling reactions in liquid-phase and gas-solid phase-reaction systems. The latest developments in specific features derived from the morphology and characteristics of graphitized nanocarbon-supported metal catalysts are highlighted, as well as the differences in the catalytic behavior of graphitized nanocarbon-supported metal catalysts versus other related catalysts.

Recent Advances on the Preparation and Catalytic Applications of Metal Complexes Supported-Mesoporous Silica MCM-41 (Review)

DOI: 10.1007/s10904-020-01689-1

Abstract-Summary

Mesoporous silica, in particular MCM-41 was widely used in several fields, including catalysis and catalytic support, due to its remarkable textural properties. The immobilization of metal complexes on the surface of mesoporous silica is one of the most popular methods. The metal complexes immobilized on the mesoporous silica MCM-41 exhibit significant catalytic activities due to the increased dispersion of the active sites and the faster diffusion of large organic molecules. This review mainly discusses the immobilization strategies of different metal complexes supported on the mesoporous silica MCM-41. A recent study was presented and well detailed based on the different preparation methods, catalytic applications and the stability of metal complexes supported on mesoporous silica MCM-41.

Extended:

Several reviews were published on metal complexes supported on different mesoporous silicas and their applications as heterogeneous catalysts for a wide variety in organic synthesis [14, 15, 16–17]. The metal complexes supported on MCM-41 have known wide application in organic synthesis and were used in several types of reaction due to their diversity. The metal complexes supported on MCM-41 have attracted attention because of their wide applications in heterogeneous catalysis.

Conclusions

The mesoporous silica MCM-41 supported by metal complexes was presented. The metal complexes supported on MCM-41 have attracted attention because of their wide applications in heterogeneous catalysis. These kinds of catalysts have been widely tested in several types of reactions such as oxidation, ozonation, reduction and photocatalysis. It is very interesting to widen the application field of metals complexes via this kind of reaction. Polymers have also been known for their effectiveness to stabilize metallic nanoparticles, so it is very interesting to prepare and test the complexes polymer-metal supported on MCM-41 in water treatment.

Graphene-supported metal single-atom catalysts: a concise review

DOI: 10.1007/s40843-019-1286-1

Abstract-Summary

SACs could greatly increase the availabilities of the active metal atoms in many catalytic reactions by reducing the size to single atom scale. Graphene-supported metal SACs have also drawn considerable attention due to the unique lattice structure and physicochemical properties of graphene, resulting in superior activity and selectivity for several chemical reactions. We review recent progress in the fabrications, advanced characterization

tools and advantages of graphene-supported metal SACs, focusing on their applications in catalytic reactions such as CO oxidation, the oxidation of benzene to phenol, hydrogen evolution reaction, methanol oxidation reaction, oxygen reduction reaction, hydrogenation and photoelectrocatalysis.

N-Heterocyclic carbenes as tunable ligands for catalytic metal surfaces

DOI: 10.1038/s41929-021-00607-z

Abstract-Summary

The active sites of these heterogeneous catalysts are often metal surfaces, which consist of a large ensemble of metal atoms, and their properties differ significantly from metal complexes bearing highly developed ligands typically used in homogeneous catalysis. A highly interesting approach is the combination of these sophisticated ligand systems from homogeneous catalysis with metal surfaces to improve parameters such as stability, reactivity and selectivity. This review summarizes developments in this area, covering fundamental properties, preparation methods, important analytical techniques and reactions of NHC-modified metal surfaces.

Conclusions and outlook

NHCs have been used to control a variety of metal-surface properties, such as stability and solubility, but also important catalytic features like selectivity and activity. Crucial for this development has been the fundamental understanding of the binding of NHCs to surfaces. A plethora of analytical techniques for the analysis of surfaces modified with NHCs have been established, and further development is essential. Design strategies of tailor-made NHCs for specific applications in catalysis are highlighted and we expect that the growing understanding of NHC-modified surfaces will lead to further groundbreaking developments. Future developments should aim at expanding the repertoire of reactions with these catalytically active metal surfaces, making use of the full structural diversity of NHCs to broaden existing approaches and identify new design strategies. The key to success should be the establishment of principles to determine which subclass of NHCs is most promising for the modification of a given surface, which is so far still challenging.

Heterogeneous single-atom catalysis

DOI: 10.1038/s41570-018-0010-1

Abstract-Summary

Aided by recent advances in practical synthetic methodologies, characterization techniques and computational modelling, we now have a large number of single-atom catalysts (SACs) that exhibit distinctive performances for a wide variety of chemical reactions. SACs have well-defined active centres, such that unique opportunities exist for the rational design of new catalysts with high activities, selectivities and stabilities. Given a certain practical application, we can often design a suitable SAC; thus, the field has developed very rapidly and afforded promising catalytic leads. The control we have over certain SAC structures

paves the way for designing base metal catalysts with the activities of noble metal catalysts.

Conclusions and future directions

To supported metal NP or nanocluster catalysts, in which metal-metal bonding between like atoms dominates the chemistry, the present catalysts feature atomically dispersed metal centres — no homoatomic metal-metal bonds are present, and the metal atoms are attached to the support surface through either heteroatoms, in the case of SACs, or other metals, in the case of SAAs. The single metal sites in SACs more or less resemble the peripheral atoms at the NP-support interface of supported NP catalysts. The non-uniformity of support materials means that not all of the single metal centres in SACs are equally accessible or equally active. The rapid development of single-atom catalysis in recent years suggests that it is not unreasonable to expect speedy access to robust SACs with high stability, selectivity and activity for industrially important reactions.

Ultra-stable metal nano-catalyst synthesis strategy: a perspective

DOI: 10.1007/s12598-019-01350-y

Abstract-Summary

The small particles exhibit superior catalytic activity in comparison with the larger particles because of an increase in low-coordinated metal atoms on the particle surface that work as active sites, such as edges and corner atoms. These small NPs are typically unstable and tend to migrate and coalesce to reduce their surface free energy during the real catalytic processes, particularly in high-temperature reactions. A means to fabricate stable small metal NP catalysts with excellent sinter-resistant performance is necessary for maintaining their high catalytic activity. At the end of this review, we highlight our recent work on the preparation of high-stability metal catalysts via a unique interfacial plasma electrolytic oxidation technology, that is, metal NPs are well embedded in a porous MgO layer that has both high thermal stability and excellent catalytic activity.

Extended:

We provide our viewpoints about the future development of ultra-stable supported metal nano-catalyst synthesis.

Introduction

Catalysts based on metal nanoparticles (NPs) have attracted great attention because of their excellent catalytic activities. Enormous efforts have been devoted to improving the performance of supported metal catalysts by downsizing NPs [76, 77]. Noble metal NPs, as a type of dominant-supported catalyst, show excellent catalytic activity in various reactions due to their special electron structures and small particle sizes that generate a high fraction of surface active atoms. Rationally and effectively stabilizing ultra-small metal NPs on supports against sintering and aggregation are of great significance for heterogeneous catalysis in practical applications. The ideal sinter-resistant catalyst typically has the following characteristics [78]: (1) its integrated components are thermally stable and without structural collapse under high-temperature

conditions; (2) its active sites are fully accessible by reactants without substantial mass transfer resistance; (3) its catalytic activity remains unchanged even after treatment at elevated temperatures. Recent theoretical and experimental studies demonstrate that either a thermodynamic approach or a kinetic approach [78, 79, 80–81] can effectively stabilize noble metal NPs on supports.

Thermodynamic approach

The thermodynamic approach aims to reduce the difference in chemical potential and surface energy between the NPs by which the Ostwald ripening can be effectively suppressed. They found that particle size and distribution are essential factors for determining their stability and a narrow size and homogeneous distribution suppresses the Ostwald ripening rate due to the NPs similar chemical potential and surface energy. A support with high surface activation energy can generate the same effect for restraining the Ostwald ripening action.

Kinetic approach

The dynamical approach mainly takes advantage of an external medium to restrain the growth of NPs in the harsh condition during the catalytic reaction, e.g., high temperature, high pressure, etc. In this section, three strategies including space confinement, coating structure and strong metal–support interaction are proposed to stabilize the NPs. There are also some other important approaches focusing on the stabilization of tiny metal NPs within zeolite matrix to improve their sintering resistance, for instance, incorporating Pt clusters into high-silica zeolites MCM-22 via the transformation of two-dimensional (2D) zeolite into a three-dimensional (3D) [82] structure, stabilizing CoO clusters within silicalite-1 crystals using a steam-assisted method [83], etc. Even so, simpler and more universal strategies should be put forward to enrich the types of catalysts to meet the increasing demand of industrial applications. This unique structure makes the Au NPs partially encapsulated and partially exposed to the air, which generates a strong interaction between the Au NPs and the mixed supports that facilitate the stability of the Au particles, and also enhances their catalytic activity due to the partially exposed surface.

Interfacial plasma electrolytic oxidation technology

Unlike the methods above, a new preparation technology, termed interfacial plasma electrolytic oxidation technology (PEO), has been successfully applied to fabricate a high-quality Au/MgO catalyst with superior stability and activity for catalytic reactions. During the PEO process, noble metal precursors are in situ decomposed and transformed into metal NPs along with their encapsulation into the MgO porous layer. Owing to this unique embedded structure, the obtained Au/MgO catalysts possess excellent thermal stability and sintering resistance. Because the oxide layer is firmly attached to metal substrate, the concentration of oxygen vacancies in MgO cannot be annihilated by high-temperature annealing. The foremost characteristic of this approach is the simultaneous in situ formation of metal NPs and an oxide support that generates a unique embedded structure between them and endows the catalyst outstanding thermal stability and recyclability.

Summary and outlook

Two main paths including thermodynamic and kinetic approaches were performed during the entire developed solution. Most solutions involve the kinetic approaches including channel confinement, coating and SMSI. Consideration SMSI is only suitable for some special metal–support pairs that have strictly limited the application in the field of catalysis, our group developed an SMSI based on universal strategy–interfacial plasma electrolytic oxidation technology for the preparation of ultra-stable supported catalysts, which is appropriate for various noble or transition metal catalysts and hence largely extends the scope of SMSI.

Whither Goest Thou, Catalysis

DOI: 10.1007/s10562-016-1865-8

Abstract-Summary

While the history of catalysis goes back to antiquity, catalysis as we know it today began in the nineteenth century with catalytic hydrogenation having its beginning with the report by Sabatier in 1897 on the hydrogenation of ethylene over a reduced NiO catalyst. About the middle of the last century, though, catalysis, particularly catalytic hydrogenations and oxidations, began to be used more extensively in synthetic applications. The last quarter of the past century saw an increased interest in understanding the details of the chemistry taking place on the catalyst surface. EHMO calculations provided information on the nature of the interaction between the substrate and metal catalyst surface. This approach was recently replaced by the use of DFT calculations to obtain information on the energetics of the interaction of a metal surface and the substrate or presumed reaction intermediates. Another twenty-first century innovation was the introduction of “nano-technology” with nano-particles of metals being used as catalysts. Has the research leading to a more detailed understanding of the catalyst surface led to the preparation of more active and selective catalysts or are the better catalysts still being prepared by the old trial and error approach? More efficient catalysts could be designed if there were a better understanding of what was taking place on the surface of ‘real world’ catalysts rather than on idealized substitutes. The presentation will cover a brief review of catalysis with emphasis on catalytic hydrogenation including proposals about the nature of catalytic active sites which were made through the years.

Where Do We Go From Here?

A high percentage of these DFT calculations have been concerned with the adsorption energies of various species on the (111) face of a catalytically active metal even though it is generally accepted that few reactions take place on these face atoms. Another factor is that in studies of hydrogenation reactions these calculations seldom include the simultaneous adsorption of hydrogen even though it has been shown that covering the catalyst surface with hydrogen inhibits adsorption on (111) face atoms [112]. Could a mixed metal composition of a catalyst to be used for a specific, highly selective reaction be determined in advance of any reaction studies? We have a number of new techniques which have been developed to obtain information about the substrate-

catalyst interaction, the detailed composition of many catalysts, the nature of the active sites on catalysts and other features of catalytic reactions.

Oxygen Reduction Reactions of Fe-N-C Catalysts: Current Status and the Way Forward

DOI: 10.1007/s41918-019-00030-w

Abstract-Summary

Fe-N-C materials are considered to be among the most important oxygen reduction reaction (ORR) catalysts, because they are potential substitutes for Pt-based catalysts and are therefore promising in the development of non-noble metal-based catalysts. From a chemical stand point, improvements can be made through the better understanding of mechanisms in Fe-N-C-based ORR catalysis along with a deeper understanding of the chemical origin of active sites on Fe-N-C catalyst surfaces. Based on these, this comprehensive review will focus on the energy conversion, transformation kinetics and electron transfer of the ORR process as catalyzed by Fe-N-C catalysts. This review focuses on the profound understanding of heterogeneous oxygen reduction reaction on Fe-N-C materials from the following aspects: (1) thermodynamics of energy conversion in ORR processes, (2) kinetics of ORR processes based on Fe-N-C catalysts, (3) the textural features of Fe-N-C and analytic results known as far, (4) fundamental principle for Fe-N-C materials synthesis and (5) practical application for fuel cell and metal-air batteries.

Introduction

One may note that from the stand point of a larger impact, Fe-N-C ORR materials are also relevant to other areas, such as selective oxidation reaction [113, 114, 115–116], CO₂ reduction [117, 118] and hydrogenation [119, 120]. A timely comprehensive review on this rapidly growing category of Fe-N-C for ORR catalysis is of great significance to a vast body of readers. Several review articles [121, 122, 123, 124, 125, 126–127], related or referred to the preparation and electrochemical performance of Fe-N-C materials for ORR catalysis, have been published. We engage to the profound understanding of heterogeneous oxygen reduction reaction on Fe-N-C materials from the following aspects: (1) the thermodynamics of energy conversion in the ORR process, (2) the kinetics of the ORR process based on Fe-N-C catalysts, (3) the textural features of Fe-N-C and analytic results known as far, (4) the fundamental principles for Fe-N-C materials synthesis and (5) the practical applications in fuel cells and metal-air batteries.

Thermodynamic Description of the ORR Process

In fuel cells, the high efficiency of energy conversion (i.e., from chemical to electrical) in terms of the theoretical thermodynamics makes it be a promising technique for an energy-sufficient in future. The thermal efficiency of ideal fuel cells operating reversibly on pure hydrogen and oxygen at standard conditions is: Then, an actual cell thermal efficiency is: At standard state, in which $E_{ideal} = 1.23$ V, and hence: In a fuel cell, oxygen (O₂) is electrochemically reduced at the cathode through the mediation of ORR. Taking the overpotential (E_{op}) into consideration for a real fuel cell, the actual cell efficiency is found

to be: Therefore, a high E_{ORR} with low E_{op} is anticipated, where the E_{ORR} depends on the process of electron transfer pathway and the E_{op} is up to the cathodic electrode materials and the electrolyte.

Kinetic Mechanisms of ORR Processes

The kinetic mechanism of reaction can be changed by a catalyst, and doing so would not affect the thermodynamics at all. As a promising non-precious metal catalysis, studying the kinetics of ORR on Fe-N-C is very useful in understanding the mechanism of ORR and for further improving the catalytic performance. A suitably chosen cationic surfactant can modulate the ORR selectivity on a Fe-N-C catalyst by kinetic promotion through Coulombic interaction with the peroxo-Fe complexes [128]. As the first step during ORR, the adsorption and activation of O₂ on catalysts involves associative or dissociative pathways, or a combination of these. It may be noted that the kinetics of ORR is determined to a large extent by the choice of electrode materials and the electrolyte chosen. A clear understanding of the kinetic mechanisms involved in ORR on Fe-N-C would facilitate further research to design, synthesize and investigate ORR catalysts.

[Section 4]

The Fe atom in Fe-N-C materials could be coordinated by the pyridine/pyrrole nitrogen, carbon or a combination of C and N [129]. For the sake of the effective catalyst design, it is hence reasonable to identify and ideally, quantify the Fe-N-C structure-ORR catalytic activity correlations [130, 131]. To unravel the nature of Fe-N-C structure, the techniques of X-ray photoelectron spectroscopic (XPS), electron microscopy, Mössbauer spectroscopic and X-ray absorption fine structure (XAFS) are mostly available. XPS is effective to elucidate the chemical composition and nitrogen bonding configuration for Fe-N-C materials. This peak differentiation principle is widely used in the research on structure of the Fe-N-C catalysts and their correlations with the electrochemical performance for ORR [132]. Pure FeO, Fe₂O₃ or iron phthalocyanine are used as references to clarify that Fe in Fe-N-C materials is coordinated with nitrogen but not oxygen [132, 133, 134].

[Section 5]

For ORR on Fe-N-C materials, to improve the activity (i.e., for facilitating substance transformation and to enhance electron transfer rate), similar to the traditional heterogeneous catalyst, there are two strategies: (1) increasing the intrinsic activity of Fe-N-C or (2) increasing the number of active site on a given electrode (e.g., through increased loading or tuned catalyst structure to expose more active sites per gram) [135]. Hence, a catalyst consisting of abundant Fe-N-C site with high intrinsic activity is desirable; in particular there would be advantages to have sufficient Fe-N₂ species on the edge of carbon support. A high content of Fe-N-C active sites is essential to deliver high ORR catalytic performance. It is generally recognized that the avoidance of carbide formation during pyrolysis represents a promising way to enhance the density of ORR active sites on Fe-N-C catalysts [136].

Application for Energy Conversion Systems

Currently, the dominant limiting factor in PEMFCs, unlike APEFCs, which is the PEM, is the electrocatalyst [137], and therefore, the focus of this review will be on the application of Fe-N-C catalysts for PEMFCs. In comparison with Pt/C, the nominally high power density of the reported Fe-N-C catalyst was related to higher mass loadings. This can be explained by the facts that Fe-N-C catalysts are carbonized at high temperatures (> 700 °C) and are more hydrophobic, and that although the porous structure of Fe-N-C catalysts can contribute to higher surface areas for active site dispersion and mass transport enhancement, it also lightens bulk density and cause these catalysts to be much thicker than Pt/C at same mass loading. The Fe-N-C materials show promising applications for the booming activities in Zn-air battery (ZABs).

Challenges and the Way Forward: a Perspective

Significant progress has been made in developing Fe-N-C materials for oxygen reduction reactions in both alkaline and acidic media. Most of the work relating to Fe-N-C for ORR being reported recently is focused on novel methods for material preparation; however, the activity seems to be stagnate [138, 139]. In acidic media, the activity of Fe-N-C materials is much less than Pt/C with ~ 50 mV lower of $E_{1/2}$. Is it the extreme value for actual Fe-N-C materials, although the activity of Fe-N-C materials can be further theoretically enhanced by the structural optimization? Despite the many challenges, there is reason to be hopeful about Fe-N-C for ORR since advancements in situ and ex situ characterization techniques will continue to give insights of relevance to progressively move toward champion catalysts.

Molecular enhancement of heterogeneous CO₂ reduction

DOI: 10.1038/s41563-020-0610-2

Abstract-Summary

The electrocatalytic carbon dioxide reduction reaction (CO₂RR) addresses the need for storage of renewable energy in valuable carbon-based fuels and feedstocks, yet challenges remain in the improvement of electrosynthesis pathways for highly selective hydrocarbon production. Organic molecules or metal complexes adjacent to heterogeneous active sites provide additional binding interactions that may tune the stability of intermediates, improving catalytic performance by increasing Faradaic efficiency (product selectivity), as well as decreasing overpotential. We introduce present-day challenges in molecular strategies and describe a vision for CO₂RR electrocatalysis towards multi-carbon products. These strategies provide potential avenues to address the challenges of catalyst activity, selectivity and stability in the further development of CO₂RR.

Conclusion and outlook

This Perspective has highlighted the potential of applying molecular strategies to enhance heterogeneous electrochemical CO₂RR. A distinct advantage of molecular enhancement approaches is that structure–function relationships can be more precisely defined. Molecularly enhanced heterogeneous CO₂RR catalysts offer the potential to overcome major challenges in tunability and stability as a frontier opportunity for CO₂RR electrocatalysis.

Modeling Ceria-Based Nanomaterials for Catalysis and Related Applications

DOI: 10.1007/s10562-016-1799-1

Abstract-Summary

Atomistic and electronic structure details of the functioning of ceria in catalysis can nowadays be successfully uncovered with the help of computational modeling based on the density functional theory (DFT). The majority of such computational studies undertaken so far relied on extended models of surfaces, which are adequate for the description of surface science processes and phenomena, but neglect the nanostructured nature of ceria in many catalysts. This Perspective focuses on discussing DFT calculations of various nanostructured models of ceria and its composites relevant for catalysis. Pivotal consequences of ceria nanostructuring for its role in catalysts derived from the computational studies are documented and supported by experimental results. How prone are metal particles deposited on ceria to sintering or dispersion and how is this interplay controlled by the nanostructuring of the support? Under what conditions will the transfer of lattice oxygen atoms from ceria support to the metal particles deposited thereon become energetically favorable? The discussed examples show that accounting for ceria nanostructuring in catalysts is essential for performing trustworthy computational modeling.

Introduction

It means that common surface-science models in the form of ordered extended single-crystal ceria surfaces often inadequately represent the structure and reactivity of active sites on the nanostructured ceria. In other articles reviewing DFT studies of metal-oxide nanostructures relevant for catalysis [150, 151] results for ceria-based nanomaterials were not presented in due details. We consider timely to discuss in this Perspective recent research efforts to theoretically model the structure and reactivity of ceria-related catalytic nanomaterials and to overview the achieved advances and remaining issues. The authors have been actively involved in the theoretical modeling of nanostructured ceria and its nanocomposites with transition metals from the opening of this research area 10 years ago [152, 153], over the past decade (e.g. [154, 155, 156]), and up to very recently (e.g. [157–158]). That whenever possible, we refrain from discussing in this article technical details and problems of the DFT-based description of metal-oxide materials such as ceria and of their reactivity and refer for more information to two recent Perspective articles [159, 160].

Outlook and Concluding Remarks

Despite of the successful progress, computational studies involving explicit ceria NP models are still scarce, mainly due to the substantial cost of DFT calculations involving size-representative models of large nanostructures combined with multitude of surface sites exposed by the latter. Our understanding of the catalytic properties of nanostructured ceria-based catalysts and, especially, of their particularities with respect to extended surfaces, should benefit from more systematically addressing reaction mechanisms of different reactions on such models. This should subsequently allow

evaluating the catalytic properties of sites found on different ceria-based nanostructured systems without the need of explicit reaction mechanism calculations, which ought to be especially attractive for studying large nanostructured models. Despite of its rather recent commencement, such modeling has been successfully used in combination with experimental studies for characterizing systems where the properties of ceria-based systems are strongly affected by their nanostructure.

Recent progress and prospect of carbon-free single-site catalysts for the hydrogen and oxygen evolution reactions

DOI: 10.1007/s12274-021-3680-9

Abstract-Summary

The key challenge for scalable production of hydrogen from water lies in the rational design and preparation of high-performance and earth-abundant electrocatalysts to replace precious metal Pt and IrO₂ for hydrogen evolution reaction (HER) and oxygen evolution reaction (OER). Developing highly active and stable OER electrocatalysts is the key for electrochemical water splitting. This review presents feasible design strategies for fabricating carbon-free single-site catalysts and their applications in HER/OER and overall water splitting.

Catalytic conversion of solar to chemical energy on plasmonic metal nanostructures

DOI: 10.1038/s41929-018-0138-x

Abstract-Summary

The demonstrations of visible-light-driven chemical transformations on plasmonic metal nanostructures have led to the emergence of a new field in heterogeneous catalysis known as plasmonic catalysis. In this Review, we provide a fundamental overview of plasmonic catalysis with emphasis on recent advancements in the field. It is our objective to stress the importance of the underlying physical mechanisms at play in plasmonic catalysis and discuss possibilities and limitations in the field guided by these physical insights.

Current trends and outlook

These multi-electron processes have been observed mainly when charge scavengers have been employed, so to fully understand these process it is critical to: (1) establish that the products are actually derived from the reactants (N₂ or CO₂) rather than from the scavengers or impurities, (2) evaluate the quantum efficiencies in terms of the reaction rates obtained and the light intensity used in the experiments — very low rates or large intensity requirements would be discouraging in this context — and (3) critically assess the overall thermodynamic efficiencies of these processes as these processes often employ high-energy scavenger molecules. Engineering selective chemistry will require engineering of not only optical properties of the plasmonic metal, but also the electronic structure of the reactants adsorbed on the active centres as well as the ground and excited potential energy surfaces.

Bridging homogeneous and heterogeneous catalysis by heterogeneous single-metal-site catalysts

DOI: 10.1038/s41929-018-0090-9

Abstract-Summary

In heterogeneous single-metal-site catalysts (HSMSCs) the active metal centres are located individually on a support and are stabilized by neighbouring surface atoms such as nitrogen, oxygen or sulfur. Modern characterization techniques allow the identification of these individual metal atoms on a given support, and the resulting materials are often referred as single-atom catalysts. Their electronic properties and catalytic activity are tuned by the interaction between the central metal and the neighbouring surface atoms, and their atomically dispersed nature allows for metal utilization of up to 100%.

Challenges and perspectives

Heterogeneous single-metal-site catalysts combine features of homogeneous and heterogeneous catalysis. In metal-based catalysts, any metal atom constitutes a single low-coordinated active site. Researchers have already sensed the importance of using specific ligands for the fabrication of HSMSCs; for example, a well-defined active site containing single cobalt atoms was reported [191]. Structural studies at the atomic level play an important role for understanding the essential factors of single-metal-site catalysts. New characterization tools on an atomic level are required for the detailed understanding and coherent synthesis of HSMSCs; for example, in homogeneous catalysis the steric and electronic nature of the active centre are in part described as a result of the so-called cone angle or bite angle of the metal with certain ligands.

Single-Atom Catalysts: From Design to Application

DOI: 10.1007/s41918-019-00050-6

Abstract-Summary

Single-atom catalysis is a powerful and attractive technique with exceptional performance, drastic cost reduction and notable catalytic activity and selectivity. In single-atom catalysis, supported single-atom catalysts contain isolated individual atoms dispersed on, and/or coordinated with, surface atoms of appropriate supports, which not only maximize the atomic efficiency of metals, but also provide an alternative strategy to tune the activity and selectivity of catalytic reactions.

Introduction

To address these issues, the downsizing of noble metals from nanoclusters to isolated single atoms is the most effective method to provide optimal active sites in corresponding catalysts to maximize metal atom efficiency and maintain necessary catalytic performances [192, 193–194]. Single-atom catalysts (SACs), a class of catalysts in which catalytically active individual and isolated metal atoms are anchored to supports, have emerged as a novel class of catalysts that can exhibit optimal metal utilization, with all metal atoms being exposed to reactants and available for catalytic reactions [194]. Despite the

observed performances for various reactions however, significant challenges associated with the synthesis and stabilization of SACs exist as well in which a key challenge in the application of SACs is the stabilization of isolated metals on supports without the compromise of catalytic activity, especially at high temperatures or under harsh reaction conditions [195, 196, 197–198].

Conclusion and Perspectives

The choice of supports and corresponding properties are important for the design of novel SACs because different supports can provide different anchoring sites to stabilize single metal atoms and provide different activities [215, 216, 217, 218–219]. To achieve high loading of single metal atoms on supports, high surface area and robust supports with large numbers of anchor sites are needed in which anchor sites on support materials can determine the active and stability of metal SACs. A deep understanding of both sintering mechanisms and active mechanisms for single metal atoms under working conditions can provide insights into the design of high-performance catalytic systems and provide useful criteria for the design of industrial catalysts. 4. Characterization methods advanced characterization methods such as HAADF-STEM, STM, XAS spectroscopy and IR spectroscopy are essential to develop highly active and stable SACs.

Single-Atom Catalysts: Advances and Challenges in Metal-Support Interactions for Enhanced Electrocatalysis

DOI: 10.1007/s41918-021-00124-4

Abstract-Summary

Since metal-support interactions (MSIs) in SACs exert a substantial influence on the catalytic properties, gaining a profound understanding and recognition of catalytic reactions depends greatly on investigating MSIs both experimentally and computationally. The engineering and modulation of MSIs are regarded as one of the most efficient methods to rationally design SACs with disruptively enhanced catalytic properties. We then discuss the existing MSIs in SACs and elucidate the significant role of strong MSIs in catalytic properties and mechanisms. The correlation between strong MSIs and electrocatalytic activities in SACs, including an outlook to increase our understanding of MSIs, is discussed. The present review provides some perspectives and an in-depth understanding of strong MSIs to advance high-performing SACs.

Extended:

The essential role of strong MSIs is not limited to improving electron transfer in SACs [220]. The strategies mentioned above, the ball-milling method [221], selected soft-landing method [222], plasma sputtering [223], photochemical reduction [224, 225], etc., aim to develop SACs by regulating MSIs. The investigation of MSIs in SACs is expected to play an essential role in the future development of heterogeneous electrocatalysis to develop renewable and environmentally friendly energy resources. The large-scale commercial application of SACs will be realized in the near future, and the development of economically

green energy conversion and storage technologies as well as catalytic sciences will be improved by SACs with strong MSIs.

Conclusion and Perspectives

Depending on the energy conversion process, an ideal SAC can be prepared by effectively balancing its own activity and stability through MSIs, where neither an MSI that is too strong, which keeps SAs centered away from activity inhibition, nor an MSI that is too weak, which results in a decrease in stability, is favored. By precisely regulating the MSIs, the location, content, and distribution of the SAs as well as the architecture of the support, can be well controlled, and the electronic and geometric environments of the SACs can be further modified; therefore, a group of high-performance SACs can be generated to advance electrocatalytic applications. Efforts should be directed toward further dynamic and in situ characterizations of SACs and reaction intermediates and studying the electronic and geometric environment of the catalytic centers to gain a deeper understanding of MSIs.

Beyond Nanoparticles: The Role of Sub-nanosized Metal Species in Heterogeneous Catalysis

DOI: 10.1007/s10562-019-02734-6

Abstract-Summary

Titanate nanostructures are of great interest for catalytic applications because their high surface area and cation exchange capacity create the possibility to achieve high metal dispersion. Due to the large amount of defects, titanate nanotubes (TNT) can stabilize sub-nanosized gold clusters, presumably in Au₂₅ form. This perspective summarizes the previous results obtained in the photocatalytic transformation of methane in which the size of gold nanoclusters plays an important role. Photocatalytic measurements revealed that methane is active towards photo-oxidation. Based on recent additional results, we stress here that gold clusters (Au₂₅) may be directly involved in the photo-induced reactions, namely in the direct activation of the methane/Au₂₅^{δ+} complex during irradiation. Another new finding is that gold nanoparticles supported on TNT exhibit high catalytic activity in CO₂ hydrogenation. Our results revealed fundamental differences in the reaction schemes as the products of the two routes are CO (thermal process) and CH₄ (photocatalytic route), indicating the importance of photogenerated electron–hole pairs in the reaction. Gold in nano and sub-nano sizes promotes the adsorption and scission of reactants, important for both types of reactions. Gold ions (Au⁺), in the cationic sites of the titanate lattice promote the photocatalytic transformation of formate (which is one of the intermediates), thus advancing the reaction further towards the fully reduced product.

Concluding Remarks

Recent literature data indicates that sub-nanosized gold clusters (Au₈) on MgO and Au₂₅ on CeO₂ rods can be prepared and characterized. Ion exchange allows titanate nanostructures to incorporate metal adatoms in their framework, which may create another type of active center besides metal clusters. Similar to CeO₂ rods, TNT can also stabilize sub-nanosized gold

clusters in Au₂₅ form. Au/TNT decorated with sub-nanosized gold clusters exhibited the highest photocatalytic activity in methane transformation. Small metal clusters (Au₂₅, probably with a partial positive charge) can bind strongly to defect sites in TNT. These clusters may be directly involved in photo-induced reactions, namely in the direct activation of the methane-Au₂₅ complex during irradiation. We should mention that small, even sub-nanosized, clusters can be prepared on non-oxide type supports as well. Very small Au clusters can also be prepared on hexagonal boron nitride [258, 259].

Advances in transition metal oxide catalysts for carbon monoxide oxidation: a review

DOI: 10.1007/s42114-019-00126-3

Abstract-Summary

The performances of transition metal catalysts are highly dependent on the crystallite size, surface area, and pore volume of the catalysts. The chemisorptions of CO over transitional metal and supported catalysts were studied in this review. The transition metal catalysts have been represented an excellent catalyst from lower cost, thermally, activity, and selectivity point of view. This investigation will show scientific basis for potential design of transition metal oxide catalysts for CO oxidation.

Extended:

The performances of most active transition metal oxides, such as Co₃O₄, CuOx, Ni₂O₄, ZnOx, or MnOx, are highly dependent on the reaction conditions [260]. The performances of silver catalysts are mostly dependent upon their surface structure and composition [261]. The transition metal oxides (TMOs) constructions, buildings, designing, and structures have been represented as one of the most important useful elements in the area of catalysis, fuel cells, energy storage, air pollution control, and so on. The transition metal oxides have superior potential for reduction of CO in the atmosphere so that it is mostly used in a catalytic converter [262, 263]. The transition metal catalysts are highly prominent metal oxide catalysts for ambient temperature CO oxidation.

Conclusions

The transition metal catalysts are highly prominent metal oxide catalysts for ambient temperature CO oxidation. The CO oxidation over transition metal catalysts to be associated in the presence of several forms of chemisorbs reactants, products, and intermediates on the surface. The accumulation of suitable promoters, supports, pretreatment, and superior preparation methods would result to improvement in the performances of transition metal catalyst toward CO oxidation. The relative ease of preparation, good thermal and chemical stability, and high activity of transition metal catalysts offer better activity for automobile vehicle pollution control applications.

Recent advances in gold-metal oxide core-shell nanoparticles: Synthesis, characterization, and their application for heterogeneous catalysis

DOI: 10.1007/s11705-015-1551-1

Abstract-Summary

This paper reviews the most recent work and research in coreshell catalysts utilizing noble metals, specifically gold, as the core within a metal oxide shell. The advantage of the core-shell structure lies in its capacity to retain catalytic activity under thermal and mechanical stress, which is a pivotal consideration when synthesizing any catalyst. The selective oxidation of carbon monoxide and reduction of nitrogen containing compounds, such as nitrophenol and nitrostyrene, have been studied over the past few years to evaluate the functionality and stability of the core-shell catalysts. Different factors that could influence the catalyst's performance are the size, structure, choice of metal oxide shell and noble metal core and thereby the interfacial synergy and lattice mismatch between the core and shell. This review covers the synthesis and characterization of gold-metal oxide core-shell structures, as well as how they are utilized as catalysts for carbon monoxide (CO) oxidation and selective reduction of nitrogen-containing compounds.

Chapter model systems in heterogeneous catalysis at the atomic level: a personal view

DOI: 10.1007/s11426-019-9671-0

Abstract-Summary

Novel instruments and technique developments, as well as their applications are reported, in an attempt to cover studies on model systems of increasing complexity, including some of the key ingredients of an industrially applied heterogeneous catalyst and its fabrication. The review is intended to demonstrate the power of model studies in understanding heterogeneous catalysis at the atomic level.

Catalytic CO Oxidation on Nanocatalysts

DOI: 10.1007/s11244-018-0920-7

Abstract-Summary

Since CO can be easily adsorbed on active metals like Au, Pt, Pd, Rh, and Ru, many researchers have attempted to observe surface phenomena, including adsorption, surface restructuring, and oxidation kinetics on diverse metal surfaces ranging from single crystals to nanoparticles (NPs). The rapid advances in nanochemistry have further stimulated studies of catalytic reactions, and in-depth understanding of CO oxidation is possible based on analyses of how the size, shape, and composition affect the activity and determine the most effective active site of metal NPs. Recent research has demonstrated that the CO oxidation activity varies with the size of metallic NPs. The oxidation state of the NPs varies as a function of the size, and the surface oxide layers formed on NPs have been found to be important in enhancing or suppressing CO oxidation. The NP surfaces undergo significant adsorbate-induced structural changes, as confirmed by various in situ characterization techniques under catalytically relevant CO oxidation conditions. Using in situ characterization techniques combined with well-defined NPs, it is possible to study CO oxidation on the molecular level in order to gain vital mechanistic insights under catalytic working conditions.

Summary and Outlook

Classical studies of CO adsorption and dissociation studies on single crystals offer valuable information about the properties of metal surfaces and their dynamic behaviors, such as adsorbate-induced surface restructuring and changes in the oxidation states. As single crystal studies shift to the use of NPs, CO oxidation remains a valuable model catalytic reaction. The current trends in heterogeneous catalysis involve molecular level investigation of nanostructured catalysts under catalytically relevant environments to study surface phenomena using in situ characterization tools. By maintaining catalytically relevant reaction environments in specially designed cells, the dynamic behavior on NP surfaces can be investigated to monitor the real motion of catalysts during reaction by employing surface instruments.

Integrating the Fields of Catalysis: Active Site Engineering in Metal Cluster, Metal Organic Framework and Metal Single Site

DOI: 10.1007/s11244-020-01248-5

Abstract-Summary

Research evolved using nanoparticles synthesized and characterized under reaction conditions opened the door to study all three fields of catalysis: heterogeneous, homogenous, and enzyme. We envision that the combination of active site engineering and unifying fields of catalysis could be applied to solve practical issues of science-based technology and develop new fields useful in energy research.

Introduction

We successfully synthesized a heterogeneous-enzyme hybrid catalyst by incorporating the enzyme-like active sites into metal organic frameworks (MOFs) for selective oxidation methane to methanol. These supported DEMCs could be readily modulated to combine the advantages of both heterogeneous and homogeneous catalysts: (1) DEMCs could catalyze homogenous reactions while typical heterogeneous catalyst could not realize; (2) tunable selectivity and activity by changing the dendrimer generation and terminal functional groups; (3) easy recyclability compared to homogeneous catalysts. Although the catalysts deactivate after the first cycle as a result of water molecules strongly bonded to the active sites, MOF-808-Bzz-Cu shows the highest reported selective methanol productivity of $71.8 \mu\text{mol g}^{-1}$ at this temperature. Zr-MOFs could also function as catalyst support to promote the activity and selectivity of Cu catalyst via the strong metal support interaction (SMSI) between the guest copper nanocrystals (NCs) and the zirconium oxide secondary building units (SBUs) [300].

Outlook and Summary

As summarized in our previous perspective, several approaches have been designed to construct enzyme hybrid catalysts, including support-bound, entrapment, cross-linking, cooperation with homogenous metal complexes, and dispersion in reverse micelles. MOF could serve as an ideal platform to incorporate artificial enzyme active sites. The design of enzyme mimicking catalysts with a high level of control could be achieved

by MOF support with simplified enzyme active sites. Selective methane oxidation to methanol could be realized by incorporating only enzyme active site onto MOF catalysts. The research will focus on enhancing the reaction selectivity and use single site catalyst as a new example to bridge homogenous and heterogeneous catalysis.

The kinetics of elementary thermal reactions in heterogeneous catalysis

DOI: 10.1038/s41570-019-0138-7

Abstract-Summary

The kinetics of elementary reactions is fundamental to our understanding of catalysis. We present a short Perspective on recent experimental advances in the measurement of rates of elementary reactions at surfaces that rely on a stroboscopic pump-probe concept for neutral matter. The topic is discussed within the context of a specific but highly typical surface reaction, CO oxidation on Pt, which, despite more than 40 years of study, was only clarified after experiments with velocity-resolved kinetics became possible. This deceptively simple reaction illustrates fundamental lessons concerning the coverage dependence of activation energies, the nature of reaction mechanisms involving multiple reaction sites, the validity of transition-state theory to describe reaction rates at surfaces and the dramatic changes in reaction mechanism that are possible when studying reactions at low temperatures.

Outlook

Modern synchrotron XPS and STM methods operating at high or near-ambient pressure have revealed significant structural changes to the surface, suggesting that it is challenging to extrapolate UHV experiments on model catalysts to 'real-world' systems [314]. The first combined experimental results obtained in UHV experiments on single-crystal metals with DFT calculations [315, 316, 317, 318, 319–320] to devise a kinetic model for a high-pressure reactor comprised of nanoparticles. In that study, basic knowledge derived from the study of model systems could be used to predict product selectivity for oxygen-assisted esterification of methanol over gold-nanoparticle catalysts under high-pressure catalytic conditions [321]. Had the leaders of that same company had greater vision, they might have invested a small fraction of these losses in the basic research of heterogeneous catalysis to improve our ability to design new catalysts by principles based on physical understanding.

Design concept for electrocatalysts

DOI: 10.1007/s12274-021-3794-0

Abstract-Summary

Metal-based electrocatalysts with different sizes (single atoms, nanoclusters, and nanoparticles) show different catalytic behaviors for various electrocatalytic reactions. Regulating the coordination environment of active sites with precision to rationally design an efficient electrocatalyst is of great significance for boosting electrocatalytic reactions. This review

summarizes the recent process of heterogeneous supported single atoms, nanoclusters, and nanoparticles catalysts in electrocatalytic reactions, respectively, and figures out the construct strategies and design concepts based on their strengths and weaknesses.

Recent progress on functional mesoporous materials as catalysts in organic synthesis

DOI: 10.1007/s42247-020-00086-1

Abstract-Summary

Mesoporous materials have been used as catalysts or their supports for homogeneous catalysis in the past decades. This review concerns the very recent development in this area, including the catalyst design, the types of active species, and the reaction catalyst by this kind of catalysts. Mesoporous catalysts can be classified as supported catalyst and bulk one. The supported catalyst includes active site in the pore wall framework, the active site on the pore wall surface, and the active site encapsulated in the mesopores. The bulk one can be directly used as catalyst, which includes metal oxides and carbon nitrides. Four different types of active sites, nanoparticles, highly distributed metals, anchored organic catalysts, and immobilized enzymes, are summarized in this review.

Summary and outlook

Tremendous advances have been made for the design and synthesis of mesoporous material-based catalysts for heterogenization of homogeneous organic reactions. With the development of the mesoporous materials science, an increasing number of organic reactions are developed for various fields of daily lives of the human beings. This review has tried to summarize the very recent progress in the design and synthesis of mesoporous material-based catalysts and their applications in a range of organic reactions. In spite of the great development of the design and synthesis of mesoporous material-based catalysts, a simple and universal method for the preparation of the stable metal centers with ultrasmall size and adjusted mesostructures is still lacking.

Catalysis using metal–organic framework-derived nanocarbons: Recent trends

DOI: 10.1557/jmr.2020.166

Abstract-Summary

Recent trends in the area of catalytic applications of metal–organic framework (MOF)-derived nanocarbons are covered. Differences between conventional porous carbons and MOF-derived carbons are in pore volumes, surface area, and presence of ad-atoms. The morphology of the MOF-derived nanocarbons can be adjustable with uniform dopant distribution. Good catalytic performance is related with highly dispersed heteroatoms, density of catalytic active sites, controllable porosity, and high surface area.

Extended:

Differences between conventional porous carbons and MOF-derived carbons are in pore volumes, surface area, presence of ad-atoms (doping atoms), all is in favor of the MOF-derived nanocarbons.

Conclusions and further outlook

Photoredox properties of MOFs and their derivatives are related with inherent high porosity, so the nanocarbons can act as hosts for photoredox species as metal nanoparticles. Structures of MOF-derived materials include MOF-derived porous carbon, MOF-derived hollow structures, compositions of MOF-derived materials (metal-free nanocarbon, transition metal/metal compound-decorated nanocarbon, and micro/nanostructured MOF-derived composites), and MOF-supported noble metal NPs. Differences between conventional porous carbons and MOF-derived carbons are in pore volumes, surface area, presence of ad-atoms (doping atoms), all is in favor of the MOF-derived nanocarbons. Transition metals and carbon are the basis of the MOF-derived electrocatalysts, together with N-dopation. Among many reported MOFs, a relatively small number of their derived nanocarbons are currently used for photocatalysis purposes (in particular, for photocatalytic CO₂ reduction), so, undoubtedly, this is also a niche for intensive further investigations, as well as for meeting requirements for practical applications.

Recent progress and perspective of electrochemical CO₂ reduction towards C₂-C₅ products over non-precious metal heterogeneous electrocatalysts

DOI: 10.1007/s12274-021-3335-x

Abstract-Summary

Compared with traditional C₁ products, high-value multicarbon products converted from atmospheric CO₂ via CO₂ER have attracted dramatic interest due to their significant economic efficiency, however desired catalytic selectivity of multicarbon products is difficult to achieve because of the high thermodynamic barriers and complex reaction pathways. Although certain progress has been made, there are still few systematic reports on the non-precious metal heterogeneous (NPMH) CO₂ER electrocatalysts for efficient conversion of CO₂ to multicarbon products. We summarize the latest research advances in recent developments of NPMH electrocatalysts, including nanostructured Cu, Cu-based bimetallic catalysts, Cu-based complexes, and carbon-based Cu-free catalysts for electroreduction of CO₂ into high-value multicarbon products. Key strategies and characterization techniques for catalytic mechanism insights, and unsolved issues and future trends for enhancing the CO₂ER performance of NPMH electrocatalysts are highlighted, which provides a constructive guidance on the development of CO₂ER electrocatalysts with high activity and selectivity for multicarbon products.

Metallic Nanoparticles in Heterogeneous Catalysis

DOI: 10.1007/s10562-020-03477-5

Abstract-Summary

Many factors including the particle size, shape and metal-support interfaces can have significant influences on the catalytic properties of metal catalysts. In this Review, the size and shape dependent catalytic chemistry of metal nanoparticles and their electronic properties will be discussed. The unique catalytic chemistry at the metal-support interfaces will be discussed in details.

Conclusions

Size and shape dependent catalytic chemistry is of great interest and importance for designing highly active and selective catalysts. Although particle size has a major effect on catalytic activity, other factors such as oxidation state of the metal NPs and presence of low coordinated step and corner sites are also playing significant role. Unusual high catalytic activity can be obtained by tuning the metal-support interfaces.

Selective Oxidation: From a Still Immature Technology to the Roots of Catalysis Science

DOI: 10.1007/s11244-016-0684-x

Abstract-Summary

The design of heterogeneous selective oxidation catalysts based upon complex metal oxides is governed at present by a set of empirical rules known as “pillars of oxidation catalysis”. They serve as practical guidelines for catalyst development and guide the reasoning about the catalyst role in the process. The present work extends the ideas of the pillar rules and develops the concept of considering a selective oxidation catalyst as enabler for the execution of a reaction network. The enabling function is controlled by mutual interactions between catalyst and reactants. This concept is based upon physical observables and could allow for a design strategy based upon a kinetic description that combines the processes between reactants with the processes between catalyst and reactants.

Extended:

This concept is based upon rigid reconstructed active surface sites that are covered and uncovered by adsorption and desorption. It is the purpose of this paper to show that the worlds of local static active sites and sites on oxidation catalysts are not different from one another and that the unifying concept of dynamical active sites can lead to a functional understanding of selective oxidation connected with physical concepts.

Theory-guided design of catalytic materials using scaling relationships and reactivity descriptors

DOI: 10.1038/s41578-019-0152-x

Abstract-Summary

A physical or chemical property of the reaction system, termed as a reactivity descriptor, scales with another property often in a linear manner, which can describe and/or predict the catalytic performance. In this Review, we describe scaling relationships and reactivity descriptors for heterogeneous catalysis, including electronic descriptors represented by d-band theory, structural

descriptors, which can be directly applied to catalyst design, and, ultimately, universal descriptors. The prediction of trends in catalytic performance using reactivity descriptors can enable the rational design of catalysts and the efficient screening of high-throughput catalysts.

Extended:

In this Review, we discuss reactivity descriptors in different catalytic systems, taking into consideration the limitations of scaling relationships and strategies to break these established scaling relationships. We aim to lay foundations for the future computational design of catalysts.

Outlook

The ability of scaling relationships to simplify our understanding of catalysis inspires us to extract specific reactivity descriptors to predict the reaction trends and to screen for new catalysts. The complexity of catalytic systems leads to numerous reactivity descriptors, which are specifically explored to describe certain sections of the catalysis. As our insight into catalysis deepens, a universal reactivity descriptor for multi-catalytic systems is gaining attention. The goal is to develop reactivity descriptors that can be used simultaneously in various types of catalyst and reaction systems, namely, universal descriptors. In the short term, the discovery of a universal reactivity descriptor for all materials and reactions is not achievable, but it is possible to extract regionally universal descriptors, which are accurate for catalytic reactions within a subfield, such as the ORR, the OER or dehydrogenation.

Bibliography

- [1] Freund HJ, Kuhlenbeck H, Libuda J, Rupprechter G, Baumer M, Hamann H (2001) *Top Catal* 15(2–4):201–209
- [2] Somorjai GA, Park JY (2008) *Top Catal* 49(3–4):126–135
- [3] Qadir K, Kim SH, Kim SM, Ha H, Park JY (2012) *J Phys Chem C* 116(45):24054–24059
- [4] Goddeti KC, Kim SM, Lee YK, Kim SH, Park JY (2014) *Catal Lett* 144(8):1411–1417
- [5] Kim SH, Jung C-H, Sahu N, Park D, Yun JY, Ha H, Park JY (2013) *Appl Catal A* 454(0):53–58
- [6] Haruta M (2002) *CATTECH* 6(3):102–115
- [7] Boronat M, Corma A (2010) *Langmuir* 26(21):16607–16614
- [8] Liu J, Liu GL, Li MZ, Shen WZ, Liu ZY, Wang JX, Zhao JC, Jiang L, Song YL (2010) *Energy Environ Sci* 3(10):1503–1506
- [9] Truong N, Yoo J, Altomarea M, Schmuki P (2014) *Chem Commun* 50(68):9653–9656
- [10] Yang JH, Wang DG, Han HX, Li C (2013) *Acc Chem Res* 46(8):1900–1909
- [11] Rosseler O, Shankar MV, Du MKL, Schmidlin L, Keller N, Keller V (2010) *J Catal* 269(1):179–190
- [12] Park SH, Kim SH, Park SJ, Ryoo S, Woo K, Lee JS, Kim TS, Park HD, Park H, Park YI, Cho J, Lee JH (2016) *J Membr Sci* 513:226–235
- [13] Ito T, Kunimatsu M, Kaneko S, Hirabayashi Y, Soga M, Agawa Y, Suzuki K (2012) *Talanta* 99:865–870
- [14] R.K. Kankala, H. Zhang, C.G. Liu, K.R. Kanubaddi, C.H. Lee, S.B. Wang, W. Cui, H.A. Santos, K. Lin, A.Z. Chen, *Adv. Funct. Mater.* 29, 1902652 (2019)
- [15] A. Rajendran, M. Rajendiran, Z.F. Yang, H.X. Fan, T.Y. Cui, Y.G. Zhang, W.Y. Li, *Chem. Rec.* 19, 1–29 (2019)

- [16] M. Abd El Sater, N. Jaber, E. Schulz, *ChemCatChem* 11, 1–27 (2019)
- [17] P. Veerakumar, P. Thanasekaran, K.L. Lu, S.B. Liu, S. Rajagopal, A.C.S. Sustain, *Chem. Eng.* 5, 6357–6376 (2017)
- [18] D.A. Alonso, A. Baeza, R. Chinchilla, C. Gómez, G. Guillena, I.M. Pastor, D.J. Ramón, *Catalysts* 8, 202 (2018)
- [19] G. Martínez-Edo, A. Balmori, I. Pontón, A.M. del Rio, D. Sánchez-García, *Catalysts* 8, 617 (2018)
- [20] M.E. Davis, *Nature* 417, 813–821 (2002)
- [21] J.S. Beck, J.C. Vartulli, W.J. Roth, M.E. Leonowicz, C.T. Kresge, K.D. Schmitt, C.T.W. Chu, D.H. Olson, E.W. Sheppard, S.B. McCullen, J.B. Higgings, J.L. Schlenker, *J. Am. Chem. Soc.* 114, 10834 (1992)
- [22] X.S. Zhao, G.Q. Lu, *J. Phys. Chem. B* 102, 1556–1561 (1998)
- [23] M. Nikoorazm, A. Ghorbani-Choghmarani, N. Noori, B. Tahmasbi, *Appl. Organomet. Chem.* 30, 843–851 (2016)
- [24] A. Ahmadi, T. Sedaghat, R. Azadi, H. Motamedi, *Catal. Lett.* 150, 112–126 (2020)
- [25] Mallat, T., Orglmeister, E. & Baiker, A. Asymmetric catalysis at chiral metal surfaces. *Chem. Rev.* 107, 4863–4890 (2007).
- [26] Schoenbaum, C. A., Schwartz, D. K. & Medlin, J. W. Controlling the surface environment of heterogeneous catalysts using self-assembled monolayers. *Acc. Chem. Res.* 47, 1438–1445 (2014).
- [27] Peris, E. Smart N-heterocyclic carbene ligands in catalysis. *Chem. Rev.* 118, 9988–10031 (2018).
- [28] Liu, L. & Corma, A. Metal catalysts for heterogeneous catalysis: from single atoms to nanoclusters and nanoparticles. *Chem. Rev.* 118, 4981–5079 (2018).
- [29] Liu, L. & Corma, A. Evolution of isolated atoms and clusters in catalysis. *Trends Chem.* 2, 383–400 (2020).
- [30] Ranganath, K. V. S., Kloesges, J., Schäfer, A. H. & Glorius, F. Asymmetric nanocatalysis: N-heterocyclic carbenes as chiral modifiers of Fe₃O₄/Pd nanoparticles. *Angew. Chem. Int. Ed.* 49, 7786–7789 (2010). Enantioselective catalysis by NHC-modified heterogeneous catalysts.
- [31] Lara, P. et al. Ruthenium nanoparticles stabilized by N-heterocyclic carbenes: ligand location and influence on reactivity. *Angew. Chem. Int. Ed.* 50, 12080–12084 (2011).
- [32] MacLeod, M. J. & Johnson, J. A. PEGylated N-heterocyclic carbene anchors designed to stabilize gold nanoparticles in biologically relevant media. *J. Am. Chem. Soc.* 137, 7974–7977 (2015).
- [33] Levratovsky, Y. & Gross, E. High spatial resolution mapping of chemically-active self-assembled N-heterocyclic carbenes on Pt nanoparticles. *Faraday Discuss.* 188, 345–353 (2016).
- [34] Cao, Z. et al. A molecular surface functionalization approach to tuning nanoparticle electrocatalysts for carbon dioxide reduction. *J. Am. Chem. Soc.* 138, 8120–8125 (2016).
- [35] Crudden, C. M. et al. Simple direct formation of self-assembled N-heterocyclic carbene monolayers on gold and their application in biosensing. *Nat. Commun.* 7, 12654 (2016).
- [36] Jiang, L. et al. N-Heterocyclic carbenes on close-packed coinage metal surfaces: bis-carbene metal adatom bonding scheme of monolayer films on Au, Ag and Cu. *Chem. Sci.* 8, 8301–8308 (2017).
- [37] Larrea, C. R. et al. N-Heterocyclic carbene self-assembled monolayers on copper and gold: dramatic effect of wingtip groups on binding, orientation and assembly. *ChemPhysChem* 18, 3536–3539 (2017).
- [38] Bakker, A. et al. Elucidating the binding modes of N-heterocyclic carbenes on a gold surface. *J. Am. Chem. Soc.* 140, 11889–11892 (2018).
- [39] Zeng, Y., Zhang, T., Narouz, M. R., Crudden, C. M. & McBreen, P. H. Generation and conversion of an N-heterocyclic carbene on Pt(111). *Chem. Commun.* 54, 12527–12530 (2018).
- [40] Bakker, A. et al. An electron-rich cyclic (alkyl)(amino)carbene on Au(111), Ag(111), and Cu(111) surfaces. *Angew. Chem. Int. Ed.* 59, 13643–13646 (2020).
- [41] Dery, S. et al. Flexible NO₂-functionalized N-heterocyclic carbene monolayers on Au (111) surface. *Chem. Eur. J.* 25, 15067–15072 (2019).
- [42] Lovat, G. et al. Determination of the structure and geometry of N-heterocyclic carbenes on Au(111) using high-resolution spectroscopy. *Chem. Sci.* 10, 930–935 (2019).
- [43] Dery, S. et al. Elucidating the influence of anchoring geometry on the reactivity of NO₂-functionalized N-heterocyclic carbene monolayers. *J. Phys. Chem. Lett.* 10, 5099–5104 (2019).
- [44] Dery, S. et al. Strong metal-adsorbate interactions increase the reactivity and decrease the orientational order of OH-functionalized N-heterocyclic carbene monolayers. *Langmuir* 36, 697–703 (2020).
- [45] Weidner, T. et al. NHC-based self-assembled monolayers on solid gold substrates. *Aust. J. Chem.* 64, 1177–1179 (2011).
- [46] Rakers, L. et al. Ruthenium nanoparticles ligated by cholesterol-derived NHCs and their application in the hydrogenation of arenes. *Chem. Commun.* 54, 7070–7073 (2018).
- [47] Rühling, A. et al. Modular bidentate hybrid NHC-thioether ligands for the stabilization of palladium nanoparticles in various solvents. *Angew. Chem. Int. Ed.* 55, 5856–5860 (2016). Application of bidentate NHC ligands to modulate stability and solubility of nanoparticles.
- [48] Richter, C., Schaepe, K., Glorius, F. & Ravoo, B. J. Tailor-made N-heterocyclic carbenes for nanoparticle stabilization. *Chem. Commun.* 50, 3204–3207 (2014).
- [49] Ferry, A. et al. Negatively charged N-heterocyclic carbene-stabilized Pd and Au nanoparticles and efficient catalysis in water. *ACS Catal.* 5, 5414–5420 (2015).
- [50] Ernst, J. B., Muratsugu, S., Wang, F., Tada, M. & Glorius, F. Tunable heterogeneous catalysis: N-heterocyclic carbenes as ligands for supported heterogeneous Ru/K-Al₂O₃ catalysts to tune reactivity and selectivity. *J. Am. Chem. Soc.* 138, 10718–10721 (2016).
- [51] de los Bernardos, M. D., Pérez-Rodríguez, S., Gual, A., Claver, C. & Godard, C. Facile synthesis of NHC-stabilized Ni nanoparticles and their catalytic application in the Z-selective hydrogenation of alkynes. *Chem. Commun.* 53, 7894–7897 (2017).
- [52] Kaeffer, N., Mance, D. & Copéret, C. N-Heterocyclic carbene coordination to surface copper sites in selective semihydrogenation catalysts from solid-state NMR spectroscopy. *Angew. Chem. Int. Ed.* 59, 19999–20007 (2020).
- [53] Kaeffer, N., Liu, H.-J., Lo, H.-K., Fedorov, A. & Copéret, C. An N-heterocyclic carbene ligand promotes highly selective alkyne semihydrogenation with copper nanoparticles supported on passivated silica. *Chem. Sci.* 9, 5366–5371 (2018).
- [54] Fedorov, A., Liu, H.-J., Lo, H.-K. & Copéret, C. Silica-supported Cu nanoparticle catalysts for alkyne semihydrogenation: effect of ligands on rates and selectivity. *J. Am. Chem. Soc.* 138, 16502–16507 (2016).

- [55] Kaeffer, N., Larmier, K., Fedorov, A. & Copéret, C. Origin of ligand-driven selectivity in alkyne semihydrogenation over silica-supported copper nanoparticles. *J. Catal.* 364, 437–445 (2018).
- [56] Asakura, K., Nagahiro, H., Ichikuni, N. & Iwasawa, Y. Structure and catalytic combustion activity of atomically dispersed Pt species at MgO surface. *Appl. Catal. A Gen.* 188, 313–324 (1999).
- [57] Yang, M. et al. Catalytically active Au-O(OH)_x species stabilized by alkali ions on zeolites and mesoporous oxides. *Science* 346, 1498–1501 (2014).
- [58] Yang, M. et al. A common single-site Pt(ii)-O(OH)_x- species stabilized by sodium on “active” and “inert” supports catalyzes the water–gas shift reaction. *J. Am. Chem. Soc.* 137, 3470–3473 (2015).
- [59] Lin, J. et al. Remarkable performance of Ir₁/FeO_x single-atom catalyst in water gas shift reaction. *J. Am. Chem. Soc.* 135, 15314–15317 (2013).
- [60] Yang, M., Allard, L. F. & Flytzani-Stephanopoulos, M. Atomically dispersed Au-(OH)_x species bound on titania catalyze the low-temperature water-gas shift reaction. *J. Am. Chem. Soc.* 135, 3768–3771 (2013).
- [61] Wang, C., Yang, M. & Flytzani-Stephanopoulos, M. Single gold atoms stabilized on nanoscale metal oxide supports are catalytic active centers for various reactions. *AIChE J.* 62, 429–439 (2016).
- [62] Guan, H. et al. Enhanced performance of Rh₁/TiO₂ catalyst without methanation in water–gas shift reaction. *AIChE J.* 63, 2081–2088 (2017).
- [63] Fei, H. et al. Atomic cobalt on nitrogen-doped graphene for hydrogen generation. *Nat. Commun.* 6, 8668 (2015).
- [64] Kyriakou, G. et al. Isolated metal atom geometries as a strategy for selective heterogeneous hydrogenations. *Science* 335, 1209–1212 (2012).
- [65] Qiao, B. et al. Highly efficient catalysis of preferential oxidation of CO in H₂-rich stream by gold single-atom catalysts. *ACS Catal.* 5, 6249–6254 (2015).
- [66] Jones, J. et al. Thermally stable single-atom platinum-on-ceria catalysts via atom trapping. *Science* 353, 150–154 (2016).
- [67] Zhang, Z. et al. Thermally stable single atom Pt/m-Al₂O₃ for selective hydrogenation and CO oxidation. *Nat. Commun.* 8, 16100 (2017).
- [68] Qiao, B. T. et al. Ultrastable single-atom gold catalysts with strong covalent metal–support interaction (CMSI). *Nano Res.* 8, 2913–2924 (2015).
- [69] Nie, L. et al. Activation of surface lattice oxygen in single-atom Pt/CeO₂ for low-temperature CO oxidation. *Science* 358, 1419–1423 (2017).
- [70] Wang, Y.-G., Yoon, Y., Glezakou, V.-A., Li, J. & Rousseau, R. The role of reducible oxide–metal cluster charge transfer in catalytic processes: new insights on the catalytic mechanism of CO oxidation on Au/TiO₂ from ab initio molecular dynamics. *J. Am. Chem. Soc.* 135, 10673–10683 (2013).
- [71] Wang, Y.-G., Mei, D. H., Glezakou, V. A., Li, J. & Rousseau, R. Dynamic formation of single-atom catalytic active sites on ceria-supported gold nanoparticles. *Nat. Commun.* 6, 6511 (2015).
- [72] Liu, J.-C., Wang, Y.-G. & Li, J. Toward rational design of oxide-supported single-atom catalysts: atomic dispersion of gold on ceria. *J. Am. Chem. Soc.* 139, 6190–6199 (2017).
- [73] Wang, J. et al. Formation, migration, and reactivity of Au–CO complexes on gold surfaces. *J. Am. Chem. Soc.* 138, 1518–1526 (2016).
- [74] Lang, R. et al. Hydroformylation of olefins by a rhodium single-atom catalyst with activity comparable to RhCl(PPh₃)₃. *Angew. Chem. Int. Ed.* 55, 16054–16058 (2016).
- [75] He, L., Weniger, F., Neumann, H. & Beller, M. Synthesis, characterization, and application of metal nanoparticles supported on nitrogen-doped carbon: catalysis beyond electrochemistry. *Angew. Chem. Int. Ed.* 55, 12582–12594 (2016).
- [76] Huda M, Minamisawa K, Tsukamoto T, Tanabe M, Yamamoto K. Aerobic toluene oxidation catalyzed by subnano metal particles. *Angew Chem Int Edit.* 2019;58(4):1002.
- [77] Imaoka T, Akanuma Y, Haruta N, Tsuchiya S, Ishihara K, Okayasu T, Chun WJ, Takahashi M, Yamamoto K. Platinum clusters with precise numbers of atoms for preparative-scale catalysis. *Nat Commun.* 2017;8:688.
- [78] Arnal PM, Comotti M, Schuth F. High-temperature-stable catalysts by hollow sphere encapsulation. *Angew Chem Int Edit.* 2006;45(48):8224.
- [79] Prieto G, Zecevic J, Friedrich H, de Jong KP, de Jongh PE. Towards stable catalysts by controlling collective properties of supported metal nanoparticles. *Nat Mater.* 2013;12(1):34.
- [80] Li WZ, Kovarik L, Mei DH, Liu J, Wang Y, Peden CHF. Stable platinum nanoparticles on specific MgAl₂O₄ spinel facets at high temperatures in oxidizing atmospheres. *Nat Commun.* 2013;4:2481.
- [81] Dong JH, Fu Q, Jiang Z, Mei BB, Bao XH. Carbide-supported Au catalysts for water–gas shift reactions: a new territory for the strong metal-support interaction effect. *J Am Chem Soc.* 2018;140(42):13808.
- [82] Liu LC, Diaz U, Arenal R, Agostini G, Concepcion P, Corma A. Generation of subnanometric platinum with high stability during transformation of a 2D zeolite into 3D. *Nat Mater.* 2017;16(12):132.
- [83] Yan Y, Zhang ZH, Bak SM, Yao SY, Hu XB, Shadike Z, Do-Thanh CL, Zhang F, Chen H, Lyu XL, Chen KQ, Zhu YM, Lu XY, Ouyang PK, Fu J, Dai S. Confinement of ultrasmall cobalt oxide clusters within silicalite-1 crystals for efficient conversion of fructose into methyl lactate. *ACS Catal.* 2019;9(3):1923.
- [84] Somorjai GA (1976) *Acc Chem Res* 9:248–256
- [85] White JM (1982) *Science* 218:429–433
- [86] Taylor HS (1922) *Chem Age* 30:309–314
- [87] Lewis WCMcC (1920) *J Chem Soc* 623–638
- [88] Taylor, H. S. A theory of the catalytic surface. *Proc. R. Soc. Lond. A* 108, 105–111 (1925).
- [89] Taylor HS (1924) *J Phys Chem* 28:898–942
- [90] Taylor HS (1948) *Adv Catal* 1:1–26
- [91] Kistiakowsky GB (1927) *Proc Natl Acad Sci USA* 13:1–4
- [92] Armstrong EF, Hilditch TP (1919) *Proc R Soc Lond Ser A* 96:137–146
- [93] Taylor HS (1921) *J Ind Eng Che* 13:75–78
- [94] Armstrong EF, Hilditch TP (1925) *Chem & Ind* 44:701–709
- [95] Langmuir I (1918) *J Am Chem Soc* 40:1361–1403
- [96] Langmuir I (1916) *J Am Chem Soc* 38:2221–2295
- [97] Bond GC (1966) *Disc Faraday Soc* 41:200–214
- [98] Siegal S, Smith GV (1960) *J Am Chem Soc* 82:6082–6087
- [99] Mitsui S, Imaizumi S, Nanbu A, Senda Y (1975) *J Catal* 36:333–337

- [100] Augustine RL (1995) *Heterogeneous catalysis for the synthetic chemist*. Dekker, New York, p 321
- [101] Bond GC, Sermon PA, Webb G, Buchanan DA, Wells PB (1973) *Chem Commun* 444–445
- [102] Sermon P.A, Bond GC, Wells PB (1979) *J Chem Soc Faraday Trans 1* 75:385–394
- [103] Augustine R.L, Meng L (1996) *Chem Ind* 68:15–30
- [104] Bond, GC, Webster DE (1969) *Ann NY Acad Sci* 158:540–559
- [105] Bond GC, Webster DE (1966) *Platin Metals Rev* 10:10–13
- [106] Bowden FP (1928) *Nature* 122:647–648
- [107] Vogel D, Spiel C, Schmid M, Stoger-Pollach M, Schlogl R, Suchorski Y, Rupperechter G (2013) *J Phys Chem C* 117:12054–12060
- [108] Cheronis ND (1947) *Organic chemistry, an introduction to the carbon compounds*. Crowell, New York, pp 232–233
- [109] Blakely DW, Somorjai GA (1976) *J Catal* 42:181–196
- [110] Goodman DW (1984) *Acc Chem Res* 17:194–200
- [111] Haruta M (1997) *Catal Today* 36:153–166
- [112] Chizallet C, Bonnard G, Krebs E, Bisson L, Thomazeau C, Raybaud P (2011) *J Phys Chem C* 115:12135–12149
- [113] Saha, B., Gupta, D., Abu-Omar, M.M., et al.: Porphyrin-based porous organic polymer-supported iron(III) catalyst for efficient aerobic oxidation of 5-hydroxymethyl-furfural into 2,5-furandicarboxylic acid. *J. Catal.* 299, 316–320 (2013)
- [114] Deng, D., Chen, X., Yu, L., et al.: A single iron site confined in a graphene matrix for the catalytic oxidation of benzene at room temperature. *Sci. Adv.* 1, 1500462 (2015)
- [115] Zhang, P., Chen, X.F., Lian, J.S., et al.: Structural selectivity of CO oxidation on Fe/N/C catalysts. *J. Phys. Chem. C* 116, 17572–17579 (2012)
- [116] Liu, W. et al. Discriminating catalytically active Fe_{Nx} species of atomically dispersed Fe–N–C catalyst for selective oxidation of C–H bond. *J. Am. Chem. Soc.* 139, 10790–10798 (2017).
- [117] Ju, W., Bagger, A., Hao, G.P., et al.: Understanding activity and selectivity of metal-nitrogen-doped carbon catalysts for electrochemical reduction of CO₂. *Nat. Commun.* 8, 944 (2017)
- [118] Huan, T.N., Ranjbar, N., Rousse, G., et al.: Electrochemical reduction of CO₂ catalyzed by Fe–N–C materials: a structure-selectivity study. *ACS Catal.* 7, 1520–1525 (2017)
- [119] Xu, S., Yu, D., Liao, S., et al.: Nitrogen-doped carbon supported iron oxide as efficient catalysts for chemoselective hydrogenation of nitroarenes. *RSC Adv.* 6, 96431–96435 (2016)
- [120] Li, J., Jj, Zhang, Liu, H., et al.: Graphitic carbon nitride (g-C₃N₄)-derived Fe–N–C catalysts for selective hydrodeoxygenation of 5-hydroxymethylfurfural to 2,5-dimethylfuran. *ChemistrySelect* 2, 11062–11070 (2017)
- [121] Shao, M., Chang, Q., Dodelet, J.P., et al.: Recent advances in electrocatalysts for oxygen reduction reaction. *Chem. Rev.* 116, 3594–3657 (2016)
- [122] Nie, Y., Li, L., Wei, Z.: Recent advancements in Pt and Pt-free catalysts for oxygen reduction reaction. *Chem. Soc. Rev.* 44, 2168–2201 (2015)
- [123] Scofield, M.E., Liu, H., Wong, S.S.: A concise guide to sustainable PEMFCs: recent advances in improving both oxygen reduction catalysts and proton exchange membranes. *Chem. Soc. Rev.* 44, 5836–5860 (2015)
- [124] Raj, C.R., Samanta, A., Noh, S.H., et al.: Emerging new generation electrocatalysts for the oxygen reduction reaction. *J. Mater. Chem. A* 4, 11156–11178 (2016)
- [125] Xia, W., Mahmood, A., Liang, Z., et al.: Earth-abundant nanomaterials for oxygen reduction. *Angew. Chem. Int. Ed.* 55, 2650–2676 (2015)
- [126] Xia, Z., An, L., Chen, P., et al.: Non-Pt nanostructured catalysts for oxygen reduction reaction: synthesis, catalytic activity and its key factors. *Adv. Energy Mater.* 6, 1600458 (2016)
- [127] Wenling, G., Liuyong, H., Jing, L., et al.: Recent advancements in transition metal-nitrogen-carbon catalysts for oxygen reduction reaction. *Electroanalysis* 30, 1217–1228 (2018)
- [128] Wu, K.H., Shi, W., Wang, D., et al.: In situ electrostatic modulation of path selectivity for the oxygen reduction reaction on Fe–N doped carbon catalyst. *Chem. Mater.* 29, 4649–4653 (2017)
- [129] Xu, H., Cheng, D., Cao, D., et al.: A universal principle for a rational design of single-atom electrocatalysts. *Nat. Catal.* 1, 339–348 (2018)
- [130] Zitolo, A. et al. Identification of catalytic sites for oxygen reduction in iron- and nitrogen-doped graphene materials. *Nat. Mater.* 14, 937–942 (2015).
- [131] Malko, D., Kucernak, A., Lopes, T.: In situ electrochemical quantification of active sites in Fe–N/C non-precious metal catalysts. *Nat. Commun.* 7, 13285 (2016)
- [132] Jiang, W., Gu, L., Li, L., et al.: Understanding the high activity of Fe–N–C electrocatalysts in oxygen reduction: Fe/Fe₃C nanoparticles boost the activity of Fe–Nx. *J. Am. Chem. Soc.* 138, 3570–3578 (2016)
- [133] Miao, Z., Wang, X., Tsai, M., et al.: Atomically dispersed Fe–Nx/C electrocatalyst boosts oxygen catalysis via a new metal-organic polymer supramolecule strategy. *Adv Energy Mater* 8(24), 1801226 (2018)
- [134] Fei, H., Dong, J., Feng, Y., et al.: General synthesis and definitive structural identification of MN₄C₄ single-atom catalysts with tunable electrocatalytic activities. *Nat. Catal.* 1, 63–72 (2018)
- [135] Seh, Z.W., Kibsgaard, J., Dickens, C.F., et al.: Combining theory and experiment in electrocatalysis: insights into materials design. *Science* 355, 146–157 (2017)
- [136] Kramm, U.I., Herrmann-Geppert, I., Fiechter, S., et al.: Effect of iron-carbide formation on the number of active sites in Fe–N–C catalysts for the oxygen reduction reaction in acidic media. *J. Mater. Chem. A* 2, 2663–2670 (2014)
- [137] Zhou, T., Shao, R., Chen, S., et al.: A review of radiation-grafted polymer electrolyte membranes for alkaline polymer electrolyte membrane fuel cells. *J. Power Sources* 293, 946–975 (2015)
- [138] Zhang, Z., Sun, J., Wang, F., et al.: Efficient oxygen reduction reaction (ORR) catalysts based on single iron atoms dispersed on a hierarchically structured porous carbon framework. *Angew. Chem. Int. Ed.* 130, 9176–9181 (2018)
- [139] Hu, B., Wu, Z., Chu, S., et al.: SiO₂-protected shell mediated templating synthesis of Fe–N-doped carbon nanofibers and their enhanced oxygen reduction reaction performance. *Energy Environ. Sci.* 11, 2208–2215 (2018)
- [140] Hori, Y. In *Modern Aspects of Electrochemistry* (eds. Vayenas, C. G., White, R. E. & Gamboa-Aldeco, M. E.) 89–189 (Springer, 2008).
- [141] Nitopi, S. et al. Progress and perspectives of electrochemical CO₂ reduction on copper in aqueous electrolyte. *Chem. Rev.* 119, 7610–7672 (2019).

- [142] Cui, X., Li, W., Ryabchuk, P., Junge, K. & Beller, M. Bridging homogeneous and heterogeneous catalysis by heterogeneous single-metal-site catalysts. *Nat. Catal.* 1, 385–397 (2018).
- [143] Chapovetsky, A. et al. Pendant hydrogen-bond donors in cobalt catalysts independently enhance CO₂ reduction. *ACS Cent. Sci.* 4, 397–404 (2018).
- [144] Göttle, A. J. & Koper, M. T. M. Determinant role of electrogenerated reactive nucleophilic species on selectivity during reduction of CO₂ catalyzed by metalloporphyrins. *J. Am. Chem. Soc.* 140, 4826–4834 (2018).
- [145] Kornienko, N. et al. Metal–organic frameworks for electrocatalytic reduction of carbon dioxide. *J. Am. Chem. Soc.* 137, 14129–14135 (2015).
- [146] Buss, J. A., VanderVelde, D. G. & Agapie, T. Lewis acid enhancement of proton induced CO₂ cleavage: bond weakening and ligand residence time effects. *J. Am. Chem. Soc.* 140, 10121–10125 (2018).
- [147] Chen, S., Liu, Y. & Chen, J. Heterogeneous electron transfer at nanoscopic electrodes: importance of electronic structures and electric double layers. *Chem. Soc. Rev.* 43, 5372–5386 (2014).
- [148] Raciti, D., Mao, M. & Wang, C. Mass transport modelling for the electroreduction of CO₂ on Cu nanowires. *Nanotechnology* 29, 44001 (2017).
- [149] Limburg, B., Bouwman, E. & Bonnet, S. Molecular water oxidation catalysts based on transition metals and their decomposition pathways. *Coord. Chem. Rev.* 256, 1451–1467 (2012).
- [150] Bromley ST, de Moreira IPR, Neyman KM, Illas F (2009) Approaching nanoscale oxides: models and theoretical methods. *Chem Soc Rev* 38:2657–2670. doi: 10.1039/b806400h
- [151] Kozlov SM, Neyman KM (2013) Catalysis from first principles: towards accounting for the effects of nanostructuring. *Top Catal* 56:867–873. doi: 10.1007/s11244-013-0050-1
- [152] Loschen C, Bromley ST, Neyman KM, Illas F (2007) Understanding ceria nanoparticles from first-principles calculations. *J Phys Chem C* 111:10142–10145. doi: 10.1021/jp072787m
- [153] Loschen C, Migani A, Bromley ST et al (2008) Density functional studies of model cerium oxide nanoparticles. *Phys Chem Chem Phys* 10:5730–5738. doi: 10.1039/b805904g
- [154] Bruix, A. et al. Maximum noble-metal efficiency in catalytic materials: atomically dispersed surface platinum. *Angew. Chem. Int. Ed.* 53, 10525–10530 (2014).
- [155] Vayssilov GN, Lykhach Y, Migani A et al (2011) Support nanostructure boosts oxygen transfer to catalytically active platinum nanoparticles. *Nat Mater* 10:310–315. doi: 10.1038/nmat2976
- [156] Bruix A, Rodriguez JA, Ramírez PJ et al (2012) A new type of strong metal-support interaction and the production of H₂ through the transformation of water on Pt/CeO₂(111) and Pt/CeO_x/TiO₂(110) catalysts. *J Am Chem Soc* 134:8968–8974. doi: 10.1021/ja302070k
- [157] Lykhach Y, Kozlov SM, Skála T et al (2016) Counting electrons on supported nanoparticles. *Nat Mater* 15:284–288. doi: 10.1038/nmat4500
- [158] Figueroba A, Kovács G, Bruix A, Neyman KM (2016) Towards stable single-atom catalysts: strong binding of atomically dispersed transition metals on the surface of nanostructured ceria. *Catal Sci Technol.* doi: 10.1039/C6CY00294C
- [159] Pacchioni G (2014) First principles calculations on oxide-based heterogeneous catalysts and photocatalysts: problems and advances. *Catal Letters* 145:80–94. doi: 10.1007/s10562-014-1386-2
- [160] Paier J (2016) Hybrid density functionals applied to complex solid catalysts: successes, limitations, and prospects. *Catal Letters* 146:861–885. doi: 10.1007/s10562-016-1735-4
- [161] Vayssilov GN, Mihaylov M, St Petkov P et al (2011) Reassignment of the vibrational spectra of carbonates, formates, and related surface species on ceria: a combined density functional and infrared spectroscopy investigation. *J Phys Chem C* 115:23435–23454. doi: 10.1021/jp208050a
- [162] Trovarelli A, de Leitenburg C, Boaro M, Dolcetti G (1999) The utilization of ceria in industrial catalysis. *Catal Today* 50:353–367. doi: 10.1016/S0920-5861(98)00515-X
- [163] Bernal S, Calvino J, Cauqui M et al (1999) Some recent results on metal/support interaction effects in NM/CeO₂ (NM: noble metal) catalysts. *Catal Today* 50:175–206. doi: 10.1016/S0920-5861(98)00503-3
- [164] Lykhach Y, Figueroba A, Camellone MF et al (2016) Reactivity of atomically dispersed Pt₂₊ species towards H₂: model Pt–CeO₂ fuel cell catalyst. *Phys Chem Chem Phys* 18:7672–7679. doi: 10.1039/c6cp00627b
- [165] Lindstrom, C. D. & Zhu, X.-Y. Photoinduced electron transfer at molecule–metal interfaces. *Chem. Rev.* 106, 4281–4300 (2006). Review paper summarizing mechanisms of electron transfer at molecule–metal interfaces with emphasis on the role of chemical bonding at the interface.
- [166] Frischkorn, C. & Wolf, M. Femtochemistry at metal surfaces: nonadiabatic reaction dynamics. *Chem. Rev.* 106, 4207–4233 (2006).
- [167] White, J. M. Using photons and electrons to drive surface chemical reactions. *J. Mol. Catal. Chem.* 131, 71–90 (1998).
- [168] Busch, D. G. & Ho, W. Direct observation of the crossover from single to multiple excitations in femtosecond surface photochemistry. *Phys. Rev. Lett.* 77, 1338–1341 (1996).
- [169] Linic, S., Christopher, P., Xin, H. & Marimuthu, A. Catalytic and photocatalytic transformations on metal nanoparticles with targeted geometric and plasmonic properties. *Acc. Chem. Res.* 46, 1890–1899 (2013).
- [170] Christopher, P., Xin, H. & Linic, S. Visible-light-enhanced catalytic oxidation reactions on plasmonic silver nanostructures. *Nat. Chem.* 3, 467–472 (2011). Demonstration of visible-light-enhanced reactions on plasmonic Ag nanostructures with systematic experiments uncovering the role of hot charge carriers in activating chemical bonds.
- [171] Mukherjee, S. et al. Hot electrons do the impossible: plasmon-induced dissociation of H₂ on Au. *Nano Lett.* 13, 240–247 (2013).
- [172] Marimuthu, A., Zhang, J. & Linic, S. Tuning selectivity in propylene epoxidation by plasmon mediated photo-switching of Cu oxidation state. *Science* 339, 1590–1593 (2013). A unique case in which plasmon excitation causes a change in the oxidation state of a metal catalyst under operating conditions resulting in a significant improvement of product selectivity.
- [173] Linic, S., Aslam, U., Boerigter, C. & Morabito, M. Photochemical transformations on plasmonic metal nanoparticles. *Nat. Mater.* 14, 567–576 (2015).

- [174] Kale, M. J., Avanesian, T. & Christopher, P. Direct photocatalysis by plasmonic nanostructures. *ACS Catal.* 4, 116–128 (2014).
- [175] Zhang, Y. et al. Surface-plasmon-driven hot electron photochemistry. *Chem. Rev.* 118, 2927–2954 (2018).
- [176] Zhang, X., Chen, Y. L., Liu, R.-S. & Tsai, D. P. Plasmonic photocatalysis. *Rep. Prog. Phys.* 76, 046401 (2013).
- [177] Maier, S. A. *Plasmonics: Fundamentals and Applications* (Springer Science and Business Media, Bath, 2007).
- [178] Kelly, K. L., Coronado, E., Zhao, L. L. & Schatz, G. C. The optical properties of metal nanoparticles: the influence of size, shape, and dielectric environment. *J. Phys. Chem. B* 107, 668–677 (2002).
- [179] Halas, N. J., Lal, S., Chang, W.-S., Link, S. & Nordlander, P. Plasmons in strongly coupled metallic nanostructures. *Chem. Rev.* 111, 3913–3961 (2011).
- [180] Evanoff, D. D. & Chumanov, G. Size-controlled synthesis of nanoparticles. 2. Measurement of extinction, scattering, and absorption cross sections. *J. Phys. Chem. B* 108, 13957–13962 (2004).
- [181] Jain, P. K., Lee, K. S., El-Sayed, I. H. & El-Sayed, M. A. Calculated absorption and scattering properties of gold nanoparticles of different size, shape, and composition: applications in biological imaging and biomedicine. *J. Phys. Chem. B* 110, 7238–7248 (2006).
- [182] Bosbach, J., Hendrich, C., Stietz, F., Vartanyan, T. & Träger, F. Ultrafast dephasing of surface plasmon excitation in silver nanoparticles: influence of particle size, shape, and chemical surrounding. *Phys. Rev. Lett.* 89, 257404 (2002).
- [183] Bonn, M. et al. Phonon- versus electron-mediated desorption and oxidation of CO on Ru(0001). *Science* 285, 1042–1045 (1999). Demonstration of unique chemical reaction outcomes for electron-mediated processes versus phonon-mediated processes on bulk metals under laser excitation.
- [184] Ageev, V. N. Desorption induced by electronic transitions. *Prog. Surf. Sci.* 47, 55–203 (1994).
- [185] Christopher, P., Xin, H., Marimuthu, A. & Linic, S. Singular characteristics and unique chemical bond activation mechanisms of photocatalytic reactions on plasmonic nanostructures. *Nat. Mater.* 11, 1044–1050 (2012). Combined experimental and theoretical study uncovering the role of hot carriers in plasmon-driven chemical reactions.
- [186] Qiao, B. T. et al. Single-atom catalysis of CO oxidation using Pt1/FeOx. *Nat. Chem.* 3, 634–641 (2011). The first practical Pt single site catalyst on FeOx was fabricated and displayed high activity and stability for both CO oxidation and preferential oxidation of CO in H2.
- [187] Wei, H. S. et al. FeOx-supported platinum single-atom and pseudo-single-atom catalysts for chemoselective hydrogenation of functionalized nitroarenes. *Nat. Commun.* 5, 5634 (2014).
- [188] Hu, P. P. et al. Electronic metal- support interactions in single-atom catalysts. *Angew. Chem. Int. Ed.* 53, 3418–3421 (2014).
- [189] Addou, R. et al. Influence of hydroxyls on Pd atom mobility and clustering on rutile TiO2(011)-2 x 1. *ACS Nano* 8, 6321–6333 (2014).
- [190] Zhou, X. et al. Stable Pt single atoms and nanoclusters on ultrathin CuO film and their performances in CO oxidation. *J. Phys. Chem. C* 120, 1709–1715 (2016).
- [191] Liu, W. G. et al. Single-atom dispersed Co-N-C catalyst: structure identification and performance for hydrogenative coupling of nitroarenes. *Chem. Sci.* 7, 5758–5764 (2016). The isolated Co site catalyst was successfully synthesized by pyrolysis of Co-phen complex and the resulting material displayed good reactivity on preparation of azo products by the hydrogenation of nitrobenzenes.
- [192] Tyo, E.C., Vajda, S.: Catalysis by clusters with precise numbers of atoms. *Nat. Nanotechnol.* 10, 577–588 (2015)
- [193] Liang, S., Hao, C., Shi, Y.: The power of single-atom catalysis. *ChemCatChem* 7, 2559–2567 (2015)
- [194] Yang, X., Wang, A., Qiao, B., et al.: Single-atom catalysts: a new frontier in heterogeneous catalysis. *Acc. Chem. Res.* 46, 1740–1748 (2013)
- [195] Flytzani-Stephanopoulos, M., Gates, B.C.: Atomically dispersed supported metal catalysts. *Annu. Rev. Chem. Biomol. Eng.* 3, 545–574 (2012)
- [196] Corma, A., et al.: Exceptional oxidation activity with size-controlled supported gold clusters of low atomicity. *Nat. Chem.* 5, 775–781 (2013)
- [197] Moliner, M., Concepción, P., Boronat, M., et al.: Reversible transformation of Pt nanoparticles into single atoms inside high-silica chabazite zeolite. *J. Am. Chem. Soc.* 138, 15743–15750 (2016)
- [198] Peterson, E.J., DeLaRiva, A.T., Lin, S., et al.: Low-temperature carbon monoxide oxidation catalysed by regenerable atomically dispersed palladium on alumina. *Nat. Commun.* 5, 4885 (2014)
- [199] Qiao, B., Wang, A., Yang, X., et al.: Single-atom catalysis of CO oxidation using Pt1/FeOx. *Nat. Chem.* 3, 634–641 (2011)
- [200] Vilé, G., Albani, D., Nachttegaal, M., et al.: A stable single-site palladium catalyst for hydrogenations. *Angew. Chem. Int. Ed.* 54, 11265–11269 (2015)
- [201] Pei, G.X., Liu, X.Y., Wang, A., et al.: Ag alloyed Pd single-atom catalysts for efficient selective hydrogenation of acetylene to ethylene in excess ethylene. *ACS Catal.* 5, 3717–3725 (2015)
- [202] Pei, G.X., Liu, X.Y., Wang, A., et al.: Promotional effect of Pd single atoms on Au nanoparticles supported on silica for the selective hydrogenation of acetylene in excess ethylene. *New J. Chem.* 38, 2043–2051 (2014)
- [203] Aich, P., Wei, H., Basan, H., et al.: Single-atom alloy Pd–Ag catalyst for selective hydrogenation of acrolein. *J. Phys. Chem. C* 119, 18140–18148 (2015)
- [204] Boucher, M.B., Zugic, B., Cladaras, G., et al.: Single atom alloy surface analogs in Pd0.18Cu0.15 nanoparticles for selective hydrogenation reactions. *Phys. Chem. Chem. Phys.* 15, 12187–12196 (2013)
- [205] Cao, X.R., Ji, Y.F., Luo, Y.: Dehydrogenation of propane to propylene by a Pd/Cu single-atom catalyst: insight from first-principles calculations. *J. Phys. Chem. C* 119, 1016–1023 (2015)
- [206] Boucher, M.B., Marcinkowski, M.D., Liriano, M.L., et al.: Molecular-scale perspective of water-catalyzed methanol dehydrogenation to formaldehyde. *ACS Nano* 7, 6181–6187 (2013)
- [207] Shan, J.J., Lucci, F.R., Liu, J., et al.: Water co-catalyzed selective dehydrogenation of methanol to formaldehyde and hydrogen. *Surf. Sci.* 650, 121–129 (2016)
- [208] Zhang, H.J., Kawashima, K., Okumura, M., et al.: Colloidal Au single-atom catalysts embedded on Pd nanoclusters. *J. Mater. Chem. A* 2, 13498–13508 (2014)
- [209] Cheng, X., Zhao, Y., Li, F., et al.: Catalytic mechanisms of Au11 and Au11–nPt_n (n = 1–2) clusters: a DFT investigation on the oxidation of CO by O2. *J. Mol. Model.* 21, 1–11 (2015)

- [210] Yao, Y.X., Goodman, D.W.: New insights into structure–activity relationships for propane hydrogenolysis over Ni–Cu bimetallic catalysts. *RSC Adv.* 5, 43547–43551 (2015)
- [211] Zhang, L., Wang, A., Miller, J.T., et al.: Efficient and durable Au alloyed Pd single-atom catalyst for the Ullmann reaction of aryl chlorides in water. *ACS Catal.* 4, 1546–1553 (2014)
- [212] Lucci, F.R., Marcinkowski, M.D., Lawton, T.J., et al.: H₂ activation and spillover on catalytically relevant Pt–Cu single atom alloys. *J. Phys. Chem. C* 119, 24351–24357 (2015)
- [213] Wei, H.S., Liu, X., Wang, A., et al.: FeO_x-supported platinum single-atom and pseudo-single-atom catalysts for chemoselective hydrogenation of functionalized nitroarenes. *Nat. Commun.* 5, 5634 (2014)
- [214] Gu, X.K., Qiao, B., Huang, C.Q., et al.: Supported single Pt₁/Au₁ atoms for methanol steam reforming. *ACS Catal.* 4, 3886–3890 (2014)
- [215] Vasileff, A., Xu, C., Jiao, Y., et al.: Surface and interface engineering in copper-based bimetallic materials for selective CO₂ electroreduction. *Chem* 4, 1809–1831 (2018)
- [216] Liu, J., Zhu, D., Zheng, Y., et al.: Self-supported earth-abundant nanoarrays as efficient and robust electrocatalysts for energy-related reactions. *ACS Catal.* 8, 6707–6732 (2018)
- [217] Jiao, Y., Zheng, Y., Chen, P., et al.: Molecular scaffolding strategy with synergistic active centers to facilitate electrocatalytic CO₂ reduction to hydrocarbon/alcohol. *J. Am. Chem. Soc.* 139, 18093–18100 (2017)
- [218] Vasileff, A., Zheng, Y., Qiao, S.: Carbon solving carbon's problems: recent progress of nanostructured carbon-based catalysts for the electrochemical reduction of CO₂. *Adv Energy Mater.* 7, 1700759 (2017)
- [219] Bayatsarmadi, B., Zheng, Y., Vasileff, A., et al.: Recent advances in atomic metal doping of carbon-based nanomaterials for energy conversion. *Small* 13, 1700191 (2017)
- [220] Hu, P.P., Huang, Z.W., Amghouz, Z., et al.: Electronic metal-support interactions in single-atom catalysts. *Angew. Chem. Int. Ed.* 53, 3418–3421 (2014). <https://doi.org/10.1002/anie.201309248>
- [221] Jeon, I.Y., Zhang, S., Zhang, L.P., et al.: Edge-selectively sulfurized graphene nanoplatelets as efficient metal-free electrocatalysts for oxygen reduction reaction: the electron spin effect. *Adv. Mater.* 25, 6138–6145 (2013). <https://doi.org/10.1002/adma.201302753>
- [222] Vajda, S., White, M.G.: Catalysis applications of size-selected cluster deposition. *ACS Catal.* 5, 7152–7176 (2015). <https://doi.org/10.1021/acscatal.5b01816>
- [223] Yamazaki, K., Maehara, Y., Kitajima, R., et al.: High-density dispersion of single platinum atoms on graphene by plasma sputtering in N₂ atmosphere. *Appl. Phys. Express* 11, 095101 (2018). <https://doi.org/10.7567/apex.11.095101>
- [224] Lee, B.H., Park, S., Kim, M., et al.: Reversible and cooperative photoactivation of single-atom Cu/TiO₂ photocatalysts. *Nat. Mater.* 18, 620–626 (2019). <https://doi.org/10.1038/s41563-019-0344-1>
- [225] Wei, H. et al. Iced photochemical reduction to synthesize atomically dispersed metals by suppressing nanocrystal growth. *Nat. Commun.* 8, 1490 (2017).
- [226] Tang, Y. et al. Single rhodium atoms anchored in micropores for efficient transformation of methane under mild conditions. *Nat. Commun.* 9, 1231 (2018).
- [227] Zhang, H.B., Liu, G.G., Shi, L., et al.: Single-atom catalysts: emerging multifunctional materials in heterogeneous catalysis. *Adv. Energy Mater.* 8, 1701343 (2018). <https://doi.org/10.1002/aenm.201701343>
- [228] Chen, S., Chen, Z.N., Fang, W.H., et al.: Ag₁₀Ti₂₈-oxo cluster containing single-atom silver sites: atomic structure and synergistic electronic properties. *Angew. Chem. Int. Ed.* 58, 10932–10935 (2019). <https://doi.org/10.1002/anie.201904680>
- [229] Cao, S.F., Zhao, Y.Y., Lee, S., et al.: High-loading single Pt atom sites [Pt–O(OH)_x] catalyze the CO PROX reaction with high activity and selectivity at mild conditions. *Sci. Adv.* 6, eaba3809 (2020). <https://doi.org/10.1126/sciadv.aba3809>
- [230] Liu P, Zhao Y, Qin R, et al. Photochemical route for synthesizing atomically dispersed palladium catalysts. *Science*, 2016, 352: 797–800
- [231] Zhang, L.H., Han, L.L., Liu, H.X., et al.: Potential-cycling synthesis of single platinum atoms for efficient hydrogen evolution in neutral media. *Angew. Chem. Int. Ed.* 56, 13694–13698 (2017). <https://doi.org/10.1002/anie.201706921>
- [232] Zhao, S., Chen, F., Duan, S.B., et al.: Remarkable active-site dependent H₂O promoting effect in CO oxidation. *Nat. Commun.* 10, 3824 (2019). <https://doi.org/10.1038/s41467-019-11871-w>
- [233] Therrien, A. J. et al. An atomic-scale view of single-site Pt catalysis for low-temperature CO oxidation. *Nat. Catal.* 1, 192–198 (2018).
- [234] Chen, W.X., Pei, J.J., He, C.T., et al.: Rational design of single molybdenum atoms anchored on N-doped carbon for effective hydrogen evolution reaction. *Angew. Chem. Int. Ed.* 56, 16086–16090 (2017). <https://doi.org/10.1002/anie.201710599>
- [235] Liu, L.C., Díaz, U., Arenal, R., et al.: Generation of subnanometric platinum with high stability during transformation of a 2D zeolite into 3D. *Nat. Mater.* 16, 132–138 (2017). <https://doi.org/10.1038/nmat4757>
- [236] Lee, S., Fan, C.Y., Wu, T.P., et al.: CO oxidation on Au_n/TiO₂ catalysts produced by size-selected cluster deposition. *J. Am. Chem. Soc.* 126, 5682–5683 (2004). <https://doi.org/10.1021/ja049436v>
- [237] Lei, Y., Mehmood, F., Lee, S., et al.: Increased silver activity for direct propylene epoxidation via subnanometer size effects. *Science* 328, 224–228 (2010). <https://doi.org/10.1126/science.1185200>
- [238] Li, Z.J., Wang, D.H., Wu, Y.E., et al.: Recent advances in the precise control of isolated single-site catalysts by chemical methods. *Natl. Sci. Rev.* 5, 673–689 (2018). <https://doi.org/10.1093/nsr/nwy056>
- [239] Zhang, Z.Q., Chen, Y.G., Zhou, L.Q., et al.: The simplest construction of single-site catalysts by the synergism of micropore trapping and nitrogen anchoring. *Nat. Commun.* 10, 1675 (2019). <https://doi.org/10.1038/s41467-019-09596-x>
- [240] Kuang, P.Y., Wang, Y.R., Zhu, B.C., et al.: Pt single atoms supported on N-doped mesoporous hollow carbon spheres with enhanced electrocatalytic H₂-evolution activity. *Adv. Mater.* 33, 2008599 (2021). <https://doi.org/10.1002/adma.202008599>
- [241] Lu, J., Fu, B., Kung, M.C., et al.: Coking- and sintering-resistant palladium catalysts achieved through atomic layer deposition. *Science* 335, 1205–1208 (2012). <https://doi.org/10.1126/science.1212906>
- [242] O'Neill, B.J., Jackson, D.H.K., Crisci, A.J., et al.: Stabilization of copper catalysts for liquid-phase reactions by atomic layer

- deposition. *Angew. Chem. Int. Ed.* 52, 13808–13812 (2013). <https://doi.org/10.1002/anie.201308245>
- [243] Lu, J., Elam, J.W., Stair, P.C.: Synthesis and stabilization of supported metal catalysts by atomic layer deposition. *Acc. Chem. Res.* 46, 1806–1815 (2013). <https://doi.org/10.1021/ar300229c>
- [244] Qiu, H.-J. et al. Nanoporous graphene with single-atom nickel dopants: an efficient and stable catalyst for electrochemical hydrogen production. *Angew. Chem. Int. Ed.* 54, 14031–14035 (2015).
- [245] Zhang, T., Fu, L.: Controllable chemical vapor deposition growth of two-dimensional heterostructures. *Chem* 4, 671–689 (2018). <https://doi.org/10.1016/j.chempr.2017.12.006>
- [246] Zhao, J., Deng, Q., Bachmatiuk, A., et al.: Free-standing single-atom-thick iron membranes suspended in graphene pores. *Science* 343, 1228–1232 (2014). <https://doi.org/10.1126/science.1245273>
- [247] Tavakkoli, M., Holmberg, N., Kronberg, R., et al.: Electrochemical activation of single-walled carbon nanotubes with pseudo-atomic-scale platinum for the hydrogen evolution reaction. *ACS Catal.* 7, 3121–3130 (2017). <https://doi.org/10.1021/acscatal.7b00199>
- [248] Strasser, P.: Free electrons to molecular bonds and back: closing the energetic oxygen reduction (ORR)-oxygen evolution (OER) cycle using core-shell nanoelectrocatalysts. *Acc. Chem. Res.* 49, 2658–2668 (2016). <https://doi.org/10.1021/acs.accounts.6b00346>
- [249] Taylor K, Pettiette-Hall CL, Cheshnovsky O, Smalley RE (1992) *J Chem Phys* 96:3319–3329
- [250] Fu Q, Wagner (2007) *Surf Sci Rep* 62:431–498
- [251] Li H, Li L, Li Y (2013) *Nanotechnol Rev* 2:515–528
- [252] Puzsztai P, Puskás R, Varga E, Erdőhelyi A, Kukovecz Á, Kónya Z, Kiss J (2014) *Phys Chem Chem Phys* 16:26786–26797
- [253] László B, Baán K, Varga E, Oszkó A, Erdőhelyi A, Kónya Z, Kiss J (2016) *Appl Catal B* 199:473–484
- [254] Kukovecz Á, Pótári G, Oszkó A, Kónya Z, Erdőhelyi A, Kiss J (2011) *Surf Sci* 605:1048–1055
- [255] Kiss J, Puzsztai P, Óvári L, Baán K, Merza G, Erdőhelyi A, Kukovecz Á, Kónya Z (2014) *e-J Surf Sci Nanotechnol* 12:252–258
- [256] Lee J, Shim HS, Lee M, Song JK, Lee D (2011) *J Phys Chem Lett* 2:2840–2845
- [257] Schmid G (2008) *Chem Soc Rev* 37:1909–1930
- [258] Patterson MC, Habenicht BF, Kurrztz RL, Liu L, Xu Y, Sprunger PT (2014) *Phys Rev B* 89:205423
- [259] Gubó R, Vári G, Kiss J, Farkas AP, Óvári L, Berkó A, Kónya Z (2018) *Phys Chem Chem Phys* 20:15473–15485
- [260] Dey S, Dhal GC, Mohan D, Prasad R (2018) Synthesis and characterization of AgCoO₂ catalyst for oxidation of CO at a low temperature. *Polyhedron* 155:102–113
- [261] Dey S, Dhal GC, Mohan D, Prasad R (2019) Synthesis of silver promoted CuMnOx catalyst for ambient temperature oxidation of carbon monoxide. *J Sci: Adv Mater Devices* 4:47–56
- [262] Dong RT, Wang HL, Zhang Q, Xu XT, Wang F, Li B (2015) Shape-controlled synthesis of Mn₂O₃ hollow structures and their catalytic properties. *CrystEngComm* 17:7406–7413
- [263] Dey S, Dhal GC, Mohan D, Prasad R (2018) The choice of precursors in the synthesizing of CuMnOx catalysts for maximizing CO oxidation. *Int J Ind Chem* 9:199–214
- [264] Wu Y, Wang DS, Li YD (2014) Nanocrystals from solutions: catalysts. *Chem Soc Rev* 43:2112–2124
- [265] Yuan CZ, Wu HB, Xie Y, Lou XW (2014) Mixed transition-metal oxides: design, synthesis, and energy-related applications. *Angew Chem Int* 53:1488–1504
- [266] Dey S, Dhal GC, Prasad R, Mohan D (2016) Total oxidation of CO by CuMnOx catalyst at a low temperature. *Int J Sci Eng Res* 7(10):1730–1737
- [267] Abu Bakar WAW, Toemen RAS (2012) Catalytic methanation reaction over supported nickel–ruthenium oxide base for purification of simulated natural gas. *Sci Iran* 19(3):525–534
- [268] Hashemnejad SM, Parvari M (2011) Deactivation and regeneration of nickel-based catalysts for steam-methane reforming. *Chin J Catal* 32(2):273–279
- [269] Grillo F, Natile MM, Glisenti A (2004) Low temperature oxidation of carbon monoxide: the influence of water and oxygen on the reactivity of a Co₃O₄ powder surface. *Appl Catal B Environ* 48:267–274
- [270] Kraum M, Baerns M (1999) Fischer–Tropsch synthesis: the influence of various cobalt compounds applied in the preparation of supported cobalt catalysts on their performance. *Appl Catal A Gen* 186:189–200
- [271] Larsson PO, Berggren H, Andersson A, Augustsson O (1997) Supported metal oxides for catalytic combustion of CO and VOCs emissions: preparation of titania over layers on a macroporous support. *Catal Today* 35:137–144
- [272] Luo M, Fang P, He M, Xie Y (2005) In situ XRD, Raman, and TPR studies of CuO/Al₂O₃ catalysts for CO oxidation. *J Mol Catal A Chem* 239:243–248
- [273] Li P, Miser DE, Rabiei S, Yadav RT, Hajaligol MR (2003) The removal of carbon monoxide by iron oxide nanoparticles. *Appl Catal B Environ* 43:151–162
- [274] Fazlollahi F, Sarkari M, Gharebaghi H, Atashi H, Zarei MM, Mirzaei AA, Hecker WC (2013) Preparation of Fe–Mn/K/Al₂O₃ Fischer–Tropsch catalyst and its catalytic kinetics for the hydrogenation of carbon monoxide. *Catal Kinet React Eng* 21:507–519
- [275] Podyacheva OY, Stadnichenko AI, Yashnik SA, Stonkus OA, Slavinskaya EM, Boronin AI, Puzynin AV, Ismagilov ZR (2014) Catalytic and capacity properties of nano composites based on cobalt oxide and nitrogen-doped carbon nanofibers. *Chin J Catal* 35:960–969
- [276] Chien C, Chuang W, Huang T (1995) Effect of heat treatment conditions on Cu–Cr/γ-alumina catalyst for carbon monoxide and propane oxidation. *Applied Catalysis A : General* 131:73–87
- [277] Nagase K, Zheng Y, Kodama Y, Kakuta J (1999) Dynamic study of the oxidation state of copper in the course of carbon monoxide oxidation over powdered CuO and Cu₂O. *J Catal* 187:123–130
- [278] Konova P, Stoyanova M, Naydenov A, Christoskova S, Mehandjiev D (2006) Catalytic oxidation of VOCs and CO by ozone over alumina supported cobalt oxide. *Appl Catal A Gen* 298:109–114
- [279] Wagloehner S, Reichert D, Leon-Sorzano D, Balle P, Geiger B, Kureti S (2008) Kinetic modeling of the oxidation of CO on Fe₂O₃ catalyst in excess of O₂. *J Catal* 260:305–314
- [280] Kasmi AE, Tian Z, Vieker H, Beyer A, Chafik T (2016) Innovative CVD synthesis of Cu₂O catalysts for CO oxidation. *Appl Catal B Environ* 186:10–18

- [281] White B, Yin M, Hall A, Le D, Stolbov S, Rahman T, Turro N, O'Brien S (2006) Complete CO oxidation over Cu₂O nanoparticles supported on silica gel. *Nano Lett* 6:2095–2098
- [282] Rattan G, Kaur R (2015) Total oxidation of CO using Cu & Co catalyst: kinetic study and calcinations effect. *Bull Chem React Eng Catal* 10(3):281–293
- [283] Chen CS, Chen TC, Chen CC, Lai YT, You JH, Chou TM, Chen CH, Lee J (2012) Effect of Ti³⁺ on TiO₂ supported Cu catalysts used for CO oxidation. *ACS Lang* 28:9996–10006
- [284] Tang Y, Dong L, Deng C, Huang M, Li B, Zhang H (2016) In-Situ FTIR investigation of CO oxidation on CuO/TiO₂ catalyst. *Catal Commun* 28:1–17
- [285] Punde SS, Tatarchuk BJ (2012) Microfibrous entrapped catalysts for low temperature CO oxidation in humid air. *Catal Commun* 27:9–12
- [286] Védrine JC (2017) Heterogeneous catalysis on metal oxides. *Catalysts* 7:341–365
- [287] Somorjai GA, Park JY (2008) *Angew Chem Int Edit* 47(48):9212–9228
- [288] An K, Somorjai GA (2015) *Catal Lett* 145:233
- [289] An K, Somorjai GA (2012) *Chemcatchem* 4:151
- [290] Grass ME, Zhang YW, Butcher DR, Park JY, Li YM, Bluhm H, Bratlie KM, Zhang TF, Somorjai GA (2008) *Angew Chem Int Edit* 47:8893
- [291] Joo SH, Park JY, Renzas JR, Butcher DR, Huang WY, Somorjai GA (2010) *Nano Lett* 10:2709
- [292] Qadir K, Joo SH, Mun BS, Butcher DR, Renzas JR, Aksoy F, Liu Z, Somorjai GA, Park JY (2012) *Nano Lett* 12:5761
- [293] Berlowitz PJ, Peden CHF, Goodman DW (1988) *J Phys Chem* 92:5213
- [294] Su X, Cerner PS, Shen YR, Somorjai GA (1997) *J Am Chem Soc* 119:3994
- [295] Rioux RM, Song H, Hoefelmeyer JD, Yang P, Somorjai GA (2004) *J Phys Chem B* 109:2192
- [296] Park JY, Aliaga C, Renzas JR, Lee H, Somorjai GA (2009) *Catal Lett* 129:1
- [297] Joo SH, Park JY, Tsung C-K, Yamada Y, Yang P, Somorjai GA (2009) *Nat Mater* 8:126
- [298] Lee DG, Kim SM, Kim SM, Lee SW, Park JY, An K, Lee IS (2016) *Chem Mater* 28:9049
- [299] Aijaz A, Akita T, Tsumori N, Xu Q (2013) *J Am Chem Soc* 135:16356
- [300] Rungtaweeworanit B, Baek J, Araujo JR, Archanjo BS, Choi KM, Yaghi OM, Somorjai GA (2016) Copper nanocrystals encapsulated in Zr-based metal-organic framework for highly selective CO₂ hydrogenation to methanol. *Nano Lett* 16:7645–7649
- [301] Becker, C. A., Cowin, J. P., Wharton, L. & Auerbach, D. J. CO₂ product velocity distributions for CO oxidation on platinum. *J. Chem. Phys.* 67, 3394–3395 (1977).
- [302] Campbell CT, Ertl G, Kuipers H, Segner J (1980) *J Chem Phys* 73:5862
- [303] Gland, J. L. & Kollin, E. B. Carbon monoxide oxidation on the Pt(111) surface: Temperature programmed reaction of coadsorbed atomic oxygen and carbon monoxide. *J. Chem. Phys.* 78, 963–974 (1983).
- [304] Segner, J., Campbell, C. T., Doyen, G. & Ertl, G. Catalytic oxidation of CO on Pt(111): the influence of surface defects and composition on the reaction dynamics. *Surf. Sci.* 138, 505–523 (1984).
- [305] Neugeboren, J. et al. Velocity-resolved kinetics of site-specific carbon monoxide oxidation on platinum surfaces. *Nature* 558, 280–283 (2018). This article describes a velocity-resolved ion-imaging technique for accurate measurement of reaction kinetics at gas–surface interfaces. The method is applied to CO oxidation on Pt surfaces and the experimental results are successfully described using a coverage-independent microkinetic model.
- [306] Zhou, L., Kandratsenka, A., Campbell, C. T., Wodtke, A. M. & Guo, H. Origin of thermal and hyperthermal CO₂ from CO oxidation on Pt surfaces: the role of post-transition-state dynamics, active sites, and chemisorbed CO₂. *Angew. Chem. Int. Ed.* 58, 6916–6920 (2019).
- [307] Madix, R. J. & Telford, S. G. The kinetic isotope effect for C–H bond activation on Cu(110): the effects of tunnelling. *Surf. Sci.* 277, 246–252 (1992).
- [308] Falconer, J. L. & Schwarz, J. A. Temperature-programmed desorption and reaction: applications to supported catalysts. *Catal. Rev. Sci. Eng.* 25, 141–227 (1983).
- [309] Xu, J. Z. & Yates, J. T. Catalytic oxidation of CO on Pt(335): a study of the active site. *J. Chem. Phys.* 99, 725–732 (1993).
- [310] Zaera, F. New advances in the use of infrared absorption spectroscopy for the characterization of heterogeneous catalytic reactions. *Chem. Soc. Rev.* 43, 7624–7663 (2014).
- [311] Fuhrmann, T. et al. Activated adsorption of methane on Pt(111) - an in situ XPS study. *New J. Phys.* 7, 107 (2005).
- [312] Papp, C. & Steinrück, H. P. In situ high-resolution X-ray photoelectron spectroscopy - Fundamental insights in surface reactions. *Surf. Sci. Rep.* 68, 446–487 (2013).
- [313] Wintterlin, J., Völkening, S., Janssens, T. V. W., Zambelli, T. & Ertl, G. Atomic and macroscopic reaction rates of a surface-catalyzed reaction. *Science* 278, 1931–1934 (1997). This work uses scanning tunnelling microscopy to measure accurate kinetics of CO oxidation on Pt(111) terraces at low temperature (230–275K) by directly counting the disappearance of O atoms on a timescale of minutes to hours. Under the conditions used in this work, reactions occur at domain boundaries between the not completely mixed CO and O islands. This work is an excellent example of how low-temperature studies of surface chemistry can be dramatically different to those carried out closer to the high temperatures used in real-world applications.
- [314] van Spronsen MA, Frenken JWM, Groot IMN. *Chem Soc Rev*, 2017, 46: 4347–4374
- [315] Xu, B. J., Madix, R. J. & Friend, C. M. Predicting gold-mediated catalytic oxidative-coupling reactions from single crystal studies. *Acc. Chem. Res.* 47, 761–772 (2014). This article describes the elucidation of the microkinetic mechanism for oxidative-coupling-reaction networks on gold catalysts via first-principles studies on single-crystal gold surfaces.
- [316] Stowers, K. J., Madix, R. J. & Friend, C. M. From model studies on Au(111) to working conditions with unsupported nanoporous gold catalysts: Oxygen-assisted coupling reactions. *J. Catal.* 308, 131–141 (2013).
- [317] Xu, B. J., Haubrich, J., Baker, T. A., Kaxiras, E. & Friend, C. M. Theoretical study of O-assisted selective coupling of methanol on Au(111). *J. Phys. Chem. C* 115, 3703–3708 (2011).
- [318] Xu, B. J. & Friend, C. M. Oxidative coupling of alcohols on gold: Insights from experiments and theory. *Faraday Discuss.* 152, 307–320 (2011).
- [319] Outka, D. A. & Madix, R. J. Acid-base and nucleophilic chemistry of atomic oxygen on the Au(110) surface: reactions

- with formic acid and formaldehyde. *Surf. Sci.* 179, 361–376 (1987).
- [320] Wachs, I. E. & Madix, R. J. The surface intermediate H₂COO. *Appl. Surf. Sci.* 5, 426–428 (1980).
- [321] Reece, C., Redekop, E. A., Karakalos, S., Friend, C. M. & Madix, R. J. Crossing the great divide between single-crystal reactivity and actual catalyst selectivity with pressure transients. *Nat. Catal.* 1, 852–859 (2018). This work demonstrated the use of fundamental studies on single-crystal gold to correctly predict the oxidative coupling of methanol on a nanoporous gold catalyst. Such studies demonstrate how the pressure and materials ‘gaps’ between surface science and real-world catalysis can be closed.
- [322] I. Coric, B. List, *Nature* 483, 315–319 (2012)
- [323] C. Li, *Catal. Rev. Sci. Eng.* 46, 419–492 (2004)
- [324] J. Cejka, *Appl. Catal. A* 254, 327–338 (2003)
- [325] Q. Yang, J. Liu, L. Zhang, C. Li, *J. Mater. Chem.* 19, 1945–1955 (2009)
- [326] J. Liang, Z. Liang, R. Zou, Y. Zhao, *Adv. Mater.* 29 (2017)
- [327] A. Taguchi, F. Schüth, *Microporous Mesoporous Mater.* 77, 1–45 (2005)
- [328] C. Perego, R. Millini, Porous materials in catalysis: challenges for mesoporous materials. *Chem. Soc. Rev.* 42, 3956–3976 (2013)
- [329] T. Cheng, Q. Zhao, D. Zhang, G. Liu, *Green Chem.* 17, 2100–2122 (2015)
- [330] N. Pal, A. Bhaumik, *RSC Adv.* 5, 24363–24391 (2015)
- [331] G.M. Ziarani, N. Lashgari, A. Badiei, *J. Mol. Catal. A Chem.* 397, 166–191 (2015)
- [332] Y.-P. Zhu, T.-Z. Ren, Z.-Y. Yuan, *Catal. Sci. Technol.* 5, 4258–4279 (2015)
- [333] Y.Y. Sun, S. Walspurger, J.P. Tessonier, B. Louis, J. Sommer, *Appl. Catal. A* 300, 1–7 (2006)
- [334] C.Y. Ma, B.J. Dou, J.J. Li, J. Cheng, Q. Hu, Z.P. Hao, S.Z. Qiao, *Appl. Catal. B* 92, 202–208 (2009)
- [335] J.N. Kuhn, W. Huang, C.-K. Tsung, Y. Zhang, G.A. Somorjai, *J. Am. Chem. Soc.* 130, 14026–1402+ (2008)
- [336] W. Huang, J.N. Kuhn, C.-K. Tsung, Y. Zhang, S.E. Habas, P. Yang, G.A. Somorjai, *Nano Lett.* 8, 2027–2034 (2008)
- [337] C. Deraedt, R. Ye, W.T. Ralston, F.D. Toste, G.A. Somorjai, Dendrimer-Stabilized Metal Nanoparticles as Efficient Catalysts for Reversible Dehydrogenation/Hydrogenation of N-Heterocycles. *J. Am. Chem. Soc.* 139, 18084–18092 (2017)
- [338] R. Ye, A.V. Zhukhovitskiy, C.V. Deraedt, F.D. Toste, A. Somorjai, Supported dendrimer-encapsulated metal clusters: toward heterogenizing homogeneous catalysts. *Acc. Chem. Res.* 50, 1894–1901 (2017)
- [339] X. Wei, M. Zhou, X. Zhang, X. Wang, Z. Wu, Amphiphilic mesoporous sandwich-structured catalysts for selective hydrogenation of 4-nitrostyrene in water. *ACS Appl. Mater. Interfaces* 11, 39116–39124 (2019)
- [340] G.H. Wang, X. Deng, D. Gu, K. Chen, H. Tuysuz, B. Spliethoff, H.J. Bongard, C. Weidenthaler, W. Schmidt, F. Schüth, *Angew. Chem. Int. Ed.* 55, 11101–11105 (2016)
- [341] J. Dou, H.C. Zeng, *J. Phys. Chem. C* 116, 7767–7775 (2012)
- [342] Z. Sun, B. Sun, M. Qiao, J. Wei, Q. Yue, C. Wang, Y. Deng, S. Kaliaguine, D. Zhao, *J. Am. Chem. Soc.* 134, 17653–17660 (2012)
- [343] R. Goyal, D. Dumbre, L.N.S. Konathala, M. Pandey, A. Bordoloi, *Catal. Sci. Technol.* 5, 3632–3638 (2015)
- [344] Y. Liu, H. Dai, J. Deng, S. Xie, H. Yang, W. Tan, W. Han, Y. Jiang, G. Guo, *J. Catal.* 309, 408–418 (2014)
- [345] J. Yang, C.-Y. Mou, *Appl. Catal. B* 231, 283–291 (2018)
- [346] X. Zhang, D. Wang, M. Jing, J. Liu, Z. Zhao, G. Xu, W. Song, Y. Wei, Y. Sun, *Chemcatchem* 11, 2089–2098 (2019)
- [347] X.F. Lin, Mingli, H. He, J. Wu, L. Chen, D. Ye, Y. Hu, Y. Wang, W. Wen, *Acta Phys. -Chim. Sin.* 34, 719–730 (2018)
- [348] K. Engstrom, E.V. Johnston, O. Verho, K.P.J. Gustafson, M. Shakeri, C.-W. Tai, J.-E. Backvall, *Angew. Chem. Int. Ed.* 52, 14006–14010 (2013)
- [349] T. Himiyama, M. Waki, Y. Maegawa, S. Inagaki, *Angew. Chem. Int. Ed.* 58, 9150–9154 (2019)
- [350] R. Zhang, J. Jiang, J. Zhou, Y. Xu, R. Xiao, X. Xia, Z. Rao, *Adv. Mater.* 30 (2018)
- [351] W. Wang, W. Jing, L. Sheng, D. Chai, Y. Kang, Z. Lei, *Appl. Catal. A* 538, 123–130 (2017)
- [352] P. Cruz, Y. Perez, I. del Hierro, M. Fajardo, *Microporous Mesoporous Mater.* 220, 136–147 (2016)
- [353] F. Chen, S. Zhao, T. Yang, T. Jiang, J. Ni, Q. Zhang, L. Xiaonian, *Acta Phys. -Chim. Sin.* 35, 775–786 (2019)
- [354] L. Geng, X. Zhang, W. Zhang, M. Jia, G. Liu, Highly dispersed iron oxides on mesoporous carbon for selective oxidation of benzyl alcohol with molecular oxygen. *Chem. Commun.* 50, 2965–2967 (2014)
- [355] A.L. Canepa, V.R. Elias, V.M. Vaschetti, E.V. Sabre, G.A. Eimer, S.G. Casuscelli, *Appl. Catal. A* 545, 72–78 (2017)
- [356] X. Dong, D. Wang, K. Li, Y. Zhen, H. Hu, G. Xue, *Mater. Res. Bull.* 57, 210–220 (2014)
- [357] M. Li, X. Fu, L. Peng, L. Bai, S. Wu, Q. Kan, J. Guan, *Chemistryselect* 2, 9486–9489 (2017)
- [358] C.-W. Kung, P.-C. Han, C.-H. Chuang, and K.C.-W. Wu: Electronically conductive metal–organic framework-based materials. *APL Mater.* 7, 110902 (2019).
- [359] E. Pérez-Mayoral, I. Matos, M. Bernardo, and I.M. Fonseca: New and advanced porous carbon materials in fine chemical synthesis. Emerging precursors of porous carbons. *Catalysts* 9(2), 133 (2019).
- [360] L. Song, T. Xu, D. Gao, X. Hu, C. Li, S. Li, and G. Chen: Metal-organic framework (MOF)-derived carbon-mediated interfacial reaction for the synthesis of CeO₂–MnO₂ catalysts. *Chem. Eur. J.* 25(26), 6621–6627 (2019).
- [361] X. Lin, S. Wang, W. Tu, Z. Hu, Z. Ding, Y. Hou, R. Xu, and W. Dai: MOF-derived hierarchical hollow spheres composed of carbon-confined Ni nanoparticles for efficient CO₂ methanation. *Catal. Sci. Technol.* 9, 731–738 (2019).
- [362] Z. Dong, X. Le, Y. Liu, C. Dong, and J. Ma: Metal-organic framework derived magnetic porous carbon composite supported gold and palladium nanoparticles as highly efficient and recyclable catalysts for reduction of 4-nitrophenol and hydrodechlorination of 4-chlorophenol. *J. Mater. Chem. A* 2, 18775–18785 (2014).
- [363] H. Zhang, H. Osgood, X. Xie, Y. Shao, and G. Wu: Engineering nanostructures of PGM-free oxygen-reduction catalysts using metal-organic frameworks. *Nano Energy* 31, 331–350 (2017).
- [364] Y. Zhou, Y. Zhang, X. Xu, S. Zhao, Z. Guo, K.-H. Wu, C. Tan, and Z. Wang: Bimetallic metal-organic framework derived metal-carbon hybrid for efficient reversible oxygen electrocatalysis. *Front. Chem.* 7, 747 (2019).
- [365] Y. Cao, Y. Lu, E.H. Ang, H. Geng, X. Cao, J. Zheng, and H. Gu: MOF-derived uniform Ni nanoparticles encapsulated in carbon nanotubes grafted on rGO nanosheets as bifunctional materials

- for lithium-ion batteries and hydrogen evolution reaction. *Nanoscale* 11(32), 15112–15119 (2019).
- [366] Q. Yuan, Y. Yu, Y. Gong, and X. Bi: Three-dimensional N-doped carbon nanotube frameworks on Ni foam derived from a metal–organic framework as a bifunctional electrocatalyst for overall water splitting. *ACS Appl. Mater. Inter.* 12(3), 3592–3602 (2020).
- [367] Z. Song, L. Zhang, M. Zheng, and X. Sun: Chapter 1: MOF-derived materials for extremely efficient electrocatalysis. In *Layered Materials for Energy Storage and Conversion*, D. Geng, Y. Cheng, and G. Zhang, eds. (Royal Society of Chemistry, London, 2019); pp. 1–38.
- [368] H.-F. Wang, L. Chen, H. Pang, S. Kaskel, and Q. Xu: MOF-derived electrocatalysts for oxygen reduction, oxygen evolution and hydrogen evolution reactions. *Chem. Soc. Rev.* 49, 1414–1448 (2020).
- [369] T. Singh, C. Das, N. Bothra, N. Sikdar, S. Das, S.K. Pati, and T. Kumar Maji: MOF derived Co₃O₄@Co/NCNT nanocomposite for electrochemical hydrogen evolution, flexible zinc-air batteries, and overall water splitting. *Inorg. Chem.* 59(5), 3160–3170 (2020).
- [370] B. Weng, C.R. Grice, W. Meng, L. Guan, F. Xu, Y. Yu, C. Wang, D. Zhao, and Y. Yan: Metal–organic framework-derived CoWP@C composite nanowire electrocatalyst for efficient water splitting. *ACS Energy Lett.* 3(6), 1434–1442 (2018).
- [371] C. Guan, H. Wu, W. Ren, C. Yang, X. Liu, X. Ouyang, Z. Song, Y. Zhang, S.J. Pennycook, C. Cheng, and J. Wang: Metal–organic framework-derived integrated nanoarrays for overall water splitting. *J. Mater. Chem. A* 6, 9009–9018 (2018).
- [372] T. Quynh Ngan Tran, B. Ju Park, W. Hyun Yun, T. Nhac Duong, and H. Hee Yoon: Metal–organic framework-derived Ni@C and NiO@C as anode catalysts for urea fuel cells. *Sci. Rep.* 10, 278 (2020).
- [373] S. Chen, H. Jang, J. Wang, Q. Qin, X. Liu, and J. Cho: Bimetallic metal–organic framework-derived MoFe-PC microspheres for electrocatalytic ammonia synthesis under ambient conditions. *J. Mater. Chem. A* 8, 2099–2104 (2020).
- [374] W. Chang, D. Zheng, C. Zhao, and Y. Yang: Photocatalytic activity of MOF-derived Cu₂O/Cu/C/Ag porous composites. *S. Afr. J. Chem.* 72, 10–15 (2019).
- [375] H. Li, J. Tian, Z. Zhu, F. Cui, Y.-A. Zhu, X. Duan, and S. Wang: Magnetic nitrogen-doped nanocarbons for enhanced metal-free catalytic oxidation: Integrated experimental and theoretical investigations for mechanism and application. *Chem. Eng. J.* 354, 507–516 (2018).
- [376] Y. Gong, X. Zhao, H. Zhang, B. Yang, K. Xiao, T. Guo, J. Zhang, H. Shao, Y. Wang, and G. Yud: MOF-derived nitrogen doped carbon modified g-C₃N₄ heterostructure composite with enhanced photocatalytic activity for bisphenol a degradation with peroxymonosulfate under visible light irradiation. *Appl. Catal., B* 233, 35–45 (2018).
- [377] H. Zhang, S. Chen, H. Zhang, X. Fan, C. Gao, H. Yu, and X. Quan: Carbon nanotubes-incorporated MIL-88B-Fe as highly efficient fenton-like catalyst for degradation of organic pollutants. *Front. Environ. Sci. Eng.* 13, 18 (2019).
- [378] F-Z Song, X. Yang, and Q. Xu: Ultrafine bimetallic Pt–Ni nanoparticles achieved by metal–organic framework templated zirconia/porous carbon/reduced graphene oxide: Remarkable catalytic activity in dehydrogenation of hydrous hydrazine. *Small Methods* 4(1), 1900707 (2020).
- [379] S. Zhuang, B. Babu Nunna, and E. Soo Lee: Metal organic framework-modified nitrogen-doped graphene oxygen reduction reaction catalyst synthesized by nanoscale high-energy wet ball-milling structural and electrochemical characterization. *MRS Commun.* 8(1), 40–48 (2018).
- [380] Liu, L., Corma, A.: Metal catalysts for heterogeneous catalysis: from single atoms to nanoclusters and nanoparticles. *Chem. Rev.* 118, 4981–5079 (2018). <https://doi.org/10.1021/acs.chemrev.7b00776>
- [381] Wang J, Wang G, Zhao J (2002) *Phys Rev B* 66:035418
- [382] Tian N, Zhou Z-Y, Sun S-G, Ding Y, Wang ZL (2007) Synthesis of tetrahedral platinum nanocrystals with high-index facets and high electro-oxidation activity. *Science* 316:732. <https://doi.org/10.1126/science.1140484>
- [383] Perez J, Gonzalez ER, Villullas HM (1998) Hydrogen evolution reaction on gold single-crystal electrodes in acid solutions. *J Phys Chem B* 102:10931–10935. <https://doi.org/10.1021/jp9831987>
- [384] Zhang L, Chen D, Jiang Z, Zhang J, Xie S, Kuang Q, Xie Z, Zheng L (2012) Facile syntheses and enhanced electrocatalytic activities of Pt nanocrystals with high-index surfaces. *Nano Res* 5:181–189. <https://doi.org/10.1007/s12274-012-0198-1>
- [385] Chen M, Goodman DW (2006) Catalytically active gold: from nanoparticles to ultrathin films. *Acc Chem Res* 39:739–746. <https://doi.org/10.1021/ar040309d>
- [386] Kiss J, Kukovec A, Kónya Z (2019) Beyond nanoparticles: the role of sub-nanosized metal species in heterogeneous catalysis. *Catal Lett* 149:1441–1454. <https://doi.org/10.1007/s10562-019-02734-6>
- [387] László B, Baán K, Oszkó EA, Kiss J, Kónya Z (2018) *Top Catal* 61:875:888
- [388] Solymosi F, Pasztor M (1985) An infrared study of the influence of carbon monoxide chemisorption on the topology of supported rhodium. *J Phys Chem* 89:4789–4793. <https://doi.org/10.1021/j100268a026>
- [389] Buchanan DA, Hernandez ME, Solymosi F, White JM (1990) CO-induced structural changes of Rh on TiO₂ Support. *J Catal* 125:456–466. [https://doi.org/10.1016/0021-9517\(90\)90318-E](https://doi.org/10.1016/0021-9517(90)90318-E)
- [390] Berkó A, Solymosi F (2000) Effects of different gases on the morphology of Ir nanoparticles supported on the TiO₂(110)-(1×2) surface. *J Phys Chem B* 104:10215–10221. <https://doi.org/10.1021/jp002065u>
- [391] Berkó A, Szökő J, Solymosi F (2004) Effect of CO on the morphology of Pt nanoparticles supported on TiO₂(1 1 0)-(1 × n). *Surf Sci* 566–568:337–342. <https://doi.org/10.1016/J.SUSC.2004.05.065>
- [392] Bäumer M, Freund HJ. *Prog Surf Sci*, 1999, 61: 127–198
- [393] Campbell CT (1997) Ultrathin metal films and particles on oxide surfaces: structural, electronic and chemisorptive properties. *Surf Sci Rep* 27:1–111. [https://doi.org/10.1016/S0167-5729\(96\)00011-8](https://doi.org/10.1016/S0167-5729(96)00011-8)
- [394] Gunter PL, Niemantsverdriet JW, Ribeiro FH, Somorjai GA (1997) Surface science approach to modeling supported catalysts. *Catal Rev* 39:77–168. <https://doi.org/10.1080/01614949708006469>
- [395] Solymosi F (1985) Comments on electronic effects in strong metal-support interactions on titania-deposited metal catalysts. *J Catal* 94:581–585. [https://doi.org/10.1016/0021-9517\(85\)90226-X](https://doi.org/10.1016/0021-9517(85)90226-X)

- [396] Tauster SJ, Fung SC, Garten RL (1978) Strong metal-support interactions. Group 8 noble metals supported on titanium dioxide. *J Am Chem Soc* 100:170–175. doi: 10.1021/ja00469a029
- [397] Cook KM, Poudyal S, Miller JT, Bartholomew CH, Hecker WC (2012) Reducibility of alumina-supported cobalt Fischer-Tropsch catalysts: effects of noble metal type, distribution, retention, chemical state, bonding, and influence on cobalt crystallite size. *Appl Catal A* 449:69–80. <https://doi.org/10.1016/j.apcata.2012.09.032>
- [398] Guo Y, Mei S, Yuan K, Wang D-J, Liu H-C, Yan C-H, Zhang Y-W (2018) Low-temperature CO₂ methanation over CeO₂-supported Ru single atoms, nanoclusters, and nanoparticles competitively tuned by strong metal-support interactions and H-spillover effect. *ACS Catal* 8:6203–6215. <https://doi.org/10.1021/acsCatal7b04469>
- [399] Grasselli RK, Tenhover MA (2008) In: Knözinger G, Schüth F, Weitkamp EH (eds) *Handbook of heterogeneous catalysis*. VCH, Ann Arbor, p 3489
- [400] Grasselli RK, Suresh DD (1972) Aspects of structure and activity in uranium-antimony oxide acrylonitrile catalysts. *J Catal* 25:273–291
- [401] Schlögl R. *Angew Chem Int Ed*, 2015, 54: 3465–3520
- [402] Alnoncourt RN, Csepei LI, Hävecker M, Girgsdies F, Schuster ME, Schlögl R, Trunschke A (2014) The reaction network in propane oxidation over phase-pure MoVTenb M1 oxide catalysts. *J Catal* 311:369–385
- [403] Alnoncourt R, Kolen'ko YV, Schlögl R, Trunschke A (2012) A new way of probing reaction networks: analyzing multidimensional parameter space. *Comb Chem High Screen* 15(2):161–169
- [404] Kampe P, Giebeler L, Samuelis D, Kunert J, Drochner A, Haass F, Adams AH, Ott J, Endres S, Schimanke G, Buhrmester T, Martin M, Fuess H, Vogel H (2007) Heterogeneously catalysed partial oxidation of acrolein to acrylic acid—structure, function and dynamics of the V–Mo–W mixed oxides. *Phys Chem Chem Phys* 9:3577–3589
- [405] Geske M, Korup O, Horn R (2013) Resolving kinetics and dynamics of a catalytic reaction inside a fixed bed reactor by combined kinetic and spectroscopic profiling. *Catal Sci Technol* 3:169–175
- [406] Topsøe H, Ovesen CV, Clausen BS, Topsøe NY, Nielsen PH, Törnqvist E, Nørskov JK (1997) Importance of dynamics in real catalyst systems. *Stud Surf Sci Catal* 109:121–139
- [407] Wang SG, Temel B, Shen JA, Jones G, Grabow LC, Studt F, Bligaard T, Abild-Pedersen F, Christensen CH, Nørskov JK (2011) Universal Brønsted-Evans-Polanyi relations for C–C–O, C–N, N–O, N–N, and O–O dissociation reactions. *Catal Lett* 141:370–373
- [408] Vojvodic A, Calle-Vallejo F, Guo W, Wang S, Toftelund A, Studt F, Martinez JI, Shen J, Man IC, Rossmeisl J, Bligaard T (2011) On the behavior of Brønsted-Evans-Polanyi relations for transition metal oxides. *J Chem Phys* 134(24):244509
- [409] Zhao C, Wachs IE (2008) Selective oxidation of propylene over model supported V₂O₅ catalysts: influence of surface vanadia coverage and oxide support. *J Catal* 257:181–189
- [410] Kulkarni D, Wachs IE (2002) Isopropanol oxidation by pure metal oxide catalysts: number of active surface sites and turnover frequencies. *Appl Catal A* 237:121–137
- [411] Amakawa K, Sun LL, Guo CS, Hävecker M, Kube P, Wachs IE, Lwin S, Frenkel AI, Patlolla A, Hermann K, Schlögl R, Trunschke A (2013) How strain affects the reactivity of surface metal oxide catalysts. *Angewandte Chemie Inter Edn* 52:13553–13557
- [412] Hammer, B. & Nørskov, J. K. Why gold is the noblest of all the metals. *Nature* 376, 238–240 (1995).
- [413] Nørskov, J. K. Electronic is factors in catalysis. *Prog. Surf. Sci.* 38, 103–144 (1991).
- [414] Nilsson, A. et al. The electronic structure effect in heterogeneous catalysis. *Catal. Lett.* 100, 111–114 (2005).
- [415] Hammer, B. & Nørskov, J. K. Theoretical surface science and catalysis—calculations and concepts. *Adv. Catal.* 45, 71–129 (2000).
- [416] Kitchin, J. R., Nørskov, J. K., Barteau, M. A. & Chen, J. G. Modification of the surface electronic and chemical properties of Pt(111) by subsurface 3d transition metals. *J. Chem. Phys.* 120, 10240–10246 (2004).
- [417] Logadottir, A. et al. The Brønsted–Evans–Polanyi relation and the volcano plot for ammonia synthesis over transition metal catalysts. *J. Catal.* 197, 229–231 (2001).
- [418] Wang, S. et al. Universal Brønsted–Evans–Polanyi relations for C–C, C–O, C–N, N–O, N–N, and O–O dissociation reactions. *Catal. Lett.* 141, 370–373 (2010).
- [419] Nørskov, J. K. et al. The nature of the active site in heterogeneous metal catalysis. *Chem. Soc. Rev.* 37, 2163–2171 (2008).
- [420] Michaelides, A. et al. Identification of general linear relationships between activation energies and enthalpy changes for dissociation reactions at surfaces. *J. Am. Chem. Soc.* 125, 3704–3705 (2003).
- [421] Bligaard, T. et al. The Brønsted–Evans–Polanyi relation and the volcano curve in heterogeneous catalysis. *J. Catal.* 224, 206–217 (2004).
- [422] Loffreda, D., Delbecq, F., Vigne, F. & Sautet, P. Fast prediction of selectivity in heterogeneous catalysis from extended Brønsted–Evans–Polanyi relations: a theoretical insight. *Angew. Chem. Int. Ed.* 48, 8978–8980 (2009).
- [423] Vojvodic, A. et al. On the behavior of Brønsted–Evans–Polanyi relations for transition metal oxides. *J. Chem. Phys.* 134, 244509 (2011).
- [424] Wang, S. et al. Universal transition state scaling relations for (de)hydrogenation over transition metals. *Phys. Chem. Chem. Phys.* 13, 20760–20765 (2011).
- [425] Viñes, F., Vojvodic, A., Abild-Pedersen, F. & Illas, F. Brønsted–Evans–Polanyi relationship for transition metal carbide and transition metal oxide surfaces. *J. Phys. Chem. C* 117, 4168–4171 (2013).
- [426] Yang, B., Burch, R., Hardacre, C., Headdock, G. & Hu, P. Understanding the optimal adsorption energies for catalyst screening in heterogeneous catalysis. *ACS Catal.* 4, 182–186 (2013).
- [427] Fajín, J. L. C., Cordeiro, M. N. D. S., Illas, F. & Gomes, J. R. B. Generalized Brønsted–Evans–Polanyi relationships and descriptors for O–H bond cleavage of organic molecules on transition metal surfaces. *J. Catal.* 313, 24–33 (2014).
- [428] Greeley, J., Jaramillo, T. F., Bonde, J., Chorkendorff, I. & Nørskov, J. K. Computational high-throughput screening of electrocatalytic materials for hydrogen evolution. *Nat. Mater.* 5, 909–913 (2006).
- [429] Zhang, Y.-J., Sethuraman, V., Michalsky, R. & Peterson, A. A. Competition between CO₂ reduction and H₂ evolution on

- transition-metal electrocatalysts. *ACS Catal.* 4, 3742–3748 (2014).
- [430] Cave, E. R. et al. Trends in the catalytic activity of hydrogen evolution during CO₂ electroreduction on transition metals. *ACS Catal.* 8, 3035–3040 (2018).
- [431] Greeley, J., Nørskov, J. K., Kibler, L. A., El-Aziz, A. M. & Kolb, D. M. Hydrogen evolution over bimetallic systems: understanding the trends. *ChemPhysChem* 7, 1032–1035 (2006).
- [432] Calle-Vallejo, F., Loffreda, D., Koper, M. T. & Sautet, P. Introducing structural sensitivity into adsorption–energy scaling relations by means of coordination numbers. *Nat. Chem.* 7, 403–410 (2015).
- [433] Hong, W. T. et al. Toward the rational design of non-precious transition metal oxides for oxygen electrocatalysis. *Energy Environ. Sci.* 8, 1404–1427 (2015).
- [434] Tsai, C., Chan, K., Nørskov, J. K. & Abild-Pedersen, F. Understanding the reactivity of layered transition-metal sulfides: a single electronic descriptor for structure and adsorption. *J. Phys. Chem. Lett.* 5, 3884–3889 (2014).
- [435] Xu, H., Cheng, D., Cao, D. & Zeng, X. C. A universal principle for a rational design of single-atom electrocatalysts. *Nat. Catal.* 1, 339–348 (2018).
- [436] Wang, A., Li, J. & Zhang, T. Heterogeneous single-atom catalysis. *Nat. Rev. Chem.* 2, 65–81 (2018).
- [437] Marcinkowski, M. D. et al. Pt/Cu single-atom alloys as coke-resistant catalysts for efficient C–H activation. *Nat. Chem.* 10, 325–332 (2018).
- [438] Zhang, Z. et al. Thermally stable single atom Pt/m-Al₂O₃ for selective hydrogenation and CO oxidation. *Nat. Commun.* 8, 16100 (2017).
- [439] Mehta, P. et al. Overcoming ammonia synthesis scaling relations with plasma-enabled catalysis. *Nat. Catal.* 1, 269–275 (2018).
- [440] Sun, G. et al. Breaking the scaling relationship via thermally stable Pt/Cu single atom alloys for catalytic dehydrogenation. *Nat. Commun.* 9, 4454 (2018).
- [441] Nie, L. et al. Activation of surface lattice oxygen in single-atom Pt/CeO₂ for low-temperature CO oxidation. *Science* 358, 1419–1423 (2017).
- [442] Liu, J. et al. Tackling CO poisoning with single-atom alloy catalysts. *J. Am. Chem. Soc.* 138, 6396–6399 (2016).
- [443] Lucci, F. R. et al. Selective hydrogenation of 1,3-butadiene on platinum–copper alloys at the single-atom limit. *Nat. Commun.* 6, 8550 (2015).
- [444] Qiao, B. et al. Single-atom catalysis of CO oxidation using Pt₁/FeO_x. *Nat. Chem.* 3, 634–641 (2011).
- [445] Bruix, A. et al. Maximum noble-metal efficiency in catalytic materials: atomically dispersed surface platinum. *Angew. Chem. Int. Ed.* 53, 10525–10530 (2014).
- [446] Wei, H. et al. FeO_x-supported platinum single-atom and pseudo-single-atom catalysts for chemoselective hydrogenation of functionalized nitroarenes. *Nat. Commun.* 5, 5634 (2014).
- [447] Zhang, S. et al. Catalysis on singly dispersed bimetallic sites. *Nat. Commun.* 6, 7938 (2015).
- [448] Cheng, M.-J., Clark, E. L., Pham, H. H., Bell, A. T. & Head-Gordon, M. Quantum mechanical screening of single-atom bimetallic alloys for the selective reduction of CO₂ to C₁ hydrocarbons. *ACS Catal.* 6, 7769–7777 (2016).
- [449] Lin, L. et al. A highly CO-tolerant atomically dispersed Pt catalyst for chemoselective hydrogenation. *Nat. Nanotechnol.* 14, 354–361 (2019).
- [450] Liu, D. et al. Atomically dispersed platinum supported on curved carbon supports for efficient electrocatalytic hydrogen evolution. *Nat. Energy* 4, 512–518 (2019).
- [451] Darby, M. T., Stamatakis, M., Michaelides, A. & Sykes, E. C. H. Lonely atoms with special gifts: breaking linear scaling relationships in heterogeneous catalysis with single-atom alloys. *J. Phys. Chem. Lett.* 9, 5636–5646 (2018).